IMPROVING THE DELIVERY OF NOVEL MOLECULARLY-TARGETED THERAPIES FOR THE TREATMENT OF PRIMARY AND METASTATIC BRAIN TUMORS

A DISSERTATION
SUBMITTED TO THE FACULTY OF THE
UNVERSITY OF MINNESOTA
BY

GAUTHAM GAMPA

IN PARTIAL FULFILLMENT OF THE REQUIERMENTS
FOR THE DEGREE OF
DOCTOR OF PHILOSOPHY

WILLIAM FREDERICK ELMQUIST

JANUARY 2019

ACKNOWLEDGEMENTS

I am extremely grateful to everyone who believed in my abilities and helped me directly or indirectly. This research endeavor has become possible with the kind support of many individuals.

First and foremost, I would like to express my deep gratitude to my advisor Dr. William Elmquist for his patient guidance, constant encouragement, enthusiasm towards our research and his willingness to offer his time so generously. There are many qualities that make him a great advisor and a wonderful person to work with, and he will always have a positive influence on me. I would like to sincerely thank Dr. Jann Sarkaria for being a great mentor, and a committee member. His valuable advice and critiques have contributed appreciably in making me think rationally about the scientific outcomes from my projects. I wish to extend my gratitude to Dr. Steven Rosenfeld for being a mentor and collaborator. His insights and practical feedback have helped me shape aspects of my research work. I would also like to thank Dr. Ronald Siegel and Dr. Jayanth Panyam for serving on my committee, and offering constructive suggestions during the development of this research work. Together, the above mentioned people have been instrumental in helping me develop my scientific voice and think critically about my research work.

I would like to express my appreciation to my colleagues at the Elmquist Laboratory, past and present, for their support: Dr. Karen Parrish, Dr. Shruthi Vaidhyanathan, Dr. Shuangling Zhang, Dr. Minjee Kim, Dr. Janice Laramy, Brynna Wilken-Resman, Dr. Sani Kizilbash, Nicholas Cook-Rostie, Dr. Afroz Mohammad, Surabhi Talele, Jessica

Griffith and Katelyn Swanson. The camaraderie and support of these creative friends have helped me grow as a scientist, and I will always remember the good memories I had in the lab. This research work would not have been completed without the help of collaborators in the Sarkaria Lab and Rosenfeld Lab at the Mayo Clinic, and Strategia Therapeutics. I would like to particularly thank Danielle Burgenske, Ann Mladek, Brett Carlson, Bianca-Maria Marin and Mark Schroeder from Sarkaria Lab, Rajappa Kenchappa and James Crish from Rosenfeld Lab for ensuring the smooth conduct of some of the in vivo studies. I also wish to acknowledge the help provided by Dr. Linda Paradiso and Dr. Louis DePalatis from Strategia Therapeutics.

I am thankful to a few special teachers. I would like to thank Dr. Ronald Sawchuk for offering the SAAMII workshop. I thank Dr. Cheryl Zimmerman for teaching the courses in Pharmacokinetics. I wish to thank Dr. Richard Brundage for teaching the Pharmacometrics courses. I would like to acknowledge the help provided by Mr. James Fisher in the development of LC-MS/MS assays.

I am grateful to the Department of Pharmaceutics and the Graduate School at the University of Minnesota. I would like to thank the faculty and administrative staff at the Department of Pharmaceutics for their support throughout my graduate school education at the University of Minnesota. The Sawchuk Fellowship awarded by the Department of Pharmaceutics and the Doctoral dissertation Fellowship awarded by the Graduate School at the University of Minnesota enabled me to focus on my research and provided me with the opportunity to present my research at national and international conferences. The

projects in this dissertation were supported by grants from the National Institutes of Health and Strategia Therapeutics.

I thank my friends, Vidhi Bhatt, Kushal Patel, Jigish Parmar, Nagakiran Duggirala, Suresh Swaminathan, Siddarth Karuka, Sharan Banagiri, Nidhi Sharda, Roopesh Bhuriwale, Rohit Asawa, Hariprasad Brungi, Rajat Thakur, Abhijit Yenumulapalli and Nikhil Bojja, for their companionship, encouragement and support.

Finally, I am extremely grateful to my family for their persistent support, encouragement and faith in me. I thank my wonderful parents, Dr. Ramakrishna and Neeraja, for being my first teachers, inculcating positive values in me, motivating me all along and their endless love. I would like to wholeheartedly thank my grandfather Dr. Ranga Rao, my aunt Dr. Sudha Rani, my brother Gaurav and my wife Divya Mounica for their willingness to help, positive outlook and everlasting support.

DEDICATION

To my grandparents and parents

for their unconditional love, support and encouragement.

ABSTRACT

Tumors in the brain are challenging to diagnose and are associated with poor survival outcomes. Brain tumors are difficult to treat, in part, due to restricted drug delivery across the blood-brain barrier (BBB). Although the BBB is compromised in some regions of brain tumors, the degree of disruption is not uniform and certain tumor locations have a functionally intact BBB. A critical component of BBB that restricts entry of therapeutics into brain is active efflux. The objective of this work is to examine brain distribution of novel molecularly-targeted therapies, including evaluation of influence of P-gp and Bcrp-mediated efflux at the BBB, assessment of spatial heterogeneity in drug distribution to brain tumors, and comparison of unbound (active) drug exposures with in vitro efficacy. Ispinesib is a KIF11 inhibitor that inhibits both tumor proliferation and invasion in glioblastoma (GBM). We demonstrate that ispinesib has a limited brain delivery due to efflux by P-gp and Bcrp, and ispinesib delivery is heterogeneous to areas within a tumor in a GBM model. Furthermore, predicted unbound-concentrations in brain were less than in vitro cytotoxic concentrations, suggesting that delivery may limit in vivo efficacy. Also, pharmacological inhibition of efflux transport (elacridar co-administration) improves brain delivery of ispinesib, and future studies will evaluate if enhanced delivery will improve efficacy. CCT196969, LY3009120 and MLN2480 are panRAF inhibitors with minimal paradoxical activation of MAPK pathway and may overcome resistance observed with BRAF inhibitor therapy in melanoma. MEK inhibition is used in combination with BRAF inhibitors to delay resistance. E6201 is a potent MEK inhibitor

with a unique macrocyclic structure. While brain distribution of panRAF inhibitors is limited by efflux, E6201 has a favorable brain distribution profile and interacts minimally with P-gp and Bcrp. The delivery of E6201 is variable to regions of tumor in an intracranial melanoma model. However, predicted unbound-concentrations in brain achieve levels higher than in vitro cytotoxic concentrations for LY3009120 and E6201, suggesting possible efficacy in melanoma brain metastases. Future studies evaluating in vivo efficacy in preclinical models will reveal the utility of selected compounds in brain tumor treatment, and if improved delivery translates to superior efficacy.

Table of Contents

LIST OF TABLES

LIST OF FIGURES

LIST OF ABBREVIATIONS

ABC, ATP-binding cassette

AUC, area under the curve

BBB, blood-brain barrier

Bcrp, breast cancer resistance protein (Abcg2)

BSA, bovine serum albumin

CE-MRI, contrast-enhanced magnetic resonance imaging;

CL, clearance

Cmax, maximum drug concentration

CNS, central nervous system

DA, distribution advantage

fu, unbound (free) fraction

F, bioavailability

FBS, fetal bovine serum

FVB, friend leukemia virus strain B

GBM, glioblastoma

GFP, green fluorescent protein

HBD, hydrogen-bond donor

IC_{50}, half-maximal inhibitory concentration

Kp, brain-to-plasma ratio

Kp,uu, unbound (free) brain-to-plasma ratio/ unbound partition coefficient

LC-MS/MS, liquid chromatography tandem mass spectroscopy

MAPK, mitogen-activated protein kinase

MBM, melanoma brain metastases

MDCKII, Madin-Darby canine kidney II

NCA, non-compartmental analysis

NVU, neurovascular unit

PBS, phosphate buffered saline

OS, overall survival

P-gp, P-glycoprotein (Abcb1, Mdr1)

PDX, patient-derived xenograft

PFS, progression-free survival

RED, rapid equilibrium dialysis

TKO, triple-knockout (*Mdr1a/b*$^{-/-}$ *Bcrp1*$^{-/-}$, P-gp and Bcrp deficient)

Tmax, time at the maximum drug concentration

TPSA, total polar surface area

Vd, volume of distribution

WT, wild-type

CHAPTER I. IMPROVING DRUG DELIVERY TO TUMORS IN THE BRAIN

1.1 INTRODUCTION

The estimated new cases of cancers of the brain and other nervous system is over 23,000 in the United States in 2018, accounting for 1.4% of all cancer patients, and a similar trend is expected globally (Siegel et al., 2018, Bray et al., 2018). The incidence of brain metastases is markedly higher than primary brain tumors, and is observed in nearly 10 % of cancer patients (Barnholtz-Sloan et al., 2004, Nayak et al., 2012, Gallego Perez-Larraya and Hildebrand, 2014). Collectively, lung cancer, breast cancer and melanoma account for up to 75% of adult brain metastases (Nayak et al., 2012, Gallego Perez-Larraya and Hildebrand, 2014). While lung cancer accounts for the highest occurrence of brain metastases, melanoma has the highest predisposition to spread to the brain (Nayak et al., 2012). Moreover, the incidence of brain metastases continues to rise as the treatment of peripheral disease improves with newer targeted therapies (Kromer et al., 2017, Gampa et al., 2017).

Diagnosis of tumors in the brain is devastating to patients, and is associated with poor survival outcomes and a dismal quality of life (Ostrom et al., 2017, Nayak et al., 2012). Time and again, promising experimental therapies continue to show disappointing results in clinical trials and there is a severe need to develop efficacious treatments for tumors in the brain. Among the numerous challenges that exist in the development of effective treatments, drug delivery across an intact blood-brain barrier (BBB) is one important challenge that calls for attention. The BBB presents a major obstacle to the delivery of targeted agents to the brain, which in turn can limit the response to therapy and thereby contribute to the abysmal prognosis observed in patients with tumors in the brain

(Agarwal; Sane; et al., 2011, Gampa et al., 2017). Therefore, future drug discovery and development endeavors should lay emphasis on specifically designing brain penetrant drugs that can reach the protected tumor cells residing behind an intact BBB for improved target engagement and efficacy.

1.1.1 Glioblastoma and KIF11 inhibition

Glioblastoma (GBM) is the most common primary brain tumor in adults, accounting for about 47% of primary malignant brain tumors (Ostrom et al., 2017). The standard therapy for patients with newly diagnosed GBM is surgical resection followed by radiation therapy and treatment with temozolomide (TMZ), an alkylating agent (Stupp et al., 2005). Despite decades of intensive research, the prognosis for patients diagnosed with GBM remains dire, with 5-year survival estimates being as low as 5.5% (Ostrom et al., 2017). The clinical success for targeted therapies tested in GBM has been extremely limited with only 4 FDA approved systemic therapies: lomustine, carmustine, temozolomide and bevacizumab. Several factors contribute to such limited progress including molecular and genetic heterogeneity of malignant gliomas, diffuse infiltrative nature of GBMs, acquired resistance due to microenvironment driven changes in genetic drivers, spatial heterogeneity in the permeability of the BBB and inadequate drug delivery to the brain (Agarwal; Sane; et al., 2011, Gampa et al., 2017, Sarkaria et al., 2018). An important mechanism responsible for restricting the brain delivery of several molecularly-targeted therapies is active efflux at the BBB, mainly by P-gp and Bcrp (Table 1). Resolving the drug delivery problem will undoubtedly help us move closer to finding more efficacious treatments for GBM.

GBMs are often characterized as aggressive brain tumors with high proliferative capacities and wide spread diffuse infiltration within the brain (Chiesa-Vottero et al., 2003, Cuddapah et al., 2014, Demuth and Berens, 2004, Mastronardi et al., 1999, Stoyanov et al., 2017). Although surgical resection and radiation therapy can provide initial local disease control, systemic therapies are often necessary for long-term benefits. The rapid proliferation and extensive dissemination of glioma cells present major challenges in developing effective therapies for the management of this devastating disease. Given this, treatments inhibiting a target that is involved in both tumor cell proliferation and invasion, may improve the responses in malignant GBM (Venere et al., 2015).

Several anti-cancer agents targeting microtubules have been used in the treatment of systemic solid tumors (Wood et al., 2001). The microtubule-based cytoskeleton is essential for both mitosis and cell motility. However, dose-limiting neurotoxicity is frequently observed with anti-mitotic drugs as microtubules are vital for CNS function (Canta et al., 2009, Wood et al., 2001). A group of microtubule associated proteins that are involved in mitotic cell division are the kinesins (Cross and McAinsh, 2014, Rath and Kozielski, 2012). KIF11 is a kinesin that is involved in the separation of centrosomes in prophase, and the formation of bipolar spindle in metaphase of mitosis (Wojcik et al., 2013). Also, KIF11 has some non-mitotic functions, and has been shown to be involved in cell motility (Falnikar et al., 2011). Ispinesib (Table 2) is a potent small-molecule allosteric inhibitor of KIF11, and acts by affecting the ability of KIF11 to bind to microtubules by blocking ADP release (Lad et al., 2008). KIF11 inhibition with ispinesib

suppresses glioma cell proliferation as well as cell motility (Venere et al., 2015) (Figure 1). Also, clinical studies indicate absence of significant neurotoxicity on treatment with ispinesib (Blagden et al., 2008, Burris et al., 2011). These observations suggest that KIF11 inhibition with molecularly-targeted agents such as ispinesib may have a place in the treatment of GBM.

1.1.2 Melanoma brain metastases and MAPK inhibition

Metastatic melanoma is an aggressive form of skin cancer responsible for the majority of skin cancer related mortality. Approximately, 91,000 new cases of melanoma with more than 9000 deaths are projected for 2018 in the United States (Siegel et al., 2018). The MAPK signaling is deregulated in up to 80% of melanomas (Davies et al., 2002). Typically, signal transduction via the MAPK pathway is initiated by the binding of a growth factor, hormone or cytokine to receptor tyrosine kinase that causes the activation of RAS. Upon activation, RAS recruits RAF to the cell membrane and activates RAF, which activates MEK. MEK further phosphorylates and activates ERK kinases leading to activation of downstream pathways responsible for pro-survival and proliferation signals (Samatar and Poulikakos, 2014) (Figure 2). Oncogenic driver mutations in MAPK pathway, frequently in BRAF (~50%) and NRAS (~20%), cause an elevation of kinase activities that trigger the constitutive activation of RAS-RAF-MEK-ERK signaling and results in uncontrolled proliferation (Davies et al., 2002, Hodis et al., 2012).

Melanoma has a high propensity to metastasize to the brain and about ~70% of patients with advanced disease will show metastatic spread to the brain (Gupta et al., 1997, Damsky et al., 2014). The approved therapies have shown improvements in survival by a

few months in patients with melanoma brain metastases (MBM) (Long et al., 2012, Dummer et al., 2014, Margolin et al., 2012, Spagnolo et al., 2016, Tawbi et al., 2018). While encouraging, the management of patients with MBM still poses a significant challenge (Gampa et al., 2017). The modest efficacy in patients with MBM is related to factors including inadequate drug delivery to protected tumor cells residing behind an intact BBB and brain microenvironment driven alterations in gene expression. The FDA approved inhibitors of MAPK pathway have a restricted ability to distribute to the brain due to P-gp and/or Bcrp mediated drug efflux at the BBB, and this can impact their efficacy (Choo et al., 2014, de Gooijer et al., 2018, Mittapalli et al., 2013, Mittapalli et al., 2012, Vaidhyanathan et al., 2014, Wang et al., 2018). There is a critical need to design novel inhibitors of the MAPK pathway that are brain penetrant and can tackle issues related to resistance for improved outcomes in the treatment of MBM.

Targeted inhibition of MAPK pathway with RAF and MEK inhibitors is an important treatment strategy in BRAF-mutant melanomas (Samatar and Poulikakos, 2014) (Figure 2). Vemurafenib, dabrafenib and encorafenib are FDA approved mutant-BRAF inhibitors while cobimetinib, trametinib and binimetinib are FDA approved MEK inhibitors for melanoma. An important clinical challenge in melanoma is acquired resistance to treatment with BRAF inhibitors (Samatar and Poulikakos, 2014). Although vemurafenib/cobimetinib, dabrafenib/trametinib and encorafenib/binimetinib combinations have been approved due to improved clinical responses with BRAF/MEK inhibitor combinations over single agent treatment, patients still progress due to emergence of therapeutic resistance often due to hyperactivated downstream MEK

signaling (Wagle et al., 2014, Welsh et al., 2016). Also, treatment with some BRAF inhibitors is associated with a paradoxical activation of MAPK signaling, primarily in RAS-mutant melanomas (Hatzivassiliou et al., 2010, Poulikakos et al., 2010).

panRAF inhibition

The first generation BRAF inhibitors show efficacy in BRAF-mutant melanomas but are less effective in wild-type BRAF and RAS-mutant melanomas. Also, in RAS-mutant melanomas, treatment with some BRAF inhibitors is associated with a paradoxical activation of the MAPK pathway, which can stimulate secondary malignancies (Hatzivassiliou et al., 2010, Poulikakos et al., 2010). The BRAF-mutant melanomas function in a RAS independent manner, and can signal via mutant BRAF monomers (Freeman et al., 2013). Therefore, BRAF inhibitors should be effective in blocking RAS-RAF-MEK-ERK signaling in BRAF-mutant melanomas. However, wild-type BRAF and RAS-mutant tumors function via RAF dimers, with CRAF playing a vital role in MAPK signal transduction (Freeman et al., 2013). By occupying one partner in homo- and hetero-dimers of RAF, the BRAF inhibitors promote transactivation of drug free partner leading to a paradoxical activation of the MAPK pathway (Poulikakos et al., 2010, Samatar and Poulikakos, 2014). Hence, BRAF inhibitor therapy is commonly employed in BRAF-mutant melanomas, but contraindicated in wild-type BRAF melanomas (Hatzivassiliou et al., 2010).

The newer panRAF inhibitors may overcome issues of paradoxical activation and resistance by effective inhibition of homo and hetero dimers of BRAF and CRAF (Girotti et al., 2015, Peng et al., 2015, Rasco, 2013) (Figure 2). They may be active as first-line

treatment options for both BRAF and NRAS mutant melanomas, and also as second-line therapy for relapsed patients treated with BRAF and BRAF/MEK inhibitors (Girotti et al., 2015). CCT196969, LY3009120 and MLN2480 are three recently developed panRAF inhibitors (Table 2), that have been shown to be capable of inhibiting MAPK pathway in BRAF-mutant, wild-type BRAF and NRAS-mutant melanomas with minimal paradoxical activation (Girotti et al., 2015, Henry et al., 2015, Rasco, 2013). All the three inhibitors have low nanomolar IC_{50} against BRAF and CRAF, and show activity in preclinical models of melanoma (Elenbaas B, 2010, Girotti et al., 2015, Peng et al., 2015). LY3009120 and MLN2480 are being evaluated in phase I/II clinical trials (clinicaltrials.gov).

MEK inhibition

Another key target in the MAPK pathway is MEK, and cancers with elevated MEK activity including those with activating mutations in upstream BRAF may be responsive to MEK inhibition (Wang et al., 2007). Also, given that MEK is downstream of RAF, targeted inhibition of MEK can delay acquired resistance observed with BRAF inhibitor therapy (Flaherty; Infante; et al., 2012, Flaherty; Robert; et al., 2012). Combination therapy with BRAF and MEK inhibitors has resulted in improved efficacy over treatment with single agent BRAF or MEK inhibitors (Flaherty; Infante; et al., 2012). E6201 (Table 2) is an ATP-competitive inhibitor of MEK1 with a unique macrocyclic structure, and has low nanomolar potency in multiple melanoma cell lines, particularly BRAF-mutant melanoma lines (Babiker et al., 2018, Byron et al., 2012, Narita et al., 2014). Preclinical studies have demonstrated activity of E6201 in BRAF-mutated cancer xenografts,

including melanoma (Wu J, 2009). Also, a phase 1 trial (NCT00794781) testing E6201 in patients with advanced solid tumors shows evidence of clinical efficacy in metastatic melanoma patients, including patients with metastatic spread to the brain (Babiker et al., 2018, Tibes et al., 2018). Moreover, panRAF/MEK inhibitor combination may be a rational treatment strategy in melanoma, especially in patients with resistance to single agent MAPK inhibitors (Whittaker et al., 2015).

1.2 STATEMENT OF THE PROBLEM

Brain tumors, both primary and metastatic, are devastating and are associated with poor survival outcomes (Ostrom et al., 2017, Siegel et al., 2018). Even after diagnosis, the treatment options for brain tumors are limited and provide only modest benefits (Spagnolo et al., 2016, Stupp et al., 2005). Such a lack of success in developing effective therapies after decades of meticulous basic and translational research offers a major challenge to the scientific community. There is a critical unmet need to develop efficacious treatments that can improve the quality of life of patients with brain tumors. The chapters 2 and 3 describe various challenges that exist in the treatment of tumors in the brain, with drug delivery to the site of action being one major concern. Many of the enumerated challenges are relevant to both primary brain cancers such as glioblastoma and brain metastases in general. The treatment of tumors in the brain is impeded by at least three critical challenges: (a) early and accurate diagnosis of CNS malignancies, (b) overcoming therapeutic resistance due to brain microenvironment driven changes in genetic drivers and their expression, (c) drug delivery to achieve adequate concentrations of potent inhibitors at the site of action in the brain. The research work described in this dissertation is mainly focused on the drug delivery challenge.

Inadequate drug delivery across an intact BBB can limit efficacy in the treatment of brain tumors. T1-weighted magnetic resonance imaging (MRI) visualizes tumor regions with a disrupted BBB, represented by contrast enhancement. However, tumor cells in certain regions, particularly in infiltrative tumor sites and early low volume lesions, may be residing behind a functionally intact BBB, and thereby not only do they escape detection

by contrast-enhanced MRI but also are protected from therapies with poor permeability across the BBB (Sarkaria et al., 2018). The successful treatment of tumors in the brain with molecularly-targeted agents will depend on the ability of these therapies to permeate an intact BBB and reach the protected tumor cells, as any tumor cells that are left behind can lead to treatment failure and tumor relapse. A key mechanism that has been shown to limit the brain distribution of several anti-cancer agents is active efflux, particularly by P-glycoprotein (P-gp/Abcb1) and breast cancer resistance protein (Bcrp/Abcg2), at the BBB. Given this, examining the brain delivery of potent anti-cancer therapies and evaluating the role of active transporters expressed at the BBB in affecting drug delivery to target tumor cells in the brain is crucial to develop effective treatments for tumors in the brain.

1.3 STRUCTURE OF THE DISSERTATION

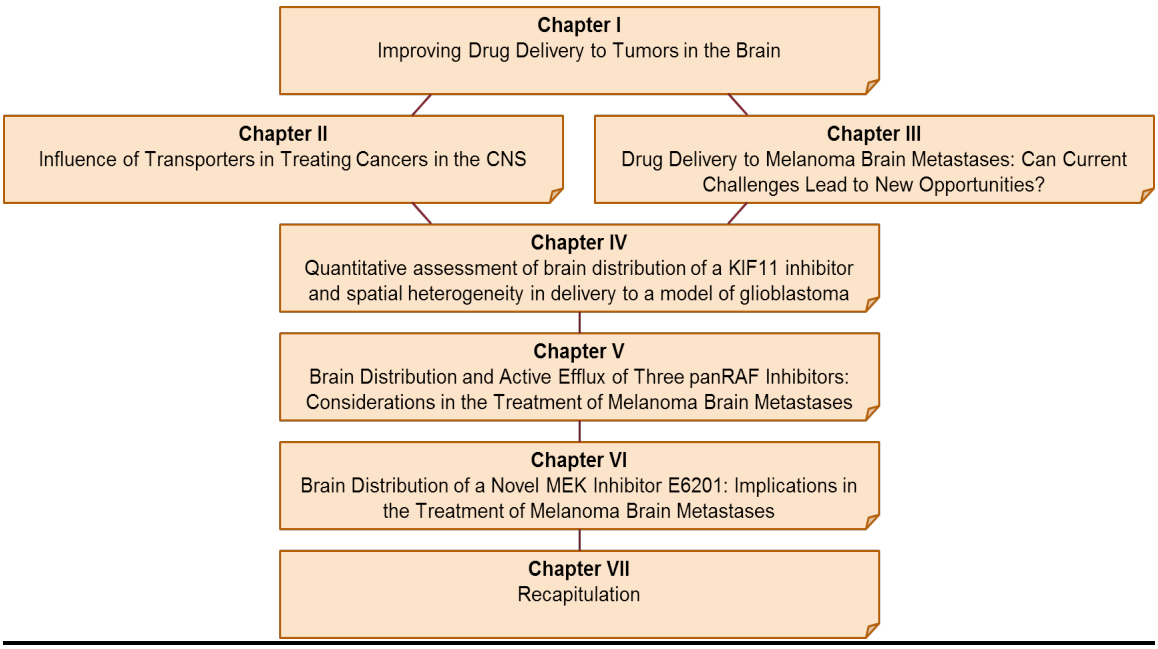

1.4 RESEARCH OBJECTIVES

The overall goal of this dissertation is to investigate the drug delivery challenges in the treatment of tumors in the brain, both primary and metastatic. The long term goal is to improve the quality of life of patients affected with brain tumors by contributing to the advancement of effective treatments through overcoming drug delivery limitations. The following research objectives were examined in this dissertation.

1) To evaluate the distribution of the KIF11 inhibitor ispinesib to the brain, and to regions in and around the tumor in a preclinical GBM model, and assess improvement in brain delivery by pharmacological inhibition of active efflux transporters (Chapter 4).

2) To compare the brain distribution profiles and in vitro efficacy of three panRAF inhibitors i.e., CCT196969, LY3009120 and MLN2480, and evaluate their potential utility in the treatment of brain metastases from melanoma (Chapter 5).

3) To examine the brain delivery of the MEK inhibitor E6201, assess distribution to intracranial tumors in a preclinical model, and understand the utility of E6201 in brain tumor treatment (Chapter 6).

These objectives are driven by the hypothesis that improving drug delivery to the protected tumor regions in the brain will enhance target engagement at the site of action and thereby efficacy.

1.5 RESEARCH PLAN

Chapter 4 is focused on examining the brain delivery of ispinesib and the mechanisms involved in limiting the brain distribution. Transgenic knockout mice that lack P-glycoprotein (P-gp/Abcb1) and/or breast cancer resistance protein (Bcrp/Abcg2) were used to investigate the role of active efflux transporters in affecting the brain delivery of ispinesib. In addition, distribution of ispinesib to regions of tumor core, tumor rim (brain adjacent to tumor, BAT) and normal (non-tumor) brain were determined in a preclinical rodent model of GBM. The effect of co-administration of elacridar, a pharmacological inhibitor of P-gp and Bcrp, as a strategy to enhance the brain delivery of ispinesib was also investigated. The predicted unbound concentrations of ispinesib in brain and plasma were compared with in vitro cytotoxic concentrations (IC_{50}) in GBM cell lines to understand the potential of ispinesib in the treatment of GBM.

Chapter 5 compares the brain delivery of three newly developed panRAF inhibitors, CCT1996969, LY3009120 and MLN2480. The role of active efflux transport at the BBB in influencing the brain distribution of these three compounds was examined using transgenic mice lacking P-gp and Bcrp. In vitro rapid equilibrium dialysis experiments were conducted to determine the unbound fractions in brain, plasma and serum-containing cell culture media, and the Kp,uu were determined for the three compounds. In vitro potency assays to determine the sensitivity of three patient derived melanoma cell lines (BRAF-mutant M12 and M27, NRAS-mutant M15) to treatment with the three panRAF inhibitors were performed and the most sensitive cell line (BRAF-mutant M12)

was selected for further correlations of in vivo unbound concentrations with the in vitro free IC_{50} estimates.

In Chapter 6, the brain distribution and influence of P-gp and/or Bcrp-mediated active efflux on affecting the delivery of E6201 across the BBB was investigated using mouse models. Moreover, spatial distribution of E6201 to tumor core, tumor rim and normal brain was evaluated in an intracranial patient-derived xenograft model (M12). A comparison of brain distribution of E6201 with the approved MEK inhibitors suggests that E6201 has a relatively favorable brain distribution profile. In vitro cytotoxicity assays indicate that BRAF-mutant M12 is most sensitive to E6201 treatment. A correlation of the unbound concentration-time profiles with in vitro free IC_{50} in BRAF-mutant M12 patient-derived melanoma cell line suggests possible activity in melanoma brain metastases.

TABLES

Table 1. 1 Some targeted agents implicated in the treatment of melanoma and GBM.

Targeted agent	Primary Target	Substrate status		Brain-to-plasma ratio, mice	Reference
		P-gp (ABCB1)	BCRP (ABCG2)		
Vemurafenib [a]	mutant BRAF	Yes	Yes	0.01	(Durmus et al., 2012, Mittapalli et al., 2012)
Dabrafenib [b]	mutant BRAF	Yes	Yes	0.04	(Mittapalli et al., 2013)
Encorafenib [c]	mutant BRAF	Yes	Yes	0.004	(Wang et al., 2018)
Trametinib [d]	MEK	Yes	No	0.15	(Vaidhyanathan et al., 2014)
Cobimetinib [e]	MEK	Yes	No	0.08	(Choo et al., 2014)
Omipalisib[a]	PI3k/mTOR	Yes	Yes	0.06	(Vaidhyanathan et al., 2016)
GDC-0980 [e]	PI3k/mTOR	Yes	Yes	0.08	(Salphati; Pang; et al., 2012)
Palbociclib [a]	CDK4/6	Yes	Yes	0.2	(de Gooijer et al., 2015, Parrish; Pokorny; et al., 2015)
Abemaciclib [d]	CDK4/6	Yes	Yes	0.21	(Raub et al., 2015)
Dasatinib [d]	BCR-Abl, EGFR	Yes	Yes	0.12	(Agarwal et al., 2013)
Lapatinib [a]	EGFR	Yes	Yes	0.03	(Polli et al., 2009)

[a] Steady state brain to plasma concentration ratios

[b] Brain to plasma ratio of AUC_{0-4} post oral dose

[c] Brain to plasma ratio of concentrations one hour post oral dose

[d] Brain to plasma ratio of $AUC_{0-tlast}$ post intravenous dose

[e] Brain to plasma ratio of concentrations one hour post oral dose

Table 1. 2 Physico-chemical properties of ispinesib, panRAF inhibitors and E6201.

	Ispinesib	**CCT196969**	**LY3009120**	**MLN2480**	**E6201**
Structure	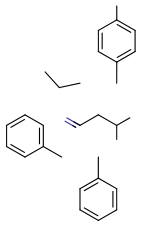	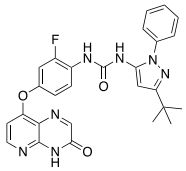	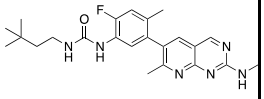	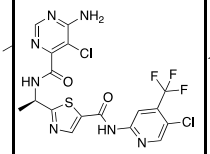	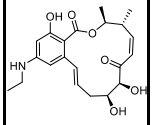
Molecular formula	$C_{30}H_{33}ClN_4O_2$	$C_{27}H_{24}FN_7O_3$	$C_{23}H_{29}FN_6O$	$C_{17}H_{12}ClF_3N_2O_3S$	$C_{21}H_{27}NO_6$
Molecular weight (g/mol)	517.07	513.53	424.52	506.29	389.45
Solubility	< 1mg/mL	< 1mg/mL	< 1mg/mL	< 1mg/mL	< 1mg/mL
logP	5.5	5.5	4.2	3	2.92
logD (pH 7.4)	3.2	5.5	4.2	3	2.92
pKa[1]	na	10.36	11.61	10.29	9.86
TPSA (A^2)	79	123	92	136	116
HBD count	1	3	3	3	4
Rotatable bond count	9	6	6	6	2

The reported properties were calculated using ChemAxon (http://www.chemicalize.com).

[1] The values represent strongest acidic pKa reported by ChemAxon

na, Not available

TPSA, Topological polar surface area

HBD, Hydrogen bond donor

FIGURES

Figure 1. 1 A schematic showing that inhibition of KIF11 hits both tumor cell proliferation and invasion, the characteristic hallmarks of GBM. GBMs are brain tumors with high proliferation index, and targeted inhibition of KIF11 using potent inhibitors such as ispinesib may be a suitable treatment strategy.

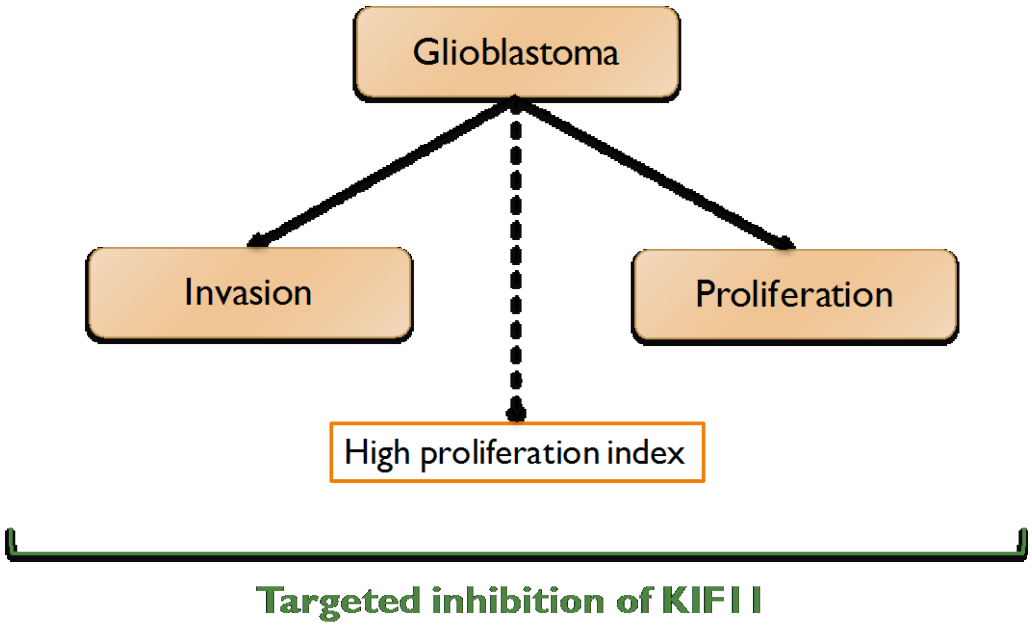

Figure 1. 2 A schematic representing the MAPK signaling cascade, and targets of approved BRAF inhibitors, approved MEK inhibitors, panRAF inhibitors and E6201.

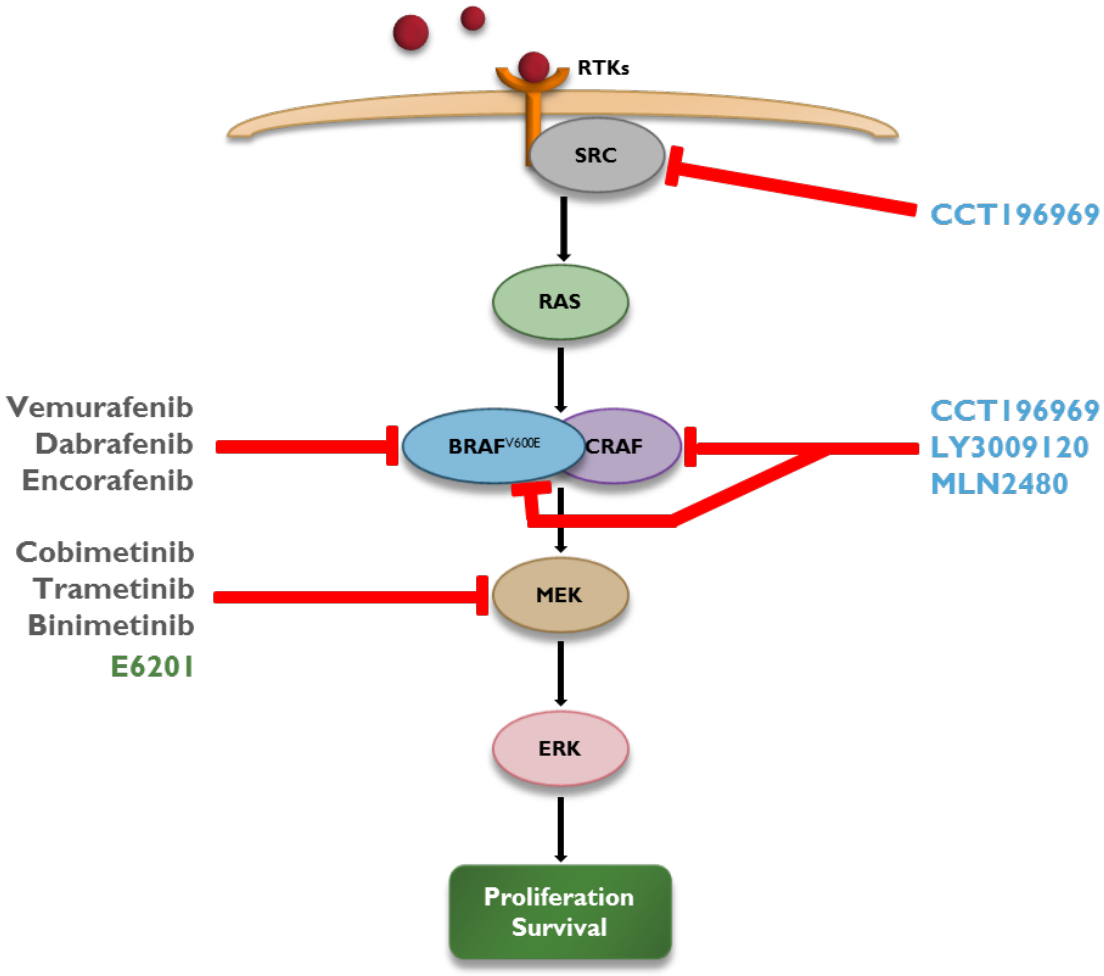

CHAPTER II. INFLUENCE OF TRANSPORTERS IN TREATING CANCERS IN THE CNS

ABSTRACT

Brain tumors are difficult to treat, in part, due to lack of adequate drug delivery across the blood-brain barrier (BBB). Although the BBB is compromised to some degree in brain tumors, it is not uniformly disrupted and some tumor locations have a relatively intact BBB. The presence of transporters (efflux) at the BBB limits the brain distribution of therapeutics intended for treatment of CNS disorders. The differences in clearance processes, arising due to differences in transporter expression and orientation in BBB vs BCSFB (blood-CSF barrier), make it complex to understand the specific influence of transporters on CNS drug delivery, and also limit the use of CSF as a surrogate for unbound brain concentrations. Several opportunities to overcome the transporter-based barrier exist and it is important to recognize that solving the drug delivery problem will open many new doors for targeted therapies to be efficacious in treatment of brain tumors.

2.1 INTRODUCTION

Over 23,000 new cases of cancers of the brain and other nervous system are expected in the year 2017 in the United States, accounting for 1.4% of all cancer patients (Siegel et al., 2017). Glioblastoma (GBM) is the third most common primary CNS tumor (14.9% of primary brain and other CNS tumors), and the most common primary malignant tumor (47.1% of primary malignant brain tumors) (Ostrom et al., 2017). The incidence of brain metastases is much higher than primary brain tumors, and is observed in 8.5-9.6% of cancer patients (Barnholtz-Sloan et al., 2004, Nayak et al., 2012, Kromer et al., 2017). Patients with lung cancer, breast cancer and melanoma exhibit the highest occurrence of brain metastases, and combined together they account for up to 75% of adult brain metastases (Nayak et al., 2012, Gallego Perez-Larraya and Hildebrand, 2014). While lung cancer accounts for the highest incidence proportion of brain metastases, melanoma has the highest propensity to metastasize to the brain (Nayak et al., 2012).

Tumors in the brain can lead to poor quality of life in affected patients (Stupp et al., 2005, Fokas et al., 2013, Bohn et al., 2016). Brain tumors are often difficult to diagnose, especially early in the disease progression (Bruzzone et al., 2012), and even after diagnosis, it is challenging to effectively treat them. The removal of tumors by surgical resection can be limited by its location, and even when the site allows for such a procedure, low-volume lesions can make resection less feasible (Patchell et al., 1990, Fife et al., 2004). Also, finding effective systemic therapies that adequately penetrate an intact blood-brain barrier (BBB), and reach the target tumor cells residing in the brain to elicit meaningful responses has proven to be extremely challenging (Agarwal; Sane; et al.,

2011, Gampa et al., 2017). As new systemic therapies continue to improve the management of extracerebral tumors, and if these therapies do not penetrate the BBB effectively, the incidence of brain tumors will continue to increase (Gallego Perez-Larraya and Hildebrand, 2014).

While the BBB/brain-tumor barrier (BTB) may be compromised in some regions of the tumors, it is critical to recognize that the BBB can be intact and fully functional in some regions of brain that contain tumor cells, especially in early non-contrast enhancing tumors, leading to restricted BBB penetration of anti-cancer agents (Essig et al., 2006, Jain et al., 2007, Lockman et al., 2010, Osswald et al., 2016, Sarkaria et al., 2018). Many small molecule anti-cancer targeted agents are substrates of active efflux transporters at the BBB, and so their brain penetration can be severely limited (Agarwal; Sane; et al., 2011, Gampa; Vaidhyanathan; Resman; et al., 2016, Gampa et al., 2017). Thus, it is crucial that future drug discovery endeavors focus on specifically designing anti-cancer agents capable of penetrating an intact BBB, to achieve effective treatment of brain tumors. Also, there have been reports indicating the expression of efflux transporters on the tumor cells that form a secondary barrier to drug delivery (Agarwal; Sane; et al., 2011). Given such dynamic complexities, understanding the role of transporters in affecting drug distribution to target tumor cells in the brain is critical to develop efficacious therapies. This chapter will discuss different aspects related to the influence of transport systems at the BBB on the treatment of cancers in the CNS.

2.2 TRANSPORTERS IN THE BRAIN BARRIERS AND CANCER CELLS

Multiple barriers, both physical and physiological, restrict the distribution of various substances into the CNS, and help maintain the precise homeostasis required for normal, healthy brain functions (Davson and Segal, 1995, Abbott, 2013). The capillaries in the brain are composed of endothelial cells held together in close proximity by tight junctions, and are surrounded by extracellular matrix components, pericytes, and astrocyte foot processes that collectively form the BBB or the neurovascular unit (NVU) (Abbott, 2013) (Figure 1). This dynamic structure restricts the paracellular movement of molecules in to the brain, and is also associated with multiple transport systems, both influx and efflux, that regulate the trafficking of molecules via transcellular route at the BBB, thereby limiting the passage of ionized, hydrophilic solutes, and large molecules (Taylor, 2002, Begley, 2004, Loscher and Potschka, 2005).

Transport proteins at the BBB play an important role in the uptake and efflux of many therapeutic agents (Agarwal; Sane; et al., 2011, Gampa et al., 2017). Influx transporters like amino acid transporters, hexose transport system and organic anion transporting polypeptides (OATPs) are primarily involved in transport of nutrients, peptides and large molecules, but fewer small-molecule targeted agents are substrates of influx transporters (Sun et al., 2003, Tamai and Tsuji, 2000, Stieger and Hagenbuch, 2014). However, a majority of small-molecule targeted agents are substrates for active efflux transporters, belonging to the ATP binding cassette (ABC) family of proteins, expressed at the BBB (Begley, 2004). P-glycoprotein (P-gp, also known as ABCB1/MDR1), multi-drug resistance associated proteins (MRPs/ABCC) and breast cancer resistant protein

(BCRP/ABCG2) are key efflux transport proteins responsible for extruding many toxins and xenobiotics, including drugs intended for the treatment of CNS disorders, out of the brain (Agarwal; Sane; et al., 2011). Multiple studies have shown that the brain distribution of various anti-cancer targeted therapies is limited by active efflux at the BBB (Agarwal; Sane; et al., 2011, Gampa et al., 2017).

There exist certain differences in the localization and expression of efflux transporters in different regions of the CNS. One important difference is the localization of P-gp. P-gp is expressed on the luminal side of the BBB to perform the function of moving substrates into the blood, while it is located on the CSF facing side of the BCSFB (blood-cerebrospinal fluid barrier), and thereby pumps substrates into the CSF (Rao et al., 1999, Ronaldson et al., 2004, Gazzin et al., 2008). No such variability in localization of MRP1 has been reported at the BBB compared to BCSFB, with MRP1 facing the blood in both the barriers (Ronaldson et al., 2004, Gazzin et al., 2008). Also, the expression of P-gp is higher in the microvasculature i.e., the BBB, whereas that of MRP1 is more pronounced in the choroid plexus representing the BCSFB, suggesting a more prominent neuroprotective role of P-gp in the brain (Gazzin et al., 2008). Understanding such intricacies in transporter expression and localization is critical in evaluating the CNS distribution of drugs, and also determining the influence of transport proteins on the CNS drug exposure.

The expression of efflux transporters has also been observed at the tumor cell level, a secondary barrier to drug delivery, which can confer multi-drug resistance to cancer cells (Loscher and Potschka, 2005, Szakacs et al., 2006, Dean et al., 2005). Efflux pumps at

the tumor cell level act as a sequential barrier along with BBB, and further protect the tumor cells in the brain (Loscher and Potschka, 2005, Lin et al., 2014, Luo et al., 2012). Drug efflux transporters including P-gp, BCRP, and some MRPs have been observed to be expressed at the tumor cell level, in both primary and metastatic brain tumors (Szakacs et al., 2006, Lin et al., 2014, Fattori et al., 2007, Demeule et al., 2001, Zhou et al., 2001, Bleau et al., 2009, Calatozzolo et al., 2005, Luo et al., 2012, Pajic et al., 2009). Even low levels of P-gp and MRP1 expression has been reported to considerably affect tumor sensitivity to drugs that are substrates of efflux proteins (Regina et al., 2001). A review of the literature suggests a differential expression of these transporters in different types of brain tumors. Reports suggest that the expression of P-gp in most primary brain tumors was similar to that of normal brain, whereas P-gp expression was much lower in metastatic brain tumors from lung adenocarcinomas and melanomas (Regina et al., 2001). Also, expression of P-gp in brain metastases from lung adenocarcinomas was similar to that in primary tumors, suggesting the expression to be somewhat a reflection of the tissue of tumor origin (Regina et al., 2001).

Matsumoto et al, studied P-gp expression in 5 glioma cell lines (GB-1, U-373 MG, T98G, A-172, U-87 MG), of which one human glioblastoma-derived cell line (GB-1) showed high expression of P-gp and was resistant to vincristine, doxorubicin and etoposide, whereas, P-gp was not observed in the other four glioma lines that were sensitive to these drugs, indicating the important role of P-gp in multi-drug resistance and efficacy (Matsumoto et al., 1991). Similarly, expression of MRP1 and BCRP in glioma cells has also been reported to play a role in therapeutic resistance (Emery et al., 2017, Zhou et al.,

2001). Multi-drug resistance due to expression of efflux transporters has also been reported in metastatic tumor cells, with primary origin outside the brain. For instance, preclinical studies have reported the expression of P-gp in brain metastases of breast cancer (Pajic et al., 2009). Human melanoma cells have also been observed to express P-gp in multiple studies (Frank et al., 2005, Chen et al., 2009, Luo et al., 2012).

While efflux transporters are inherently expressed in some cancers, they can also be upregulated upon exposure of tumor cells to anti-cancer agents, thereby leading to acquired resistance to treatment (Loscher and Potschka, 2005). For instance, a study observed that the exposure of U87 and T98G glioblastoma cells to temozolomide promoted the production of epidermal growth factor (EGF), which in turn induced the intracellular trafficking of P-gp to the cell membrane, as well as a conformational change in the inactive form of the transmembrane transporter into the active form, ultimately leading to the development of acquired resistance to therapy (Munoz et al., 2014). This shows the essential role transporters can play, in conferring multi-drug resistance to tumors. The existence of essentially two transport barriers, the BBB and tumor cell barrier, can severely restrict the delivery of anti-cancer agents to target tumor cells residing in the brain. Therefore, it is crucial to devise approaches that help in overcoming these barriers for achieving improved treatment outcomes.

2.3 DRUG PHARMACOKINETICS IN THE CNS

The complex architecture of CNS necessitates a careful application of pharmacokinetic principles in the determination of drug distribution to the CNS. The purpose of this section is to guide the reader in gaining an understanding of certain important concepts related to the neuro-pharmacokinetics of a drug intended for use in the management of CNS diseases.

2.3.1 Targeted bioavailability

The drug concentrations in blood or plasma are routinely measured as surrogates for concentrations at the site of action, due to ease of accessibility. While drug concentration in systemic circulation may somewhat reflect the concentration at the site of action when the target is in a peripheral, more accessible, tissue, their use as a surrogate for brain drug concentrations can be misleading. This is important particularly in the context of brain compared to other organs due to presence of the BBB that can severely restrict drug distribution to the brain (Agarwal; Sane; et al., 2011, Gampa et al., 2017). To differentiate the bioavailability estimated using drug concentrations at the site of action, brain in this discussion, from the traditional bioavailability determined using the systemic concentrations, we would like to use the term 'targeted bioavailability' (Elmquist, 2005) (Figure 2). Various factors can influence a compound's targeted bioavailability in the brain such as BBB permeability, drug transport by transport proteins, drug metabolism, protein binding, protein expression, receptor affinity, gene regulation and dosage regimen (Elmquist, 2005). The findings from various studies testing different anti-cancer agents indicate that the concentrations of a drug in the brain can be remarkably different from

systemic concentrations (Agarwal; Sane; et al., 2011, Pitz et al., 2011, Gampa et al., 2017). The relevance of concentration-effect relationship should be judiciously assessed when using systemic concentrations, as the variability in pharmacodynamic measurements (i.e., drug response, and toxicity) may not be reflected by the variability observed in the pharmacokinetic measurements (Elmquist, 2005). Therefore, the measurement of target site concentrations, when possible, is more appropriate to evaluate a pharmacokinetic-pharmacodynamic (PK-PD) relationship.

2.3.2 Route of drug administration

Various drugs administered via systemic routes fail to achieve efficacious concentrations at the target site in the brain due to restricted penetration cross the BBB. In an effort to overcome such delivery issues, local drug administration directly in to the CNS has been employed. The advantage of local drug delivery is precise targeting to the site of action in the brain, which in turn can reduce the dose of drug needed and thus lessen untoward off-target side effects. However, they are often invasive, expensive and have potential for ill effects such as infection and surgical complications. Local delivery methods include intracranial delivery via intrathecal, epidural, intraventricular, intraparenchymal routes, and spinal drug delivery. Intrathecal and epidural routes are more commonly employed in clinic (mainly for chronic pain management), while the other intracranial routes are used less frequently (Xing et al., 2018). In the recent years, many efforts have been directed towards nasal drug delivery for CNS targeting. While the nasal route has the advantage of being a non-invasive method capable of bypassing the BBB, it has the disadvantages of variable drug exposure and dosing volume limitation (Khan et al., 2017). Some other

local delivery methods include convection-enhanced delivery (CED), polymeric bio-degradable wafers, and intrathecal implantable pumps (Bregy et al., 2013, Bottros and Christo, 2014).

2.3.3 Drug distribution

A prerequisite for efficacy is the exposure of target to adequate drug concentrations that are necessary for target engagement, and thereby achieve the desired responses. Early drug discovery programs should incorporate this important idea and optimize drug pharmacokinetics with emphasis on improving unbound rather than total drug concentrations in the CNS (Heffron, 2018). The CNS distribution of a compound relates to both the rate and extent of drug penetration into the CNS, and it is essential to delineate the rate from the extent of drug distribution (Hammarlund-Udenaes et al., 2008).

The rate of transport describes the speed of movement of a drug across the BBB, and is estimated using the permeability-surface area product (PS) or the influx clearance (Kin, CLin) (Hammarlund-Udenaes et al., 2008). The permeability depends on both membrane properties and physicochemical characteristics of a molecule. The mechanisms of drug transfer across the BBB include passive diffusion, carrier-mediated uptake in to the brain, adsorptive or receptor-mediated transcytosis, and active efflux by transporters out of the brain (Reichel, 2015). The techniques commonly employed for measuring influx include the brain uptake index (BUI), in-situ brain perfusion technique, intravenous injection method and microdialysis (Bickel, 2005). Typically, the rate of CNS penetration approaches the cerebral blood flow for compounds with high BBB permeability, and is

limited by the net influx clearance for compounds with low BBB permeability (Reichel, 2015). Although the time to equilibrium between blood and brain is delayed for compounds with low permeability, the equilibrium itself remains unaffected.

The extent of drug delivery is more relevant to drug activity within the CNS, as most drugs are administered on a continuous (multiple dosing) basis. Traditionally, the extent of CNS penetration has been expressed as brain-to-plasma ratio (Kp) that is defined as the total AUC in brain normalized by the total AUC in plasma. Though Kp provides useful information, one has to recognize the composite nature of this metric i.e., it depends on non-specific binding of drug in brain, non-specific drug binding to plasma components, and the more specific drug transport across the BBB (Hammarlund-Udenaes et al., 2008) (Figure 3). Given that many CNS drugs are lipophilic, non-specific binding in brain can have a major contribution to Kp, thereby masking the true drug transport attributes. Attempts to improve brain penetration by increasing Kp may not result in better efficacy, since it is often accomplished by making drugs more lipophilic which leads to higher binding in the brain, but not necessarily to an increase in unbound drug concentrations required to improve target engagement (Reichel, 2015).

The unbound partition coefficient, referred to as Kp,uu, is an unbiased measure of the extent of brain penetration of free drug. It reflects the true transport equilibrium across the BBB, and is not confounded by non-specific binding (Hammarlund-Udenaes et al., 2008) (Figure 3). The estimation of Kp,uu uses the unbound fraction in plasma (fu,plasma), and the unbound fraction in brain (fu,brain), along with the Kp.

$$Kp = \frac{AUCbrain}{AUCplasma}$$

$$Kp,uu = \frac{AUCbrain}{AUCplasma}\ x\ \frac{fu,brain}{fu,plasma}$$

According to the free drug hypothesis, it is the unbound drug that is available to interact with the target and elicit pharmacological activity (Smith et al., 2010, Rankovic, 2015). While the Kp of drugs can be in a 2000-fold range, the range of Kp,uu is typically much smaller, between 0.02 and 3, i.e., a 150 fold difference, which demonstrates the influence of non-specific drug binding on Kp (Hammarlund-Udenaes et al., 2008, Loryan et al., 2014). Therefore, replacing Kp with Kp,uu as a measure of the extent of CNS penetration is more appropriate (Hammarlund-Udenaes et al., 2008, Liu et al., 2008, Di et al., 2013, Rankovic, 2015, Heffron, 2018). Table 1 shows the brain distribution of some molecularly-targeted agents that have been examined for the treatment of brain tumors.

Also, thinking about Kp,uu with respect to the actual clearance mechanisms provides a mechanistic understanding of the meaning of Kp,uu (Hammarlund-Udenaes et al., 2008, Liu et al., 2008).

$$Kp,uu = \frac{CLin}{CLout} = \frac{CLps + CLuptake}{CLps + CLefflux + CLelim}$$

In the equation above, CL in represents the summation of all clearances into the brain, CLout denotes the summation of all clearances out of the brain, CLps refers to the passive diffusional clearance across the BBB, CLuptake relates to active uptake in to the brain, CLefflux relates to transport mediated efflux out of the brain, and CLelim relates to drug elimination from the brain, both by metabolism and bulk flow into CSF. A Kp,uu

around unity suggests passive diffusion to be the main driving force with no uptake and efflux processes in place or uptake balancing efflux, while a Kp,uu less than unity suggests active efflux process to be dominant, and a Kp,uu significantly greater than unity suggests active uptake process to be dominant (Hammarlund-Udenaes et al., 2008, Di et al., 2013). The proportion of CNS drugs with a Kp,uu of unity or higher has been relatively small. Many drugs have been shown to have low Kp,uu values as they are liable to efflux at the BBB, and the limited delivery of such drugs to target sites in the brain can severely impact the responses achieved.

Also, a combination of influx and efflux processes may play a crucial role in dictating the pharmacokinetic profile of a drug. Fexofenadine, an anti-histamine agent, is a substrate of P-gp. The expectation is that upon co-administration with grapefruit juice (GFJ), there will be an increase in oral bioavailability of fexofenadine due to P-gp inhibition by GFJ in gut. However, studies show that upon co-administration with GFJ the oral bioavailability of fexofenadine decreased. GFJ is an inhibitor of both OATPs and P-gp. Therefore, the eventual extent of absorption of fexofenadine depends on the relative degree of inhibition of OATPs and P-gp, as fexofenadine is liable to both influx by OATPs and efflux by P-gp. It is likely that the effect of GFJ on OATPs is more pronounced than on enteric P-gp, causing reduced bioavailability of oral fexofenadine (Hanley et al., 2011, Pasko et al., 2017). Talinolol and celiprolol also exhibit similar drug-food interaction with GFJ (Hanley et al., 2011). A similar interplay of influx and efflux transporters is possible at the BBB, which may ultimately determine the brain exposure of drugs that are substrates of both influx and efflux transporters.

2.3.4 CSF vs brain exposures

Cerebrospinal fluid (CSF) is considered to be essentially free of drug protein binding, as the protein concentrations are very low in CSF compared to plasma. Given this, the concentrations measured in CSF are often considered to serve as unbound drug concentrations (Bonati et al., 1982). The use of CSF concentration as a surrogate for unbound drug concentration in the brain is not always appropriate, and can be misleading because of differences in BBB and BCSFB properties (Shen et al., 2004, Westerhout et al., 2011, de Lange, 2013, Di et al., 2013, Pardridge, 2016, Jacus et al., 2016). Figure 4 depicts the blood, brain and CSF compartments, and the drug distribution processes occurring between them. CSF may be a good surrogate for unbound brain concentrations with compounds that freely diffuse across these barriers to achieve a rapid distributional equilibrium (Kpuu ~ 1) between brain or CSF, and plasma (Lin, 2008, Di et al., 2013). However, unbound plasma concentration can be used as a surrogate for unbound brain concentration with compounds that achieve such a distributional equilibrium, thereby providing no additional value with CSF measurement (Di et al., 2013). Also, CSF is not a well-stirred compartment and depending on the site/time of sampling, body posture or route of drug administration, the drug concentrations in CSF are expected to vary significantly (Rong, 2012, Di et al., 2013). It is thus advisable to use CSF drug concentrations in combination with corresponding plasma unbound concentrations to better estimate the unbound brain concentration even for drugs that are not substrates of transport proteins (Di et al., 2013).

For compounds that are transporter substrates, CSF concentration is not an accurate substitute for unbound brain concentration. The BCSFB and the BBB differ both anatomically and physiologically, including the localization and function of transporters (Gazzin et al., 2008, Westerhout et al., 2011, Rong, 2012). For instance, P-gp substrates are pumped into CSF from blood at the BCSFB, as opposed to efflux into blood at the BBB, and consequently the CSF concentration of a drug that is a P-gp substrate tends to overestimate unbound concentration in the brain, misinforming the drug development process (Rao et al., 1999, Gazzin et al., 2008, Lin, 2008, Keep and Smith, 2011) (Figure 4). Preclinical and clinical studies have shown the unbound drug concentrations in CSF to be higher than in brain ECF under steady-state conditions (Rambeck et al., 2006, Kodaira et al., 2011, de Lange, 2013, Huang et al., 2015). Consequently, it is difficult to reliably predict brain unbound concentrations even with access to CSF concentration data for many compounds.

A limitation in the clinical phase of drug development process for CNS drugs is the lack of access to direct measurement of brain ECF concentrations. Techniques such as intracerebral microdialysis and PET imaging can provide useful information; however, ethical considerations of employing an invasive technique in healthy volunteers often limits direct measurement of brain ECF unbound drug concentrations (Lin, 2008). Also, such procedures are laborious and are low-throughput. On the other hand, sampling CSF from the lumbar region is relatively simple, and thus use of CSF concentrations as surrogate for unbound drug concentration in the brain is appealing in early drug

development endeavors (Lin, 2008, de Lange, 2013). Nonetheless, the utility of CSF concentrations to predict target site concentrations in the brain is often questionable.

Intracerebral microdialysis has been proposed as a tool for assessing drug disposition to brain, as it can allow measurement of unbound drug concentrations near the site of action in the brain. Microdialysis probes may also be used to deliver drugs, and simultaneous monitor pharmacodynamic response to therapy (Elmquist and Sawchuk, 1997, Benjamin et al., 2004, Goodman, 2011). Also, the measurement of drug concentrations at multiple locations in the brain can be accomplished by placement of more than one catheter at a given time. The results of a microdialysis study in four GBM patients to assess the distribution of p-boronophenylalanine (BPA) into normal brain, tumor and brain around tumor showed lower BPA distribution to normal brain compared to tumor and brain around tumor regions, within the same patient (Bergenheim et al., 2005). Another clinical study was performed in patients with recurrent high-grade gliomas, where catheters were placed during surgery to measure methotrexate concentrations in either contrast enhancing or non-enhancing tumor tissue (Blakeley et al., 2009). The results show variable distribution of methotrexate, with high concentrations in contrast enhancing and lowest concentrations in non-contrast enhancing tumor regions. These results provide clinical evidence of variability in drug distribution to different regions of brain tumors, suggesting heterogeneity in BBB permeability in brain tumors.

Although intracerebral microdialysis can provide useful information on the tissue pharmacokinetics, it has several limitations. It is a laborious and invasive technique requiring hospitalization of patients. The placement of catheter cannot only lead to

complications like infection or hemorrhage, but can also disrupt the BBB due to trauma, thereby overestimating drug distributional kinetics to the brain (Groothuis et al., 1998, Blakeley and Portnow, 2010). Another disadvantage is the adsorption of macromolecules from the surrounding interstitium to the probe membrane and gliosis, which can decrease permeability and reduce recovery (Benjamin et al., 2004). The catheter placement into regions of interest is often challenging, and a skilled team is needed to execute the study with minimal errors (Blakeley and Portnow, 2010, Liu et al., 2014). The technique requires careful catheter calibration and sensitive analytical methods to detect drug concentrations. Also, this technique is not amenable to many drugs including those with high lipophilicity or high molecular weight or high protein binding (Blakeley and Portnow, 2010). Given these shortcomings, the use of intracerebral microdialysis as a routine technique for screening the neuro-pharmacokinetics of drugs is less appealing.

2.4 STRATEGIES TO OVERCOME TRANSPORT BARRIERS

The delivery of adequate concentrations of anti-cancer targeted therapies to tumor cells residing in the brain has proven to be a significant challenge. Various approaches to overcome the delivery barrier have been considered, some of which are briefly described in this section (Figure 5).

2.4.1 Structural modification for CNS delivery

Designing drug molecules that are capable of crossing the BBB to attain optimal concentrations in the brain should be a priority for CNS drug discovery programs. This can be achieved by identification of key physicochemical properties that aid in BBB penetration, followed by rational structural modifications to impart such properties in the molecules intended for use as CNS therapeutics. In this direction, critical physicochemical properties have been studied, and computational models developed to optimize key attributes necessary for successful brain delivery (Rankovic, 2015, Heffron, 2016). Wager et. al., have developed a multi-parameter optimization (MPO) approach to screen molecules for optimal neuro-pharmacokinetic and safety profiles. The key physicochemical properties used/desired were: (a) lipophilicity, partition coefficient (ClogP) ≤ 3 being desirable; (b) distribution coefficient (ClogD) with a desirable value ≤ 2; (c) molecular weight (MW) with a desirable value ≤ 360; (d) topological polar surface area (tPSA) with a desirable value between 40-90; (e) number of hydrogen bond donors (HBD) with a desirable value ≤ 0.5; (f) most basic center of the molecule (pKa) with a desirable value ≤ 8 (Wager et al., 2010). Each of the six properties were equally weighted with a desirability score between 0-1, with final CNS MPO score ranging from 0-6,

allowing multiple ways to achieve a particular score depending on the property optimized. Application to 119 marketed CNS drugs validated the utility of the algorithm with 74% drugs showing high CNS MPO scores. These drugs also displayed desirable ADME properties like high permeability, low P-gp efflux liability, and higher stability (Wager et al., 2010).

The use of CNS MPO score approach on a set of thienopyrimidine molecules and screening for a score greater than 4.5 has led to the identification of brain penetrant PI3K inhibitors, GNE-317 and GDC-0084, that showed significantly greater tumor growth inhibition in GBM mouse models as compared to BBB impenetrant PI3K inhibitors (Sutherlin et al., 2010, Salphati; Heffron; et al., 2012, Osswald et al., 2016) (Figure 6). Another example is AZD3759, a potent brain penetrant EGFR inhibitor, which was developed using gefitinib as the initial lead. Techniques like repositioning of fluoro moiety and reduction of rotatable side chain were employed for overcoming P-gp and BCRP efflux to improve brain penetration, while maintaining the quinazoline scaffold necessary for activity (Zeng et al., 2015). One more example is the structural modification of crizotinib, an ALK inhibitor, leading to the development of BBB penetrant lorlatinib (PF-06463922). Cyclization of crizotinib to form the macrocyclic lorlatinib led to a reduction in the effective HBDs and rotatable bond count, thereby decreasing its interaction with efflux transporters and improving CNS distribution (Johnson et al., 2014, Basit et al., 2017). These examples demonstrate that utilization of structure-guided drug design early in CNS drug discovery programs, can aid in the development of brain penetrant drugs.

2.4.2 Transporter modulation

As a strategy to overcome transporter-mediated drug delivery limitations, inhibition of transporters, particularly P-gp and BCRP, has been investigated (Baumert and Hilgeroth, 2009). The first generation inhibitors comprised of marketed drugs known to inhibit efflux transporters include drugs such as verapamil, cyclosporine-A, and quinidine (Tsuruo et al., 1981, Slater et al., 1986). However, these inhibitors have low potency and selectivity, and require high doses (Benson et al., 1985, Verweij et al., 1991). An analog of cyclosporine-A, valspodar (PSC-833), was developed as a second generation inhibitor with more potent inhibition of P-gp, but it interfered with cytochrome P450 function (Twentyman and Bleehen, 1991). As a consequence, third generation inhibitors including tariquidar, elacridar, and zosuquidar, were developed (Roe et al., 1999, Hyafil et al., 1993, Dantzig et al., 1996). Although co-administration of tariquidar improved the brain exposure of targeted agents and corresponding efficacy without any toxicity concerns in preclinical studies, two phase III clinical trials in non-small cell lung cancer (NSCLC) patients have been terminated early due to toxicity when used in combination with paclitaxel/carboplatin or vinorelbine (Fox and Bates, 2007). Similarly, toxicity concerns were reported in clinical studies investigating the use of zosuquidar and elacridar (Rubin et al., 2002, Sandler et al., 2004, Kuppens et al., 2007). Co-administration of probenecid, an inhibitor of organic anion transporter (OAT), was shown to increase the brain concentration of bumetanide in mice, but its clinical use to improve brain penetration of a drug was found to be limited (Tollner et al., 2015, Kenneth, 1969).

To date, there is no specifically designed inhibitor of efflux transporters that is approved by either the FDA or European regulatory agencies. The lack of success in achieving clinically relevant drug-drug interactions at the BBB to improve brain delivery of CNS therapeutics has been attributed to the following reasons: (a) the increase in drug exposure due to drug-drug interactions is much lower than expected (Zamek-Gliszczynski et al., 2009) (b) achieving systemic concentrations of inhibitor required to saturate efflux transporters at the BBB is often challenging (Kalvass et al., 2013) (c) the toxicity potential due to drug-drug interactions at the BBB is another important concern for clinical implementation of this strategy (Kalvass et al., 2013, Kuppens et al., 2007, Fox and Bates, 2007, Rubin et al., 2002, Sandler et al., 2004).

Another means of transporter modulation is to alter transporter expression, which has been observed in situations like pathological conditions, xenobiotic exposures, stress, and inflammation (Miller, 2010). The approaches considered are mainly based on RNA interference technology that trigger gene silencing by using small interfering RNA (siRNA), short hairpin RNA (shRNA), or microRNA (Widmer et al., 2007, Gu et al., 2015, Zhu et al., 2008). An increase in intracellular drug concentrations in drug-resistant tumor cells has been observed by using such approaches (Widmer et al., 2007). Also, some compounds such as cantharidin and metformin have been shown to inhibit the expression of P-gp, but their clinical application as transporter modulators has not been investigated (Zheng et al., 2008, Kim et al., 2011). Given that modulation of transporter expression occurs in a non-specific manner and is more complex than transient transporter inhibition, it is crucial to develop precise techniques for site-targeted down-

regulation of specific efflux transporters, so that the drug concentrations and related efficacy can be better predicted.

2.4.3 Tight Junction Modification

A selective disruption of the BBB followed by administration of anti-cancer agents provides for a promising approach to enhance drug delivery to the brain in the treatment of brain tumors (Madsen et al., 2010). Various techniques have been employed to cause transient BBB disruption as briefly discussed below.

Osmotic disruption of the BBB:

The administration of hypertonic solutions causes disruption of the BBB due to shrinkage of endothelial cells and opening up of tight junctions between them, thereby allowing paracellular movement of drugs (Kemper et al., 2004). The transient BBB disruption followed by administration of anti-cancer agents has been employed as a strategy to overcome brain drug delivery limitations (Neuwelt et al., 1980, Kroll et al., 1998). However, this approach is invasive, complex to perform and is associated with toxic side effects (Madsen et al., 2010).

Focused Ultrasound:

Focused Ultrasound (FUS) is based on the concentration of acoustic energy onto a focal spot that results in BBB disruption. However, reliable BBB opening without damage to normal brain has not yet been confirmed (Madsen et al., 2010, Poon et al., 2017). Microbubble (MB) enhanced FUS involves oscillation of MBs in the presence of FUS to cause BBB disruption (Hynynen et al., 2006). This approach has demonstrated improvements in delivery and efficacy of anti-cancer agents in glioma models (Oberoi et

al., 2016). Also, significant downregulation of localized P-gp expression with no apparent damage to brain endothelial cells was observed, suggesting the potential use of MB-FUS for targeted brain delivery of drugs that are liable to efflux by P-gp (Cho et al., 2016, Mcmahon et al., 2017). However, the long-term effects of FUS on the brain microvasculature have not been extensively investigated.

Photosensitizer based techniques:

Photodynamic therapy (PDT) involves the administration of a photo-sensitizing agent that localizes in the tumor followed by photo-activation, which can result in a direct inhibitory effect on tumor cells and also a localized disruption of BBB that can aid in the delivery of other anti-cancer agents to the brain tumor. Hirschberg et. al evaluated the ability of 5-aminolevulinic acid (ALA)-mediated PDT to open the BBB in rats and observed that the BBB was reversibly disrupted 2 hours following PDT and recovered 80-100% after 72 hours, with no signs of tissue damage (Hirschberg et al., 2008, Semyachkina-Glushkovskaya et al., 2017). Photochemical internalization (PCI) is another similar novel technique, wherein photosensitizers capable of preferentially localizing in the membrane of endocytotic vesicles are used, followed by light assisted activation to cause localized disruption of the BBB (Madsen et al., 2010).

Chemical agents:

Adenosine, a product of ATP catabolism, has been shown to increase the BBB permeability by signaling through A1 and A2A adenosine receptors (AR), expressed on BBB cells. Administration of regadenoson (Lexiscan®), A2A agonist, and NECA, a broad spectrum AR agonist, also enhanced the permeability of BBB in a transient manner

(Carman et al., 2011, Bynoe et al., 2015). In another study, the same group also observed that the administration of regadenoson and NECA caused the downregulation of P-gp and BCRP at the BBB, in a reversible and time dependent manner (Kim and Bynoe, 2016). These studies suggest that modulation of AR signaling can be utilized as a strategy to increase BBB permeability and improve delivery of drugs to the brain. However, further studies to investigate and validate the relationship between the time of dosing and increase in BBB permeability using these compounds must be carried out (Carman et al., 2011).

RMP-7, a novel bradykinin analog, was shown to have selective bradykinin B2 agonizing activity that led to a dose- and time-dependent enhancement in the permeability of BBB and BTB (Bartus et al., 1996, Sanovich et al., 1995). However, the results of a phase 2 study in glioma patients showed that RMP-7 did not improve the efficacy of carboplatin (Prados et al., 2003).

2.4.4 Local drug delivery approaches

Local drug administration directly in to the CNS has been employed as a strategy to precisely deliver drug to the target site in the brain. Some methods employed include convection-enhanced delivery (CED), bio-degradable wafers placed in the tumor cavity post resection, and intrathecal implantable pumps. CED is a bulk-flow (hydrostatic pressure differential) driven invasive technique that allows continuous delivery of small- and large-molecular-weight compounds into the brain tissue through infusion catheters implanted during surgery (Lonser et al., 2015). The brain tissue in close proximity to the catheter may receive effective drug delivery, but the concentrations decrease steeply as

the distance from the catheter tip increases, due to competing forces of convective flow through brain parenchyma and drug diffusion into capillaries (Morrison et al., 1994). The use of bio-degradable wafers such a Gliadel® (carmustine) that are placed in the tumor cavity post resection for sustained drug release over a few days has also been considered for improving drug delivery to brain tumors post resection (Bregy et al., 2013). Intrathecal implantable pumps have also been employed for local delivery of analgesics to the CNS over prolonged periods, particularly for the management of chronic pain (Bottros and Christo, 2014). One problem with any local drug delivery technique is that molecules with high permeability or active efflux liability essentially leak out from the brain tissue into blood capillaries following local brain delivery. This phenomenon, namely the "sink effect", can influence the volume of brain tissue captured (Lonser et al., 2015, Parrish; Sarkaria; et al., 2015). The brain, a highly perfused organ, has capillaries in close proximity to each other with an average distance of 40 microns between them, and so the diffusion distance is 20 microns; thereby the probability of drug diffusion into capillary bed is high (Zlokovic and Apuzzo, 1998, Pardridge, 2016). Thus the selection of (i) a suitable drug candidate that has minimal liability to sink effect, and (ii) optimization of delivery parameters (such as infusion parameters for CED) to capture the required brain tissue volume (e.g., brain tumor), are critical to achieve beneficial responses with local delivery methods.

2.4.5 Other drug delivery based approaches

Various delivery strategies and formulation-based approaches have been considered for improving drug delivery to the CNS (Blasi et al., 2007, Pardridge, 2012, Kreuter, 2014).

The utilization of receptor-mediated uptake is one such strategy of interest that has been investigated by attaching a drug/antibody/nanocarrier to a factor that targets an uptake receptor at the BBB (van Tellingen et al., 2015). An example of this is GRN1005, an angiopep-2 peptide conjugated to paclitaxel, which gets across the BBB via transcytosis using the lipoprotein receptor related protein 1 (LRP1) (Drappatz et al., 2013). Another example is 2B3-101 which is a pegylated liposome conjugated with glutathione, and actively transported across the BBB. This formulation showed enhancement in the uptake and delivery when compared to the conventional doxorubicin liposomal formulation (Gaillard et al., 2014). The reader is directed to a review by Pardridge that discusses these "Trojan Horse" mechanisms and prodrug strategies with multiple examples in greater detail (Pardridge, 2012). Other formulation based approaches including nanoparticulate and liposomal drug delivery systems have also been widely studied and the reader is directed to comprehensive reviews that discuss these ideas (Blasi et al., 2007, Kreuter, 2014).

2.5 CONCLUSIONS

The diagnosis and treatment of brain tumors has been challenging, leading to a poor quality of life in the affected patients. While surgical resection and radiation therapy can provide initial local disease control, treatment with systemic therapies is often necessary for long-term benefits. Though systemic therapies have shown improvements in the management of extracerebral tumors, the responses in the brain have not been as effective, and also variable. This is attributed to the brain microenvironment that plays a key role in the emergence of resistance to therapy as well as in limiting the delivery of therapies to target sites in the brain. Although the BBB is relatively compromised in brain tumors, the degree of disruption and permeability to targeted therapies is heterogeneous at different sites within the same tumor, and between tumors in the same brain. Given this, drug penetration across sites with an intact BBB poses a significant hurdle, and the exposure of all tumor cells to efficacious drug concentrations is critical for efficacy, as any tumor cells that are left behind can lead to treatment failure and tumor relapse.

The interaction of anti-cancer agents with efflux transporters expressed at the BBB is a critical reason for inadequate drug delivery to brain tumors. P-gp and BCRP have been recognized as two major transporters at the BBB that efflux a majority of targeted therapies intended for use in the treatment of brain disorders. The expression of efflux transporters at the tumor cell level forms a secondary barrier, and further complicates the issue of drug delivery to brain tumors. Also, the differences in orientation and expression of transporters in the BBB vs the BCSFB influences the clearance processes that govern the movement of drug into the CNS, making it complex to understand the impact of

transporters on CNS drug delivery. This also limits the use of CSF as a surrogate for brain unbound concentrations, especially for drugs that are substrates for active efflux at the BBB. When determining the CNS pharmacokinetics of a drug, it is important to consider the bioavailability at the target site, and use unbound partition coefficient as a measure of the extent of drug distribution to account for drug binding to off-target sites.

Given the importance of drug delivery in the treatment of brain tumors, drug discovery and development programs should direct efforts to devise strategies to by-pass this key challenge. Many strategies are being developed to improve drug delivery to the CNS that include structure guided drug design to reduce transporter affinity and develop brain penetrant drugs, inhibition or downregulation of transporters, invasive and non-invasive means of transient BBB disruption, and local drug delivery directly into the brain parenchyma. However, the clinical success of such techniques has been limited, and needs further development. The problem of drug delivery is a key obstacle that needs to be tackled to achieve clinical success in the treatment of brain tumors.

FUNDING

This work was partially supported by National Institutes of Health grants from: National Institute of Neurological Diseases and Stroke R01-NS077291, R01-NS073610, and the National Cancer Institute U54-CA210180.

CONFLICT OF INTEREST STATEMENT

The authors indicate no conflict of interest with the subject matter of this review.

TABLES

Table 2. 1 Brain distribution of some drugs investigated for treatment of brain tumors. Atenolol and diazepam are examples of a hydrophilic drug with low brain distribution, and a lipophilic drug that freely diffuses across the BBB, respectively.

CNS drug	Primary Target	Kp brain	fu,blood/ plasma	fu,brain	Kp,uu brain	Reference
Atenolol	β1 receptor	0.04	NR	NR	0.01	(Summerfield et al., 2016, de Lange et al., 1994)
Diazepam	$GABA_A$	1.96	0.098	0.058	1.16	(Uchida et al., 2011)
Temozolomide	DNA alkylation	0.35	NR	NR	NR	(Goldwirt et al., 2014)
Paclitaxel	Microtubule	0.50	0.021	0.005	0.12	(Uchida et al., 2011)
AZD3759	EGFR	2.90	0.047	0.020	1.30	(Zeng et al., 2015)
Erlotinib	EGFR	0.17	0.045	0.029	0.11	(Zeng et al., 2015)
Gefitinib	EGFR	0.16	0.033	0.004	0.02	(Zeng et al., 2015)
Afatinib	EGFR	0.05	0.041	0.005	0.01	(Zeng et al., 2015)
GDC-0084	PI3K	1.39	0.29	0.067	0.41	(Salphati et al., 2016)
GNE-317	PI3K	1.32	NR	NR	0.48	(Salphati et al., 2014)
Pictilisib[a]	PI3K	0.02	NR	NR	0.001	(Salphati et al., 2014)
E6201	MEK	2.66	0.034	0.001	0.14	(Gampa et al., 2018)
Ribociclib	CDK4/6	NR	NR	NR	0.12	(Patel, 2016)
Abemaciclib	CDK4/6	0.21	0.054	0.008	0.03	(Raub et al., 2015)
Palbociclib	CDK4/6	0.06	0.2	0.02	0.01	(Raub et al., 2015, Parrish; Sarkaria; et al., 2015)
Ponatinib	PDGFR-α, RET	0.82	0.23	0.029	0.11	(Laramy et al., 2017)
Lorlatinib	ALK, ROS1	0.64	0.36	0.12	0.21	(Johnson et al., 2014)

NR, not reported

FIGURES

Figure 2. 1 A schematic representation of the blood-brain barrier (BBB) and blood-tumor barrier (BTB). The expression of efflux transporters at the BBB/BTB (barrier 1) and tumor cell level (barrier 2) is shown, and together they form a sequential transport barrier for the movement of anti-cancer therapeutics in to the brain.

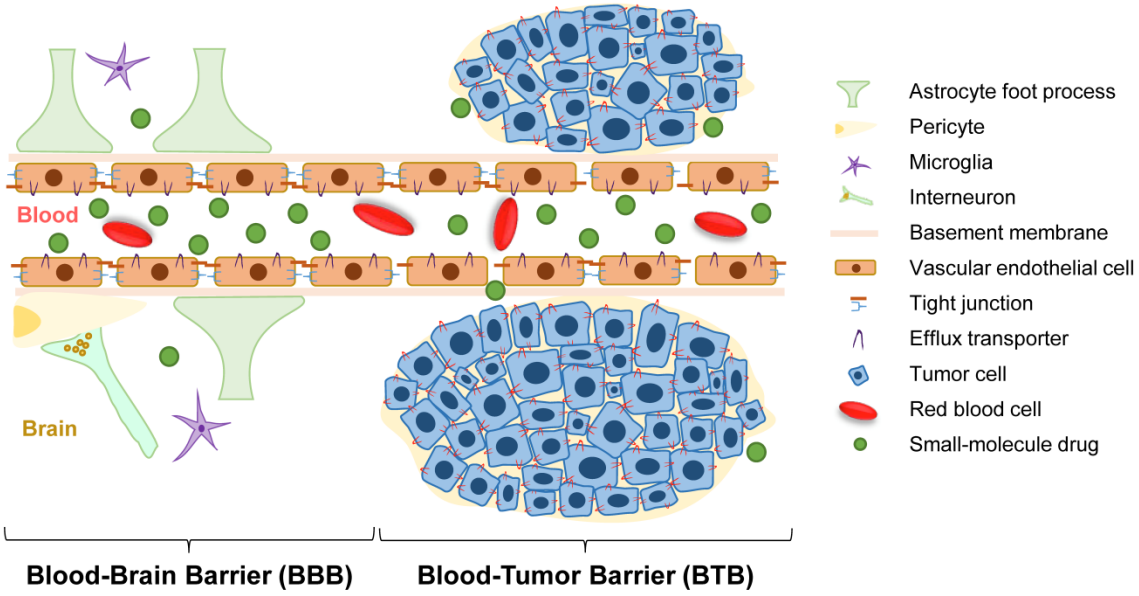

Figure 2. 2 A schematic representation of some of the barriers that an orally administered compound must pass before reaching the site of action. The barriers that a compound must pass to reach the systemic circulation are traditionally thought to contribute to the final bioavailability of a compound, whereas the barriers that must be overcome after the drug leaves the bloodstream to reach the site of action are related to drug targeting. The overall consideration of barriers from the site of administration to the site of action, which is usually extravascular, can be thought of as related to targeted bioavailability (adapted from (Elmquist, 2005), with permission).

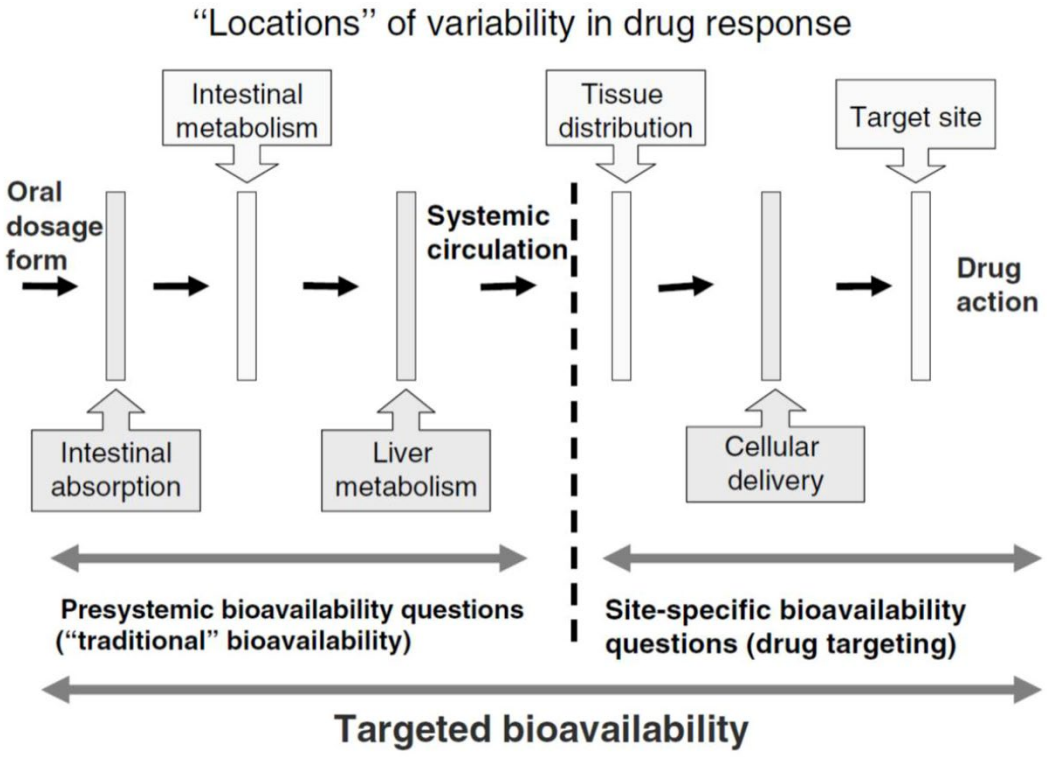

Figure 2. 3 The multiple equilibrium processes that determine the extent of drug distribution to the brain, i.e., the Kp and Kp,uu. The non-specific binding of a drug in brain and plasma can have a major influence on Kp. The Kp,uu represents the true transport equilibrium across the BBB and is not confounded by non-specific drug binding. BBB, blood−brain barrier; Kp, brain-to-plasma ratio; Kp,uu, unbound partition coefficient; CLin, summation of all clearances in to the brain; CLout, summation of all clearances out of the brain; CLps, passive diffusional clearance across the BBB; CLuptake, active uptake in to the brain; CLefflux, transport mediated efflux out of the brain; CLelim, drug elimination from the brain due to metabolism and bulk flow into CSF.

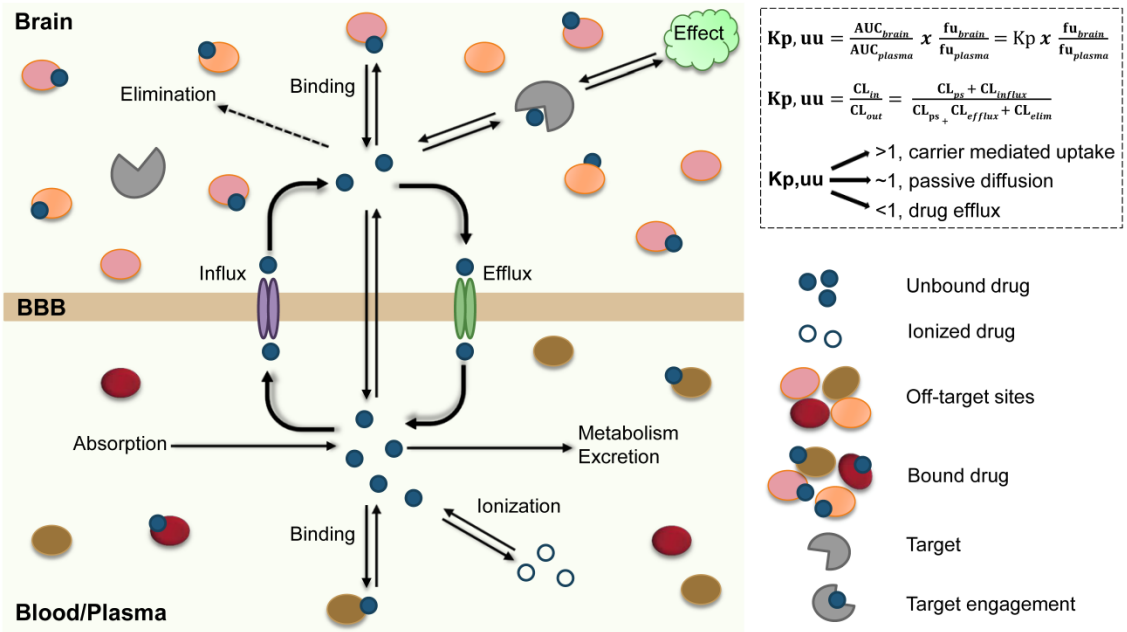

Figure 2. 4 A simplistic depiction showing unbound drug distribution equilibrium between four compartments commonly used to describe CNS pharmacokinetics, the brain ECF, the brain ICF, CSF and blood. Single broad red arrows indicate the expression of efflux transporters at the BBB and BCSFB, and the direction of drug movement due to efflux by transporters. P-gp, BCRP and MRPs are efflux transporters expressed at the BBB and BCSFB. BBB, blood−brain barrier; BCSFB, blood-cerebrospinal fluid barrier; Cp, plasma drug concentration; Cp,u, plasma unbound drug concentration; Cb,u(ECF), brain unbound drug concentration in extracellular fluid compartment; Cb(ECF), brain drug concentration in extracellular fluid compartment; Cb,u(ICF), brain unbound drug concentration in intracellular fluid compartment; Cb(ICF), brain drug concentration in intracellular fluid compartment; Ccsf, CSF drug concentration.

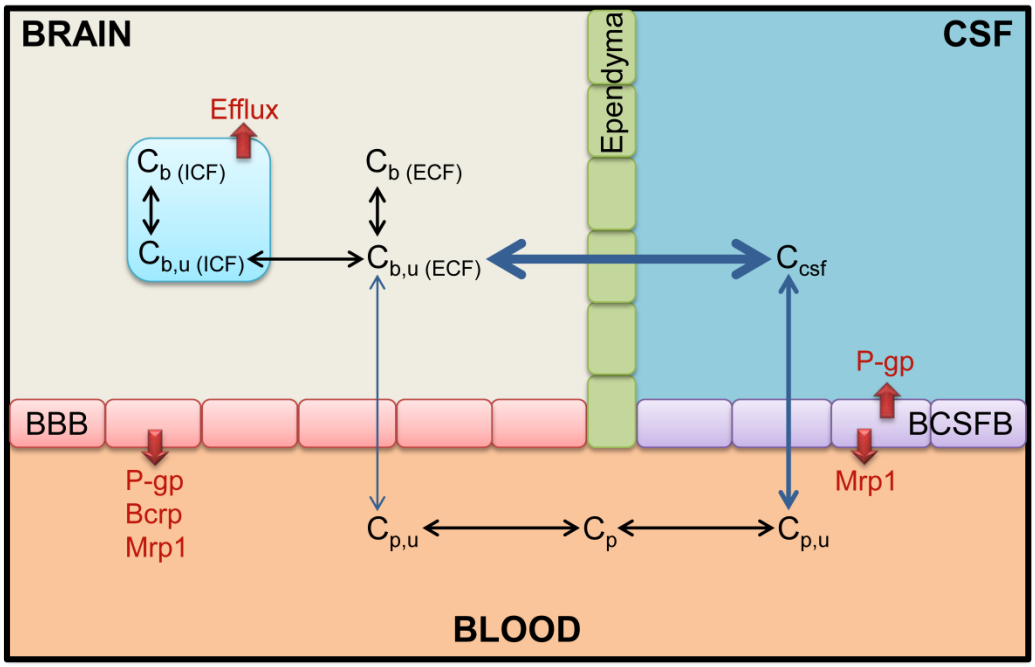

Figure 2. 5 The illustration shows various strategies that have been used to overcome the CNS drug delivery limitations due to the existence of the BBB.

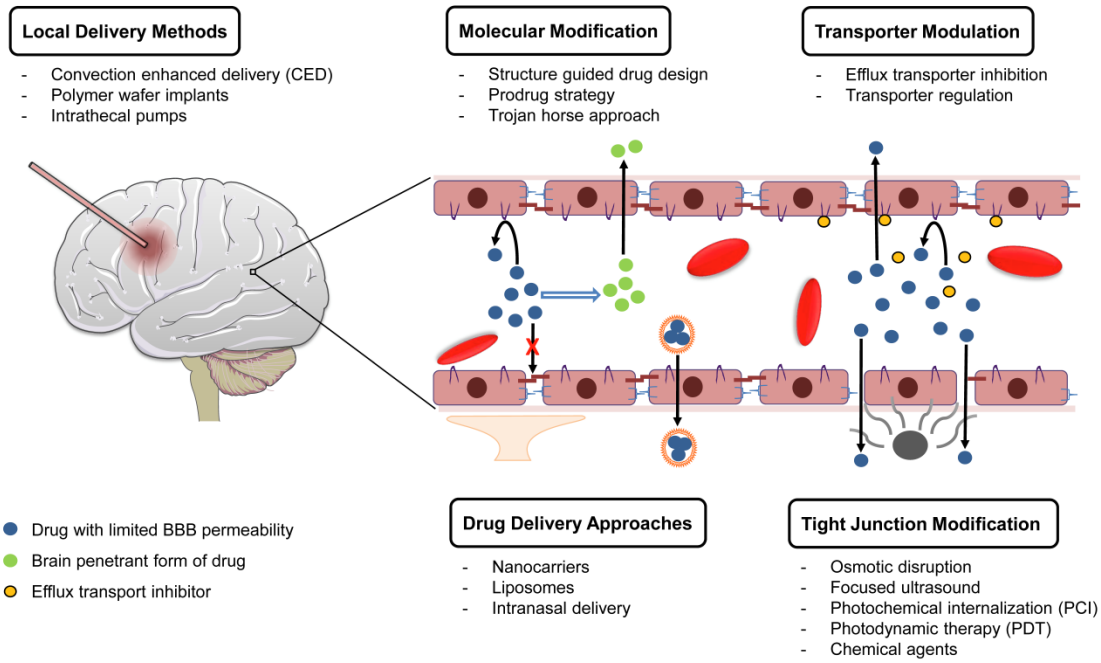

Figure 2. 6 The role of BBB permeability in the efficacy of targeted therapies for the treatment of brain metastases. A, injection of brain-tropic A2058 melanoma cells (orange) into the left cardiac ventricle of mice led to the formation of melanoma brain metastases. Sodium fluorescein (green), a brain-impermeable dye, was injected intravenously via tail vein, and its uptake into metastatic lesions was measured and used as a marker of brain metastasis permeability. Only ~29% of the brain metastases were permeable to the administered dye (green clouds). B, mice harboring both permeable (green clouds) and impermeable (no clouds) brain metastases were randomized to vehicle or two PI3 K inhibitors, GDC-0980, which is brain-impermeable, or GNE-317, which has demonstrated brain permeability. Both GDC-0980 and GNE-317 inhibited the growth of permeable metastases, while only the brain-permeable GNE-317 inhibited the growth and caused tumor apoptosis (white tumor cells with X) of impermeable metastases. These observations confirm a functional contribution of brain permeability to drug efficacy for brain metastases treatment (adapted from (Gampa et al., 2017), with permission).

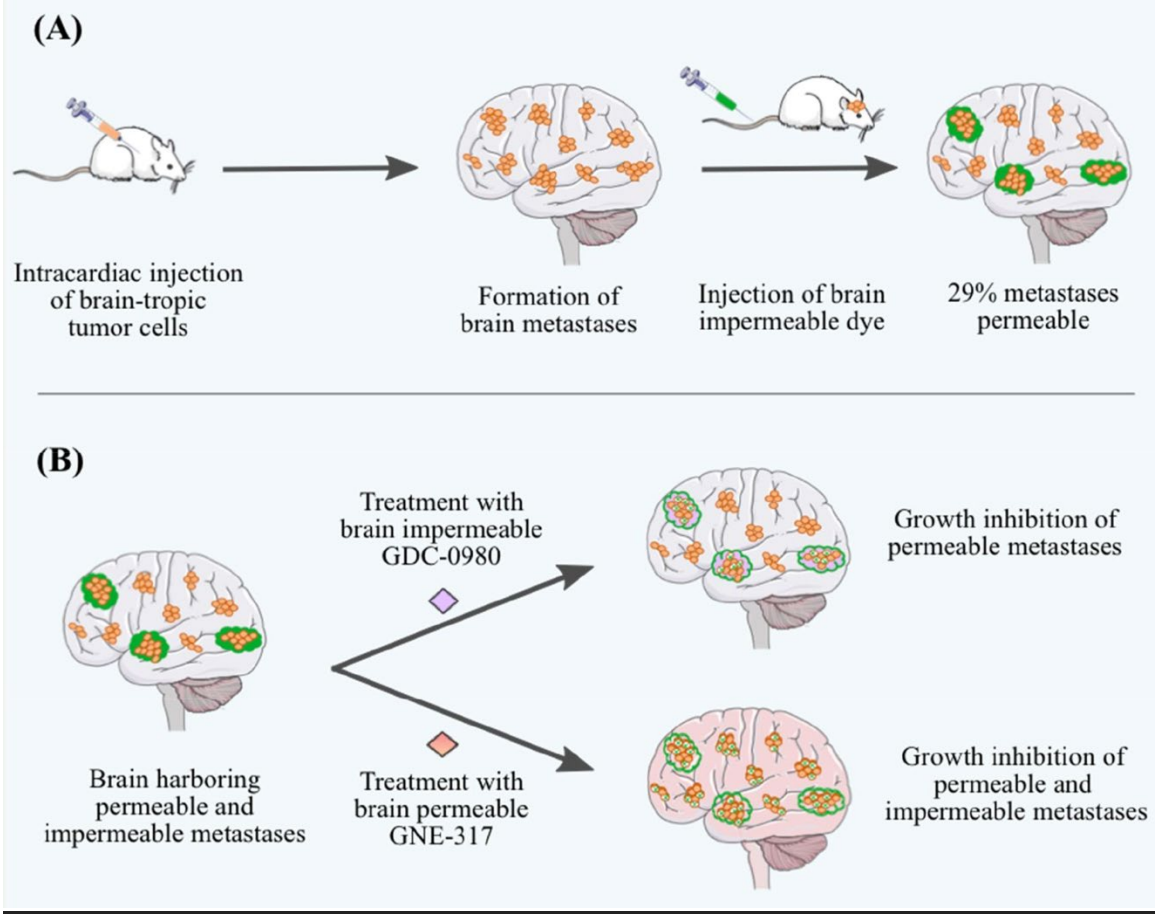
(A)
Intracardiac injection of brain-tropic tumor cells
Formation of brain metastases
Injection of brain impermeable dye
29% metastases permeable
(B)
Brain harboring permeable and impermeable metastases
Treatment with brain impermeable GDC-0980
Treatment with brain permeable GNE-317
Growth inhibition of permeable metastases
Growth inhibition of permeable and impermeable metastases

CHAPTER III. DRUG DELIVERY TO MELANOMA BRAIN METASTASES: CAN CURRENT CHALLENGES LEAD TO NEW OPPORTUNITIES?

The contents of this chapter have been published in:

Gampa G et al. (2017) Drug delivery to melanoma brain metastases: can current challenges lead to new opportunities? Pharmacological research. 123:10-25.

ABSTRACT

Melanoma has a high propensity to metastasize to the brain, and patients with melanoma brain metastases (MBM) have an extremely poor prognosis. The recent approval of several molecularly-targeted agents (e.g., BRAF, MEK inhibitors) and biologics (anti-CTLA-4, anti-PD-1 and anti-PD-L1 antibodies) has brought new hope to patients suffering from this formerly untreatable and lethal disease. Importantly, there have been recent reports of success in some clinical studies examining the efficacy of both targeted agents and immunotherapies that show similar response rates in both brain metastases and extracranial disease. While these studies are encouraging, there remains significant room for improvement in the treatment of MBM, given the lack of durable response and the development of resistance to current therapies. Critical questions remain regarding mechanisms that lead to this lack of durable response and development of resistance, and how those mechanisms may differ in systemic sites versus brain metastases. One issue that may not be fully appreciated is that the delivery of several small molecule molecularly-targeted therapies to the brain is often restricted due to active efflux at the blood-brain barrier (BBB) interface. Inadequate local drug concentrations may be partially responsible for the development of unique patterns of resistance at metastatic sites in the brain. It is clear that there can be local, heterogeneous BBB breakdown in MBM, as exemplified by contrast-enhancement on T1-weighted MR imaging. However, it is possible that the successful treatment of MBM with small molecule targeted therapies will depend, in part, on the ability of these therapies to penetrate an intact BBB and reach the protected micro-metastases (so called “sub-clinical” disease) that escape

early detection by contrast-enhanced MRI, as well as regions of tumor within MRI-detectable metastases that may have a less compromised BBB. The emergence of resistance in MBM may be related to several diverse, yet interrelated, factors including the distinct microenvironment of the brain and inadequate brain penetration of targeted therapies to specific regions of tumor. The tumor microenvironment has been ascribed to play a key role in steering the course of disease progression, by dictating changes in expression of tumor drivers and resistance-related signaling mechanisms. Therefore, a key issue to consider is how changes in drug delivery, and hence local drug concentrations within a metastatic microenvironment, will influence the development of resistance. Herein we discuss our perspective on several critical questions that focus on many aspects relevant to the treatment of melanoma brain metastases; the answers to which may lead to important advances in the treatment of this devastating disease.

GRAPHICAL ABSTRACT

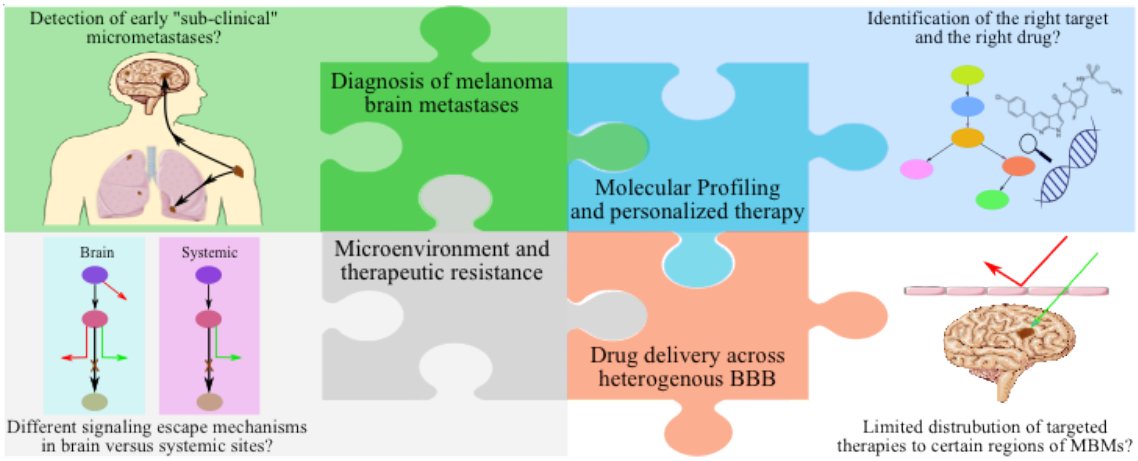

3.1 INTRODUCTION

The metastatic spread of melanoma to the brain is a major cause of morbidity and mortality in patients suffering from this disease. Metastatic melanoma, a debilitating and lethal form of skin cancer, is projected to have 87,110 new cases in 2017 in the US, with 9,730 deaths (Siegel et al., 2017). This malignancy has a high proclivity to spread to the brain, and patients with multiple brain metastases have an extremely poor prognosis, with a median overall survival (OS) of less than 6 months (Damsky et al., 2014, Sloan et al., 2009, Raizer et al., 2008, Gupta et al., 1997). The presence of brain metastases in a significant proportion (~70%) of melanoma patients at autopsy is a clear indication of an important unmet medical need (Gorantla et al., 2013, McWilliams et al., 2003).

Despite the remarkable progress seen in the overall treatment of melanoma patients (Bates, 2013), it is still difficult to treat advanced metastatic disease that has spread to the brain. Melanoma patients with multiple brain metastases can have a particularly poor survival, as short as 1-2 months. The standard of care for the management of patients with multiple brain metastases has been whole brain radiation therapy. Patients with one to three brain metastases are often candidates for surgical resection or stereotactic radiosurgery, depending on the location and size of the lesion(s) (Fife et al., 2004). Even with the advent of relatively successful targeted therapies and immunotherapies, treatments that can reliably provide major survival benefits for patients suffering from this devastating condition have still not been realized.

The small molecule targeted therapies inhibiting MAP kinase signaling (e.g., BRAF inhibitors such as vemurafenib and dabrafenib, MEK inhibitors such as trametinib and

cobimetinib) and the large molecule immune checkpoint inhibitors (e.g., cytotoxic T-lymphocyte-associated antigen 4 (CTLA-4) inhibitors such as ipilimumab and programmed cell death receptor (PD-1) inhibitors such as nivolumab) have shown some improvements in overall survival (OS) and progression-free survival (PFS) by a few months in patients with melanoma brain metastases (MBM) (Dummer et al., 2014, Rochet et al., 2012, Long et al., 2012, Falchook et al., 2012, Spagnolo et al., 2016, Davies et al., 2017). While encouraging, such modest improvements in OS are far from satisfactory, and do not represent a high probability of cure for patients suffering from this lethal condition. The results of some clinical studies suggest that the observed intracranial responses are poor compared to extracranial responses (Rochet et al., 2012, Larkin et al., 2014, Harding et al., 2015, McArthur et al., 2016, Spagnolo et al., 2016). However, there are important observations from other trials that indicate the intracranial responses are comparable to the extracranial responses (Gibney et al., 2015, Margolin et al., 2012, Di Giacomo and Margolin, 2015, Cohen et al., 2016, Spagnolo et al., 2016, Davies et al., 2017), creating a broad spectrum of reported efficacy of these therapies in MBM. Lack of durable efficacy may be due to many factors, and in MBM it may be related to resistance mechanisms that include both inadequate delivery and specific brain microenvironment characteristics that each could lead to changes in expression of genetic drivers. While small molecule molecularly-targeted therapies target key oncogenic proteins in deregulated signaling cascades, immunotherapies act by enriching prevailing immune responses to melanoma antigens. It is well appreciated that small molecule therapies must distribute to the target site to exert their action. However, it is crucial to

recognize that immune checkpoint inhibitors such as anti-CTLA-4 and anti-PD-1 therapies can cause activation and proliferation of cytotoxic T-lymphocytes in systemic sites, which are then able to gain access to the brain metastatic locations and attack the tumor cells (Engelhardt and Ransohoff, 2012, Margolin, 2016) thereby offering an important rationale for activity in MBM.

It is important to note that the patients with symptomatic MBM have frequently been excluded from pivotal clinical trials testing novel therapeutic agents (Davies et al., 2011, Cohen et al., 2016). This is due to the poor prognosis seen in this subset of patients and, at least in part, can be ascribed to the fact that several small molecule molecularly-targeted agents are substrates for active efflux at the blood-brain barrier (BBB), and so the delivery of these agents to brain metastases can be severely restricted (Durmus et al., 2015, Agarwal; Sane; et al., 2011, Parrish; Sarkaria; et al., 2015, Gampa; Vaidhyanathan; Wilken-Resman; et al., 2016). Such exclusionary practices have limited progress with regard to testing the efficacy of these agents in the treatment of MBM. While few trials have been specifically tailored for testing therapies in this subset of patients, some clinical trials are currently underway and will be important in understanding the therapeutic outcomes with the use of the recently developed therapies in patients with MBM.

It is critical to realize that the successful treatment of MBM, or any brain metastases, with molecularly-targeted agents will depend on the development of novel therapeutic agents that are not only potent at the target site, but are also capable of penetrating an intact BBB and reaching the protected metastatic tumor cells that are not clinically

detectable upon contrast-enhanced MR imaging (Murrell et al., 2016). Several critical questions surrounding the clinical diagnoses and treatment of MBM are addressed in this perspective, and adequate drug delivery is a component of each of these critical clinical questions. Figure 1 depicts the complexity involved in the discovery and development of new treatment paradigms for MBM. This "puzzle" will only be truly solved when all the key aspects influencing effective therapy are taken into consideration. For instance, it is clear that a potent drug that does not reach its intended target will be ineffective. Moreover, at least in a subset of non-responsive patients, a therapy that is initially effective in systemic (i.e, non-brain) metastases may not have efficacy in the brain due to microenvironment driven changes in tumor-growth driving targets. A broad understanding of these issues, all somewhat tied to the problem of adequate drug delivery to brain metastases, will help the scientific and medical community make appropriate decisions with respect to the discovery, development, and patient-specific selection of therapeutic agents for the treatment of MBM. Although a multi-factorial approach is needed to deal with this important problem of MBM treatment, the goal of this perspective is to focus on aspects related to drug delivery, bearing in mind other crucial factors such as microenvironment and resistance that will also need to be addressed in a comprehensive approach to this problem. In this perspective, we put forth our views on some of the critical clinical questions (Box 1) regarding the current and future treatment of MBM. However, before tackling these questions, that are largely related to drug delivery across the BBB, a brief review of the structure and function of the BBB is offered.

3.2 BLOOD-BRAIN BARRIER: AN OBSTACLE FOR DRUG DELIVERY TO BRAIN METASTASES

The BBB is comprised of several cell types, leading to various mechanisms that limit the penetration of many small and large molecule compounds into the brain. The endothelial cells in the brain microvasculature are held in close proximity by tight junctions, and are enclosed by extracellular matrix elements, pericytes and astrocyte foot processes, which collectively form the neurovascular unit (NVU), i.e., the BBB (Abbott, 2013). Such a complex architecture restricts the passive entry of many xenobiotics, including drug molecules, into the brain. Moreover, as shown in Figure 2, the entry of therapeutic agents into the brain is also strictly regulated by the presence of diverse transport systems belonging to the ATP-Binding Cassette (ABC) and Solute Carrier (SLC) families of proteins at the BBB (Taylor, 2002, Abbott et al., 2010). Of special interest are two important efflux transporters, P-glycoprotein (P-gp, MDR1, ABCB1) and breast cancer resistance protein (BCRP, ABCG2), known to limit the CNS delivery of several small molecule therapeutics that may be used for the treatment of CNS diseases (Agarwal; Hartz; et al., 2011, Wu and S, 2014, Gampa; Vaidhyanathan; Wilken-Resman; et al., 2016, Durmus et al., 2015). As examples of drugs relevant to the treatment of melanoma, there is evidence from preclinical studies that indicates an interaction of several molecularly-targeted therapies, including vemurafenib, dabrafenib, trametinib, palbociclib, cobimetinib and omipalisib, with P-gp and BCRP, resulting in poor drug distribution to the brain (Choo et al., 2014, Durmus et al., 2012, Mittapalli et al., 2013,

Mittapalli et al., 2012, Parrish; Pokorny; et al., 2015, Vaidhyanathan et al., 2014, Vaidhyanathan et al., 2016, de Gooijer et al., 2015).

The BBB in a brain tumor core has been widely considered to be compromised, allowing unrestricted drug delivery to tumor cells (Stewart, 1994, Gerstner and Fine, 2007). This belief has been supported by evidence from contrast-enhanced magnetic resonance imaging (CE-MRI) that can detect tumor locations with a permeable BBB (Fortin, 2012, Essig et al., 2006). However, the BBB disruption in brain neoplasms, both primary and metastatic, have a marked heterogeneity (Essig et al., 2006) and a review of the clinical data from 24 studies shows highly variable drug levels in brain tumor specimens for different antineoplastic agents (Pitz et al., 2011). The extent of BBB compromise in brain metastases and its impact on CNS delivery of therapeutic agents is an active area of investigation. Osswald and colleagues have measured permeability of brain metastases in a preclinical melanoma mouse model by injecting sodium fluorescein dye and determining the ratio of dye in metastases versus vessels. The results indicate that ~71% of brain metastases were non-permeable and only ~29% were permeable (Osswald et al., 2016) Lockman et al., have reported that the analysis of brain metastases from animal models of breast cancer show only partial BBB compromise in more than 89% of lesions. The magnitude of BBB compromise was observed to vary within and between metastases, and even in the leakiest brain metastases the permeability was much lower than in systemic tumors. Moreover, the BBB permeability of the tumor correlated with degree of drug uptake and effect. As seen in Figure 3, the distribution of paclitaxel into the breast cancer brain metastases is highly variable, even within a single metastatic

lesion (Lockman et al., 2010). Along these same lines, Adkins et al. observed in animal models of breast cancer brain metastases that the changes in permeability were independent of tumor size and morphology. These studies also report that less than 10% of the studied metastases exhibited a leaky enough BBB (up to ~50-fold higher permeability) to allow therapeutic agents to reach efficacious levels in the brain (Lockman et al., 2010, Adkins et al., 2016). Similarly, another preclinical study in a breast cancer brain metastases model revealed a variability of greater than 30-fold in vinorelbine concentrations between brain metastases. Vinorelbine distribution also varied widely within a single brain metastatic site due to heterogeneous permeability of the BBB (Samala et al., 2016). These examples in breast tumor brain metastases could be applicable in the context of MBM, as exemplified by Osswald et al., (Osswald et al., 2016) and are critical in guiding future research efforts in MBM.

In a commentary about the Osswald publication, Steeg and colleagues discuss important ideas related to misconceptions about the permeability of brain metastases. They highlight the confusion with respect to permeability, i.e., the belief that brain metastases are permeable to drugs since many are contrast-enhancing with gadolinium. As Steeg points out, a critical question related to this is, if permeability is uniformly increased, why does chemotherapy with activity in systematic metastases not work in the brain? (Steeg et al., 2016). This commentary emphasizes the crucial observation that various independent groups have shown, using different techniques, that brain metastases exhibit a heterogeneous permeability, and a significant fraction are poorly permeable (Steeg et al., 2016). While the laboratories of Drs. Smith and Lockman used quantitative imaging

following injection of dyes and radiolabeled drugs (Lockman et al., 2010), the laboratories of Drs. Foster and Chambers used gadolinium CE-MRI and high-resolution anatomic MRI to understand permeability of brain metastases in breast cancer models, and observed it to be heterogeneous (Murrell et al., 2016, Murrell et al., 2015). The laboratory of Dr. Winkler, confirms such findings of heterogeneity in permeability of brain metastases in a melanoma mouse model. They also went on to test a brain-permeable and brain-impermeable PI3K inhibitor alongside each other, observing that the brain-permeable inhibitor alone inhibited the growth of impermeable metastases. As suggested by Steeg, although a "brain-permeable" drug would often be defined differently, a useful definition in translational research is a drug that demonstrates an uptake sufficient to elicit a drug response (Steeg et al., 2016). The findings reported herein with regard to heterogeneity in brain permeability should also be tested in other brain metastasis model systems, such as spontaneous metastasis models. While responses and survival advantages have been observed with approved therapies, disease progression is frequent and development of brain-permeable drugs will possibly enhance drug efficacy. A first step in this direction will be to incorporate aspects favorable for increasing drug brain permeability (e.g., hydrogen bonding, lipophilicity, evading drug efflux) into early drug development programs (Heffron, 2016).

The current gold standard technique for the clinical detection of brain tumors is CE-MRI. Brain regions with a leaky BBB allow a large hydrophilic contrast agent such as gadolinium-diethylenetriamine pentaacetic acid (GAD-DTPA, molecular weight of 938 daltons) to passively diffuse into the brain parenchyma, indicating the "tumor" regions

(Essig et al., 2006). A major limitation of CE-MRI is that it can only reveal tumor locations that have a leaky BBB, while missing the detection of tumor cells in areas with an unbroken BBB, such as the micro-metastases and regions within larger tumors that have an intact BBB (Essig et al., 2006). As a consequence, this diagnostic modality can detect leaky tumors in advanced disease but not the early "sub-clinical" micro-metastases. Fidler et al., have reported that the brain metastases become leaky only after they attain a size of 0.25 mm (Fidler, 2011). An outcome is that the contrast-enhancing larger metastases with a leaky BBB may have relatively unrestricted drug delivery while the "sub-clinical" micro-metastases with an intact BBB have limited drug delivery leading to sub-therapeutic drug exposure. These ideas advocate the need for the development of brain-penetrant drugs capable of reaching not only the leaky metastases but also the "sub-clinical" micro-metastases and regions within MRI-detectable larger metastases that have an intact BBB, to achieve tumor regression and prevent tumor relapse.

3.3 CRITICAL QUESTIONS IN THE TREATMENT OF MELANOMA BRAIN METASTASES

The following discusses certain critical questions that, when successfully addressed, will almost certainly generate many hypotheses that will stimulate targeted research in MBM (see Box 1). This research, specific for the issues presented by brain metastases, will undoubtedly lead to therapeutic breakthroughs and improved clinical outcomes in the treatment of MBM.

3.3.1 Can targeted agents with limited distribution across an intact BBB be used to reliably treat MBM?

Limited drug delivery to tumor cells behind an intact BBB is undoubtedly an impediment to efficacy. Effective concentrations are not likely achieved for many of the small molecule molecularly-targeted agents in areas of micro-metastases and in regions of clinically detectable metastases that have an intact BBB. This is especially true where the drug BBB permeability is limited by efflux transport systems.

Given the discussion above regarding the heterogeneity of the BBB breakdown in many types of brain tumors, both metastatic and primary, instructive examples from breast cancer brain metastases illustrate how drug penetration through an intact BBB may strongly influence efficacy in brain metastases. A marked heterogeneity in the integrity of BBB in preclinical models of breast cancer corresponded with drug distribution, both within and between brain metastatic lesions (Adkins et al., 2016, Lockman et al., 2010, Samala et al., 2016). Lockman et al., and Adkins et al., report that less than 10% of brain metastatic lesions had a “leaky” enough BBB to allow the distribution of conventional

chemotherapeutics, such as paclitaxel and doxorubicin, to achieve effective concentrations (Lockman et al., 2010, Adkins et al., 2016). Both of these compounds are substrates for efflux pumps at the BBB. While these drugs are not used for MBM, such studies show that there can be marked differences in drug penetration, and hence efficacy, when compounds are subject to efflux at the BBB.

Targeted therapies such as BRAF and MEK inhibitors, and immune checkpoint inhibitors such as anti-CTLA4 and anti-PD1 therapies have shown significant efficacy in patients with MBM, with some studies reporting that the intracranial responses were comparable to the extracranial responses (Gibney et al., 2015, Margolin et al., 2012, Di Giacomo and Margolin, 2015, Cohen et al., 2016, Davies et al., 2017). While encouraging, the improvements in OS were limited, and certainly do not represent a possible cure for MBM patients. The absence of durable efficacy with molecularly-targeted agents, to some extent, may be related to the insufficient delivery of innovative treatments to the target sites in the brain that are behind an intact BBB. Moreover, most small molecule targeted agents have been shown to be effluxed by BBB transporters, particularly P-gp and BCRP. There is ample evidence that most of the small molecule therapies used for treatment of MBM are liable to active efflux at the BBB, which could be an important cause for the modest responses observed with these therapies. Vemurafenib has been shown to be a substrate for both P-gp and BCRP in animal models (Mittapalli et al., 2012, Durmus et al., 2012), and has very limited distribution into the CSF of melanoma patients (CSF:plasma ratio <1%) (Sakji-Dupre et al., 2015). Dabrafenib has a slightly higher permeability across an intact BBB than does vemurafenib in animal models

(Mittapalli et al., 2013), and it has a slightly better efficacy in clinical trials (Long et al., 2012). Both of the approved MEK inhibitors, trametinib and cobimetinib, have also been shown to be substrates of BBB efflux transporters (Vaidhyanathan et al., 2014, Choo et al., 2014). These reports strongly suggest that future targeted agents with an enhanced BBB permeability may result in greater and more durable efficacy in MBM treatment. As such, drug design and development goals should include creation of compounds that are not substrates of efflux proteins at the BBB (Heffron, 2016).

3.3.2 Will enhancing the brain distribution of systemically active agents improve the treatment of micro-metastatic disease in the brain?

The problem of limited drug delivery to brain tumors may be overcome by developing targeted therapies that can penetrate an intact BBB. However, important to the final result of improving delivery is the remaining question: will "therapeutic" drug levels in the brain, i.e., levels similar to those seen in systemic metastases, lead to regression of "sub-clinical" MBM? Further understanding of the brain microenvironment, and how it may be different than in the systemic metastatic sites with respect to tumor growth and development of resistance will be necessary to properly evaluate the impact of differences in systemic versus brain drug delivery.

The design and use of more BBB-penetrant drugs, in comparison to currently approved compounds, will help determine the effectiveness of such drugs and understand the emergence of different patterns of resistance. While there are a few brain-penetrant targeted drugs, a detailed evaluation of their efficacy in treating brain metastases has not yet been completed. Limited data about such brain-penetrant inhibitors exists and so it is

not clear at this point if such inhibitors will be more efficacious in brain metastases. Conduct of studies testing the efficacy of such inhibitors would help us better understand enhancements in treatment outcomes, and if development of therapeutic resistance can be delayed or avoided altogether.

Rational drug design to improve brain penetration of a drug that is effective against systemic targets is exemplified by Salphati et al., who have optimized the physiochemical properties of PI3K inhibitors using in-silico tools to develop GNE-317 and GDC-0084, both capable of penetrating the BBB. In orthotopic GBM mouse models, they observed that GNE-317 (U87, GS2, and GBM10 models) and GDC-0084 (U87 and GS2 models) achieved significant tumor growth inhibition compared to pictilisib, a brain impenetrant PI3K inhibitor. Further, it was reported that GNE-317 and GDC-0084 were homogenously distributed throughout the brain using matrix-assisted-laser-desorption-ionization mass spectrometry imaging (MALDI-MSI), and also well-distributed to both contrast-enhancing and non-enhancing brain tumors in corresponding U87 and GS2 models. In the same models, pictilisib was not detected in the normal brain and non-enhancing tumors. Even in the contrast-enhancing tumors, the detected pictilisib levels were spatially heterogeneous and varied by 6-fold within the contrast-enhancing U87 tumors (Salphati et al., 2016, Salphati; Heffron; et al., 2012, Salphati et al., 2014).

Another enlightening example is shown by the ALK inhibitors, such as alectinib, ceritinib, AP26113 and lorlatinib (PF-06463922). While these compounds have not been employed for MBM, they have demonstrated efficacy against brain metastases from lung tumors. The intracranial efficacies in NSCLC patients of alectinib (not liable to efflux by

P-gp) and ceritinib (brain-to-blood exposure ratio of ~15 % in preclinical rat model) have been attributed to the brain penetration of these compounds (Toyokawa et al., 2015). Lorlatinib, a macrocyclic ALK inhibitor, has also been specifically developed to cross the BBB (Johnson 2014). Moreover, AZD3759, an EGFR inhibitor, also induces profound regression of brain metastases in a preclinical mouse models of NSCLC (Zeng et al., 2015, Yang et al., 2016). AZD3759 has a high brain penetration with the unbound partition coefficient, Kpuu,brain (Figure 4) of 0.86 and is not a substrate of P-gp or BCRP efflux transporters (Tan et al., 2016). These are instructive examples because it can be expected that many of the same BBB-mediated issues in drug delivery are present in lung metastases as are in intracranial melanoma metastases.

3.3.3 Are therapies that can target currently "undetectable" brain micro-metastases more effective in extending progression-free or overall survival than treating larger brain metastases that are detectable by MRI?

A critical clinical question in treatment of MBM relates to, when do melanoma metastases first seed the brain during the progression of metastatic melanoma? Brain impenetrant drugs will not necessarily deter the initial seeding of metastatic tumor cells in the brain microenvironment and given this, would earlier initial diagnosis of brain metastases help influence therapeutic outcomes? An important corollary to this overriding question is determining if targeted therapies that can penetrate an intact BBB and achieve therapeutic levels early in disease progression will result in tumor growth inhibition or regression in brain sites.

Osswald et al. have observed in an important preclinical study, using a cranial window and multi-photon laser scanning microscopy, that targeting melanoma micro-metastases led to shrinkage of tumors in the brain. In this melanoma mouse model, the permeability of the brain metastases was determined by injecting sodium fluorescein dye and measuring the ratio of dye in metastases versus vessels. GNE-317, as indicated above, a PI3K inhibitor optimized to penetrate an intact BBB, showed responses in all brain metastases independent of the integrity of the BBB while therapy with non-brain permeable GDC-0980 (a related PI3K inhibitor with comparable effects on signaling inhibition in *in-vitro* experiments) led to responses only in permeable brain metastases (Figure 5). Also, GNE-317 showed significant benefits in the treatment of both non-permeable micro and macro-metastases. However, a reduction in the size of the tumor with GNE-317 therapy was observed only with micro-metastases, whereas the macro-metastases still grew (Figure 6A). Moreover, they also visualized and tracked dormant, single tumor cells in the brain. These single cells were in a BBB "impermeable" microenvironment and stable through a duration of 30 days post injection. The dormant cells, even though the surrounding BBB was intact, were observed to regress upon treatment with the BBB permeable GNE-317 (Figure 6B-E). These observations indicate that drugs engineered to have enhanced BBB permeability, thereby able to target the early micro-metastases, may prove to be more effective than less permeable drugs used to treat larger clinically detectable metastases at later stages of disease progression. While these results may seem obvious with respect to delivery across an intact BBB, it is critical

that this concept be incorporated into future drug design and use for therapies in melanoma brain metastases (Osswald et al., 2016).

Given that the current imaging methods cannot detect micro-metastatic disease in the brain, future gains in early diagnosis will be obtained through newer cutting-edge imaging methods. Are there any such methods on the horizon? A related and equally important question is how reliably does current CE-MRI predict the condition of the BBB in larger metastatic brain tumors? Are there distinct regions within a larger metastatic site that have an intact BBB; i.e., a BBB that has heterogeneous integrity leading to regions that will have inadequate drug delivery? This is clearly an area that deserves more attention in future research.

The major diagnostic tool for primary and metastatic brain tumors is CE-MRI. While MRI has advantages over computed tomography (CT) and positron emission tomography (PET)/CT in terms of higher sensitivity, it is only moderately specific such as in differentiating between actual response and pseudoprogression. Use of newer MR and PET imaging techniques based on the detection of pathological changes like alterations in function, metabolism, etc. by assessing tissue metabolites (proton MR spectroscopy), water mobility/infiltration (diffusion weighted MRI), vascularity (DSC perfusion weighted imaging), metabolism (FDG PET) and proliferation (18F-FET PET, 18F-DOPA PET), may be valuable in providing an earlier and more clear diagnosis. Combining some of these techniques (e.g., pre Gad T1 with DSC perfusion weighted imaging) may provide additional value and minimize issues of misdiagnosis and lack of early detection (Bruzzone et al., 2012). An emerging imaging technique that has been shown to be useful

in providing physiological details of a tumor such as vascularity and hemodynamic attributes is dynamic contrast-enhanced (DCE) MRI. Such information is beneficial in differentiating the aggressive hypervascular tumors from hypovascular tumors, which is not possible with conventional CE-MRI (Jung et al., 2016). Nevertheless, even with these currently existing imaging methods, future progress in early detection, and corresponding BBB integrity, will require further refinement of existing methods, or the development of new imaging methods that have greater sensitivity to detect tumor. It is important that such methods do not rely on the breakdown of the BBB to identify tumors.

3.3.4 In a related question (to #3), does the analysis of drug levels in a resected brain tumor specimen reflect drug levels in other regions of the brain that require treatment, especially in and around the micro-metastases?

Using total drug levels determined in a homogenized resected brain tumor as a measure of the drug delivery to that tumor is misleading. Regions of the resected tumor core may have a relatively leaky BBB allowing enhanced distribution of drug and may show higher drug levels than other regions of metastatic tumors in the brain (Gerstner and Fine, 2007). However, in tumor regions that have an intact BBB, like the micro-metastases or even specific volumes within a larger tumor mass, there will be restricted delivery of those compounds that have limited BBB permeability. Therefore, drug concentrations measured by examining a homogenate of a portion, or the entire excised lesion may mask the regions of inadequate drug delivery and as such will not be a good representation of regio-specific drug delivery to areas of growing tumor behind an intact BBB.

Studies on BBB integrity conducted in animal models of metastatic breast cancer have revealed some important findings that can be instructive for brain metastases in general (Lockman et al., 2010, Mittapalli et al., 2017). More than 89% of the metastatic lesions in the brain showed only partial BBB compromise, and the magnitude of compromise was observed to vary within and between metastases. The permeability of the heterogeneous BBB in the tumor correlated with degree of drug distribution and the response (Lockman et al., 2010). Moreover, less than 10% of the brain metastases had a BBB that was adequately permeable to allow therapeutic agents to reach the desired efficacious levels (Adkins et al., 2016). Mittapalli et al. have used a novel quantitative fluorescent microscopy imaging technique to determine the permeability of brain metastases in a preclinical breast cancer metastatic model (Mittapalli et al., 2017). They observed that the average within tumor BBB permeability varied broadly among individual metastases in contrast to the relatively homogenous average tumor-to-tumor permeability in RG2 gliomas. Also, the vascular pore size in the metastatic lesions was about 10-fold smaller than that observed in the glioma model, suggesting a less leaky vasculature in metastases compared to this primary brain tumor model (Mittapalli et al., 2017). Such observations highlight the heterogeneity of drug delivery to the brain metastatic lesions. Given the intricacies of a heterogeneously leaky BBB among different metastatic lesions, methods that simultaneously measure drug concentrations and the BBB integrity in a regio-specific manner will be necessary to determine correlations between delivery and efficacy.

Any technique that can enable the measurement of drug concentrations in distinct regions of the brain, with sufficient spatial resolution to correlate local concentrations with measurements of efficacy, will be extremely valuable. The use of the MALDI-MSI technique has been an important step forward in this direction. MALDI-MSI is a continually improving methodology that can be used to visualize relative drug levels in distinct regions of a brain section, allowing one to gain a spatial and temporal understanding of brain drug distribution. Liu et al. have used MALDI-MSI to describe the regional brain distribution of three model drugs with differential BBB permeability in mice and show that the correlation of drug and heme images can be used to understand drug permeability across BBB (Liu et al., 2013). Heme was validated as a robust marker for vasculature in the brain and measured in conjunction with the model compounds. The MALDI signal for RAF265, a RAF inhibitor with poor brain penetration, was observed to co-localize with the signal for heme, suggesting the confinement of drug to the vasculature and the inability to permeate an intact BBB, however, the RAF inhibitor was able to penetrate an intracranial tumor core (Figure 7). In contrast, the signal for BKM120, a PI3K inhibitor with good brain penetration, was observed to be well dispersed throughout the brain tissue, even the "normal" brain tissue, indicating the ability of this drug to permeate an intact BBB and distribute to various regions of the brain parenchyma. Also, for the case of erlotinib, an EGFR inhibitor, studied in U87 glioma xenograft tumors, the signal intensity for heme was high around the tumor margin (indicative of disruption of the BBB) and erlotinib was able to escape the tumor vasculature to evenly distribute within the tumor tissue of the U87 model (Liu et al.,

2013). However, there are significant questions about the lack of invasiveness of the U87 model, and whether it is a good model to explore spatial differences in BBB permeability to erlotinib or other targeted agents.

Recently, Aikawa et al. have studied penetration of alectinib (ALK inhibitor) to regions of non-tumor-bearing brain in preclinical mouse models using a combination of MALDI-MSI and LC-MS/MS techniques, referred to as quantitative MSI (qMSI) by the authors. The technique involved the use of serial brain sections in which the first and third sections were used for the measurement of alectinib using LC-MS/MS and the second (middle) section was used for drug analysis by MALDI-MSI (Figure 8). The integrated MSI response was then correlated to the LC-MS/MS determined drug concentrations in a homogenized slice to add a quantitative capability to the conventional MSI. However, it is important to note in this situation that any spatial differences in drug concentrations within a slice will be lost by this technique, as will the power of the MALDI-MSI to determine relative concentrations with a high spatial specificity. To address that caveat, laser microdissection (LMD) of specific regions of additional serial sections followed by LC-MS/MS drug concentration measurements in the LMD specimens was performed in an attempt to confirm the quantitative distributions of alectinib obtained by qMSI (Figure 9) (Aikawa et al., 2016). The use of such advanced techniques to understand not only the drug permeability across the BBB, but also the differential distribution to distinct regions of the "normal" brain and within brain tumors is essential to better understand and correlate drug delivery to observed response. While the development of MALDI-MSI as a tool to better understand brain drug delivery is exciting, the technique has limitations in

terms of quantitative measurements of drug levels. Therefore, there is still a pressing need for the development of novel highly-sensitive quantitative modalities to clearly understand how drug delivery to distinct regions of the brain and/or tumor may influence efficacy. Progress in finding effective therapies for the treatment of MBM and other brain tumors will rely on these new methods of analysis.

3.3.5 Will the use of drugs that have initial efficacy in systemic (i.e., non-brain) metastases, but have poor brain penetration, lead to resistant brain metastases? If so, will this be through mechanisms different than those leading to the eventual resistance at systemic sites?

It is evident that targeted therapies such as vemurafenib, dabrafenib, and their respective combinations with MEK inhibitors, cobimetinib and trametinib have improved the treatment of metastatic melanoma (Bates, 2013). However, these targeted agents have poor permeability (Choo et al., 2014, Mittapalli et al., 2013, Mittapalli et al., 2012, Vaidhyanathan et al., 2014) across the BBB likely leading to sub-therapeutic drug concentrations in areas of the brain where the BBB is intact. Current clinical data indicate that a significant proportion of patients stop responding to these targeted agents due to the development of resistance in systemic tumors (Welsh et al., 2016). It is certainly possible that the limited distribution of these drugs to the brain will lead to sub-therapeutic concentrations that may select for resistant tumor cells. The existence of locations within the metastatic lesions having an intact BBB can lead to sub-therapeutic drug exposures and the establishment of a sanctuary site. Such sub-therapeutic drug exposures, especially over prolonged periods, may induce the development of resistance to therapy by tumor

cells. The development of resistant clones of metastatic cells at non-brain sites and dissemination of the resistant cells from such sites to further seed the brain with drug resistant tumor cells can also possibly result in the growth of resistant MBMs. Furthermore, it is possible that with the development and use of agents that are BBB-penetrant, the mechanisms that drive resistance in systemic tumors and brain may become more similar. These perspectives on site-specific resistance mechanisms need further study, and future results may more clearly inform clinicians on drug choice to combat resistance.

Also, it is important to recognize that the expression of tumor targets could be different in tumors in the brain versus systemic tumor locations, possibly driven by differences in the tumor microenvironment. The hyperactivation of PI3K-AKT pathway and loss of PTEN have been implicated in the brain but not in extracerebral melanoma metastases (Bucheit et al., 2014). It was observed in preclinical mouse xenograft studies that a number of genes were reprogrammed, i.e., multiple gene expression changes occurred when tumors cells were implanted in the brain, irrespective of the type of tumor cell (Park et al., 2011). A discordance in gene expression patterns between different metastatic sites of the same tumor type was observed, while the brain metastases from diverse tumor types were more similar to each other (Park et al., 2011) which may be reflective of the similar microenvironment (a common soil). In a retrospective study involving whole-exome sequencing of 86 matched brain metastases, primary tumors, and normal tissue samples, Brastianos et al. have observed that 53% of the patients had clinically instructive alterations in brain metastases that were not detected in primary tumors (Brastianos et al.,

2015). Also interesting was that though genetically different from the primary tumors, distinct brain metastases were genetically homogenous and were associated with alterations sensitive to PI3K/AKT/mTOR, CDK, and HER2/EGFR inhibitors. Such alterations may be required for the establishment of metastatic disease in the brain, and may also influence the development of therapeutic resistance. Given these observations, characterization of the brain metastases post tissue collection from craniotomies may provide vital information not obtained from the genomic analysis of primary tumors, and would guide the selection of therapies directed towards key targets expressed in brain metastases. It is possible that diverse metastatic entities converge in common soil providing repeated, targetable features for appropriate molecularly-targeted agents (Brastianos et al., 2015, Saunus et al., 2015). The development of brain-penetrant inhibitors targeting such alterations expressed in brain metastases, and the conduct of clinical trials testing them, would delineate the clinical viability of such targets for the treatment of brain metastases, including MBM.

Given such differences in gene expression patterns between the systemic sites and the brain, it is possible that the mechanisms of resistance may be different in the brain compared to other systemic sites. However, additional research is needed in this area to clearly demarcate any such differences in resistance mechanisms. One question with respect to this: is the difference in tumor response and/or resistance between systemic sites and those in the brain related to only differences in drug delivery (i.e., achievable concentration), or are there specific influences of the different microenvironments, beyond drug delivery, that could lead to differences in efficacy and/or resistance?

We do not yet have a comprehensive understanding of other roles of the tumor microenvironment in the brain compared to the periphery (i.e., outside the brain) that may influence therapeutic outcomes. The microenvironment could be dictating the changes in gene expression profiles that, along with limited drug exposure, may lead to emergence of unique patterns of resistance and ultimately determine the choice of targets and subsequent drugs considered for the treatment of metastatic disease in the brain.

An important question related to the influence of the microenvironment is: will brain-only failure during targeted therapy portend the emergence of peripheral (i.e., non-brain) resistance? Given that the lack of adequate drug delivery and different gene expression patterns distinguishes the MBM from systemic metastases, systemic metastases could be responsive to targeted therapy and show initial tumor regression, during which time there may be "brain-only" failure to therapy. The question then becomes: will tumor cells from such resistant brain metastases reseed regions outside the brain, leading to the development of resistant systemic metastases? This is clearly an important clinical question that needs further study; in spite of its multi-factorial complexity.

3.3.6 What are the mechanisms responsible for the homing of tumor cells to the brain and how does the integrity of the BBB at the metastatic site affect the homing process? Also, will the integrity of the BBB at a metastatic site influence the rate of tumor growth in individual brain metastases?

Specific interactions that lead to the homing of melanoma tumor cells to the brain are not well understood. However, a few recent findings indicate some possible mechanisms implicated in the establishment of MBMs. The expression of PLEKHA5 has been found

to be linked to the increased transmigration of melanoma cells across the BBB and is associated with a higher risk of MBM formation (Jilaveanu et al., 2015, Eisele et al., 2015). Also, β1 integrins have been implicated to play a vital role in furthering the metastatic process by regulating the shift of cells to active and migratory mode, likely an important step in the formation of MBM (Barkan and Chambers, 2011) Another study suggests that matrix metalloproteinase proteins (MMPs) may be playing a role in the process of invasion of melanoma cells to the brain. Overexpression of MMPs such as MMP2 and MMP9 was suggested to aid the melanoma cells in permeating the BBB (Rizzo et al., 2015). Furthermore, it has been reported that claudin1, a tight junction protein, was responsible for the suppression of the malignant phenotype in melanoma (Izraely et al., 2015). It is known that claudins are important transmembrane proteins of the tight junctions between endothelial cells in the BBB. Given this, the integrity of the BBB may be playing an essential role in the process of homing of the metastatic tumor cells to the brain. A further elucidation of the key driving mechanisms responsible for homing of the metastatic melanoma cells to the brain will be useful in devising strategies for the prevention and treatment of MBM.

Osswald et.al, has examined the relationship between the integrity of BBB at the tumor site and the speed of tumor growth in preclinical animal models with MBMs. They report that the MBMs with a leaky BBB had a higher growth rate compared to that of MBMs with an intact BBB. Such an observation was attributed to a possibly more robust supply of growth factors and nutrients to the “BBB-permeable” metastases. Clearly more studies in this area are needed to further clarify the mechanisms involved (Osswald et al., 2016) .

3.3.7 In drug discovery, design and development, how can we find drugs that are active against the relevant targets, have adequate BBB permeability, and limit the development of resistance; the critical issues currently limiting the treatment of MBM?

To achieve significant improvements in treatment outcomes in patients with MBM, it is necessary to design and develop drugs that are potent in inhibiting key oncogenic targets, limit the emergence of therapeutic resistance and are capable of penetrating an intact BBB. All of these aspects should be considered early in the drug development process to guide the design of novel drugs. When using potent combination therapies to overcome resistance, it is required that all the individual drugs in the combinations penetrate the BBB to achieve therapeutically active drug levels in the brain. Until all of these necessary elements of drug design are met, we will likely be frustrated in our quest to find effective treatments for MBM. Also important, is the use of appropriate animal models for testing new investigational drugs. Preclinical studies with high predictive and clinical relevance are invaluable in the drug development process, and can greatly expedite the search for efficacious treatments.

A few examples of such medicinal chemistry tailored approaches have been described by Heffron in a recent perspective. The physicochemical properties of kinase inhibitors recognized as CNS penetrating (n = 20; molecules with meaningful free brain concentrations or are not substrates of P-gp/BCRP) to those that have limited CNS penetration (n = 48; molecules with low brain concentrations or are substrates of P-gp/BCRP), as well as 119 marketed CNS drugs, were compared. The median and mean

values of cLogP, cLogD7.4, total polar surface area (TPSA), hydrogen bond donor (HBD) count, and molecular weight between the two categories of kinase inhibitors were notably similar, and the only significant disparity was the calculated pKa (which can affect HBD count for those compounds that are sufficiently basic). The CNS penetrating inhibitors had a lower median pKa than both kinase inhibitors and CNS drugs incapable of crossing the BBB. Such examples illustrate the importance of subtle differences in the fundamental properties of the therapeutic compounds, and how they critically impact the brain delivery of these compounds. These ideas should be incorporated into future drug development efforts in the pursuit of brain-penetrant inhibitors for the treatment of CNS disorders (Heffron, 2016).

In particular, Heffron's article describes the discovery of three molecules; AZD3759, lorlatinib, and TAK-960, from five compounds that were initially designed with the intent of improving brain penetration, where intramolecular hydrogen bonds were exploited to mask at least 1 HBD (this masking would not be accounted for in calculated physicochemical properties of those molecules) and would also affect the effective polar surface area. As Heffron points out, it is possible that other CNS penetrant kinase inhibitors, whether intentionally or not, also employ a similar design strategy to avoid efflux (Heffron, 2016). Regardless, this is an approach that is worth consideration in the development of brain-penetrant inhibitors for treatment of CNS disorders, including brain metastases. If the lessons learned from the development of currently employed compounds are applied in a positive way, early in the development of future therapeutic compounds intended for treatments related to CNS, we will likely see more targeted

therapies that are capable of penetrating the BBB and overcoming this key hurdle. Achieving this would be a major leap in the struggle to find more efficacious treatments, even cures, for CNS disorders, specifically for MBM that are protected by an uncompromised BBB.

Optimal drug design and development efforts should be complimented by appropriate subsequent preclinical testing, pertinent to the research objectives. Preclinical animal models are indispensable tools that aid in gaining mechanistic insights of the disease biology, and in screening activity of drugs in the developmental pipeline. A useful animal model should be reproducible and closely recapitulate the human disease. Such models developed to study MBM would be most beneficial if they generate spontaneous tumors and form metastatic lesions with high propensity to seed the brain, as seen clinically (Kerbel, 2015). Patient-derived xenograft (PDX) models are biologically stable across passages and preserve the primary histopathological, genetic and molecular characteristics of patient tumor. Due to their value as predictive tools of clinical outcomes, PDXs are being used for various applications including preclinical drug activity testing, biomarker identification, and developing personalized medicine approaches (Tentler et al., 2012, Hidalgo et al., 2014). Establishment of PDXs is achieved by implanting tumor cells isolated from patients into immunodeficient mice (subcutaneous or orthotopic), and such an approach is suitable for melanoma (Hidalgo et al., 2014, Quintana et al., 2008). PDXs are useful as “avatars” for testing anti-cancer therapies, with a high predictive value of potential clinical outcomes (Quintana et al., 2012, Einarsdottir et al., 2014). For example, Krepler and colleagues have used mouse

PDXs in combination with targeted sequencing and phosphoproteomics for the conduct of personalized "preclinical trials", that led to successful identification of second-line targeted therapies for treating drug resistant tumors (Krepler et al., 2016). Another useful preclinical model is the genetically engineered mouse model (GEMM) that harbors mutations common to MBM, and has growth patterns resembling human disease. One advantage of GEMMs over PDX models is that the lesions develop in an immunocompetent host, allowing testing of both targeted and immunotherapies with appreciable predictive and clinical relevance (Ruggeri et al., 2014). Another valuable model is the spontaneous metastasis model that is capable of recapitulating all the events involved in the multi-step process of metastatic spread. The technique involves an *in-vivo* serial selection process for isolation of enriched aggressive metastatic cells, which are then orthotopically implanted in mice to allow the formation of distant visceral metastases (Kerbel, 2015). The observed metastatic patterns are variable between animals, providing a realistic representation of the clinical situation (Francia et al., 2011). These models have been used in a few translational studies, and an example is a study showing the growth of relapsed spontaneous brain metastases in mice with advanced systemic metastatic melanoma but without brain disease, after systemic disease control upon drug treatment (Cruz-Munoz et al., 2008).

A major challenge with preclinical models, given the important role of tumor microenvironment in cancer biology, is the change of stromal components from predominantly human to predominantly mice. PDX and spontaneous metastases models employ immunocompromised hosts, which prevents their use for testing

immunotherapies. Also, generation of models from a patient tumor isolated at a single time point cannot capture the broad diversity of the dynamic course of disease progression (Francia et al., 2011, Hidalgo et al., 2014, Tentler et al., 2012). In spontaneous metastases models, a problem is the regrowth of primary tumors at the location of surgical resection, and also resection of primary tumors itself can cause complications. Also, the selection of aggressive subpopulations of metastatic tumor cells can need multiple cycles of in-vivo selection (Francia et al., 2011, Kerbel, 2015). The major challenges with the development of GEMMs are asynchronous development of tumors in the transgenic host, and lack of availability of tissue-specific promoters for developing certain cancers (Ruggeri et al., 2014). Despite the unique advantages offered, establishment of GEMMs and spontaneous metastases models is complex, expensive and time consuming, which may limit their practical utilization in testing therapeutics for MBM (Kerbel, 2015, Ruggeri et al., 2014).

Given that each of the described models have certain advantages and disadvantages, the selection of an appropriate model for studying a given research question is critical, and it is beneficial to perform evaluations in more than one kind of model when feasible. A multi-model approach with spontaneous metastatic models as secondary screens in conjunction with GEMMs or PDX models can provide a broader picture of the likely outcomes of an investigational therapy in clinic (Kerbel, 2015). While the development of strategies such as “humanized mice” with reconstituted human immune system (Krepler et al., 2016, Kalscheuer et al., 2012) to overcome the use of an immunocompromised host are underway, the current PDX and spontaneous metastases

models are nevertheless valuable tools. Preclinical testing in the right animal model can guide the conduct of clinical studies and help make informed decisions, all of which play a pivotal role in improving the success rate of finding better therapies.

3.3.8 Are potential advances in the treatment of melanoma patients negatively impacted by the exclusion of patients with brain metastases from pivotal clinical trials testing novel targeted therapies?

It is important to include patients with symptomatic MBM in clinical trials to fully test the effectiveness of the novel targeted therapies. Achieving systemic disease control in a trial testing patients with detectable systemic metastases, but no brain metastases, might not be enough, as most of the patients ultimately die with brain metastases. Autopsy results show the presence of brain metastases in 70% of the studied melanoma patient population, suggesting a grave need to treat MBMs to improve therapeutic outcomes in patients with advanced melanoma or else the progress achieved with systemic disease control will remain incremental (Gorantla et al., 2013, McWilliams et al., 2003). One traditional drug development model has been to conduct clinical trials designed to test the safety and therapeutic efficacy of novel therapeutics in patients with systemic disease burden, while excluding patients with detectable brain disease. The reason for such exclusionary practices has been the dismal prognosis associated with this patient population.

The pivotal clinical trials testing novel therapeutics associated with the treatment of melanoma comprised of more than 6000 metastatic melanoma patients but excluded patients with active MBMs (Cohen et al., 2016). Smaller trials testing these agents in

MBM populations were opened later and included 234 patients, representing only 4.1% of the patients enrolled; clearly insufficient (Cohen et al., 2016). Given the growing evidence that suggests differences in the microenvironment of the brain versus systemic sites, in terms of both the expression of genomic drivers and restricted drug delivery to the brain, it is critical to include patients with brain involvement early in clinical trials to gain insight into the mechanisms that may lead to therapeutic failure (Brastianos et al., 2015). For instance, the PI3K inhibitors would historically have been tested in patients with systemic disease while this target may actually be more important in brain metastases (Chen et al., 2014, Bucheit et al., 2014, Niessner et al., 2016, Peng et al., 2016). The exclusionary practices in clinical trial testing of novel therapeutic agents could result in an incomplete understanding of key concepts. Thus, inclusion of patients with active MBMs early in clinical trials testing novel therapies, along with trials specifically tailored to this population, would help accelerate the development of therapies to treat the debilitating MBMs.

3.4 OPPORTUNITIES FOR THE FUTURE

The eight major questions that have been posed in this perspective emphasize significant gaps in our knowledge that, if answered, will directly address several critical unmet needs in the treatment of MBM. Research that can answer these questions, both preclinical and clinical, will undoubtedly move the field toward more efficacious treatments.

One aspect of many of the questions is how we can ensure adequate drug delivery to melanoma metastases that are protected by an uncompromised BBB. The small molecule molecularly-targeted agents are restricted by their ability to permeate an intact BBB, mainly due to active efflux by BBB transporters, particularly P-gp and BCRP (Agarwal; Sane; et al., 2011, Gampa; Vaidhyanathan; Wilken-Resman; et al., 2016, Parrish; Sarkaria; et al., 2015). Also, it has been reported that melanoma cells previously treated with targeted agents are capable of expressing the ATP-dependent efflux transporter ABCB5, while a side-population of melanoma stem cells have been identified to express ABCB5 intracellularly and ABCB1 on the plasma membrane (Chartrain et al., 2012, Luo et al., 2012). Existence of such efflux mechanisms at the level of tumor cells forms a secondary barrier, which can further limit the delivery of small molecule molecularly-targeted therapies to the tumor cells. The exposure of metastatic tumor cells to sub-therapeutic drug levels will lead to poor treatment outcomes in patients with MBM due to the establishment of the brain as a pharmacological sanctuary site, possibly leading to the development of resistance. It was observed in preclinical models of metastatic melanoma that effective control of systemic metastatic burden for a period of time can result in an increased rate of relapse of brain metastases. The efficacy benefit in controlling systemic

metastatic disease is possibly allowing the seeded micro-metastases in the brain to have more time to expand into detectable macroscopic metastases (Cruz-Munoz et al., 2008). Thus, it is important to enhance the drug delivery of targeted therapies to the brain. The development of brain-penetrant inhibitors, and their evaluation in preclinical and clinical studies, will help us understand the target-engagement related improvements in efficacy by improving drug delivery to MBM, thus eliminating one variable that could affect efficacy. Also important and related to this line of questioning is the development of techniques that can facilitate reliable measurements of drug concentrations at distinct locations of the brain, with adequate spatial resolution to correlate local drug concentrations with biomarkers of target engagement and overall efficacy.

A key area that needs attention in future research is the development of imaging modalities that can detect micro-metastatic disease early in the disease progression. This would help clinicians to develop a fundamental understanding of the timing of the first appearance of the brain metastases compared to the systemic melanoma tumors, and evaluate if any improvements in treatment outcomes can be achieved by using brain-penetrant targeted therapies early in the disease progression. A deeper elucidation of the driving mechanisms responsible for homing of the metastatic melanoma cells to the brain will be extremely useful in identifying potential new targets, and devising novel strategies for both the prevention and treatment of MBM. Such advances will definitely help us better understand the disease progression, and move forward in the quest for a cure to treat MBM.

Additional research is also required to clearly demarcate any differences in resistance mechanisms in the brain versus the systemic sites. While differences in drug delivery to the target sites is an important reason for differences in tumor response and/or resistance between systemic and brain metastatic sites, it is crucial to understand if there are any other specific influences of the different microenvironments that could lead to alterations in target expression, efficacy and/or resistance. As discussed above, the microenvironment of a metastatic site could be dictating the changes in gene expression profiles that, along with limited drug exposure, may lead to emergence of unique patterns of resistance and ultimately determine the choice of targets and subsequent drugs, possibly as combination therapies, that will be considered for the treatment of metastatic disease in the brain. Given the differences in gene expression patterns between the systemic sites and the brain, it is also possible that the mechanisms of resistance may be different in the brain compared to the systemic sites, leading to a "brain-only" pattern of failure. These viewpoints on site-specific resistance mechanisms need additional evaluation, and future results may clearly inform clinicians on the apt choice of drug(s) to combat resistance.

To achieve meaningful enhancements in treatment outcomes in patients with MBM, it is vital to design and develop drugs that are potent in inhibiting key oncogenic targets, limit the emergence of therapeutic resistance and are capable of penetrating an intact BBB. All of these aspects should be considered early in the drug development process to guide the design of novel drugs (Figure 10). Drugs specifically designed with the intent of treating brain metastases, all the while recognizing the source of primary tumor (e.g., melanoma,

breast, lung cancer), might be more important than screening and developing agents for the treatment of a particular systemic tumor. Testing candidates from such a screening for use in the treatment of brain metastases growing from that specific cancer type may not include important "brain-specific" development parameters, such as blood-brain barrier penetration or efficacy against unique drivers that are preferentially expressed in the brain tumor. This is essential considering the critical idea that the brain, a common soil for the systemic tumor "seeds", may be fostering the growth of specific clones of tumor cells and also causing changes in the tumor gene expression patterns, an adaptation that may be necessary for the tumor cells to grow in the privileged microenvironment of the brain. Such observations imply that brain metastases growing from different primary tumors may be more similar in terms of gene expression patterns, compared to the primary tumors from which they originate. Thus, developing brain-penetrant inhibitors specifically designed to be effective against brain metastases emerging from various primary tumors, might be a viable strategy to test in future drug development endeavors for the treatment of brain metastases. It is important to note the fact that drug delivery to the target sites and potency of the developed therapeutic agents in inhibiting the metastatic tumor cells in the brain, both dictate the ultimate outcome seen in the treatment of the brain metastatic disease.

Achieving a modest improvement in the overall survival by the use of targeted therapies (e.g., vemurafenib and dabrafenib, combined with MEK inhibitors) in metastatic melanoma may be significant, but is still far from being sufficient to improve the MBM patient's dire situation. We need therapies that can treat the metastatic disease in the brain

and prolong the survival to such an extent that it makes an impact on quality of life, beyond a meagre increase in survival of the patient by few months. It is therefore critical to include patients with active MBMs early in future clinical trials testing targeted agents, along with design of trials specifically tailored to test the MBM population, to help accelerate the development of therapies to treat the debilitating MBMs.

This perspective reviewed many of the critical issues that remain in developing effective treatments for MBM. The task of adequate delivery of potent agents to protected sites in the brain must be solved to avoid the possibility of brain-only failure and emergence of unique patterns of resistance. A better understanding of how the tumor microenvironment influences tumor growth is also required to help match effective drugs to appropriate patient. Great progress has been made, and future research, guided by the right questions, will undoubtedly improve the outlook for patients with MBM.

FUNDING

This work was partially supported by National Institutes of Health grant from: National Institute of Neurological Diseases and Stroke R01-NS077291 (WFE, JNS), R01-NS073610 (WFE), U54-CA210180 (WFE, JNS).

CONFLICT OF INTEREST STATEMENT

The authors indicate no conflict of interest with the subject matter of this review.

Box 1: Critical questions in the treatment of MBM

1. Can targeted agents with limited distribution across an intact BBB be used to reliably treat MBM?

2. Will enhancing the brain distribution of systemically active agents improve the treatment of micro-metastatic disease in the brain?

3. Are therapies that can target currently "undetectable" brain micro-metastases more effective in extending progression-free or overall survival than treating larger brain metastases that are detectable by MRI?

4. In a related question (to #3), does the analysis of drug levels in a resected brain tumor specimen reflect drug levels in other regions of the brain that require treatment, especially in and around the micro-metastases?

5. Will the use of drugs that have initial efficacy in systemic (i.e., non-brain) metastases, but have poor brain penetration, lead to resistant brain metastases? If so, will this be through mechanisms different than those leading to the eventual resistance at systemic sites?

6. What are the mechanisms responsible for the homing of tumor cells to the brain and how does the integrity of the BBB at the metastatic site affect the homing process? Also, will the integrity of the BBB at a metastatic site influence the rate of tumor growth in individual brain metastases?

7. In drug discovery, design and development, how can we find drugs that are active against the relevant targets, have adequate BBB permeability, and limit the development of resistance; the critical issues currently limiting the treatment of MBM?

8. Are potential advances in the treatment of melanoma patients negatively impacted by the exclusion of patients with brain metastases from pivotal clinical trials testing novel targeted therapies?

FIGURES

Figure 3. 1 A complex, dynamic puzzle of interrelated pieces necessary to improve the treatment of melanoma brain metastases (MBM) includes: (a) improved imaging modalities for diagnosis of early "sub-clinical" micro-metastases, (b) improved identification of the brain-specific targets and selection of suitable targeted therapies, (c) improved recognition of brain-specific resistance mechanisms, and, (d) improved drug design to overcome BBB delivery issues and yield effective combination therapies.

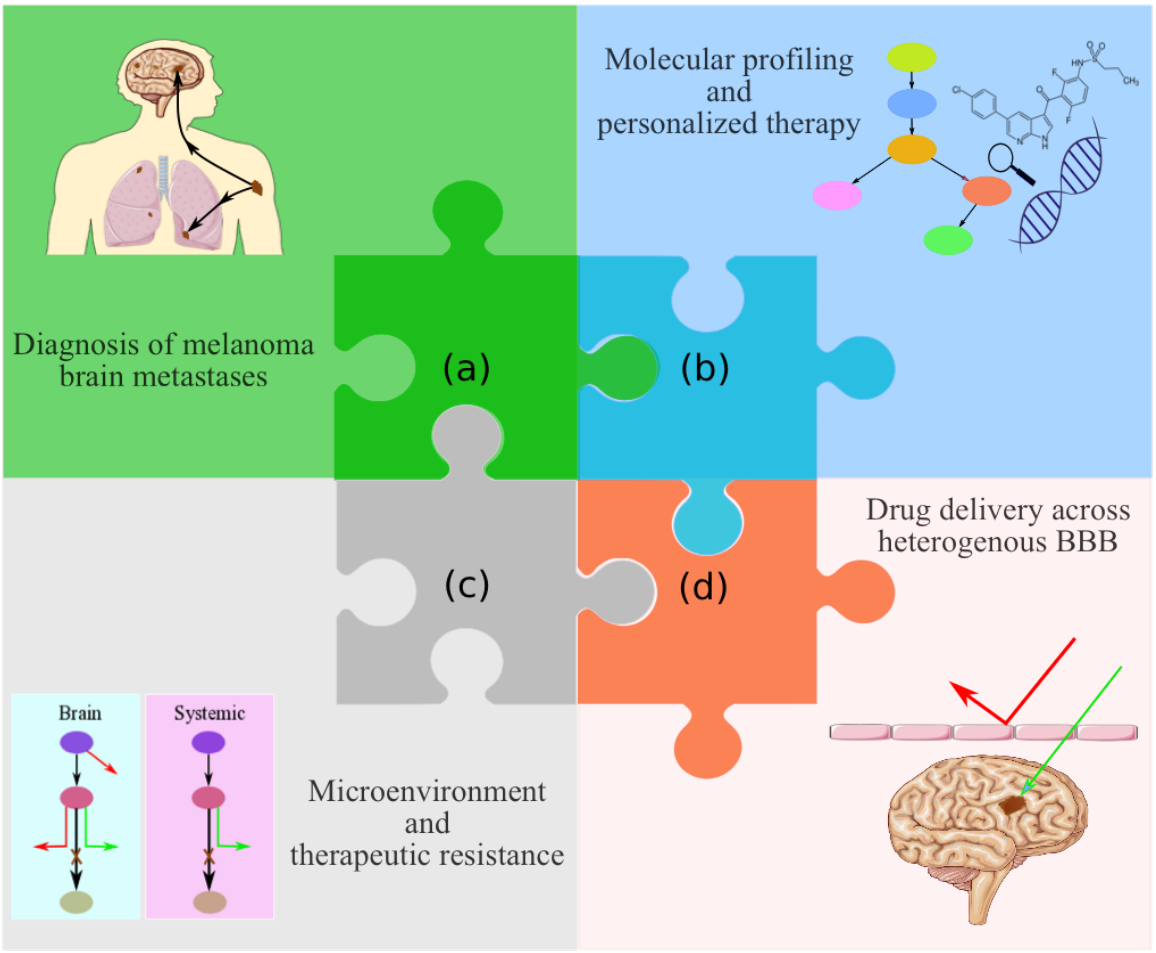

Figure 3. 2 The blood-brain barrier (BBB). A) The BBB (also referred to as the neurovascular unit, NVU) architecture, and cell associations that form the BBB. B) various routes of trafficking across the BBB that includes transcellular passive diffusion, active efflux, carrier mediated influx, receptor mediated transcytosis (RMT), adsorptive-mediated transcytosis (AMT), diapedesis and modulation of tight junctions (TJ) (adapted from (Abbott, 2013), with permission).

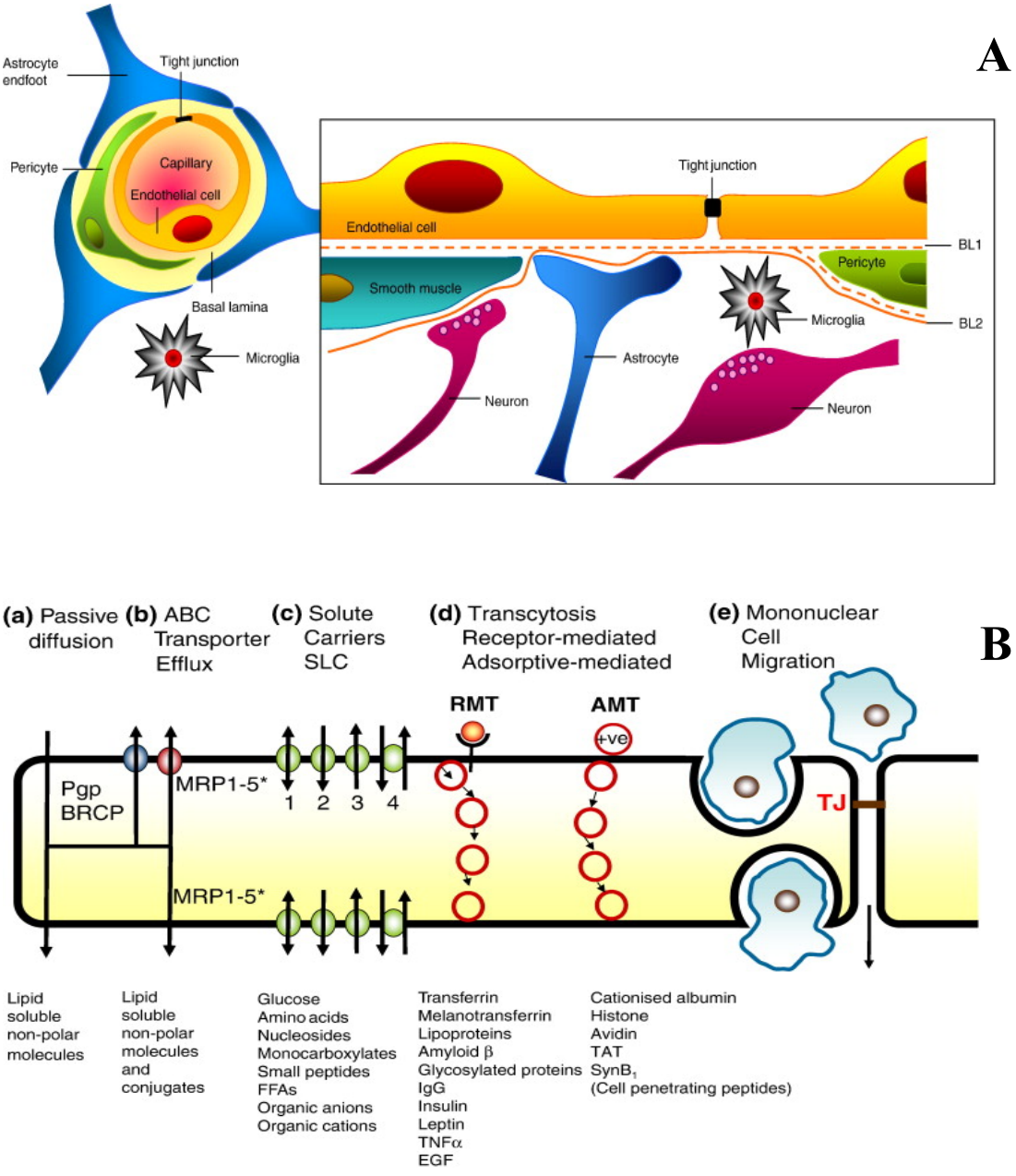

Figure 3. 3 Variable paclitaxel uptake in 231-BR-HER2 brain metastases that correlates with 3-kDa Texas Red dextran accumulation. 14C-Paclitaxel distribution in 231-BR-HER2 metastases after intravenous administration of 10 mg/kg of paclitaxel (Taxol formulation). Distribution of eGFP (A), 3-kDa Texas Red dextran [10-minute circulation (B)], and 14C-paclitaxel [8 hours (C)], followed by a 30-second vascular washout. White scale bar represents 1 mm. Heterogeneous distribution is shown within one representative brain metastasis (D, eGFP; E, 14C-paclitaxel; and F, 3-kDa Texas Red dextran). G, 14C-paclitaxel concentration (ng/g) in brain and 231-BR-HER2 brain metastases. Values represent the percentage of all metastases in each group, and the mean ± SD of 14C-paclitaxel concentration in each group. H, mean brain metastasis drug concentration was measured at different times (30 minutes–8 hours) and related to that in brain distant from tumor, plasma, blood, and systemic tissues (n = 3 animals per point). Yellow areas show highest and lowest concentrations observed in brain metastases at the 3 time points. Calculated area under the curve cumulative exposure (in μg h/g) equaled 0.18 in brain, 2.9 in average brain metastasis, and 80 to 400 in systemic tissues (adapted from (Lockman et al., 2010), with permission).

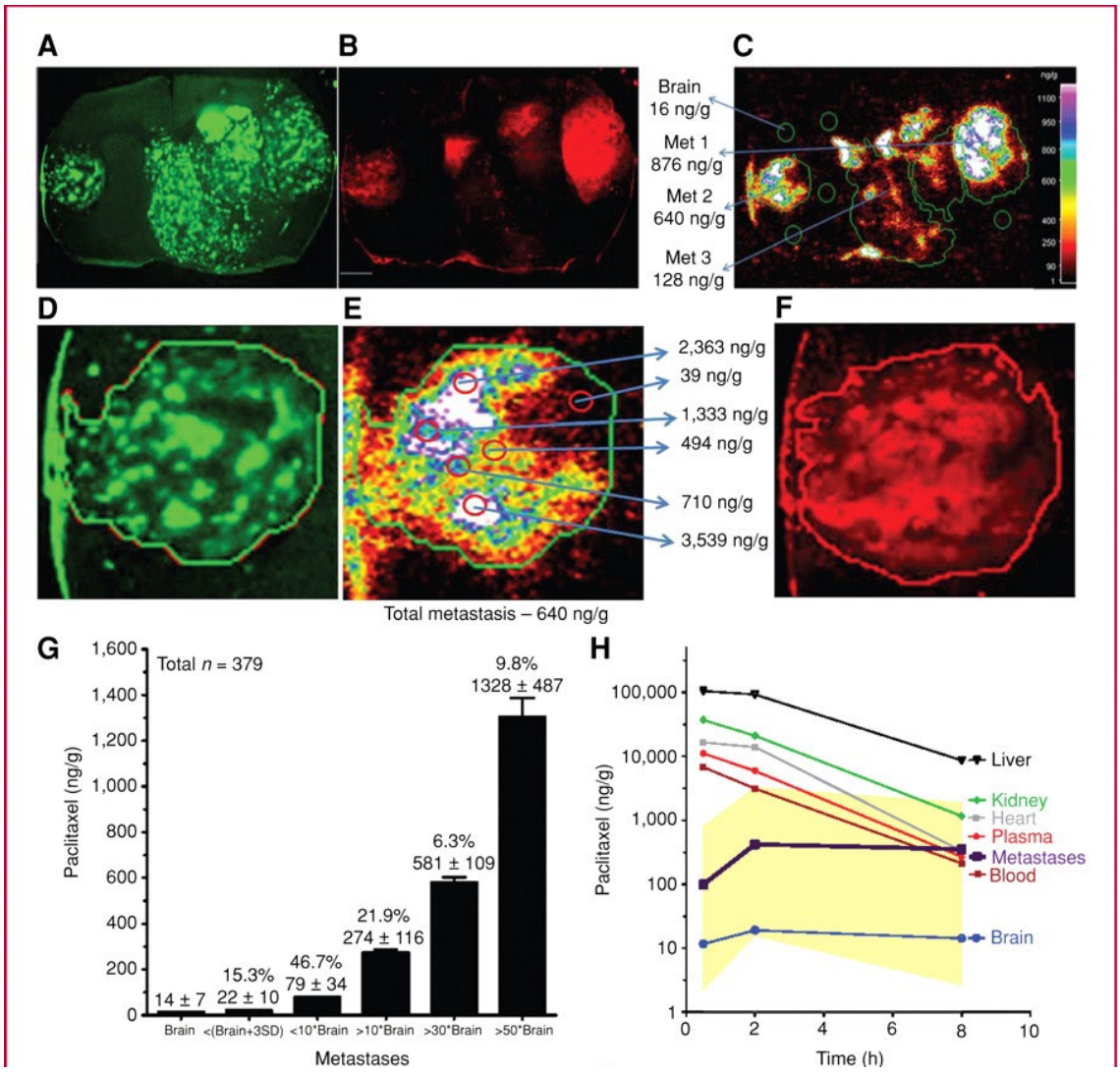
A
B
C
Brain
16 ng/g
Met 1
876 ng/g
Met 2
640 ng/g
Met 3
128 ng/g
D
E
F
2,363 ng/g
39 ng/g
1,333 ng/g
494 ng/g
710 ng/g
3,539 ng/g
Total metastasis – 640 ng/g
G
Total n = 379
Paclitaxel (ng/g)
9.8%
1328 ± 487
6.3%
581 ± 109
21.9%
274 ± 116
46.7%
79 ± 34
15.3%
22 ± 10
14 ± 7
Brain
<(Brain+3SD)
<10*Brain
>10*Brain
>30*Brain
>50*Brain
Metastases
H
Paclitaxel (ng/g)
Liver
Kidney
Heart
Plasma
Metastases
Blood
Brain
Time (h)

Figure 3. 4 Elucidation of the unbound partition coefficient, Kpuu. The diagram represents the protein-bound and unbound drug molecules in the blood and brain compartments. The Kpuu, brain to plasma unbound drug concentration ratio, is determined using the total drug concentrations (C_{total}) and unbound fractions (f_u), in both the blood and brain compartments. P-gp, an efflux transporter, is also shown on the luminal (blood) side of the BBB (adapted from, (Dolgikh et al., 2016)).

$$K_{p,uu} = \frac{C_{total,brain}}{C_{total,plasma}} \cdot \frac{f_{u,brain}}{f_{u,plasma}}$$

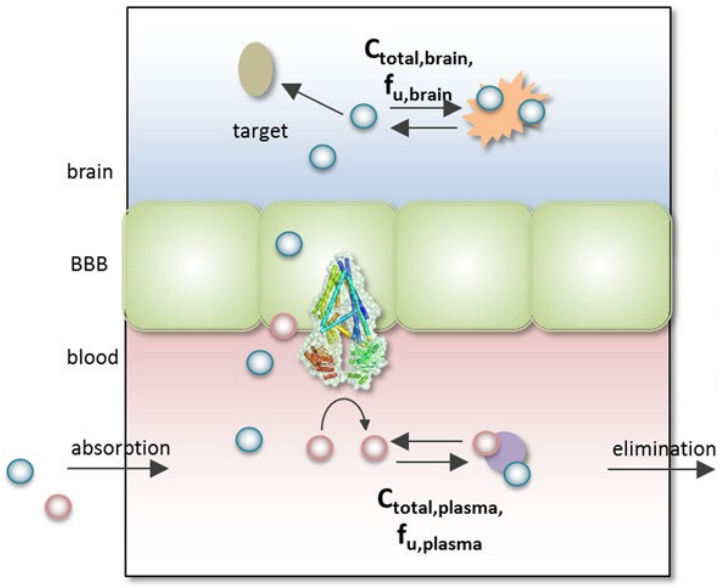

Figure 3. 5 The role of BBB permeability in the efficacy of targeted therapies for the treatment of brain metastases. A, injection of brain-tropic A2058 melanoma cells (orange) into the left cardiac ventricle of mice led to the formation of MBMs. Sodium fluorescein (green), a brain-impermeable dye, was injected intravenously via tail vein, and its uptake into metastatic lesions was measured and used as a marker of brain metastasis permeability. Only ~29% of the brain metastases were permeable to the administered dye (green clouds). B, mice harboring both permeable (green clouds) and impermeable (no clouds) brain metastases were randomized to vehicle or two PI3K inhibitors, GDC-0980, which is brain-impermeable, or GNE-317, which has demonstrated brain permeability. Both GDC-0980 and GNE-317 inhibited the growth of permeable metastases, while only the brain-permeable GNE-317 inhibited the growth and caused tumor apoptosis (white tumor cells with X) of impermeable metastases. These observations confirm a functional contribution of brain permeability to drug efficacy for brain metastases treatment (modified and redrawn from (Steeg et al., 2016)).

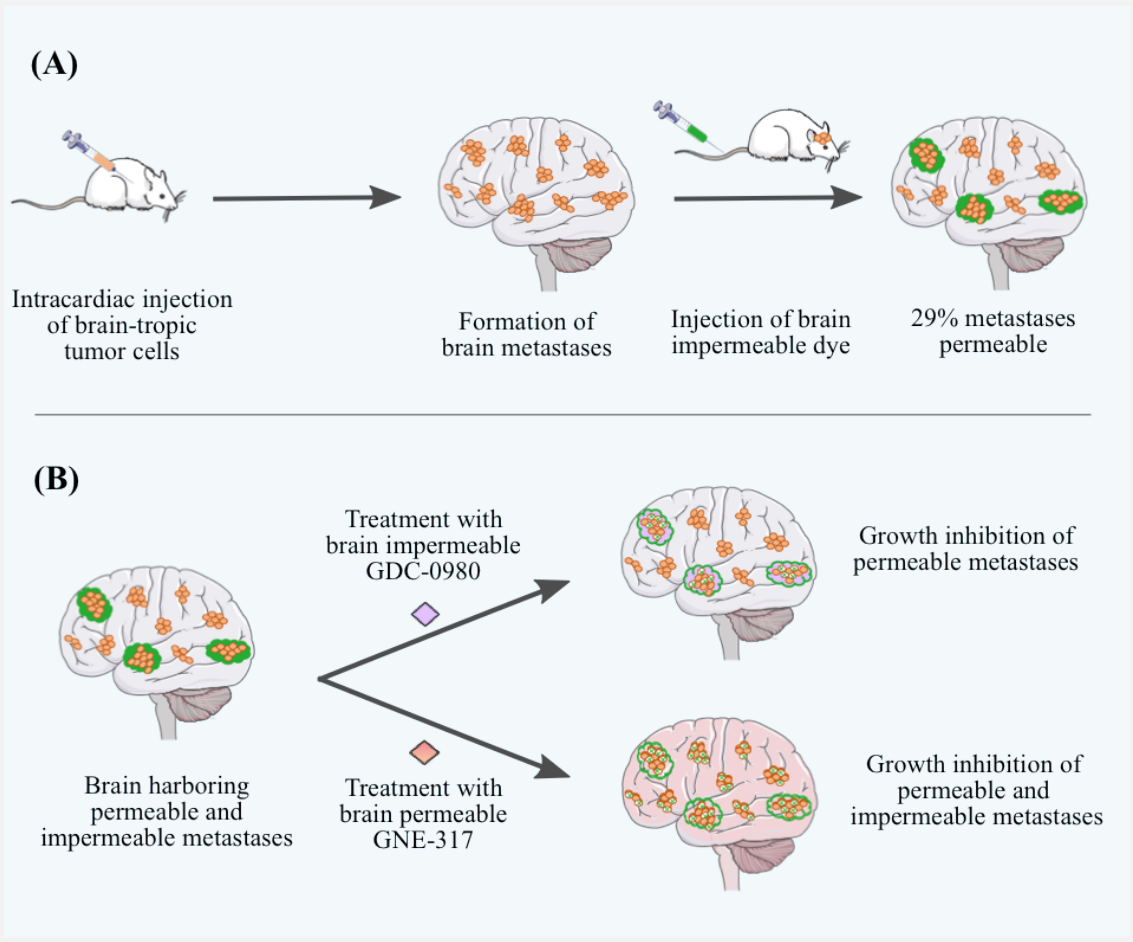
(A)
Intracardiac injection of brain-tropic tumor cells
Formation of brain metastases
Injection of brain impermeable dye
29% metastases permeable
(B)
Brain harboring permeable and impermeable metastases
Treatment with brain impermeable GDC-0980
Treatment with brain permeable GNE-317
Growth inhibition of permeable metastases
Growth inhibition of permeable and impermeable metastases

Figure 3. 6 GNE-317 targets micro-metastases and dormant tumor cells. A, Subgroup analysis of GNE-317 treated metastases, separately for non-permeable micro- (n=10) and macro-metastases (n=6) (***, P < 0.001 and *, P=0.033; two- sided t tests). B–E, Treatment response of single, long-term, non-proliferating and non-regressing, thus dormant, melanoma cells. The single cells are slowly moving during dormancy. After start of treatment with GNE-317 at D31 (C), the dormant cells regressed within 8 days (E) (adapted from (Osswald et al., 2016), with permission).

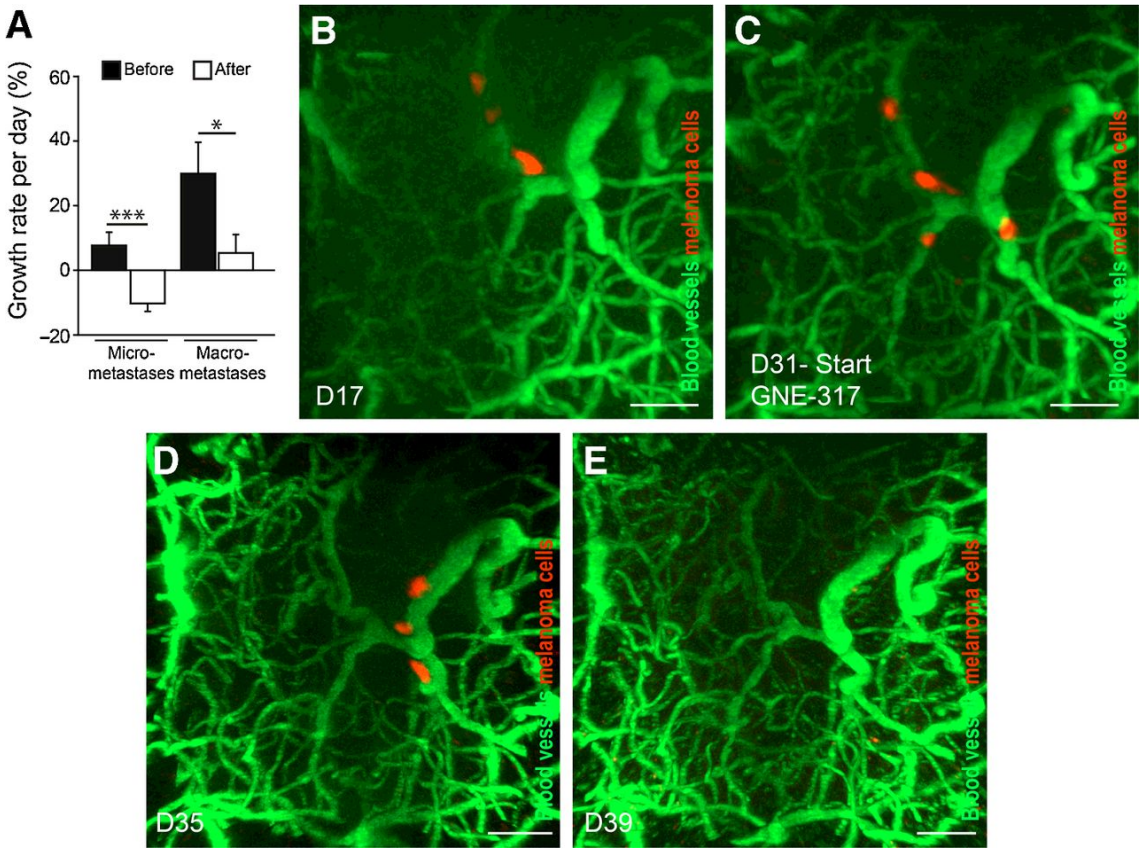

Figure 3. 7 3D reconstruction of (A) RAF265 (in green), (B) tumor (in purple) and ventricles (lateral ventricles in yellow, 3rd ventricle in light green, dorsal 3rd ventricle in orange, 4th ventricle in magenta) from optical images of H&E staining sections. Serial sections were collected with 30-50 μm intervals and imaged by mass spectrometer with 100 μm spatial resolution or microscope. 3D models were reconstructed using 3D Doctor (adapted from (Liu et al., 2013), with permission).

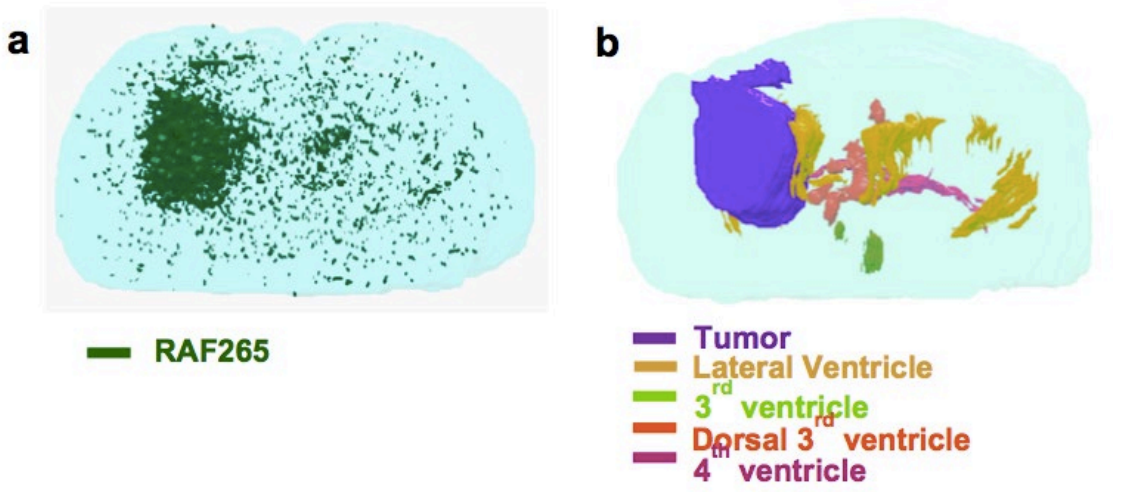

Figure 3. 8 A schematic representation of the quantitative MSI (qMSI) approach. Three serial sections isolated from non-tumor bearing normal brain specimens were used to create the qMSI image. One brain section was used to detect the alectinib distribution by MALDI-MSI, whereas the other two sections were used to quantify the amount of alectinib. The signal intensity of the images detected by MALDI-MSI was converted into the absolute quantity of alectinib found in the serial section (adapted from (Aikawa et al., 2016), with permission).

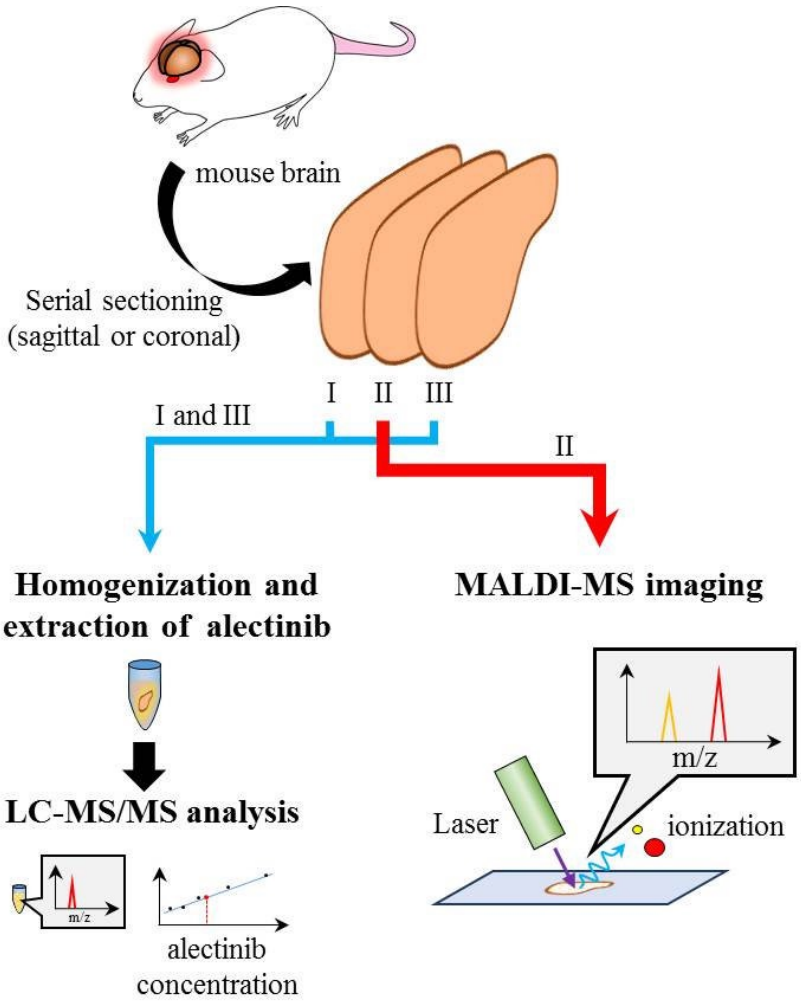

Figure 3. 9 Validation of the quantitative distribution of alectinib with qMSI by using laser microdissection technique. A, mouse brain sections isolated at 1 hour after administration of 20 mg/kg alectinib were used to confirm the quantitative alectinib distribution in the qMSI image (80 μm resolution) in FVB and MDR1$^{a/b}$ knockout mice. Laser microdissection was used to cut out eight separate regions (R1-R8) of additional brain sections, and alectinib in those tissue regions was quantified by LC-MS/MS. B, correlation between the amounts of alectinib measured from dissected R1-R8 regions and those determined from complementary R1-R8 regions of qMSI images was examined. FVB: blue, R1-R4; MDR1$^{a/b}$ knockout: red, R5-R8. (adapted from (Aikawa et al., 2016), with permission).

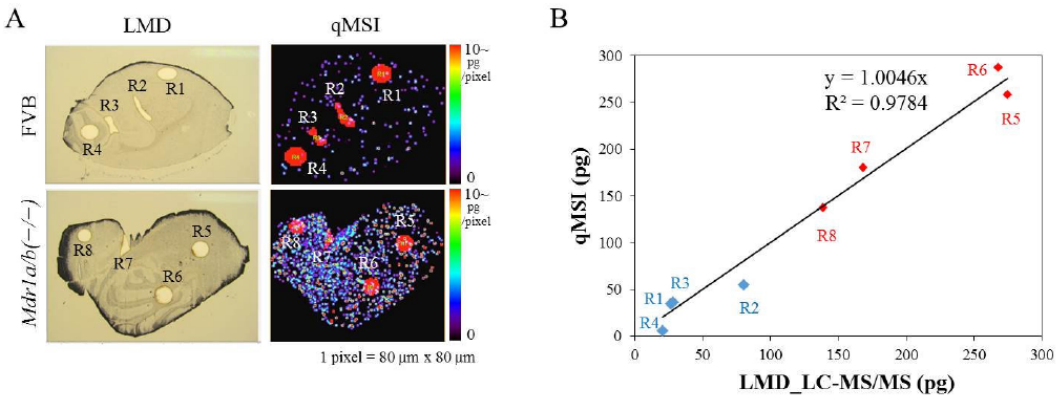

Figure 3. 10 Flow chart depicting the sequence of steps that need to be considered for the treatment of a patient with MBM. Some of the key limitations in the current practice are listed in dashed boxes, the answers to which can help in the advancement of the treatment of MBMs. The ultimate goal is to find a suitable targeted therapy that is not just palliative but can provide a cure to the debilitating MBM.

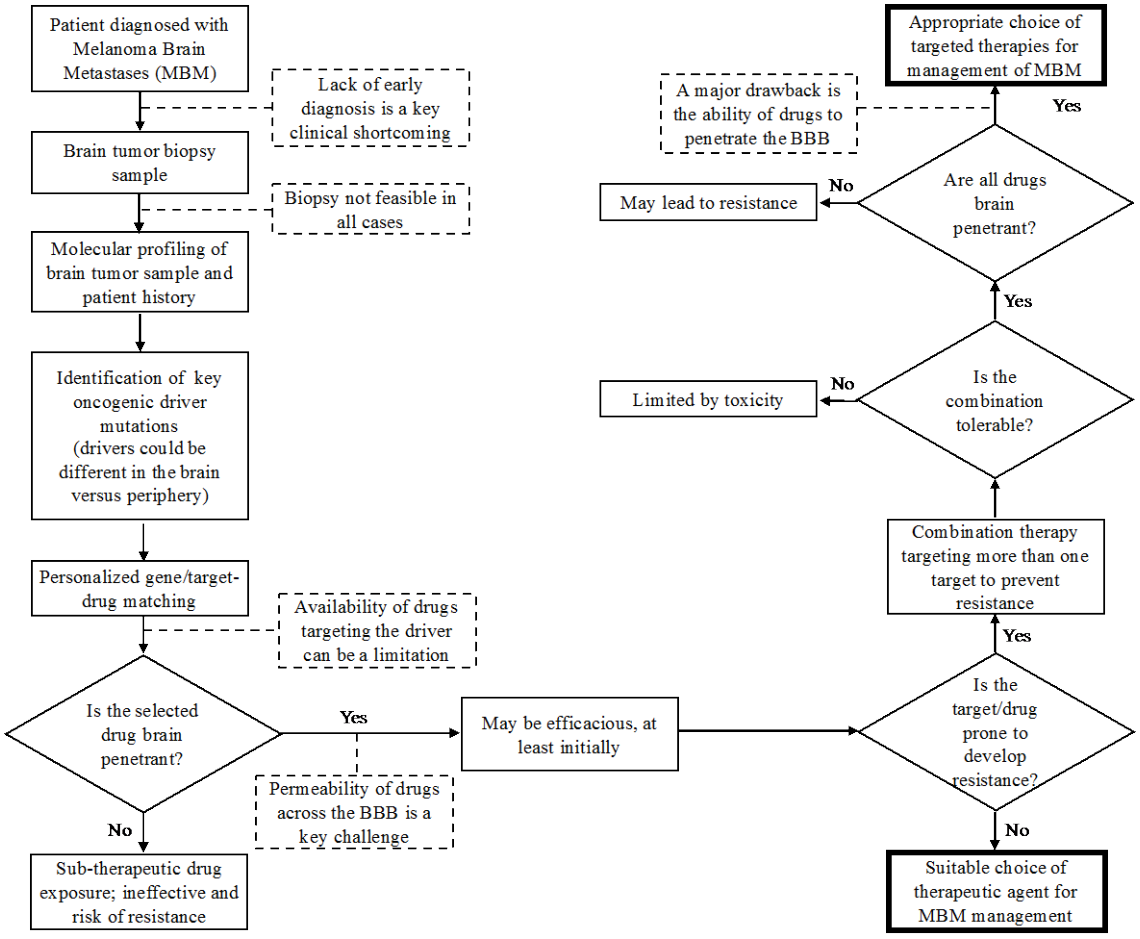

CHAPTER IV. QUANTITATIVE ASSESSMENT OF BRAIN DISTRIBUTION OF A KIF11 INHIBITOR AND SPATIAL HETEROGENEITY IN DELIVERY TO A MODEL OF GLIOBLASTOMA

ABSTRACT

Glioblastoma multiforme (GBM) is a malignant brain tumor characterized by rapid proliferation and extensive local invasion. KIF11 is a kinesin protein involved in both proliferation and invasion. Inhibition of KIF11 with potent molecularly-targeted agents, such as ispinesib, may be a suitable strategy for GBM treatment. However, many anti-cancer agents have a restricted brain delivery, mainly due to active efflux by P-gp and Bcrp at the BBB, and this can result in inadequate drug exposure at the site of action and poor response to therapy. The purpose of the current study was to examine aspects related to the brain delivery of ispinesib and understand how this may possibly impact efficacy. Brain distribution studies in non-tumor bearing FVB mice show that P-gp and Bcrp play a co-operative role in restricting the brain delivery of ispinesib. In vitro binding assays indicate that ispinesib is highly bound in both plasma and brain, and the Kp,uu in wild-type and *Mdr1a/b*$^{-/-}$ *Bcrp1*$^{-/-}$ mice were 0.02 and 1.01, respectively. The in vitro efficacy studies show that MGPP3 GBM cell line has low nanomolar sensitivity to ispinesib. A comparison of unbound concentrations with in vitro IC_{50} suggests that the unbound concentrations in brain do not reach the vitro IC_{50}. Furthermore, a regional heterogeneity in delivery was observed in a rat model of GBM, with a high Kp in the necrotic tumor core and a low Kp in the normal (non-tumor) brain. The Kp in the tumor rim was in-between that in tumor core and normal brain, suggesting a restricted delivery of ispinesib to the invasive edge of the tumor. Pharmacological inhibition of efflux transport by elacridar co-administration significantly enhanced the delivery of ispinesib to the brain, and the unbound concentrations in brain will likely achieve the in vitro cytotoxic

concentrations. Hence, devising approaches to overcome the drug delivery limitations is important to improve target engagement and responses. We intend to conduct subsequent studies in preclinical models of GBM to evaluate the in vivo efficacy of ispinesib and also test if enhancements in drug delivery will translate to improved efficacy in the treatment of GBM.

4.1 INTRODUCTION

Glioblastoma multiforme (GBM) is a type of brain cancer that accounts for nearly 47% of primary malignant brain tumors, and is associated with a dismal prognosis (Ostrom et al., 2017). GBMs are aggressive and lethal with high proliferative capacities (Mastronardi et al., 1999, Chiesa-Vottero et al., 2003, Stoyanov et al., 2017). Moreover, though GBM rarely spreads outside the CNS, the highly infiltrative nature and wide spread dissemination within the brain suggest that GBM is a disease of the whole-brain (Matsukado et al., 1961, Demuth and Berens, 2004, Cuddapah et al., 2014). To improve efficacy in GBM, an important consideration is to develop therapies that inhibit both (a) mitotic cell division necessary for tumor proliferation, as well as (b) cell motility needed for tumor cell dispersion (Venere et al., 2015). Consequently, treatments for GBM should ideally target both tumor cell proliferation and invasion, the characteristic hallmarks of GBM, and also have adequate brain penetration for target engagement at the site of action in the brain.

The microtubule-based cytoskeleton is involved in mitosis and cell motility, and several anti-mitotic agents targeting microtubules, including taxanes and vinca alkaloids, have been used in the treatment of non-CNS solid tumors (Wood et al., 2001). However, microtubules are vital for normal CNS function and dose-limiting neurotoxicity concerns are observed with the traditional anti-mitotic drugs (Wood et al., 2001, Canta et al., 2009). This has led to efforts directed at identifying cellular targets that are associated with microtubule function and have an essential role in mitosis, but lack neurotoxicity upon inhibition. One such group of microtubule-associated molecular motor proteins are

kinesins, which are involved in various stages of the mitotic cell division (Rath and Kozielski, 2012, Cross and McAinsh, 2014). KIF11 (kinesin-5, Eg5, HsEg5, KSP) is plus-end directed kinesin required for the separation of centrosomes in prophase and formation of bipolar spindle in metaphase of mitosis (Sarli and Giannis, 2008, Wojcik et al., 2013). KIF11 has been shown to be involved in cell motility (Falnikar et al., 2011, Wang and Lin, 2014). Venere et al., have shown that KIF11 is a driver of glioma cell division and motility, and targeting KIF11 with molecularly-targeted therapies inhibits both proliferation and invasion (Venere et al., 2015). Also, the expression of KIF11 is substantially low in non-proliferating cells relative to proliferating cells, and in normal cells compared to tumor cells (Hegde PS, 2003). Hence, KIF11 is an appealing target in GBM treatment.

Ispinesib (SB-715992) (Fig. 1) is the first KIF11 inhibitor to be tested clinically. Ispinesib alters the ability of KIF11 to bind to microtubules by locking the KIF11 motor in the ADP state due to inhibition of ADP release (Lad et al., 2008). Inhibition of KIF11 with potent targeted agents such as ispinesib suppresses proliferation of both tumor-initiating cell (TIC) and non-TIC populations. KIF11 inhibition by ispinesib also decreases glioma cell motility possibly due to altered microtubule lengthening in migrating tumor cells (Venere et al., 2015). The results of clinical studies testing ispinesib show no significant neurotoxicity concerns with ispinesib treatment (Blagden et al., 2008, Souid et al., 2010, Burris et al., 2011, Gomez et al., 2012). These observations suggest that targeted inhibition of KIF11 with ispinesib may be a viable strategy for the treatment of GBM.

The development of targeted therapies that can penetrate an intact blood-brain barrier (BBB) to reach the target tumor cells and elicit clinically meaningful responses has proven to be an exceedingly difficult task (Agarwal; Sane; et al., 2011, Gampa et al., 2017). Many small-molecule anti-cancer therapies are prone to active efflux at the BBB, particularly by p-glycoprotein (P-gp/Abcb1) and breast cancer resistance protein (Bcrp/Abcg2), and this can result in a severely limited drug distribution to the brain (Agarwal; Sane; et al., 2011, Gampa; Vaidhyanathan; Resman; et al., 2016). Although the BBB may be relatively compromised in certain regions of tumors, early non-contrast enhancing low-volume lesions and infiltrative tumor cells may be residing behind a functionally intact BBB, which can lead to inadequate drug delivery to these tumor cells and establishment of a pharmacological sanctuary (Jain et al., 2007, Osswald et al., 2016, Sarkaria et al., 2018). Thus, addressing the drug delivery challenge is crucial to improve clinical outcomes in patients with brain tumors such as GBM.

Ispinesib has a unique mechanism of action in that it hits both glioma cell proliferation and invasion. Also, GBM is a malignant brain tumor with a high proliferation index and so the fraction of cells undergoing mitotic cell division at any particular time is expected to be relatively high, which is important for KIF11 inhibitors to be effective. Given this, targeted inhibition of KIF11 with ispinesib may find a place in the treatment of GBM. However, an important consideration for efficacy in brain tumors is adequate brain drug exposure to elicit target engagement, especially at sites with a functionally intact BBB. Hence, we sought out to test this critical aspect. The objective of the current study is to evaluate the brain distribution of ispinesib and examine active efflux mechanisms that

may influence the delivery of ispinesib across the BBB, assess differences in drug delivery to regions of tumor and normal (non-tumor) brain in a rodent model of GBM, as well as compare that drug delivery with in vitro efficacy.

4.2 MATERIALS AND METHODS

4.2.1 Chemicals

Ispinesib, N-(3-aminopropyl)-N-[(1R)-1-(3-benzyl-7-chloro-4-oxoquinazolin-2-yl)-2-methylpropyl]-4-methylbenzamide, was purchased from Selleck Chemicals (Houston, TX). Elacridar [GF-120918, N-[4-[2-(6,7-dimethoxy-3,4-dihydro-1H-isoquinolin-2-yl)ethyl]phenyl]-5-methoxy-9-oxo-10H-acridine-4-carboxamide] was purchased from Toronto Research Chemicals Inc. (Ontario, Canada). Cell culture reagents were purchased from Invitrogen (Carlsbad, CA), and all other chemicals used were of high-performance-liquid-chromatography or reagent grade and were obtained from Sigma-Aldrich (St. Louis, MO).

4.2.2 In vitro assay for determination of unbound (free) fractions

The unbound fractions of ispinesib in plasma and brain were determined by performing rapid equilibrium dialysis (RED) experiments as per the protocol described by the manufacturer (Thermo Fisher Scientific), with some modifications suggested in the literature (Kalvass and Maurer, 2002, Friden et al., 2007). RED experiments for ispinesib were conducted at four concentrations (1, 2, 5 and 10 μM) and two time points (4 and 6 hr), and the results suggest that the unbound fractions were linear up to 2 μM concentration and equilibrium was achieved by 4 hours. Consequently, unbound fractions determined at 1 μM concentration and 4 hr time point were utilized for estimation of Kp,uu and free concentrations of ispinesib. A RED base plate (Thermo Fisher Scientific), and single-use RED inserts (Thermo Fisher Scientific) with a dialysis membrane having a

molecular weight cut off (MWCO) of 8 kDa were used in these experiments. In brief, the matrices used in these experiments comprised of fresh plasma and brain homogenates (prepared in 3 volumes of PBS, w/v) from FVB mice. Plasma and brain homogenate aliquots were spiked with 0.1 mg/mL ispinesib (in DMSO) to obtain final concentrations of 1 µM. 300 µL of 1 µM ispinesib spiked matrix was placed in sample chamber (donor), and 500 µL of phosphate buffered saline (1x PBS at pH 7.4; 100 mM sodium phosphate and 150 mM sodium chloride) was placed in buffer chamber (receiver) of RED inserts in triplicates. The inserts were placed in a base plate, assembly was covered with a sealing tape and incubated on a Bioshaker (MBR-022UP, Taitec Corporation) maintained at 37^{o}C and 1000 rpm for 4 hours. The samples collected from both the donor and receiver chambers after dialysis were stored at -80°C until subsequent LC-MS/MS analysis.

4.2.3 In vitro cytotoxicity assay

In vitro cytotoxicity testing of ispinesib was performed in two murine GBM cell lines, MGPP3 (PDGF overexpression, $p53^{-/-}$ and $PTEN^{-/-}$ double knockout, murine primary cell line) and GL261. Briefly, GBM cells were seeded into 96-well plates (pre-coated with fibronectin) at a density of 5,000 cells per well in DMEM media with 1% nitrogen supplement, 10 ng/ml of FGF and 10 ng/ml of PDGFAA. At 24 hours following plating (~70% confluency), the cells were exposed to different concentrations of ispinesib (n = 10 wells per concentration) ranging from 0.025 - 600 nM. The plates were incubated for 72 hours after treatment, and the cell viability was measured using a CellTiter-Glo ATP-based assay (Promega) read on a luminometer (Perkin-Elmer).

4.2.4 In vivo studies

Animals:

Friend leukemia virus strain B (FVB) wild-type (WT), P-gp knockout (*Mdr1a/b*$^{-/-}$, PKO, P-gp deficient), Bcrp knockout (*Bcrp1*$^{-/-}$, BKO, Bcrp deficient) and triple knockout (*Mdr1a/b*$^{-/-}$ *Bcrp1*$^{-/-}$, TKO, P-gp and Bcrp deficient) mice of either sex (balanced), were used in the in vivo pharmacokinetic studies using non-tumor-bearing animals (Taconic Farms, Germantown, NY). All mice used were 8-16 week-old adults, and approximately 15 - 35 g at the time of experiments. Mice were housed in a 12-hour light/dark cycle with unlimited access to food and water. All studies conducted were in agreement with the guidelines for the Care and Use of Laboratory Animals (National Institutes of Health, Bethesda, MD), and approved by Institutional Animal Care and Use Committee (IACUC) at University of Minnesota.

Sprague-Dawley rats, balanced for sex, were used for the in vivo pharmacokinetic studies that followed tumor implantation. All studies described were approved by the Institutional Animal Care and Use Committee at the Mayo Clinic, and conducted in accordance with the guidelines for the Care and Use of Laboratory Animals (National Institutes of Health, Bethesda, MD). Rats were housed in a standard 12-hour dark/light cycle with unlimited access to food and water.

Pharmacokinetics following intravenous and intraperitoneal administration of ispinesib:

All dosing solutions were prepared on the day of the study. In the intravenous study, a single intravenous dose of 5 mg/kg ispinesib (vehicle: ethanol, Tween 80 and distilled

water in the volume ratio of 20:2.5:77.5) was administered to FVB wild-type and *Mdr1a/b*$^{-/-}$ *Bcrp1*$^{-/-}$ mice. Blood and brain samples were collected at 0.17, 0.5, 1, 2, 4, 8 and 15 hours post-dose (n = 4 at each time point).

The brain distribution studies were also conducted in FVB wild-type, *Mdr1a/b*$^{-/-}$, *Bcrp1*$^{-/-}$, and *Mdr1a/b*$^{-/-}$ *Bcrp1*$^{-/-}$ mice following administration of a single dose of 10 mg/kg ispinesib via intraperitoneal (ip) route (microemulsion vehicle: Cremophor EL, Carbitol, Captex 355 and distilled water in a volume ratio of 20:10:3:67). Blood and brain samples were collected at 2 and 6 hours post dose (n = 4 per time point).

A serial sacrifice (destructive sampling) design was employed for sample collection in the pharmacokinetic studies. At the pre-determined sampling time points, mice were euthanized using a carbon dioxide chamber. Blood was collected by cardiac puncture and transferred to sample tubes coated with heparin. The whole brain was isolated from the skull and rinsed with ice-cold distilled water, and superficial meninges were removed by blotting with tissue paper. Plasma was separated by centrifugation of blood samples at 3500 rpm and 4°C for 15 minutes. The plasma and brain samples were stored at -80°C, until analysis for ispinesib concentrations by LC-MS/MS. Assuming a vascular volume of 1.4% in mouse brain (Dai et al., 2003), the concentrations in brain were corrected for residual drug in brain vasculature.

Brain distribution of ispinesib with and without co-administration of a pharmacological inhibitor of efflux transporters:

In another intraperitoneal dosing study, FVB wild-type mice received a single dose of 10 mg/kg ip ispinesib with or without simultaneous co-administration of 10 mg/kg ip

elacridar, a pharmacological inhibitor of P-gp and Bcrp (microemulsion vehicle). Blood and brain specimens were harvested at 2 and 6 hours post dose (n = 4 per time point). Plasma was obtained by centrifugation of whole blood samples at 3500 rpm and 4°C for 15 minutes. The samples were stored at -80°C until analysis by LC-MS/MS.

Spatial distribution of ispinesib in a rat model of GBM:

A rat model of GBM was utilized for the spatial drug distribution studies. The GBM tumors were induced by PDGF-IRES-tdTomato retroviral intracranial stereotactic injections in rat pups. The PDGF-IRES-tdTomato retrovirus was produced as described previously (Assanah et al., 2009). For intracranial injections, P4 (postnatal day 4) neonatal Sprague-Dawley rats were anesthetized by hypothermia. Briefly, each pup was carefully wrapped in several layers of gauze and placed in ice. Approximately after 12 minutes, the head was placed in a DKI 963 Stereotaxic Alignment Instrument (David Kopf Instruments). The bregma was identified, and a small hole was made in the skull with a sterile 18 gauge needle, 1 mm rostral and 2 mm to the right of the bregma. A 27-gauge Hamilton microsyringe was then inserted to a depth of 1.5 mm, and 1.5 µL of virus (titre: 1 x 10^6/mL) was injected slowly at a rate of 0.2 µL/min. The rats with GBM tumors were randomized to receive a single dose of 10 mg/kg ip ispinesib (microemulsion vehicle) with or without simultaneous co-administration of 10 mg/kg ip elacridar (microemulsion vehicle), on day 24 following intracranial injections. The blood and brain (tumor-bearing) samples were collected at 2 hours post dose (n = 9). The harvested whole brains were immediately flash frozen. Plasma was obtained by

centrifugation of blood samples at 3500 rpm and 4°C for 15 minutes. The brain and plasma samples were stored at -80°C until further processing.

A fluorescent microscopy based method was employed for the isolation of tumor core, tumor rim (brain adjacent to tumor, BAT) and normal (non-tumor) brain regions from the flash frozen brain samples. Briefly, an acrylic adult rat brain matrix (WPI) was used to obtain thick coronal brain sections that were 1-2 mm thick. A fluorescent microscope (Nikon AZ100M) was used to visualize the tdTomato labelled tumors in the brain slices. The borders of the core of the tumors were identified by relative fluorescence signal, and biospy punches (Harris Uni-Core, Miltex) with varying diameters were utilized to isolate the tumor core and tumor rim tissues. The tumor core was defined as the tumor region with a fluorescence signal that was 5-fold or higher relative to the background fluorescence signal observed in the normal brain. The tumor rim was identified as the region adjacent to the tumor core with a fluorescence signal 3 to 5-fold higher relative to the background fluorescence signal. The brain tissue away from the tumor with a similar or lower signal than the background fluorescence was collected as the normal brain specimen. The samples were stored at -80°C, and the concentrations of ispinesib in the tumor regions, brain and plasma samples were determined using LC-MS/MS.

4.2.5 LC-MS/MS analysis

The concentrations of ispinesib in samples from in vitro and in vivo experiments were determined using a sensitive LC-MS/MS assay. Uniform brain homogenate samples were obtained by addition of three volumes of 5% bovine serum albumin (BSA) to the brain specimens followed by homogenizing using a mechanical tissue homogenizer (PowerGen

125; Thermo Fisher Scientific, Waltham, MA). For analysis of unknowns, an aliquot of sample was spiked with 25 ng of dasatinib as the internal standard and liquid-liquid extraction was performed by addition of 1-2 volumes of pH 11 buffer and 5–10 volumes of ethyl acetate, followed by vigorous shaking for 5 minutes and centrifugation at 7500 rpm and 4°C for 5 minutes. The organic layer was collected in to microcentrifuge tubes and dried under nitrogen. The dried residue was reconstituted in 100 µL of mobile phase and transferred to high-performance liquid chromatography vials with disposable glass microinserts. The chromatographic analysis was performed on a AQUITY ultra performance liquid chromatography system (Waters, Milford, MA) with a Phenomenex Synergi 4 µ Polar-RP 80A column (75 x 2 mm; Torrance, CA). An isocratic method (55% A and 45% B) was used and the mobile phase (1 mM ammonium formate with 0.1% formic acid (A) and acetonitrile with 0.1% formic acid (B)) was delivered at a constant flow rate of 0.5 mL/min.

The column effluent was monitored using a Micromass Quattro Ultima mass spectrometer (Waters, Milford, MA). The instrument was equipped with an electrospray interface, and was controlled by the MassLynx (Version 4.1; Waters) data system. An electrospray probe in positive-ionization mode operating at a spray voltage of 4.62 kV was utilized. Samples were introduced into the interface through a heated probe with the source and desolvation temperatures set at 100°C and 350°C, respectively. The m/z transitions were 517.20 - 246.96 for ispinesib and 488.21 - 400.99 for dasatinib. The retention time was 2.48 minutes for ispinesib and 0.61 minutes for dasatinib. The runtime was 4 minutes.

4.2.6 Calculations

The unbound fractions (fu) in plasma and brain homogenate were calculated as the ratio of concentration of ispinesib in buffer to matrix (Kalvass and Maurer, 2002).

$$\text{fu, diluted} = \frac{\text{Drug concentration in buffer (receiver)}}{\text{Drug concentration in matrix (donor)}} \quad (Equation\ 1)$$

The unbound fraction in brain was estimated from the measured unbound fraction in diluted brain homogenate (fu,diluted), using the following equation (Kalvass and Maurer, 2002).

$$\text{fu, brain} = \frac{1/\text{D}}{(1/\text{fu, diluted} - 1) + 1/\text{D}} \quad (Equation\ 2)$$

where D (equal to 4) represents a dilution factor, accounting for the diluted brain homogenate.

The brain-to-plasma ratio (Kp) was calculated using the area under the concentration-time curve (AUC) or the concentrations (C), in plasma and brain.

$$\text{Kp} = \frac{\text{AUCbrain}}{\text{AUCplasma}} \quad (Equation\ 4)$$

$$\text{Kp} = \frac{\text{Cbrain}}{\text{Cplasma}} \quad (Equation\ 5)$$

A comparison of relative drug exposure in the brains of wild-type and knockout (*Mdr1a/b*$^{-/-}$, *Bcrp1*$^{-/-}$, *Mdr1a/b*$^{-/-}$ *Bcrp1*$^{-/-}$) mice were made using the distribution advantage (DA), which was expressed as the Kp in the strain under consideration normalized by the Kp in wild-type mice.

$$\text{DA} = \frac{\text{Kp}, knockout}{\text{Kp}, wild\ type} \quad (Equation\ 6)$$

The unbound partition coefficient (Kp,uu) was determined using the following equation.

$$\text{Kp, uu} = \frac{\text{AUCbrain x fu, brain}}{\text{AUCplasma x fu, plasma}} \quad (Equation\ 7)$$

The data from in vitro cytotoxicity experiments was fitted to "log(inhibitor) vs. normalized response - variable slope" equation using GraphPad Prism version 6.04 (GraphPad, La Jolla, CA) software to determine the half maximal inhibitory concentration (IC_{50}).

4.2.7 Pharmacokinetic data analysis

The pharmacokinetic parameters from the concentration-time profiles in plasma and brain were determined by non-compartmental analysis (NCA) using Phoenix WinNonlin version 6.4 (Certara USA, Inc., Princeton, NJ). The areas under the concentration-time curve (AUC) for plasma (AUC_{plasma}) and brain (AUC_{brain}) were calculated using the linear trapezoidal method. The standard errors around the means of AUC and Cmax were estimated by the sparse sampling module in WinNonlin (Nedelman and Jia, 1998).

4.2.8 Statistical analysis

GraphPad Prism version 6.04 (GraphPad, La Jolla, CA) software was employed for statistical analysis. The sample sizes used were based on previous work and were determined based on approximately 80% power to detect 50% difference between groups. Data from all experiments are represented as mean ± standard deviation (S.D.) or mean ± standard error of the mean (S.E.M), unless otherwise indicated. Comparisons between two groups were made using an unpaired t-test. Comparisons between multiple groups were made using one-way analysis of variance (ANOVA), followed by Bonferroni's

multiple comparison test. A significance level of $P < 0.05$ was used for all statistical testing.

4.3 RESULTS

4.3.1 Unbound (free) fractions of ispinesib in matrices of interest

In vitro rapid equilibrium dialysis experiments indicate that ispinesib exhibits high binding in both plasma and brain. The percent unbound fractions (equations 1 and 2) in plasma and brain are 0.6 ± 0.1 % and 0.05 ± 0.02 %, respectively. The unbound fractions in plasma and brain were used in the determination of unbound concentrations and unbound partition coefficients, Kp,uu, of ispinesib.

4.3.2 In vitro efficacy in GBM cell lines

The in vitro efficacy studies were performed in MGPP3 and GL261 murine GBM cell lines. GL261 cell line was not sensitive to ispinesib treatment even at high nanomolar concentrations. The IC_{50} for ispinesib was estimated from the observed dose-response curves in MGPP3 cell line. The dose-response curve for ispinesib in MGPP3 cells is shown in Fig. 2, and the estimated IC_{50} is 1.9 nM. The cells were cultured in serum-free media and as such minimal binding can be expected. The results suggest that MGPP3 cell line is highly sensitive to ispinesib treatment.

4.3.3 Brain distribution in FVB wild-type and transgenic mice

The pharmacokinetic profiles of ispinesib were determined in FVB wild-type and transporter deficient mice following intravenous and intraperitoneal drug administration. The plasma and brain concentration time profiles and brain-to-plasma ratios in FVB wild-type and *Mdr1a/b*$^{-/-}$ *Bcrp1*$^{-/-}$ mice following a single intravenous bolus dose of 5 mg/kg ispinesib are as shown in Fig. 3. The total brain concentrations at the indicated time

points are significantly lower than the total plasma concentrations in wild-type mice, and the resulting brain-to-plasma concentration ratios are less than one at all time points. In *Mdr1a/b*$^{-/-}$ *Bcrp1*$^{-/-}$ mice, the total brain concentrations at all the time points are significantly higher than that in wild-type mice, and the brain-to-plasma concentration ratios are higher than one at all time points. Table 1 summarizes the estimated pharmacokinetic parameters following intravenous drug administration in wild-type and *Mdr1a/b*$^{-/-}$ *Bcrp1*$^{-/-}$ mice. The brain-to-plasma AUC ratios (Kp, equation 4) for ispinesib in wild-type and *Mdr1a/b*$^{-/-}$ *Bcrp1*$^{-/-}$ mice are 0.23 and 12.12, respectively. The unbound partition coefficients (Kp,uu, equation 7) in wild-type and *Mdr1a/b*$^{-/-}$ *Bcrp1*$^{-/-}$ mice are 0.02 and 1.01, respectively.

The plasma and brain concentrations, and brain-to-plasma ratios in FVB wild-type, *Mdr1a/b*$^{-/-}$, *Bcrp1*$^{-/-}$ and *Mdr1a/b*$^{-/-}$ *Bcrp1*$^{-/-}$ mice at 2 and 6 hours post intraperitoneal administration of 10 mg/kg ispinesib are as shown in Fig. 4. The plasma concentrations were similar in the four genotypes of mice at both the time points. The brain concentrations are significantly higher in the TKO mice compared to wild-type mice. The brain-to-plasma concentration ratios at 2 hour time point in wild-type, *Bcrp1*$^{-/-}$, *Mdr1a/b*$^{-/-}$ and *Mdr1a/b*$^{-/-}$ *Bcrp1*$^{-/-}$ mice are 0.11, 0.08, 0.35 and 3.07, respectively (Table 2). The brain-to-plasma concentration ratios at 6 hour time point in wild-type, *Mdr1a/b*$^{-/-}$, *Bcrp1*$^{-/-}$ and *Mdr1a/b*$^{-/-}$ *Bcrp1*$^{-/-}$ mice are 0.16, 0.15, 1.52 and 5.20, respectively (Table 2).

4.3.4 Brain distribution of ispinesib with and without elacridar co-administration

The plasma concentrations, brain concentrations and brain-to-plasma ratios in FVB wild-type mice at 2 and 6 hours post intraperitoneal administration of 10 mg/kg ispinesib with

and without elacridar co-administration are as shown in Fig. 5. The plasma concentrations were similar in the 2 groups of mice at both the time points, while the brain concentrations are significantly higher in the group with elacridar co-administration. The corresponding brain-to-plasma concentration ratios of ispinesib at 2 and 6 hour time points are approximately 10-fold higher when elacridar was co-administered, suggesting that pharmacological inhibition of P-gp and Bcrp-mediated efflux by elacridar improves the brain distribution of ispinesib (Table 3).

4.3.5 Spatial distribution of ispinesib in a preclinical GBM model

The representative images of a brain slice and the isolated regions of interest, as well as the concentrations in plasma, tumor core, tumor rim and normal brain at 2 hours following a single intraperitoneal dose of 10 mg/kg ispinesib with or without elacridar co-administration are as shown in Fig. 6. The brain (tumor tissue)-to-plasma concentration ratios in tumor core, tumor rim and normal brain are also shown in Fig. 6. The observations indicate a heterogeneous distribution of ispinesib across the BBB in the rat model of GBM, with a higher drug accumulation in the tumor core and lower drug accumulation in the normal brain. The tumor rim had a Kp lower than that in the tumor core and higher than that in the normal brain (Table 4). These results suggest that the uptake of ispinesib is relatively restricted to the growing edge of the intracranial GBM tumor (tumor rim) when compared with the drug accumulation in the necrotic tumor core. The trend was similar in both the treatment groups. However, there was an approximately 10-fold increase in Kp in the tumor rim and normal brain regions and a 4-fold increase in Kp in the tumor core region when elacridar was co-administered with ispinesib (Table 4).

4.4 DISCUSSION

Proliferation and invasion are characteristic hallmarks of GBM. Targeted inhibition of both these processes is essential for treatments to be efficacious in GBM. KIF11 is a molecular motor protein that is involved in both these processes, and is a well-suited target for the treatment of GBM (Venere et al., 2015). Also, actively dividing tumors such as GBM are expected to have a high proportion of tumor cells undergoing mitotic cell division at any given time, and so inhibition of KIF11 will likely result in a high fractional cell kill that is important for efficacy. Ispinesib is a potent inhibitor of KIF11 and has been shown to impede both tumor cell proliferation and GBM cell motility. However, a prerequisite for efficacy is the exposure of an appropriate target to adequate concentrations of a potent inhibitor. Previous studies have shown that anti-cancer agents with a restricted brain delivery can have poor activity in brain tumors (Agarwal; Mittapalli; et al., 2012, Parrish; Pokorny; et al., 2015, Kim; Ma; et al., 2018). A key mechanism responsible for limiting the brain delivery of several targeted agents is P-gp and Bcrp-mediated active efflux at the BBB. In the current study, we have examined the brain distribution and active efflux liability of ispinesib, as well as differences in site-specific distribution in a rodent model of GBM.

In vivo pharmacokinetic studies following intravenous dosing in FVB mice show that the brain distribution of ispinesib is limited by active efflux at the BBB. The brain-to-plasma AUC ratio in FVB mice deficient in P-gp and Bcrp was about 50-fold higher than that observed in the wild-type mice (Table 1). Another set of studies examined the brain distribution of ispinesib at 2 and 6 hour post 10 mg/kg intraperitoneal administration of

ispinesib in wild-type or transporter knockout FVB mice. The brain partitioning was about 30-fold higher in *Mdr1a/b*$^{-/-}$ *Bcrp1*$^{-/-}$ mice when compared to wild-type mice at both the time points. There was an increase in Kp by 3 and 10-fold in *Mdr1a/b*$^{-/-}$ mice and the Kp was similar in *Bcrp1*$^{-/-}$ mice when compared to the wild-type mice, at 2 and 6 hour time points, respectively (Fig. 4, Table 2). These results indicate a co-operative role of P-gp and Bcrp in limiting the brain distribution of ispinesib.

In another intraperitoneal dosing study, the influence of simultaneous administration of elacridar, a pharmacological inhibitor of P-gp and Bcrp, on the brain delivery of ispinesib was assessed at 2 and 6 hour time points. The brain concentrations of ispinesib were significantly higher in the co-administered group compared to the ispinesb only group, and there was a corresponding increase in Kp by about 10-fold at both the time points in the co-dosed group (Fig. 5, Table 3). These observations demonstrate that co-administration of elacridar significantly improves the delivery of ispinesib to the brain.

The in vitro cytotoxicity studies show that the MGPP3 (PDGF overexpression, p53$^{-/-}$ and PTEN$^{-/-}$ double knockout) GBM cell line is sensitive to ispinesib, with a low nanomolar IC_{50} of 1.9 nM (Fig. 2). On the other hand, GL261 was not sensitivity to ispinesib treatment even at high nanomolar concentrations. Hence, we have used the IC_{50} in MGPP3 cells for comparisons with in vivo concentrations of ispinesib. The rapid equilibrium dialysis experiments show that ispinesib has a high binding in both plasma and brain. The unbound (free) fractions and the Kp from the in vivo studies following 5 mg/kg intravenous dosing of ispinesib were used to estimate the unbound partition coefficient i.e., the Kp,uu. The Kp,uu in wild-type and *Mdr1a/b*$^{-/-}$ *Bcrp1*$^{-/-}$ mice was 0.02

and 1.01, respectively (Table 1). Furthermore, the unbound concentration-time profile for ispinesib in plasma and brain was predicted using the total concentrations in wild-type mice and the unbound fractions from rapid equilibrium dialysis experiments, and was compared with the IC_{50} in MGPP3 GBM cells (Fig. 7). The results suggest that the unbound concentrations of ispinesib in brain in wild-type mice will be lower than the in vitro cytotoxic concentrations (IC_{50}). However, the unbound concentrations of ispinesib in the brain will reach levels just about the IC_{50} if there is a 10-fold increase in concentrations as seen with elacridar co-administration, suggesting that improved brain delivery due to pharmacological inhibition of efflux transport can result in possibly enhanced in vivo efficacy.

In the clinic, contrast enhanced-MRI (CE-MRI) is typically used for the diagnosis of brain tumors. Such a technique relies on the accumulation of a hydrophilic (gadolinium based) contrast agent within tumor locations that have a relatively leaky BBB (Sarkaria et al., 2018). As a consequence, the bulk of the tumor i.e., the necrotic tumor core is identified as the tumor region and removed by surgical debulking. However, the regions surrounding the resection area (tumor rim) and certain infiltrative tumor sites can have invasive tumor cells residing behind an intact BBB, and escape detection by CE-MRI (Sarkaria et al., 2018). Therefore, it is important that therapeutic agents intended for the treatment of GBM penetrate an intact BBB to reach these protected sites, as any tumor cells that are left behind can cause treatment failure. Given this, we sought to perform a quantitative assessment of site-differential distribution of ispinesib to tumor core, tumor rim (brain adjacent to tumor, BAT) and normal (non-tumor) brain regions in a rat model

of GBM (Fig. 6, Table 4). The results demonstrate that the Kp in normal brain (Kp = 0.11 ± 0.09 for ispinesib group, Kp = 1.21 ± 0.71 for ispinesib and elacridar group) was consistent with the Kp observed in pharmacokinetic studies performed in non-tumor bearing FVB mice at the 2 hour time point (Kp = 0.10 ± 0.08 for ispinesib group, Kp = 0.80 ± 0.37 for ispinesib and elacridar group). Of translational implications is the observation that the delivery of ispinesib was variable across the 3 regions, with the Kp being highest in the tumor core and lowest in the normal brain. The Kp in the tumor rim was in-between that in tumor core and normal brain, suggesting a restricted delivery of ispinesib to the growing edge of the tumor compared to the necrotic tumor core. Such a limited drug exposure to the invasive tumor cells remaining after surgical resection can result in lack of efficacy, and so devising strategies to enhance the delivery of ispinesib may be necessary. While the trend in the regional distribution of ispinesib was similar, the delivery of ispinesib was significantly improved when elacridar was co-administered with ispinesib in tumor regions as well as the normal brain (Table 3, Table 4). Such improved delivery will likely result in higher exposure not only in the necrotic tumor core but also more importantly in the invasive edge of the tumor, and may translate to superior treatment outcomes. Consequently, we are planning to conduct preclinical efficacy studies with ispinesib and also evaluate if the improved delivery with elacridar co-administration will result in enhanced efficacy in GBM.

In summary, the delivery of ispinesib is limited by active efflux at the BBB. The delivery of drugs with a poor BBB penetration, such as ispinesib, can be particularly restricted at the growing edge of the tumor that can contain invasive tumor cells protected by an intact

BBB, and this can result in lack of activity. Devising strategies to overcome the drug delivery challenge is important for enhanced target engagement at the site of action in the brain. Modulation of efflux transport function by elacridar co-administration resulted in improved brain delivery of ispinesib, and the unbound concentrations in the brain will likely reach levels around the cytotoxic concentrations. Future preclinical efficacy testing in animal models of GBM will reveal if the improved exposure will translate to superior efficacy. The ideal approach to overcome the drug delivery challenges is to use structure-guided drug design to develop compounds that are brain permeable and have minimal or no interaction with efflux transporters expressed at the BBB. The greater exposures in the brain achieved with brain penetrant inhibitors, similar to brain exposure of ispinesib in mice lacking efflux transporters, will likely lead to improved treatment responses. Therefore, future drug development endeavors should focus on designing targeted agents that are capable of penetrating an intact BBB to achieve superior treatment outcomes in CNS diseases.

ACKNOWLEDGEMENTS

The authors thank Jim Fisher, Clinical Pharmacology Analytical Laboratory, University of Minnesota, for his support in the development of the LC-MS/MS assays.

FOOTNOTES

This work was supported by the National Institutes of Health [Grant RO1-NS073610]. Gautham Gampa was supported by the Ronald J. Sawchuk Fellowship in Pharmacokinetics and University of Minnesota Doctoral Dissertation Fellowship (DDF).

TABLES

Table 4. 1 The pharmacokinetic parameters of ispinesib in FVB wild-type and *Mdr1a/b*$^{-/-}$ *Bcrp1*$^{-/-}$ mice following administration of single intravenous dose of 5 mg/kg. Data are presented as mean or mean ± S.E.M (n = 4).

	Wild-type		***Mdr1a/b*$^{-/-}$ *Bcrp1*$^{-/-}$**	
	Plasma	**Brain**	**Plasma**	**Brain**
Half-life (h)	4.80	4.38	6.80	9.01
$AUC_{(0-t)}$ (µg*h/mL)	7.47 ± 0.44	1.79 ± 0.19	4.66 ± 0.26	47.57 ± 3.70
$AUC_{(0-\infty)}$ (µg*h/mL)	8.40	1.96	5.83	70.69
CL (mL/min/kg)	9.91	-	14.28	-
Vd (L/kg)	4.12	-	8.38	-
Kp ($AUC_{(0-\infty)}$ ratio)	-	0.23	-	12.12
Kp,uu ($AUC_{(0-\infty)}$ ratio)	-	0.02	-	1.01
DA	-	1	-	53

$AUC_{(0-t)}$, area under the curve from zero to the time of last measured concentration
CL, clearance
Vd, volume of distribution
Kp (AUC ratio), the ratio of $AUC_{(0-t,brain)}$ to $AUC_{(0-t,plasma)}$ using total drug concentrations
Kp,uu (AUC ratio), the ratio of $AUC_{(0-t,brain)}$ to $AUC_{(0-t,plasma)}$ using free drug concentrations
DA (Distribution advantage), the ratio of $Kp_{knockout}$ to $Kp_{wild-type}$

Table 4. 2 Brain distribution in FVB wild-type, *Bcrp1*$^{-/-}$, *Mdr1a/b*$^{-/-}$ and *Mdr1a/b*$^{-/-}$ *Bcrp1*$^{-/-}$ mice following a single dose of 10 mg/kg i.p. ispinesib. Data are presented as mean or mean ± S.D.

Time	Strain	C_{plasma} (µg/mL)	C_{brain} (µg/mL)	Kp brain	Distribution advantage
2 hours	Wild-type	1.61 ± 0.72	0.18 ± 0.09	0.11 ± 0.005	1
	Bcrp1a/b$^{-/-}$	1.74 ± 0.42	0.14 ± 0.02	0.08 ± 0.02	1
	Mdr1a/b$^{-/-}$	1.75 ± 0.73	0.58 ± 0.14	0.35 ± 0.08	3
	Mdr1a/b$^{-/-}$ Bcrp1a/b$^{-/-}$	1.59 ± 1.07	3.77 ± 0.67	3.07 ± 1.69	28
6 hours	Wild-type	0.87 ± 0.54	0.14 ± 0.08	0.16 ± 0.03	1
	Bcrp1a/b$^{-/-}$	1.06 ± 0.40	0.15 ± 0.03	0.15 ± 0.05	1
	Mdr1a/b$^{-/-}$	0.87 ± 0.54	1.10 ± 0.10	1.52 ± 0.56	10
	Mdr1a/b$^{-/-}$ Bcrp1a/b$^{-/-}$	1.03 ± 0.21	5.59 ± 2.85	5.20 ± 1.94	33

Kp brain, the ratio of C_{brain} to C_{plasma} using total drug concentrations
Distribution advantage, the ratio of Kp to $Kp_{wild-type}$

Table 4. 3 Brain distribution of ispinesib in FVB wild-type mice following administration of 10 mg/kg i.p. ispinesib with or without 10 mg/kg i.p. elacridar co-administration. Data are presented as mean or mean ± S.D.

Time	Treatment	C_{plasma} (µg/mL)	C_{brain} (µg/mL)	Kp brain	Fold increase in Kp
2 hours	Ispinesib	1.11 ± 0.57	0.08 ± 0.02	0.10 ± 0.08	1
	Ispinesib + elacridar	0.72 ± 0.39	0.51 ± 0.36	0.80 ± 0.37	8
6 hours	Ispinesib	0.73 ± 0.11	0.27 ± 0.09	0.38 ± 0.14	1
	Ispinesib + elacridar	0.79 ± 0.43	2.27 ± 0.77	3.66 ± 2.64	10

Kp brain, the ratio of C_{brain} to C_{plasma} using total drug concentrations

Table 4. 4 Spatial distribution of ispinesib in a preclinical model of GBM at 2 hours following administration of 10 mg/kg ispinesib i.p. with or without 10 mg/kg i.p. elacridar co-administration. Data are presented as mean or mean ± S.D.

Treatment	Region	C_{brain} (µg/mL)	Kp brain	Fold increase in Kp[1]
Ispinesib	Normal brain	0.06 ± 0.04	0.11 ± 0.09	1
	Tumor rim	0.15 ± 0.11	0.27 ± 0.18	2.5
	Tumor core	0.38 ± 0.24	0.77 ± 0.55	7
Ispinesib + elacridar	Normal brain	0.52 ± 0.46	1.21 ± 0.71	11
	Tumor rim	0.76 ± 0.48	2.31 ± 1.25	21
	Tumor core	1.03 ± 0.42	3.08 ± 1.15	28

Kp brain, the ratio of C_{brain} to C_{plasma} using total drug concentrations
[1] compared to Kp in normal brain of ispinesib treatment group

FIGURES

Figure 4. 1 Chemical structure of ispinesib.

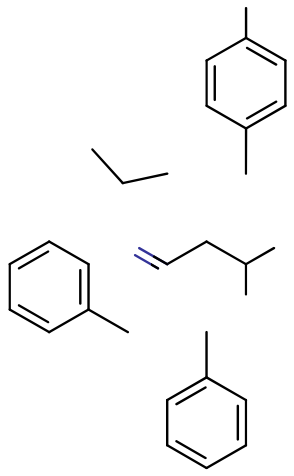

Figure 4. 2 In vitro efficacy of ispinesib in MGPP3 GBM cell line with IC_{50} estimate. Data represent the mean ± S.D.; n = 10 for all data points.

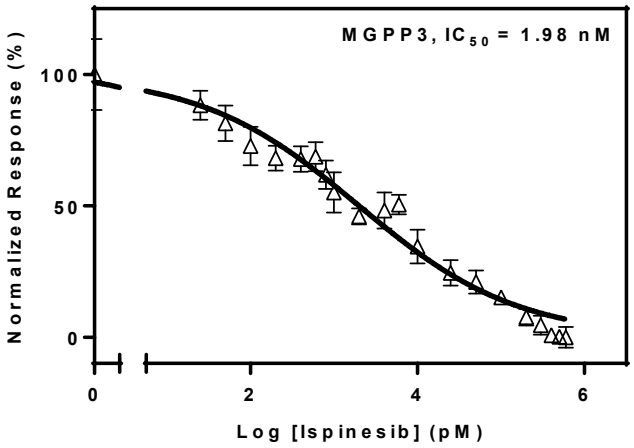

Figure 4. 3 Pharmacokinetic profiles of ispinesib in FVB wild-type and *Mdr1a/b*$^{-/-}$ *Bcrp1*$^{-/-}$ mice following intravenous (i.v.) dosing. Plasma concentrations (A), brain concentrations (B), and brain-to-plasma concentration ratios (C) of ispinesib following administration of single i.v. bolus dose of 5 mg/kg. Data represent mean ± S.D., n = 4.

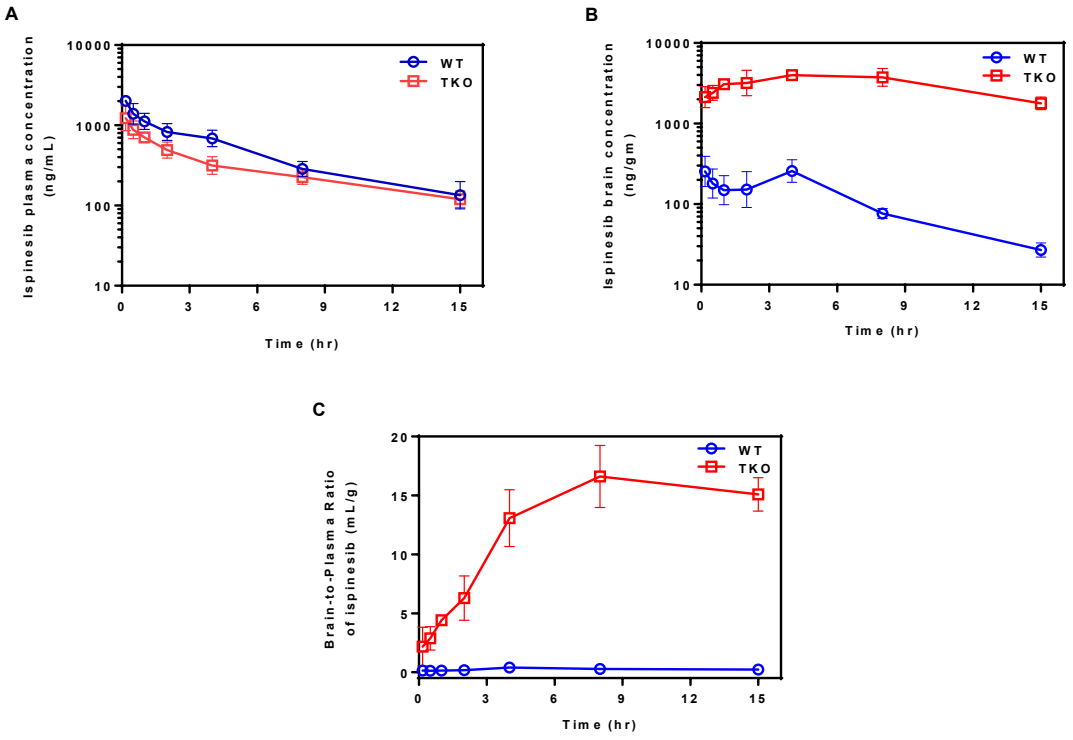

Figure 4. 4 Brain distribution of ispinesib following intraperitoneal (i.p.) administration in FVB wild-type, *Bcrp1*$^{-/-}$, *Mdr1a/b*$^{-/-}$ and *Mdr1a/b*$^{-/-}$ *Bcrp1*$^{-/-}$mice. Plasma concentrations (A), brain concentrations (B), and brain-to-plasma concentration ratios (C) at 2 and 6 hours following administration of single i.p. dose of 10 mg/kg ispinesib. **P< 0.01, ***P< 0.001 and ****P< 0.0001 when compared to the wild-type (WT) groups, for statistical testing by one-way ANOVA. Data represent mean ± S.D., n = 4.

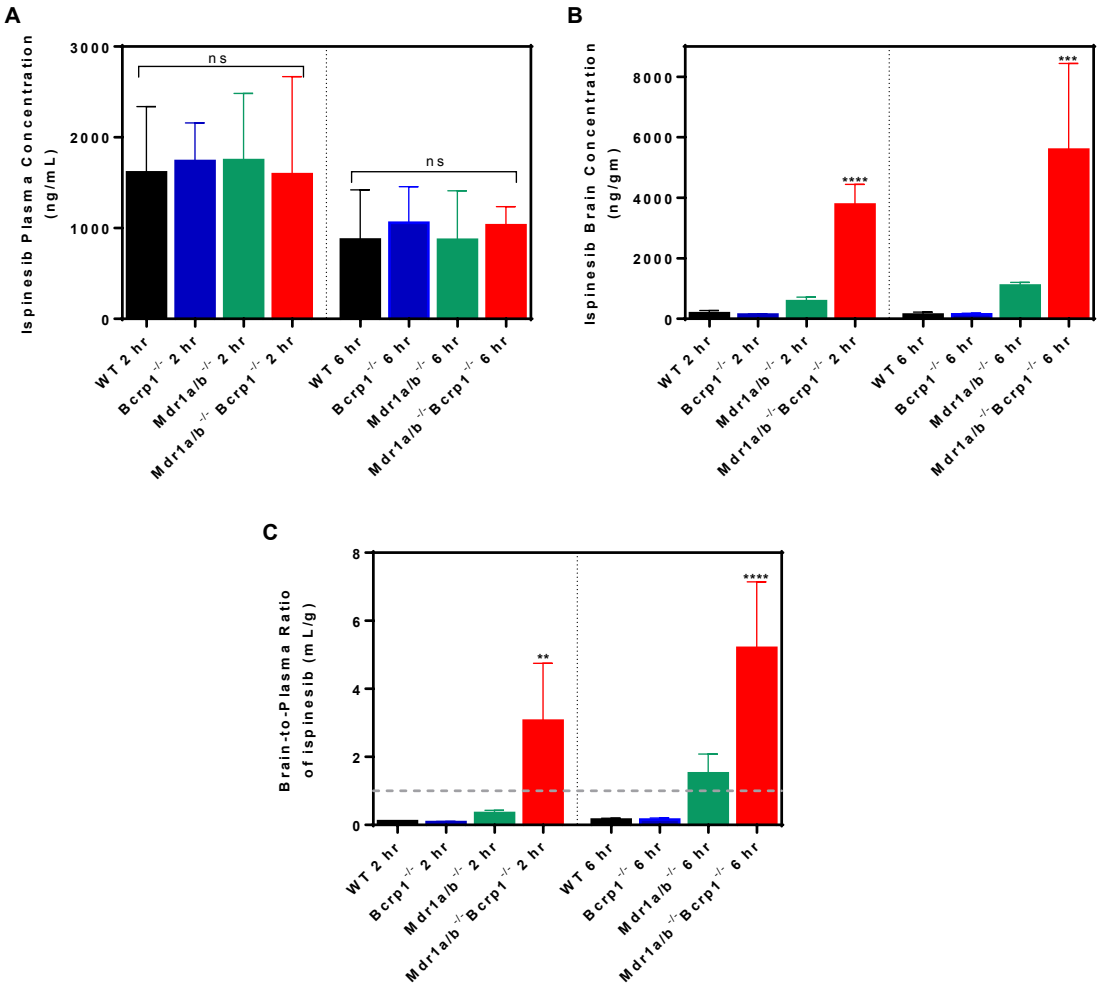

Figure 4. 5 Brain distribution of ispinesib (isp) in FVB wild-type mice with elacridar (elac) co-administration. Plasma concentrations (A), brain concentrations (B), and brain-to-plasma concentration ratios (C) of ispinesib at 2 and 6 hours following administration of ispinesib 10 mg/kg i.p. with or without simultaneous co-administration of 10 mg/kg i.p elacridar. *P< 0.05 and **P< 0.01 for statistical comparison by unpaired t-test. Data represent mean ± S.D., n = 4.

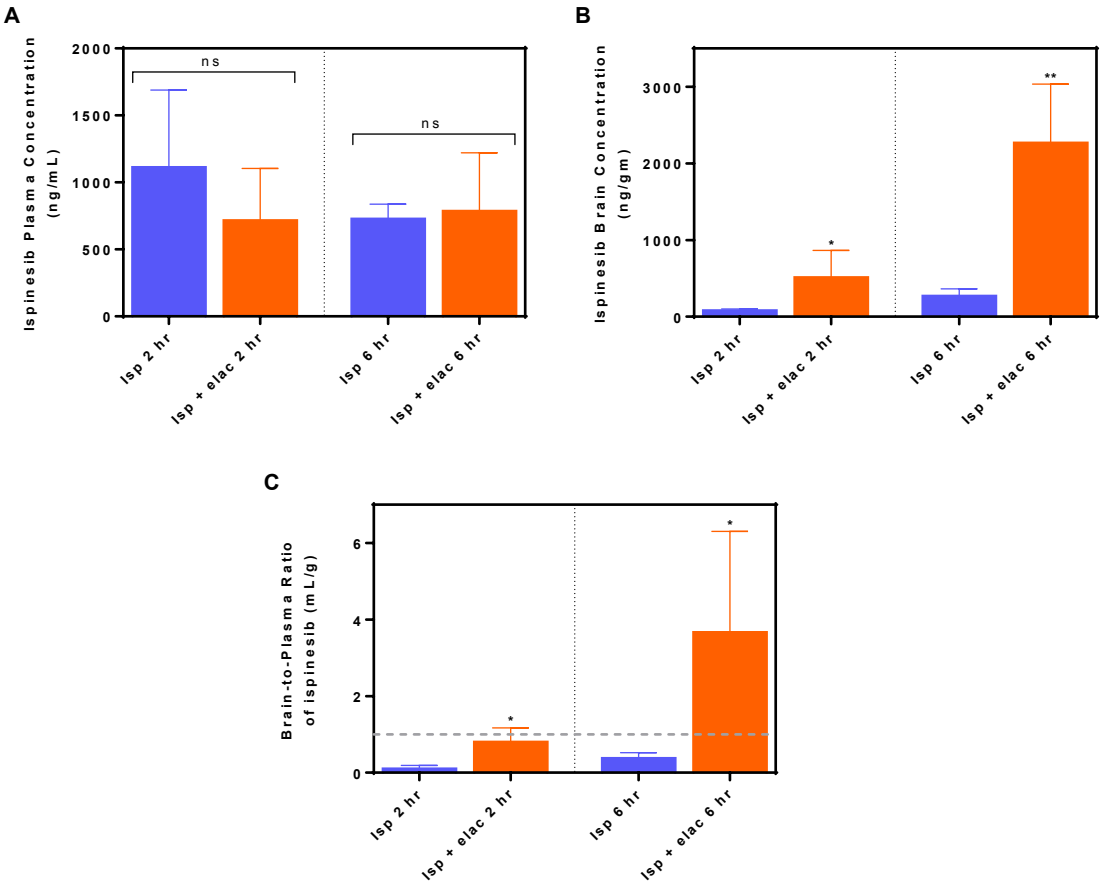

Figure 4. 6 Spatial brain distribution of ispinesib in a rat model of GBM. The figure shows representative images of a brain slice marked with the tumor core and tumor rim regions (A), and the dissected tissues (B). Also shown in the figure are bar graphs representing the concentrations (C) and brain(tumor)-to-plasma concentration ratios (D) in plasma, regions of tumor and normal brain at 2 hours following administration of ispinesib 10 mg/kg i.p. with or without simultaneous co-administration of 10 mg/kg i.p elacridar. The concentrations are significantly different in ispinesib and elacridar co-dosed group compared to ispinesib group for normal brain ($P<0.05$), tumor rim ($P<0.01$), and tumor core ($P<0.01$), statistical comparison by unpaired t-test. The brain(tumor)-to-plasma ratios are significantly different in ispinesib and elacridar co-dosed group compared to ispinesib group for normal brain ($P<0.001$), tumor rim ($P<0.01$), and tumor core ($P<0.01$), statistical comparison by unpaired t-test. *P< 0.05, **P< 0.01 and ***P< 0.001 for statistical comparison by one-way ANOVA. Data represent mean ± S.D., n = 9.

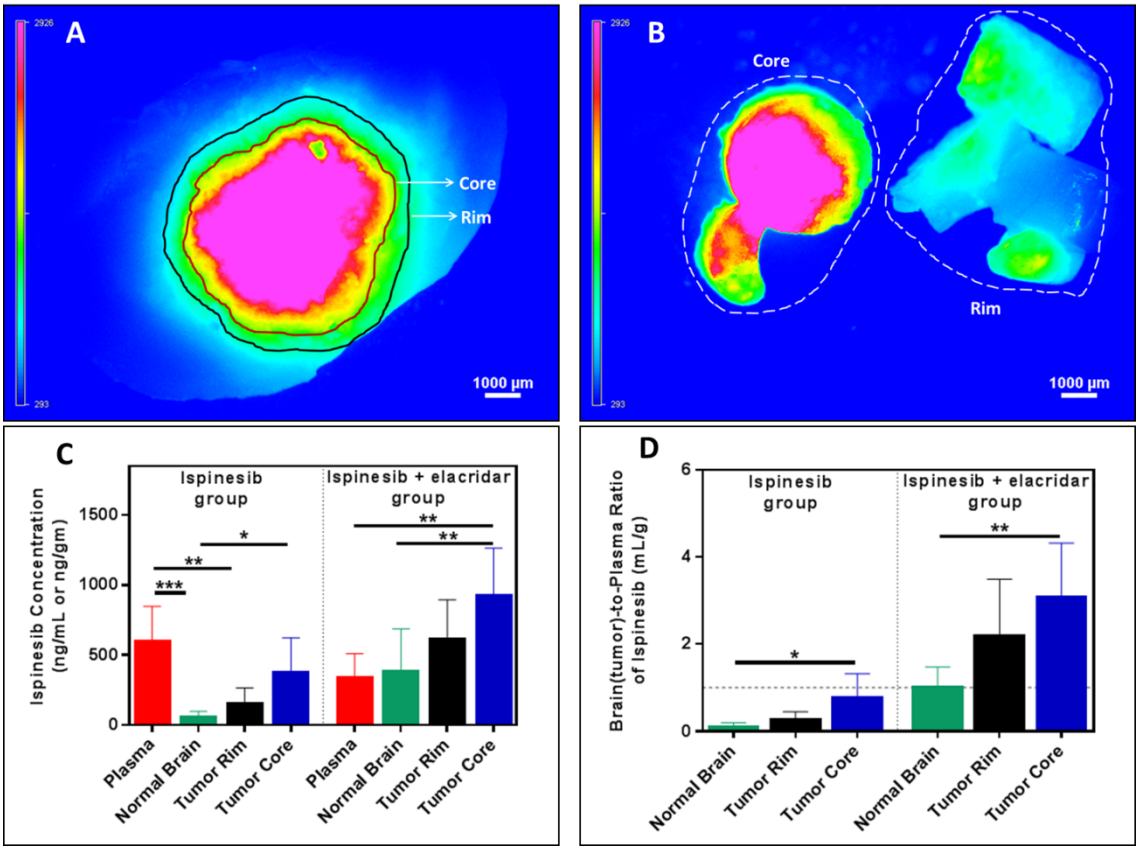

Figure 4. 7 Plasma and brain unbound concentration-time profiles of ispinesib in FVB wild-type mice following 5 mg/kg intravenous drug administration. The predicted unbound concentration profiles in brain in wild-type mice (A), with a 10-fold increase in brain concentrations as with elacridar co-administration (B), and with a 50-fold increase in brain concentrations as in P-gp and Bcrp deficient mice (C). The unbound concentrations were determined using the in vivo concentrations and the unbound fraction (fu) estimates from in vitro rapid equilibrium dialysis studies. The dashed lines represent the experimentally determined in vitro IC_{50} against MGPP3 GBM cell line. Data represent mean ± S.D., n = 4.

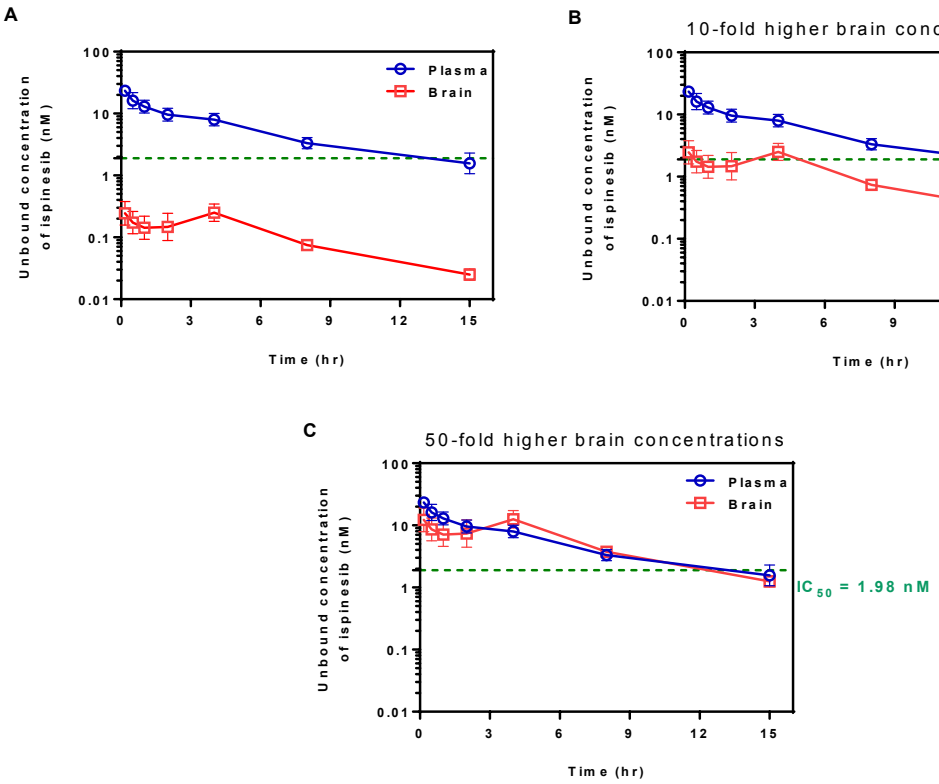

CHAPTER V. BRAIN DISTRIBUTION AND ACTIVE EFFLUX OF THREE PANRAF INHIBITORS: CONSIDERATIONS IN THE TREATMENT OF MELANOMA BRAIN METASTASES

The contents of this chapter have been published in:

Gampa G et al. (2019) Brain distribution and active efflux of three panRAF inhibitors: considerations in the treatment of melanoma brain metastases. Journal of Pharmacology and Experimental Therapeutics DOI: https://doi.org/10.1124/jpet.118.253708.

ABSTRACT

Targeted inhibition of RAF and MEK by molecularly-targeted agents has been employed as a strategy to block aberrant MAPK signaling in melanoma. While the use of BRAF and MEK inhibitors, either as a single agent or in combination, improved efficacy in BRAF-mutant melanoma, initial responses are often followed by relapse due to acquired resistance. Moreover, some BRAF inhibitors are associated with a paradoxical activation of the MAPK pathway, causing the development of secondary malignancies. The use of panRAF inhibitors, i.e., those that target all isoforms of RAF, may overcome paradoxical activation and resistance. The purpose of this study was to perform a quantitative assessment and evaluation of the influence of efflux mechanisms at the BBB in particular, Abcb1/P-gp and Abcg2/Bcrp, on the brain distribution of three panRAF inhibitors: CCT196969, LY3009120 and MLN2480. In vitro studies using transfected MDCKII cells indicate that only LY3009120 and MLN2480 are substrates of Bcrp, and none of the three inhibitors are substrates of P-gp. The three panRAF inhibitors show high non-specific binding in brain and plasma. In vivo studies in mice show that the brain distribution of CCT196969, LY3009120 and MLN2480 is limited, and is enhanced in transgenic mice lacking P-gp and Bcrp. While MLN2480 has a higher brain distribution, LY3009120 exhibits superior in vitro efficacy in patient-derived melanoma cell lines. The delivery of a drug to the site of action residing behind a functionally intact BBB along with drug potency against the target, collectively play a critical role in determining in vivo efficacy outcomes.

5.1 INTRODUCTION

Deregulated signaling of the mitogen-activated protein kinase (MAPK) pathway is commonly associated with melanomas, and often occurs due to activating mutations in BRAF (~50%) and NRAS (~20%) (Davies et al., 2002, Hocker and Tsao, 2007, Hodis et al., 2012). Inhibition of MAPK signaling by targeting RAF and MEK has been recognized as an important treatment strategy in BRAF-mutant melanomas (Samatar and Poulikakos, 2014). The improved clinical outcomes with BRAF and MEK inhibitors, either as single agents or in combination, has led to the FDA approval of BRAF inhibitors, vemurafenib, dabrafenib, encorafenib, and MEK inhibitors, cobimetinib, trametinib, binimetinib (Chapman et al., 2011, Flaherty; Infante; et al., 2012, Flaherty; Robert; et al., 2012, Long et al., 2014, Larkin et al., 2014, Ascierto et al., 2013, Delord et al., 2017, Dummer et al., 2018, Dummer et al., 2017).

A persistent clinical challenge in the management of BRAF-mutant melanomas is resistance to BRAF inhibitor therapy, both intrinsic and acquired (Shi et al., 2014, Samatar and Poulikakos, 2014). One approach to overcome resistance is combination therapy with BRAF and MEK inhibitors, causing a vertical blockade of the MAPK pathway at two central nodes. Though such combinations have improved clinical responses, patients still progress due to therapeutic resistance (Wagle et al., 2014, Welsh et al., 2016). Multiple mechanisms of acquired resistance have been identified, and reactivation of the MAPK pathway by acquisition of secondary mutations, such as mutations in RAS, is a common resistance mechanism (Shi et al., 2014, Welsh et al., 2016, Johnson et al., 2015).

In addition, BRAF inhibitors have been attributed to cause a paradoxical activation of the MAPK signaling in RAS-mutant melanomas, triggering the development of secondary malignancies (Hatzivassiliou et al., 2010, Heidorn et al., 2010, Poulikakos et al., 2010). By occupying one partner in homo- and hetero-dimers of RAF, particularly in wild-type BRAF and RAS-mutant melanomas, many BRAF inhibitors promote transactivation of the drug free partner leading to a paradoxical activation of the MAPK pathway (Poulikakos et al., 2010, Samatar and Poulikakos, 2014). Consequently, BRAF inhibitors are contraindicated in wild-type BRAF melanomas (Hatzivassiliou et al., 2010). Inhibitors targeting all isoforms of RAF, i.e., panRAF inhibitors, may show benefits by occupying and inhibiting both partners in RAF dimers, and causing a more effective blockade of the MAPK signaling. Given this multiple isoform blockade, panRAF inhibitors may be useful for first-line treatment of BRAF- and NRAS-mutant melanomas, and also as second-line treatment options in drug-resistant melanomas (Girotti et al., 2015). Furthermore, panRAF/MEK inhibitor combination may be a rational treatment strategy, especially in patients with acquired or intrinsic resistance to MAPK inhibitors (Atefi et al., 2015, Whittaker et al., 2015).

Another challenge is the effective management of melanoma patients with brain metastases. Approximately 70% of patients with metastatic melanoma will develop brain metastases, and after diagnosis of brain metastases, the median overall survival (OS) is less than 8 months (Gupta et al., 1997, Barnholtz-Sloan et al., 2004, Spagnolo et al., 2016). Several anti-cancer therapies have a restricted ability to penetrate an intact blood-brain barrier (BBB), leading to the establishment of a pharmacological sanctuary for

tumor cells, thereby limiting their efficacy in the treatment of tumors in the brain (Gampa; Vaidhyanathan; Resman; et al., 2016, Gampa et al., 2017, Kim; Kizilbash; et al., 2018). A key mechanism responsible for restricting drug delivery to the brain is active efflux at the BBB, often mediated by p-glycoprotein (Abcb1/P-gp) and breast cancer resistance protein (Abcg2/Bcrp) (Kim; Kizilbash; et al., 2018, Gampa; Vaidhyanathan; Resman; et al., 2016, Gampa et al., 2017). Previous studies have indicated that vemurafenib, dabrafenib, encorafenib, trametinib, cobimetinib and binimetinib will have limited brain distribution due to efflux by P-gp and/or Bcrp (Mittapalli et al., 2013, Mittapalli et al., 2012, Choo et al., 2014, Vaidhyanathan et al., 2014, Wang et al., 2018, de Gooijer et al., 2018). The drug delivery to brain tumors with heterogeneous disruption of the BBB can be highly variable for compounds that show a limited BBB penetration. While the BBB in the core of larger tumors may be relatively compromised, there can be regions within larger tumors, micrometastases and infiltrative tumor sites with a functionally intact BBB and thus have restricted drug distribution (Lockman et al., 2010, Osswald et al., 2016). Given this, development of potent targeted therapies capable of permeating an intact BBB is critical to improve clinical outcomes in patients with melanoma brain metastases (MBM).

CCT196969, LY3009120 and MLN2480 (Fig. 1, Table 1) are panRAF inhibitors that inhibit MAPK signaling with minimal paradoxical activation (Girotti et al., 2015, Henry et al., 2015, Rasco et al., 2013). CCT196969 has low nanomolar IC_{50} against BRAF and CRAF, and also is a potent inhibitor of SRC (Fig. 2). CCT196969 shows efficacy in melanoma cells and patient-derived xenografts that are resistant to BRAF inhibitors and

BRAF/MEK inhibitor combinations (Girotti et al., 2015). LY3009120 exhibits low nanomolar potency against ARAF, BRAF and CRAF, and shows activity in preclinical melanoma models (Fig. 2) (Henry et al., 2015, Peng et al., 2015, Chen et al., 2016). MLN2480 has a low nanomolar IC_{50} against BRAF and CRAF, and shows activity in BRAF-mutant tumors, including melanoma, in preclinical models (Sun et al., 2017, Elenbaas B, 2010). LY3009120 and MLN2480 are currently in phase I/II clinical testing (clinicaltrials.gov).

The objective of this study is to evaluate the brain distribution of CCT196969, LY3009120 and MLN2480, and examine the role of P-gp and/or Bcrp in limiting their brain delivery. Anti-RAF therapy is routinely used in combination with MEK inhibitors for the management of melanoma patients. The newer panRAF inhibitors have advantages over the traditional BRAF inhibitors, and as such panRAF/MEK inhibitor combinations may result in potential benefits in melanoma patients. However, to be effective in brain metastases, drug delivery to target sites in the brain is a key consideration. Given this, evaluation of the distribution of panRAF inhibitors to the brain is important to understand their utility in the treatment of MBM.

5.2 MATERIALS AND METHODS

5.2.1 Chemicals

CCT196969, 1-(3-(tert-butyl)-1-phenyl-1H-pyrazol-5-yl)-3-(2-fluoro-4-((3-oxo-3,4-dihydropyrido[2,3-b]pyrazin-8-yl)oxy)phenyl)urea, vemurafenib and dabrafenib were purchased from ChemieTek (Indianapolis, IN). LY3009120, 1-(3,3-Dimethylbutyl)-3-(2-fluoro-4-methyl-5-(7-methyl-2-(methylamino)pyrido(2,3-d)pyrimidin-6-yl)phenyl)urea, was purchased from Selleck Chemicals (Houston, TX). MLN2480, 4-Pyrimidinecarboxamide, 6-amino-5-chloro-N-[(1R)-1-[5-[[[5-chloro-4-(trifluoromethyl)-2-pyridinyl]amino]carbonyl]-2-thiazolyl]ethyl]-, was purchased from Medchem Express (Monmouth Junction, NJ). [^{3}H]-Vinblastine was purchased from Moravek Biochemicals (La Brea, CA). [^{3}H]-Prazosin was purchased from PerkinElmer Life and Analytical Sciences (Waltham, MA). Ko143 [(3S,6S,12aS)-1,2,3,4,6,7,12,12a-octahydro-9-methoxy-6-(2-methylpropyl)-1,4-dioxopyrazino(1',2':1,6) pyrido(3,4-b)indole-3-propanoic acid 1,1-dimethylethyl ester] was purchased from Tocris Bioscience (Ellisville, MO). Zosuquidar [LY335979, (R)-4-([1aR, 6R,10bS]-1,2-difluoro-1,1a,6,10b-tetrahydrodibenzo-[a,e] cyclopropa [c]cycloheptan-6-yl)-([5-quinoloyloxy] methyl)-1-piperazine ethanol, trihydrochloride] was provided by Eli Lilly and Co. (Indianapolis, IN). Cell culture reagents were purchased from Invitrogen (Carlsbad, CA), and all other chemicals used were of high-performance-liquid-chromatography or reagent grade and were obtained from Sigma-Aldrich (St. Louis, MO).

5.2.2 In vitro accumulation studies

Polarized Madin-Darby canine kidney II (MDCKII) cells were used for in vitro cell accumulation studies. MDCKII-wild-type (vector control) and Bcrp1-transfected (MDCKII-Bcrp1) cell lines were a kind gift from Dr. Alfred Schinkel (The Netherlands Cancer Institute). MDCKII-wild type (vector control) and human P-glycoprotein (MDR1)-transfected (MDCKII-MDR1) cell lines were kindly provided by Dr. Piet Borst (The Netherlands Cancer Institute). Cells were cultured in Dulbecco's modified Eagle's medium supplemented with 10% (v/v) fetal bovine serum, and antibiotics (penicillin, 100 U/ml and streptomycin, 100 μg/ml). Cells were grown in 25 mL tissue culture-treated flasks before seeding for the intracellular accumulation experiments, and were maintained at 37°C in a humidified incubator with 5% carbon dioxide.

The intracellular accumulation assays were performed in 12-well polystyrene plates (Corning Glassworks, Corning, NY). In brief, cells were seeded at a density of 2 x 10^5 cells and grown until ~80% confluent. On the day of experiment, culture media was aspirated and cells were washed two times with warm cell assay buffer (122 mM NaCl, 25 mM $NaHCO_3$, 10 mM glucose, 10 mM HEPES, 3 mM KCl, 2.5 mM $MgSO_4$, 1.8 mM $CaCl_2$, and 0.4 mM K_2HPO_4). The cells were then pre-incubated with cell assay buffer for 30 min, after which the buffer was aspirated and the experiment was initiated by adding 1 mL assay buffer containing 2 μM drug into each well, with further incubation for 60 minutes in an orbital shaker (ShelLab, Cornelius, OR) maintained at 37°C and 60 rpm. The drug solution was aspirated after a 60-minute incubation, followed by washing twice with ice-cold phosphate-buffered saline (PBS), and addition of 500 μL of 1%

Triton-X100 to each well for cell lysis. When an inhibitor was used, it was included in both pre-incubation and accumulation steps. The concentration of the drug of interest in solubilized cell fractions was analyzed using liquid chromatography–tandem mass spectrometry (LC-MS/ MS) as described below, and was normalized to protein content that was analyzed using a BCA protein assay (Thermo Scientific Pierce).

5.2.3 In vitro binding assays for determination of unbound (free) fractions

The unbound fractions of the panRAF inhibitors in plasma, brain and serum-containing cell culture media (10% fetal bovine serum, v/v) were determined by performing rapid equilibrium dialysis (RED) experiments as per the protocol described by the manufacturer, with some modifications suggested in the literature (Kalvass and Maurer, 2002, Friden et al., 2007). Preliminary experiments conducted at two concentrations (5 μM and 10 μM) and two time points (4 hr and 6 hr) suggest that the unbound fractions were linear across these concentrations and equilibrium was achieved by 4 hr, for each of the three inhibitors. Consequently, unbound fractions determined at 5 μM concentrations and 4 hr time point were utilized for estimation of Kp,uu and free concentrations. A RED base plate (Thermo Fisher Scientific), and single use RED inserts (Thermo Fisher Scientific) with 8 kDa molecular weight cut off (MWCO) were used for these experiments. Briefly, fresh plasma and brain homogenates (prepared in 3 volumes of PBS, w/v) isolated from wild-type FVB mice, and cell culture media were used. The drug stock in DMSO (1 mg/mL) was spiked in each matrix to obtain final concentrations of 5 μM. 300 μL of 5 μM drug spiked matrix was placed in sample chamber (donor), and 500 μL of phosphate buffered saline (1x PBS at pH 7.4; 100 mM sodium phosphate and 150

mM sodium chloride) was placed in buffer chamber (receiver) of the RED inserts in triplicates. The inserts were placed in a base plate, the assembly covered with sealing tape and incubated on an orbital shaker (ShelLab, Cornelius, OR) at 37^{o}C and 300 rpm for 4 hours. The samples collected after dialysis were stored at -80°C until subsequent LC-MS/MS analysis.

5.2.4 In vitro cytotoxicity assays in patient-derived melanoma cell lines

Short-term cultured human primary melanoma cells (BRAF-mutant M12 or BRAF-mutant M27 or NRAS-mutant M15) were maintained through serial passages in mice via subcutaneous flank implantation in immune-deficient mice (Carlson et al., 2011). Dulbecco's modified Eagle's medium supplemented with 10% (v/v) fetal bovine serum and antibiotics (penicillin, 100 U/ml and streptomycin, 100 μg/ml) was used for growing the explant cultures that were maintained at 37°C in a humidified incubator with 5% carbon dioxide.

For the determination of in vitro drug potency, melanoma cells (M12 or M27 or M15) were seeded into 96-well black clear bottom plates (Corning Incorporated, Corning, NY) at a density of 3500 cells per well in 100 μL of culture media. At 24 hours following plating (~80% confluency), the cells were treated with 9 concentrations of drug in media (n = 6 per concentration). The plates were incubated for 5 days after treatment. The cell viability in each well was determined using a CyQuant cell proliferation assay (Invitrogen) and fluorescence measurement using a BioTek Synergy HT plate reader. The relative survival of cells in the presence of drugs was normalized to the untreated controls.

5.2.5 In vivo studies

Animals:

Friend leukemia virus strain B (FVB) wild-type (WT) and triple knockout (*Mdr1a/b*$^{-/-}$ *Bcrp1*$^{-/-}$, TKO, P-gp and Bcrp deficient) mice, balanced for sex, were used in the in vivo studies (Taconic Farms, Germantown, NY). All mice used were 8-16 week-old adults, approximately 15 - 35 g at the time of experiments. Mice were maintained in a 12-hour light/dark cycle with unlimited access to food and water. All studies carried out were in agreement with the guidelines set by Principles of Laboratory Animal Care (National Institutes of Health, Bethesda, MD), and approved by Institutional Animal Care and Use Committee (IACUC) at University of Minnesota.

Plasma and brain pharmacokinetics following intravenous and oral administration of panRAF inhibitors:

All dosing solutions were prepared on the day of the experiment. A single intravenous dose of 5 mg/kg CCT196969 (vehicle: dimethyl sulfoxide, Tween 80 and distilled water in a volume ratio of 10:2.5:87.5) was administered to FVB wild-type mice. Blood and brain samples were harvested at 0.17, 0.5, 1, 2, 4, 8 and 14 hours post-dose (n = 4 at each time point). In another oral dosing study, FVB wild-type mice received a single dose of 10 mg/kg CCT196969 via oral gavage (vehicle: 5% dimethyl sulfoxide; percentage grams per volume). Brain and blood samples were collected at 0.17, 0.5, 1, 2, 4, 6, 8, 11 and 14 hours post dose (n = 4 per time point).

Brain distribution studies following single intravenous and oral doses of LY3009120 were also conducted. A single intravenous dose of 5 mg/kg LY3009120 (vehicle:

dimethyl sulfoxide, propylene glycol, Cremophor EL and distilled water in a volume ratio of 30:20:10:40) was administered to FVB wild-type mice. Blood and brain samples were harvested at 0.17, 0.5, 1, 2, 4, 7 and 11 hours post-dose (n = 4 at each time point). In the oral dosing study, FVB wild-type mice received a single dose of 25 mg/kg LY3009120 via oral gavage (vehicle: 20% hydroxyl propyl β cyclodextrin; percentage grams per volume). Brain and blood samples were collected at 0.17, 0.5, 1, 2, 4, 8 and 15 hours post dose (n = 4 per time point).

The brain distribution of MLN2480 was determined following administration of a single intravenous dose of 5 mg/kg MLN2480 (vehicle: dimethyl sulfoxide, tween 80 and distilled water in a volume ratio of 10:2.5:87.5) to FVB wild-type mice. Blood and brain samples were harvested at 0.17, 0.5, 1, 2, 4, 8 and 14 hours post-dose (n = 4 at each time point).

In another vivo brain distribution study, FVB wild-type and *Mdr1a/b*$^{-/-}$ *Bcrp1*$^{-/-}$ mice were administered a single oral dose of CCT196969 (5 mg/kg) or LY3009120 (10 mg/kg) or MLN2480 (10 mg/kg). Blood and brain samples were harvested 1-hour post-dose (n = 4).

A serial sacrifice (destructive sampling) design was employed for sampling in the pharmacokinetic studies. At the desired sampling time point, mice were euthanized using a carbon dioxide chamber. Blood was collected by cardiac puncture and transferred to heparinized tubes. The whole brain was removed from the skull and rinsed with ice-cold distilled water, and superficial meninges were removed by blotting with tissue paper. Plasma was separated by centrifugation of whole blood samples at 3500 rpm and 4°C for

15 minutes. Both plasma and brain samples were stored at -80°C, until analysis for drug concentrations by LC-MS/MS. The concentrations in brain were corrected for residual drug in brain vasculature, assuming a vascular volume of 1.4% in mouse brain (Dai et al., 2003).

Steady-state brain distribution of panRAF inhibitors:

The determination of steady-state plasma and brain concentrations of panRAF inhibitors was accomplished by implanting Alzet osmotic mini pumps (model 1003D; Durect Corporation, Cupertino, CA) loaded with CCT196969 (5 mg/mL in dimethyl sulfoxide) or LY3009120 (3 mg/mL in dimethyl sulfoxide) or MLN2480 (5 mg/mL in dimethyl sulfoxide) in the peritoneal cavity of wild-type and *Mdr1a/b*$^{-/-}$ *Bcrp1*$^{-/-}$ mice to deliver 1 μL/h drug solution as a constant infusion. The minipumps were loaded with drug solution on the day before the experiment and primed overnight in sterile PBS at 37°C. The pumps were implanted into the peritoneal cavity as described previously (Agarwal et al., 2013). Briefly, mice were anaesthetized using isoflurane, and the hair on the abdominal cavity was removed. A small incision was made in the skin on the lower right abdomen, followed by an incision in the exposed peritoneal membrane under the cutaneous opening, and the primed pump was inserted into the peritoneal cavity. The peritoneal membrane was sutured with absorbable sutures, and the opening in the skin was sealed with surgical clips. The whole procedure was performed on a heating pad until the animals fully recovered from the anesthesia. Forty-eight hours following pump implantation, the mice were sacrificed, and blood and brain samples were collected.

Plasma was obtained by centrifugation of whole blood samples at 3500 rpm and 4°C for 15 minutes. Samples were stored at -80°C until analysis by LC-MS/MS.

5.2.6 LC-MS/MS analysis

The concentrations of drugs in all samples from in vitro and in vivo studies were determined using specific and sensitive LC-MS/MS assays. Brain samples were homogenized using a mechanical homogenizer (PowerGen 125; Thermo Fisher Scientific, Waltham, MA) following the addition of three volumes of 5% bovine serum albumin (BSA) to obtain uniform homogenates. For analysis of unknowns, an aliquot of sample was spiked with 250 ng of MLN2480 or 50 ng of dabrafenib or 10 ng of CCT196969 as internal standards for analysis of CCT196969, LY3009120 and MLN2480, respectively. Liquid-liquid extraction was performed by addition of 5-10 volumes of ethyl acetate, followed by vigorous shaking for 5 minutes and centrifugation at 7500 rpm and 4°C for 5 minutes. The organic layer was separated and transferred to microcentrifuge tubes, and dried under nitrogen gas. The dried residue was reconstituted in 100 μL of mobile phase and transferred into high-performance-liquid-chromatography glass vials with disposable microinserts. The chromatographic analysis was performed on an AQUITY UPLC system (Waters, Milford, MA) using a Phenomenex Gemini 3 μ NX-C18 110A^0 column (50 mm length x 4.6 mm ID; Torrance, CA). The mobile phase (0.1% formic acid in water (A) and 0.1% formic acid in methanol (B)) was delivered at a constant flow rate of 0.35 mL/min. An isocratic method (43% A and 57% B) was employed for CCT19696 and MLN2480, and a gradient method was employed for

LY3009120 analysis. The gradient for LY3009120 was as follows: started with 50% B at 0 minutes, held at 50% B for 2 minutes, increased to 90% B over 1 minute, maintained at 90% B for 1 minute, decreased to 50% B over 0.25 minutes and maintained at 50% B for the remainder of 7 minutes.

The column effluent was monitored using a Micromass Quattro Ultima mass spectrometer (Waters, Milford, MA). The instrument was equipped with an electrospray interface, and controlled by the MassLynx (Version 4.1; Waters) data system. The samples were analyzed using an electrospray probe in negative-ionization mode operating at a spray voltage of 4.5 kV for CCT196969 and MLN2480, and positive-ionization mode operating at a spray voltage of 5 kV for LY3009120 and dabrafenib. Samples were introduced into the interface through a heated probe, in which the source temperature and desolvation temperature were set at 100°C and 350°C, respectively. The m/z transitions were 511.98 - 270.85, 425.08 - 324.00, 505.90 - 284.23 and 519.88 - 306.91 for CCT196969, LY3009120, MLN2480 and dabrafenib, respectively. The retention times for CCT19696, LY3009120, MLN2480 and dabrafenib were 3.23, 3.59, 3.10 and 4.65 minutes, respectively. The runtime was 5.5 minutes for CCT196969 and MLN2480, and 7 minutes for LY3009120. Three quality controls, representing low, medium and high concentration ranges in the calibration curve, were used to determine the between-run (interday) precision and accuracy for each of the three compounds. Precision has been expressed as percent coefficient of variation (CV%), while accuracy is expressed as percent bias. For the LC-MS/MS assays of CCT196969, LY3009120 and MLN2480, the

percent biases were less than 7%, 11% and 6%, and the percent CVs were less than 12%, 15% and 7%, respectively.

5.2.7 Calculations

The unbound (free) fractions (fu) in plasma, brain homogenate, and serum-containing cell culture media were calculated as the ratio of concentrations of the compound under investigation in buffer to matrix (Kalvass and Maurer, 2002).

$$\text{fu, diluted} = \frac{\text{Drug concentration in buffer (receiver)}}{\text{Drug concentration in matrix (donor)}} \quad (Equation\ 1)$$

The unbound fraction in brain was determined from the measured unbound fraction in diluted brain homogenate (fu,diluted), using the following equation (Kalvass and Maurer, 2002).

$$\text{fu, brain} = \frac{1/\text{D}}{(1/\text{fu, diluted} - 1) + 1/\text{D}} \quad (Equation\ 2)$$

where D (equal to 4) represents a dilution factor, accounting for the diluted brain homogenate.

The brain-to-plasma ratio (Kp) was calculated as the ratio of AUC_{brain} to AUC_{plasma}.

$$\text{Kp} = \frac{\text{AUCbrain}}{\text{AUCplasma}} \quad (Equation\ 4)$$

A comparison of relative drug exposure in the brains of wild-type and knockout (*Mdr1a/b*$^{-/-}$ *Bcrp1*$^{-/-}$) mice was made using the distribution advantage (DA), which was calculated as the Kp in the strain under consideration normalized by the Kp in wild-type mice.

$$\mathrm{DA} = \frac{\mathrm{Kp}, knockout}{\mathrm{Kp}, wild\ type} \quad (Equation\ 5)$$

The unbound partition coefficient, referred to as Kp,uu, was determined using the following equation.

$$\mathrm{Kp, uu} = \frac{\mathrm{AUCbrain\ x\ fu, brain}}{\mathrm{AUCplasma\ x\ fu, plasma}} \quad (Equation\ 6)$$

The data from in vitro cytotoxicity experiments was fitted to "log(inhibitor) vs. normalized response - variable slope" equation using GraphPad Prism version 6.04 (GraphPad, La Jolla, CA) software to determine the IC_{50} of the compounds of interest in the cell lines tested.

5.2.8 Pharmacokinetic data analysis

Pharmacokinetic parameters from the concentration-time profiles in plasma and brain were obtained by non-compartmental analysis (NCA) performed using Phoenix WinNonlin version 6.4 (Certara USA, Inc., Princeton, NJ). The areas under the concentration-time curve (AUC) for plasma (AUC_{plasma}) and brain (AUC_{brain}) were calculated using the linear trapezoidal method. The standard errors around the means of AUC and Cmax were estimated using the sparse sampling module in WinNonlin (Nedelman and Jia, 1998).

5.2.9 Statistical analysis

GraphPad Prism version 6.04 (GraphPad, La Jolla, CA) software was used for statistical analysis. The sample sizes used were based on previous work and were determined based on approximately 80% power to detect 50% difference between groups. Data from all

experiments are represented as mean ± standard deviation (S.D.) or mean ± standard error of the mean (S.E.M), unless otherwise indicated. Comparisons between two groups were made using an unpaired t-test. Comparisons between multiple groups were made using one-way analysis of variance (ANOVA), followed by Bonferroni's multiple comparison test. A significance level of $P < 0.05$ was used for all statistical analysis.

5.3 RESULTS

5.3.1 In vitro accumulation of panRAF inhibitors in MDCKII-Bcrp1 and MDCKII-MDR1 cells

The intracellular accumulation of CCT196969, LY3009120 and MLN2480 in MDCKII wild-type (vector control), Bcrp1-transfected (MDCKII-Bcrp1), and P-gp-transfected (MDCKII-MDR1) cell lines is summarized in Fig. 3. [^{3}H]-Prazosin and [^{3}H]-vinblastine were used as positive controls for Bcrp1 and MDR1 function, respectively. The cellular accumulation of [^{3}H]-prazosin is significantly lower in Bcrp1-transfected cells compared to wild-type controls (WT: 100±8%; Bcrp1: 24±2%; $P<0.0001$), and such an effect is abolished in the presence 0.2 μM Ko143, a specific Bcrp1 inhibitor. The cellular accumulation of [^{3}H]-vinblastine is also significantly lower in MDR1-transfected cells than in wild-type controls (WT: 100±1%; MDR1: 9±4%; $P<0.0001$), and such an effect is abolished in the presence of 1 μM LY335979, a specific P-gp inhibitor. The results confirm a significant elevation in functional activity of efflux transporters in the pertinent transfected cell lines.

In the same experiment, incubation with 2 μM solution of each of the three panRAF inhibitors showed that the accumulation is significantly different in Bcrp1 cells when compared with corresponding wild-type controls for LY3009120 (WT: 100±12%; Bcrp1: 30±7%; $P<0.001$), and MLN2480 (WT: 100±10%; Bcrp1: 49±10%; $P<0.01$). The addition of 0.2 μM Ko143 to the Bcrp1 cells caused a reversal of Bcrp1 mediated efflux of LY3009120 and MLN2480. For CCT196969, the cellular accumulation is not significantly different in Bcrp1 cells when compared with corresponding wild-type

controls (WT: 100±35%; Bcrp1: 60±20%; ns, P=0.16), and the addition of 0.2 μM Ko143 to Bcrp1 cells did not lead to significant differences in intracellular accumulation. Incubation with 2 μM drug solution shows no significant difference in cellular accumulation in MDR1 cells when compared with corresponding wild-type controls for CCT196969 (WT: 100±32%; MDR1: 83±15%; ns, P=0.56), LY3009120 (WT: 100±27%; MDR1: 72±40%; ns, P=0.46), and MLN2480 (WT: 100±3%; MDR1: 48±25%; ns, P=0.07). Also, the addition of 1 μM LY335979 to MDR1 cells did not lead to significant differences in intracellular accumulation when compared to transfected cells without inhibitor. These in vitro results indicate that only LY3009120 and MLN2480 are substrates of Bcrp1, and none of the three panRAF inhibitors are substrates of P-gp.

5.3.2 Unbound (free) fractions of panRAF inhibitors in matrices of interest

In vitro rapid equilibrium dialysis technique was employed for the determination of unbound fraction (fu) (equations 1 and 2) of panRAF inhibitors in plasma, brain and serum-containing cell culture media. The percent unbound fractions for CCT196969, LY3009120 and MLN2480 in plasma, brain and cell culture media are as reported in Table 2. The three panRAF inhibitors exhibit high binding in plasma and brain. The estimated unbound fractions in plasma and brain were used for the determination of unbound partition coefficient, Kp,uu, and the unbound fraction in cell culture media was utilized in the estimation of free IC_{50} of the three panRAF inhibitors in each of the cell lines tested.

5.3.3 In vitro efficacy in patient-derived melanoma cell lines

The in vitro efficacy studies were performed in BRAF-mutant M12, BRAF-mutant M27, and NRAS-mutant M15 patient-derived melanoma cell lines. The total IC_{50} for vemurafenib (control), CCT196969, LY3009120 and MLN2480 were estimated using the total drug concentration-response curves determined in the three patient-derived melanoma cell lines. The free fractions in cell culture media for CCT196969, LY3009120 and MLN2480 were used together with the total IC_{50} estimates to determine the free IC_{50} values. The dose-response curves for vemurafenib, CCT196969, LY3009120 and MLN2480 in the 3 cells lines tested are shown in Fig. 4, and the IC_{50} values are listed in Table 3., respectively. The results suggest that M12 is the most sensitive line to treatment with the four inhibitors, and LY3009120 exhibits higher potency in each of the three cell lines tested.

5.3.4 Plasma and brain pharmacokinetics in FVB mice

The pharmacokinetic profiles of panRAF inhibitors were determined in FVB wild-type and transporter deficient (knockout) mice following intravenous and oral drug administration. The brain and plasma concentration time profiles and brain-to-plasma ratios in FVB wild-type mice following a single intravenous bolus dose of 5 mg/kg CCT196969, LY3009120 and MLN2480 are as shown in Fig. 5, Fig. 6 and Fig. 7. The total brain concentrations at the indicated time points are significantly lower than the total plasma concentrations for all the three compounds. Table 4 summarizes the estimated pharmacokinetic parameters following intravenous drug administration. The brain-to-plasma AUC ratios (Kp, equation 4) for CCT196969, LY3009120 and MLN2480 are

0.006, 0.05 and 0.20, respectively, and the corresponding Kp,uu (equation 6) are 0.03, 0.02 and 0.05, respectively.

The concentration time profiles and brain-to-plasma ratios in FVB wild-type mice following a single oral dose of 10 mg/kg CCT196969 and 25 mg/kg LY3009120 are shown in Fig. 5 and Fig. 6. The estimated pharmacokinetic parameters are summarized in Table 5. The brain-to-plasma AUC ratios (Kp, equation 4) for CCT196969 and LY3009120 are 0.01 and 0.04, respectively, and are similar to that observed in the intravenous dosing studies. The corresponding Kp,uu for CCT196969 and LY3009120 (equation 6) are 0.05 and 0.02, respectively. The bioavailability (F) following oral administration is 0.77 for CCT196969 and 0.04 for LY3009120.

The brain and plasma concentrations and brain-to-plasma ratios in FVB wild-type and *Mdr1a/b*$^{-/-}$ *Bcrp1*$^{-/-}$ mice one-hour post oral administration of panRAF inhibitors (5 mg/kg CCT196969, 10 mg/kg LY3009120 and 10 mg/kg MLN2480) are as shown in Fig. 8. The brain concentrations are significantly lower than the plasma concentrations in wild-type mice for all three panRAF inhibitors, and the brain-to-plasma concentration ratios for CCT196969, LY3009120 and MLN2480 are 0.01, 0.05 and 0.24, respectively. The brain-to-plasma concentration ratios in *Mdr1a/b*$^{-/-}$ *Bcrp1*$^{-/-}$ mice are significantly higher than in wild-type mice for CCT196969, LY3009120 and MLN2480, and are 0.02, 0.32 and 2.66, respectively.

5.3.5 Steady-state brain distribution of panRAF inhibitors

The steady-state brain-to-plasma ratios for CCT196969, LY3009120 and MLN2480 are 0.01 ± 0.002, 0.01 ± 0.01, and 0.34 ± 0.10 in wild-type mice, 0.05 ± 0.02, 0.27 ± 0.12,

and 2.88 ± 0.31 in *Mdr1a/b*$^{-/-}$ *Bcrp1*$^{-/-}$ mice, respectively (Fig. 9, Table 6). The brain-to-plasma ratios are about 5, 27 and 9-fold higher for CCT196969, LY3009120 and MLN2480 in *Mdr1a/b*$^{-/-}$ *Bcrp1*$^{-/-}$ mice when compared to wild-type mice. These results are similar to the observations from the brain distribution studies in FVB wild-type and *Mdr1a/b*$^{-/-}$ *Bcrp1*$^{-/-}$ mice that evaluated the brain-to-plasma ratios one-hour post oral drug administration. Collectively, the in vivo studies show that the delivery of the three panRAF inhibitors to the brain is restricted, and active efflux by P-gp and/or Bcrp plays a role in limiting their brain distribution.

5.4 DISCUSSION

The small molecule molecularly-targeted therapies and immunotherapies approved for the treatment of melanoma have shown improvements in survival by a few months in patients with MBM (Long et al., 2012, Dummer et al., 2014, Spagnolo et al., 2016, Margolin et al., 2012, Goldberg et al., 2016, Ahmed et al., 2016, Tawbi et al., 2018). While such improvements in survival bring new optimism, the management of metastatic disease that has spread to the brain is still challenging (Gampa et al., 2017). The modest efficacy in patients with MBM may be related to factors that include inadequate drug delivery to tumor cells in the brain and specific brain microenvironment driven alterations in gene expression. As a consequence, both drug delivery and resistance concerns should be addressed to improve treatment outcomes in patients with MBM. A novel class of compounds, the panRAF inhibitors, may address both of these issues.

The panRAF inhibitors may show benefits over mutant-BRAF inhibitors in the treatment of melanoma either as single agents or in combination with a MEK inhibitor, due to their ability to overcome paradoxical activation of the MAPK pathway (Girotti et al., 2015, Peng et al., 2015). Several anti-cancer drugs have restricted brain delivery due to active efflux at the BBB, mainly by P-gp and Bcrp (Gampa et al., 2017, Kim; Kizilbash; et al., 2018). The transport of substrate compounds back into systemic circulation by efflux transporters can prevent drugs with a potential to be efficacious from reaching the target tumor cells residing behind an intact BBB. Given this, an evaluation of the brain distribution and efflux liability of therapies intended for use in CNS disorders is important. Herein we report the findings of the brain distribution, binding and in vitro

efficacy studies for three panRAF inhibitors i.e., CCT196969, LY3009120 and MLN2480. The results provide important information on the ability of these compounds to distribute across the BBB, and also allow a correlation of the in vivo concentrations with in vitro efficacy in patient-derived melanoma cell lines that will help inform in vivo efficacy studies.

In vitro intracellular accumulation studies in transfected MDCKII cells overexpressing either murine Bcrp or human P-gp, both important BBB efflux transporters, suggest that only LY3009120 and MLN2480 are substrates of Bcrp, however, none of the three inhibitors were substrates of P-gp (Fig. 3). In vitro rapid equilibrium dialysis experiments indicate that the three panRAF inhibitors exhibit high non-specific binding in brain and plasma (Table 2). The results of the in vitro efficacy testing reveal that M12, a BRAF-mutant melanoma brain metastasis patient-derived model, is the most sensitive line to treatment with CCT196969, LY3009120, MLN2480 and vemurafenib (Fig. 4, Table 3). LY3009120 has a low nanomolar $IC_{50,}$ and is the most potent inhibitor in each of the three cell lines tested.

Subsequently, experiments were conducted in mice to test the influence of P-gp and/or Bcrp on brain distribution of CCT196969, LY3009120 and MLN2480 in vivo. Pharmacokinetic studies in mice following a single intravenous or oral dose indicate that CCT196969, LY3009120 and MLN2480 all have restricted brain delivery (Fig. 5, Fig. 6 and Fig. 7). The bioavailability following oral administration of CCT196969 was promising (~77%) using the current formulation. On the other hand, the oral bioavailability of LY3009120 was poor (<5%) (Table 5). Reports indicate that

formulating LY3009120 as an amorphous solid dispersion improves the bioavailability by overcoming solubility limitations (Henry et al., 2015, Peng et al., 2015). The results of steady-state studies show that the brain distribution of CCT196969, LY3009120 and MLN2480 is enhanced in mice lacking P-gp and Bcrp (Fig. 9, Table 6). Also, studies evaluating the brain distribution one-hour post oral administration of the three panRAF inhibitors in wild-type and triple knockout mice (*Mdr1a/b*$^{-/-}$ *Bcrp1*$^{-/-}$) show similar results (Fig. 8). Together, the in vivo brain distribution studies in wild-type and transgenic knockout mice suggest that the delivery of CCT196969, LY3009120 and MLN2480 to brain is limited due to active efflux by P-gp and/or Bcrp at the BBB, with MLN2480 showing greater brain distribution. Furthermore, MLN2480 exhibits higher brain distribution than vemurafenib and dabrafenib (Table 7). However, MLN2480 shows a relatively modest in vitro efficacy, and LY3009120 exhibits superior in vitro efficacy when compared to CCT196969 and MLN2480 in patient-derived melanoma cell lines. These studies highlight the fact that the combination of drug delivery to target site in the brain and drug potency against the target will eventually influence the in vivo efficacy outcomes.

Given the importance of both drug delivery as well as drug potency in dictating treatment outcomes, a correlation of the observed in vivo concentrations of panRAF inhibitors with in vitro potencies is valuable. The average total drug concentrations post intravenous dosing at the measured time points were used together with the unbound fractions in brain and plasma to obtain unbound concentration-time profiles for CCT196969, LY3009120 and MLN2480 in wild-type mice. The unbound concentration-time profiles

were then compared to in vitro potency estimates (free IC_{50}) in M12, to evaluate the potential of CCT196969, LY3009120 and MLN2480 in the treatment of MBM (Fig. 10). The selection of cell line was guided by the results of in vitro efficacy experiments, which indicate M12 to be the most sensitive line to treatment with CCT196969, LY3009120 and MLN2480 (Fig. 4, Table 3). The unbound concentration-time profiles in brain and plasma for MLN2480 show that the unbound concentrations are substantially below the free IC_{50} in M12, when administered at a dose of 5 mg/kg intravenously. Assuming that the administration of MLN2480 at the maximum reported dose of 30 mg/kg po in mice (Sun et al., 2017) will result in a 6-fold increase in concentrations (this assumes linear kinetics and oral bioavailability of 100%), the resulting unbound plasma concentrations will just reach the free IC_{50}, and the brain concentrations will still be substantially below the free IC_{50} in M12. For CCT196969, the unbound concentrations in brain are lower and that in plasma are higher (for about 1 hour) than the free IC_{50} following 5 mg/kg iv dose. Considering that the maximum reported dose in mice for CCT196969 is 25 mg/kg po (Girotti et al., 2015) and the oral bioavailability is 77%, the concentrations will be 4-fold higher (again assuming linear kinetics) following an intravenous dose (20 mg/kg) that will result in similar exposure to 25 mg/kg po dose. The 4-fold increase in concentrations will lead to unbound plasma concentrations higher than the free IC_{50} for about 7 hours; however, the unbound brain concentrations will still be substantially below the free IC_{50}. In case of LY3009120, the unbound concentrations in plasma reach levels higher than the free IC_{50} for approximately 7 hours, and the unbound concentrations in brain are higher than the free IC_{50} in M12 for about 2 hours post-dose

after 5 mg/kg iv dosing. An intravenous dose of 10 mg/kg LY3009120 was not tolerable in FVB mice. These findings suggest that CCT196969 and LY3009120 will possibly show superior in vivo efficacy in the treatment of systemic melanoma, as the unbound plasma concentrations reach levels higher than the free IC_{50} estimates in M12 for both the compounds. However, the unbound concentrations in brain achieve levels higher than the free IC_{50} in M12 for LY3009120 alone, suggesting possible efficacy benefits with LY3009120 in the treatment of MBM. Given such insights, testing the efficacy of LY3009120 in preclinical models of MBM will be important to evaluate in vivo efficacy.

The responses to treatment with molecularly-targeted therapies have been sub-optimal and variable in patients with MBM. Such outcomes may be related to inadequate drug delivery to tumor cells in the brain and specific brain microenvironment driven changes in gene expression, both critical challenges that need to be addressed for improving the quality of life of MBM patients. The panRAF inhibitors have advantages over mutant-BRAF inhibitors in overcoming resistance and preventing the paradoxical activation of the MAPK pathway. However, the delivery of panRAF inhibitors to the site of action in the brain and their potency against the target tumor cells are key determinants of in vivo efficacy in the treatment of tumors in the brain. A correlation of unbound plasma and brain drug concentrations with in vitro potency estimates in patient-derived melanoma cell lines for CCT196969, LY3009120 and MLN2480 suggests that LY3009120 is a novel panRAF inhibitor with low nanomolar in vitro potency against mutant-BRAF (M12, M27) and NRAS (M15) patient-derived melanoma cell lines, and has adequate brain delivery to achieve therapeutically active concentrations in the brain. The novel

mechanism involving inhibition of all isoforms of RAF, as well as an appropriate balance of potency and brain delivery make LY3009120 a promising candidate for efficacy testing in preclinical models of MBM. Also, evaluating the use of a rational combination of panRAF/MEK inhibitors for achieving a better vertical blockade of MAPK signaling and in vivo efficacy in the treatment of MBM will be of interest. When using combinations, all inhibitors in a combination regimen must have adequate brain delivery to achieve therapeutic concentrations at the sites of action in the brain to elicit the desired therapeutic response, and minimize the emergence of resistance. Remarkable progress has been made in the treatment of melanoma, however, there still remains a need to develop better therapies for MBM, and drug delivery across a functionally intact BBB is an important challenge that needs to be addressed to fulfill this goal.

ACKNOWLEDGEMENTS

The authors thank Jim Fisher, Clinical Pharmacology Analytical Laboratory, University of Minnesota, for his support in the development of the LC-MS/MS assays.

FOOTNOTES

This work was supported by the National Institutes of Health [Grants RO1-NS077921, RO1-NS073610 and U54-CA210180]. Gautham Gampa was supported by the Ronald J. Sawchuk Fellowship in Pharmacokinetics and University of Minnesota Doctoral Dissertation Fellowship (DDF).

TABLES

Table 5. 1 Physico-chemical properties of panRAF inhibitors.

	CCT196969	**LY3009120**	**MLN2480**
Molecular formula	$C_{27}H_{24}FN_7O_3$	$C_{23}H_{29}FN_6O$	$C_{17}H_{12}Cl_2F_3N_7O_2S$
Molecular weight (g/mol)	513.53	424.52	506.29
Solubility	< 1mg/mL	< 1mg/mL	< 1mg/mL
logP	5.5	4.2	3
logD (pH 7.4)	5.5	4.2	3
pKa[1]	10.36	11.61	10.29
Topological polar surface area (A^2)	123	92	136
Hydrogen bond donor count	3	3	3
Rotatable bond count	6	6	6

The reported properties were calculated using ChemAxon (http://www.chemicalize.com).
[1] The values represent strongest acidic pKa reported by ChemAxon

Table 5. 2 Unbound fractions (fu) for CCT196969, LY3009120 and MLN2480 in plasma, brain and serum-containing cell culture media, determined by in vitro rapid equilibrium dialysis (RED) experiments. Data represent the mean ± S.D. (n = 3).

Inhibitor	Matrix	fu (%)
CCT196969	Plasma	0.1 ± 0.01
	Brain	0.50 ± 0.10
	Cell culture media	21.51 ± 1.58
LY3009120	Plasma	1.82 ± 0.18
	Brain	0.93 ± 0.04
	Cell culture media	27.90 ± 2.13
MLN2480	Plasma	4.21 ± 0.16
	Brain	0.98 ± 0.09
	Cell culture media	34.20 ± 1.52

fu, unbound (free) fraction

Table 5. 3 Total and free (unbound) IC_{50} for vemurafenib (control) and panRAF inhibitors in patient derived melanoma cell lines (M12 and M27, BRAF-mutant; M15, NRAS-mutant). The free IC_{50} were estimated for the panRAF inhibitors using the total IC_{50} values and the unbound fractions (fu) in cell culture media.

	IC_{50} (µM) (95% confidence intervals)			**Free IC_{50} (µM)**		
	M12	**M27**	**M15**	**M12**	**M27**	**M15**
Vemurafenib	0.14 (0.10-0.19)	0.38 (0.28-0.52)	6.16 (4.94-7.68)	-	-	-
CCT196969	0.19 (0.13-0.27)	0.53 (0.41-0.70)	1.58 (1.21-2.07)	0.04	0.11	0.33
LY3009120	0.002 (0.001-0.003)	0.001 (0.07-0.002)	0.003 (0.001-0.008)	0.0006	0.0003	0.0008
MLN2480	3.59 (3.00-4.29)	3.83 (3.11-4.71)	7.71 (6.32-9.41)	1.22	1.30	2.62

Table 5. 4 The pharmacokinetic/metric parameters of panRAF inhibitors in FVB wild-type mice following administration of single intravenous dose of 5 mg/kg. Data are presented as mean or mean ± S.E.M (n = 4).

	CCT196969		LY3009120		MLN2480	
	Plasma	**Brain**	**Plasma**	**Brain**	**Plasma**	**Brain**
Half-life (h)	2.79	3.37	2.35	1.74	6.54	7.25
$AUC_{(0-t)}$ (µg*h/mL)	150.23 ± 6.08	0.92 ± 0.02	10.86 ± 0.59	0.51 ± 0.03	17.56 ± 0.47	3.45 ± 0.09
$AUC_{(0-\infty)}$ (µg*h/mL)	155.07	0.97	10.88	0.51	22.71	4.49
CL (mL/min/kg)	0.54	-	7.66	-	3.7	-
Vd (L/kg)	0.13	-	1.56	-	2.08	-
Kp ($AUC_{(0-\infty)}$ ratio)	-	0.006	-	0.05	-	0.20
Kp,uu ($AUC_{(0-\infty)}$ ratio)	-	0.03	-	0.02	-	0.05

$AUC_{(0-t)}$, area under the curve from zero to the time of last measured concentration
$AUC_{(0-\infty)}$, area under the curve from zero to time infinity
CL, clearance
Vd, volume of distribution
Kp (AUC ratio), the ratio of $AUC_{(0-\infty,brain)}$ to $AUC_{(0-\infty,plasma)}$ using total drug concentrations
Kp,uu (AUC ratio), the ratio of $AUC_{(0-\infty,brain)}$ to $AUC_{(0-\infty,plasma)}$ using free drug concentrations

Table 5. 5 The pharmacokinetic/metric parameters of CCT196969 and LY3009120 in FVB wild-type mice following administration of single oral dose. Data are presented as mean or mean ± S.E.M (n = 4).

	CCT196969 (10 mg/kg)		**LY3009120 (25 mg/kg)**	
	Plasma	**Brain**	**Plasma**	**Brain**
Half-life (h)	3.64	3.97	2.91	2.87
Tmax (h)	4	6	0.5	1
Cmax (µg/mL)	31.09 ± 7.15	0.40 ± 0.04	1.48 ± 1.01	0.04 ± 0.009
$AUC_{(0-t)}$ (µg*h/mL)	222.01 ± 18.94	2.18 ± 0.17	2.06 ± 0.44	0.09 ± 0.02
$AUC_{(0-\infty)}$ (µg*h/mL)	241.17	2.38	2.09	0.09
CL (mL/min/kg)	0.53	-	7.98	-
Vd (L/kg)	0.16	-	2.01	-
F (%)	77	-	4	-
Kp ($AUC_{(0-\infty)}$ ratio)	-	0.01	-	0.04
Kp,uu ($AUC_{(0-\infty)}$ ratio)	-	0.05	-	0.02

Tmax, time to reach the maximum concentration
Cmax, observed maximum concentration
$AUC_{(0-t)}$, area under the curve from zero to the time of last measured concentration
$AUC_{(0-\infty)}$, area under the curve from zero to time infinity
CL, clearance
Vd, volume of distribution
F (Absolute bioavailability), ratio of the dose corrected $AUC_{(0-\infty),po}$ to dose corrected $AUC_{(0-\infty),iv}$
Kp (AUC ratio), the ratio of $AUC_{(0-\infty,brain)}$ to $AUC_{(0-\infty,plasma)}$ using total drug concentrations
Kp,uu (AUC ratio), the ratio of $AUC_{(0-\infty,brain)}$ to $AUC_{(0-\infty,plasma)}$ using free drug concentrations

Table 5. 6 Steady-state brain distribution of panRAF inhibitors in wild-type and *Mdr1a/b*$^{-/-}$ *Bcrp1*$^{-/-}$ mice. Data are presented as mean or mean ± S.D.

Inhibitor	Strain	Kp brain	Kp,uu brain	Distribution advantage
CCT196969	Wild-type	0.01 ± 0.002	0.05	1
	Mdr1a/b$^{-/-}$Bcrp1a/b$^{-/-}$	0.05 ± 0.02	0.25	5
LY3009120	Wild-type	0.01 ± 0.01	0.005	1
	Mdr1a/b$^{-/-}$Bcrp1a/b$^{-/-}$	0.27 ± 0.12	0.14	27
MLN2480	Wild-type	0.34 ± 0.10	0.08	1
	Mdr1a/b$^{-/-}$Bcrp1a/b$^{-/-}$	2.88 ± 0.31	0.66	8.5

Kp brain, the ratio of $C_{ss,brain}$ to $C_{ss,plasma}$ using total drug concentrations
Kp,uu brain, the ratio of $C_{ss,brain}$ to $C_{ss,plasma}$ using free drug concentrations
Distribution advantage, the ratio of Kp to $Kp_{wild-type}$

Table 5. 7 Comparison of brain distribution of RAF inhibitors in wild-type mice. Data are presented as means.

Inhibitor	Intravenous dose (mg/kg)	Kp brain	Kp,uu brain
Vemurafenib[a]	2.5	0.004	NR
Dabrafenib[b]	2.5	0.02	NR
CCT196969	5	0.006	0.03
LY3009120	5	0.05	0.02
MLN2480	5	0.20	0.05

Kp (AUC ratio), the ratio of $AUC_{(0-\infty,brain)}$ to $AUC_{(0-\infty,plasma)}$ using total drug concentrations
Kp,uu (AUC ratio), the ratio of $AUC_{(0-\infty,brain)}$ to $AUC_{(0-\infty,plasma)}$ using free drug concentrations
NR, not reported
[a] As reported by Mittapalli et al. 2012
[b] As reported by Mittapalli et al. 2013

FIGURES

Figure 5. 1 Chemical structure of (A) CCT196969, (B) LY3009120, and (C) MLN2480.

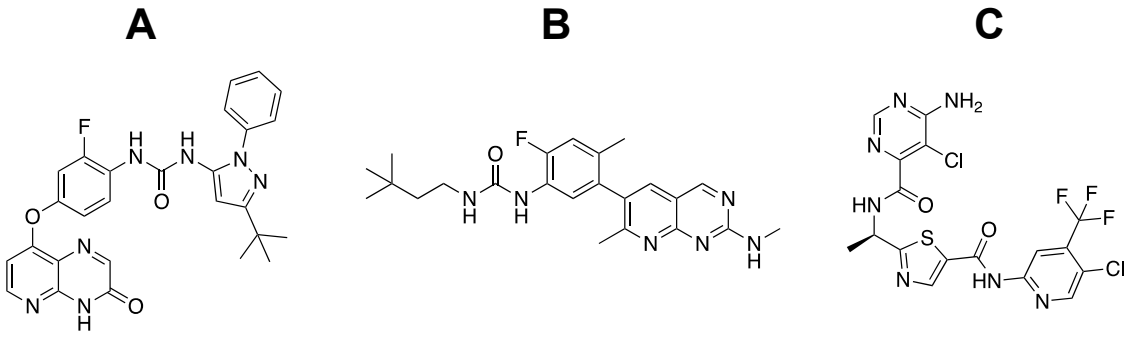

Figure 5. 2 Schematic representing the MAPK pathway, and targets of panRAF inhibitors, approved BRAF inhibitors and approved MEK inhibitors.

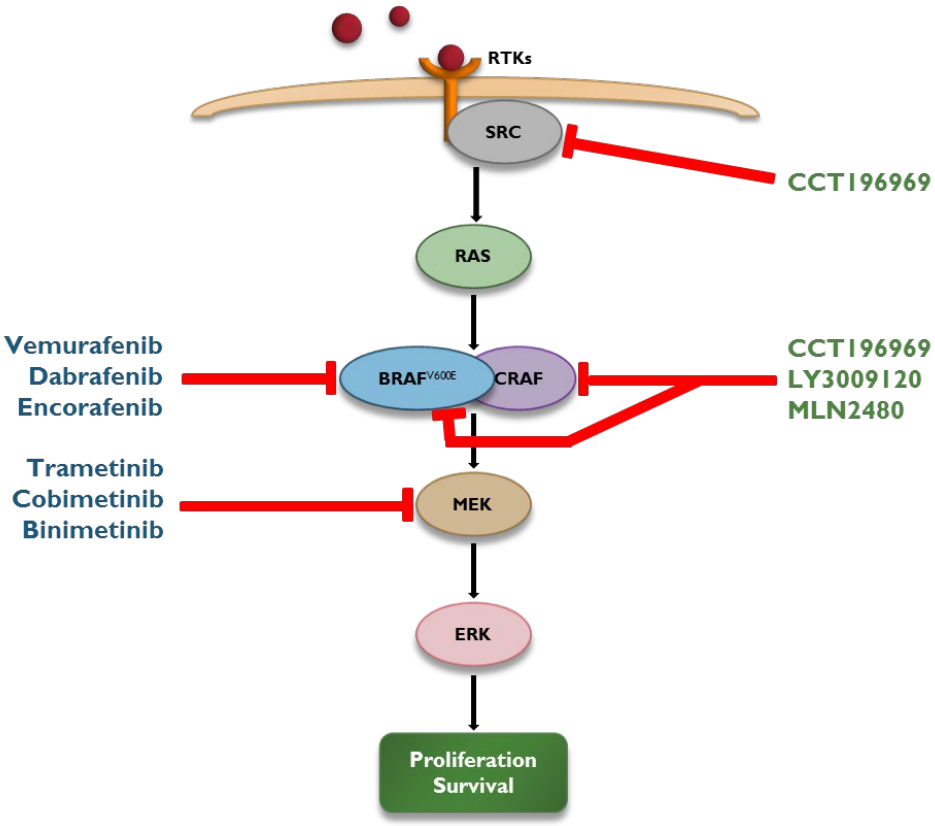

Figure 5. 3 In vitro intracellular accumulation of panRAF inhibitors. (A) The accumulation of prazosin (Bcrp probe substrate; positive control), CCT196969, LY3009120, and MLN2480 in MDCKII wild-type and Bcrp1-transfected cells with and without Bcrp inhibitor Ko143 (0.2 μM). (B) The accumulation of vinblastine (probe substrate for P-gp/MDR1; positive control), CCT196969, LY3009120, and MLN2480 in wild-type and MDR1-transfected cells with and without P-gp inhibitor LY335979 (1 μM). Data represent the mean ± S.D.; n = 3 for all data points. $$P< 0.05$ compared with the untreated transfected cell line; ^$P<$ 0.001 compared with the untreated transfected cell line; #$P<$ 0.0001 compared with the untreated transfected cell line; **$P< 0.01$ compared with respective wild-type controls; ***$P< 0.001$ compared with respective wild-type controls; ****$P< 0.0001$ compared with respective wild-type controls.

A

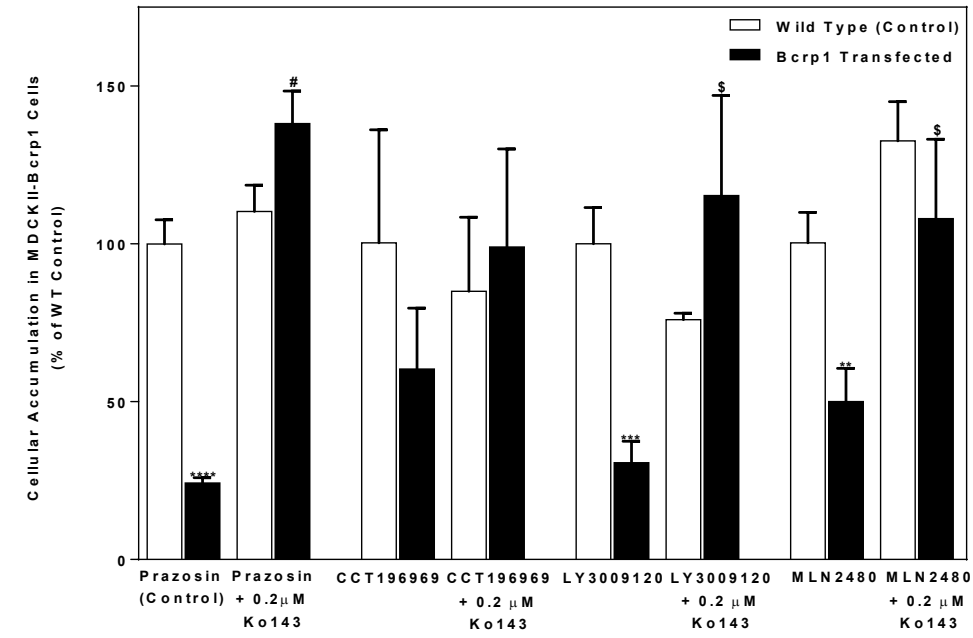
Wild Type (Control)
Bcrp1 Transfected
Cellular Accumulation in MDCKII-Bcrp1 Cells (% of WT Control)
150
100
50
0
#
$
$
****
***
**
Prazosin (Control)
Prazosin + 0.2μM Ko143
CCT196969
CCT196969 + 0.2 μM Ko143
LY3009120
LY3009120 + 0.2 μM Ko143
MLN2480
MLN2480 + 0.2 μM Ko143

B

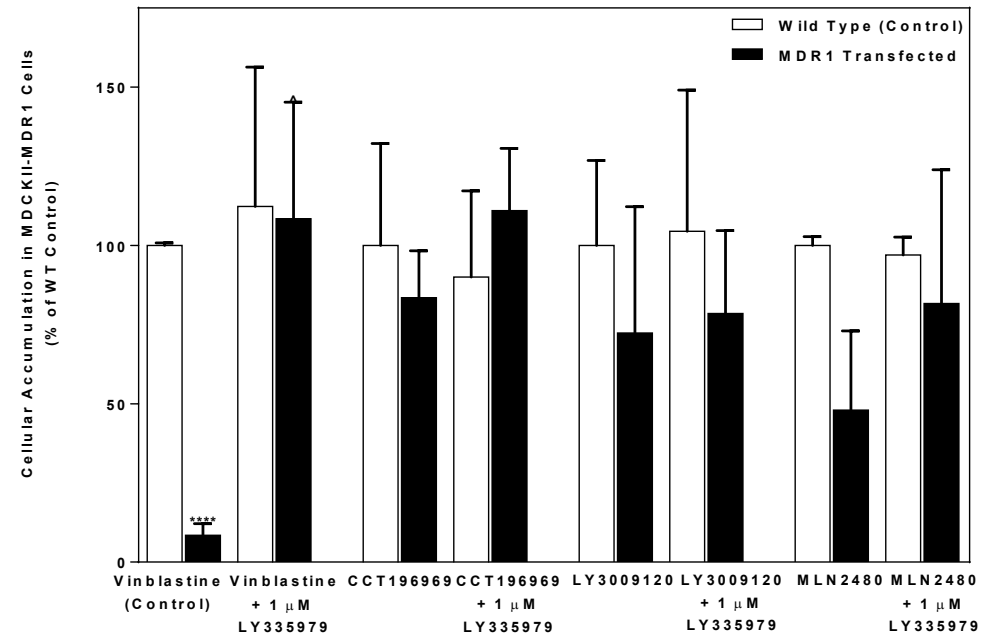
Wild Type (Control)
MDR1 Transfected
Cellular Accumulation in MDCKII-MDR1 Cells (% of WT Control)
150
100
50
0
****
Vinblastine (Control)
Vinblastine + 1 μM LY335979
CCT196969
CCT196969 + 1 μM LY335979
LY3009120
LY3009120 + 1 μM LY335979
MLN2480
MLN2480 + 1 μM LY335979

Figure 5. 4 In vitro efficacy of panRAF inhibitors in patient-derived xenograft melanoma cell lines. (A) Dose-response curves showing the effect of various concentrations of vemurafenib, CCT196969, LY3009120 and MLN2480 on BRAF-mutant M12 melanoma cell line. (B) Growth profiles showing the effect of various concentrations of vemurafenib, CCT196969, LY3009120 and MLN2480 on BRAF-mutant M27 melanoma cell line. (C) Dose-response curves showing the effect of multiple concentrations of vemurafenib, CCT196969, LY3009120 and MLN2480 on NRAS-mutant M15 melanoma cell line. Data represent the mean ± S.E.M.; n = 6 for all data points.

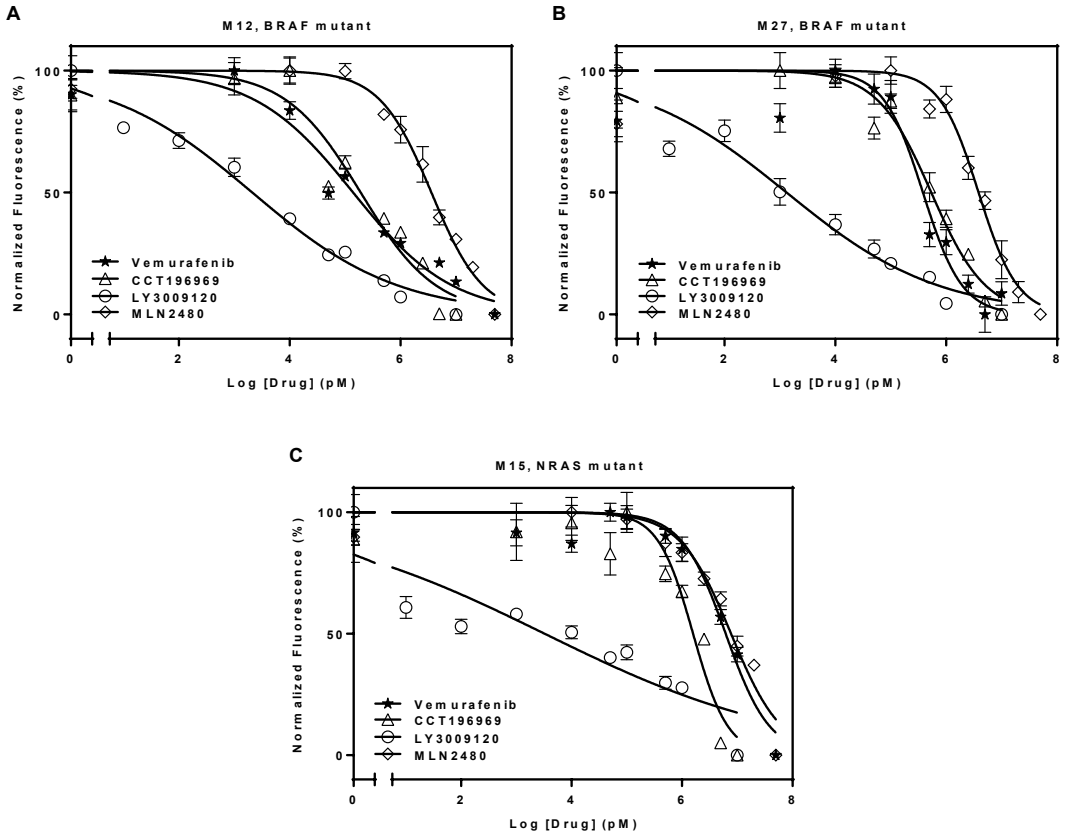

Figure 5. 5 Pharmacokinetic profiles of CCT196969 in FVB wild-type mice following intravenous (i.v.) and oral (p.o.) administration. Plasma and brain concentrations (A), and brain-to-plasma concentration ratios (B) of CCT196969 following administration of single i.v. bolus dose of 5 mg/kg. Plasma and brain concentrations (C), and brain-to-plasma concentration ratios (D) of CCT196969 post single oral dose of 10 mg/kg. Data represent mean ± S.D., n = 4.

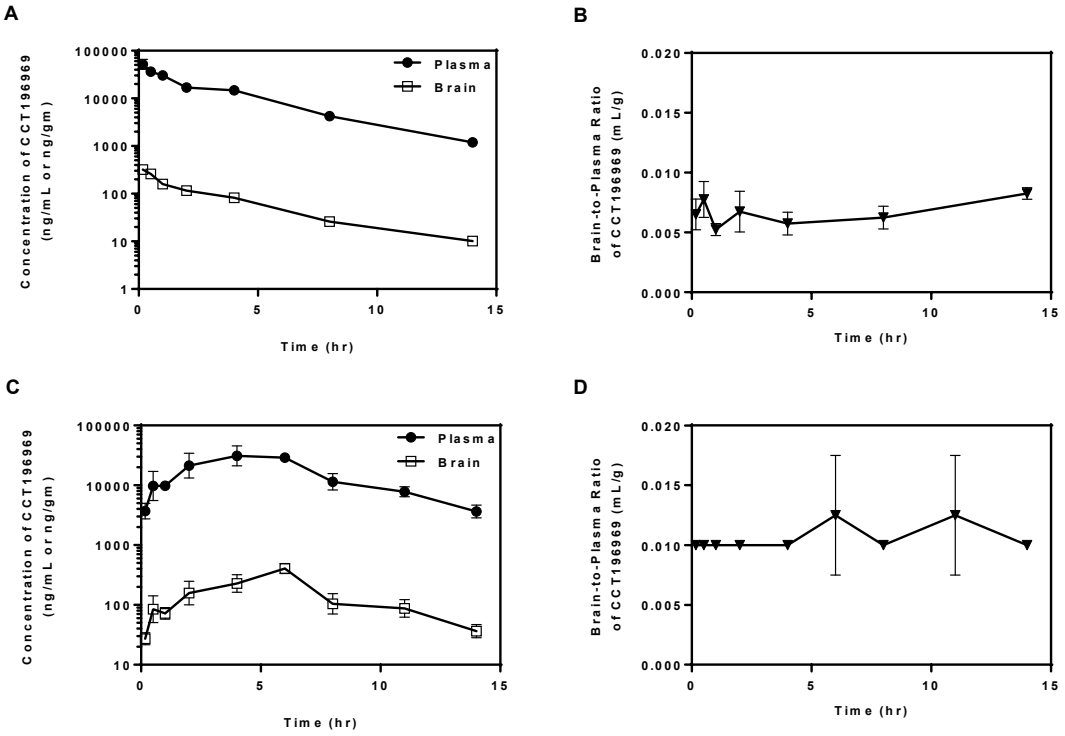

Figure 5. 6 Pharmacokinetic profiles of LY3009120 in FVB wild-type mice following intravenous (i.v.) and oral (p.o.) dosing. Plasma and brain concentrations (A), and brain-to-plasma concentration ratios (B) of LY3009120 following administration of single i.v. bolus dose of 5 mg/kg. Plasma and brain concentrations (C), and brain-to-plasma concentration ratios (D) of LY3009120 post single oral dose of 25 mg/kg. Data represent mean ± S.D., n = 4.

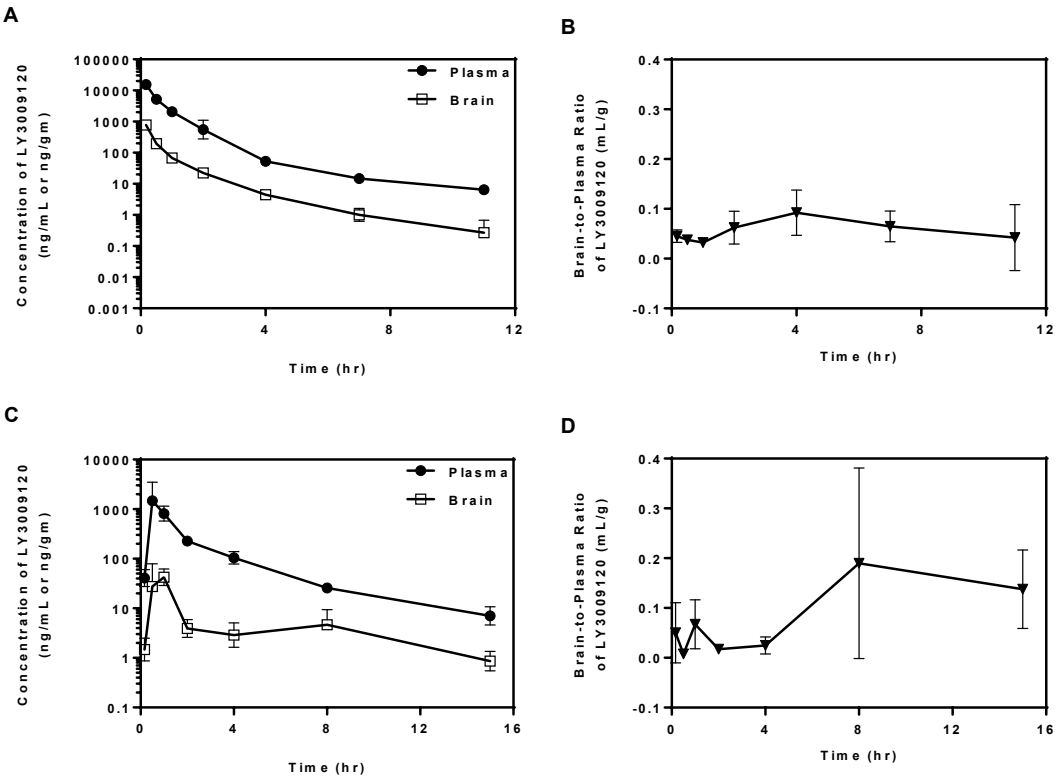

Figure 5. 7 Pharmacokinetic profiles of MLN2480 in FVB wild-type mice following intravenous (i.v.) dosing. Plasma and brain concentrations (A), and brain-to-plasma concentration ratios (B) of MLN2480 following administration of single i.v. bolus dose of 5 mg/kg. Data represent mean ± S.D., n = 4.

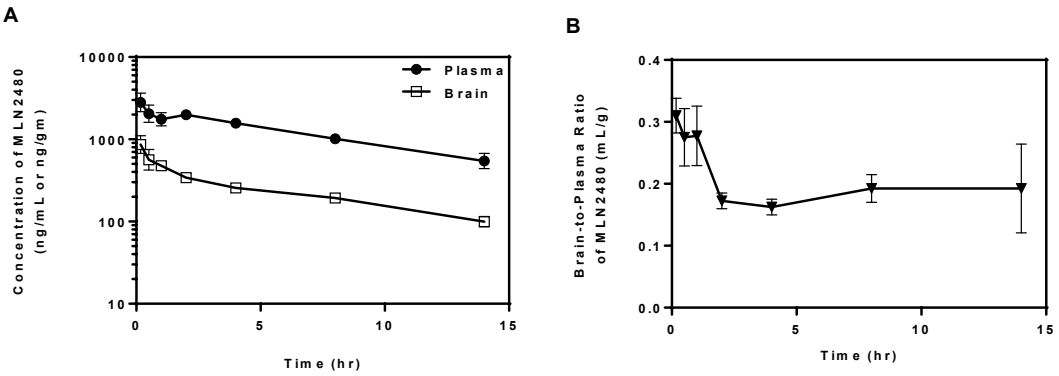

Figure 5. 8 Brain distribution one-hour following oral administration of panRAF inhibitors in FVB wild-type and *Mdr1a/b*$^{-/-}$ *Bcrp1*$^{-/-}$ mice. *P< 0.05, **P< 0.01 and ****P< 0.0001, for statistical comparison by unpaired t-test. Data represent mean ± S.D., n = 4.

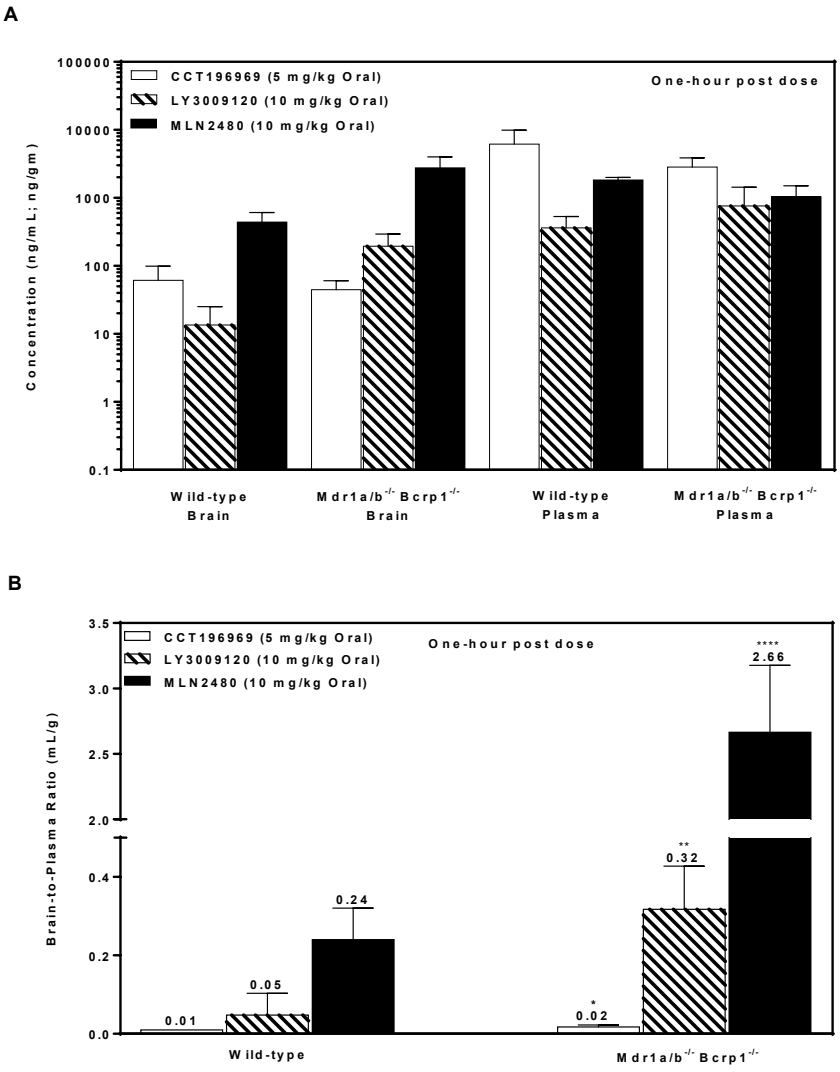

Figure 5. 9 Steady-state brain distribution of panRAF inhibitors in FVB wild-type and *Mdr1a/b*$^{-/-}$ *Bcrp1*$^{-/-}$ mice. (A) Steady-state plasma and brain concentrations of CCT196969, and (B) brain-to-plasma ratios; (C) Steady-state plasma and brain concentrations of LY3009120, and (D) brain-to-plasma ratios; (E) Steady-state plasma and brain concentrations of MLN2480, and (F) brain-to-plasma ratios. **P< 0.01 compared to wild-type brain concentration, ***P< 0.001 compared to wild-type brain concentration, ##P< 0.01 compared to wild-type brain-to-plasma ratio and ###P< 0.001 compared to wild-type brain-to-plasma ratio, for statistical comparison by unpaired t-test. Data represent mean ± S.D., n = 4.

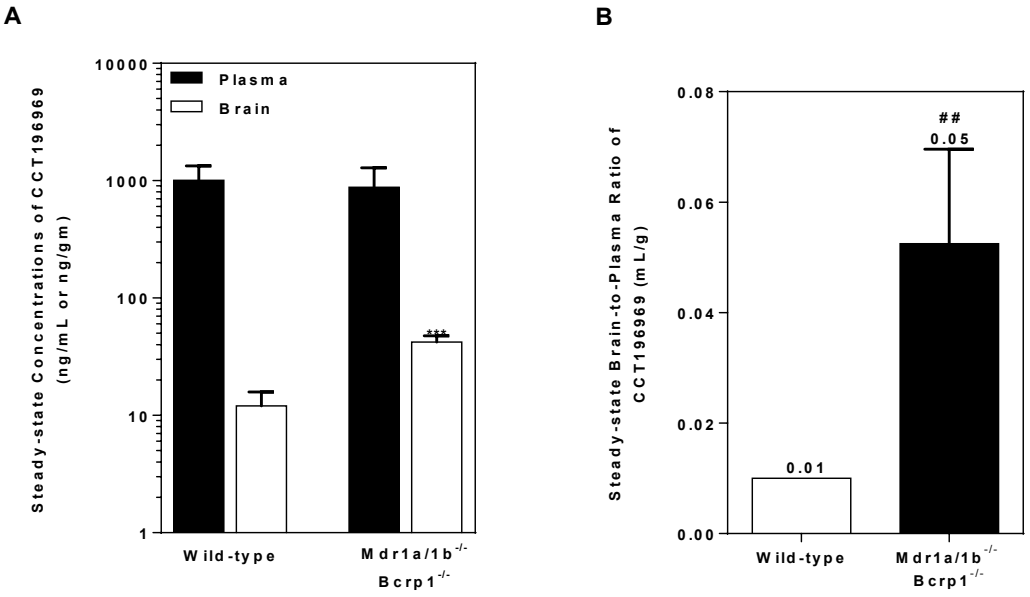

C

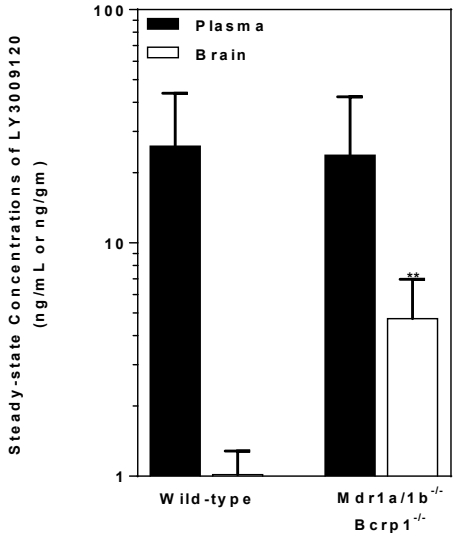
Steady-state Concentrations of LY3009120 (ng/mL or ng/gm)
100
10
1
Plasma
Brain
**
Wild-type
Mdr1a/1b-/-
Bcrp1-/-

D

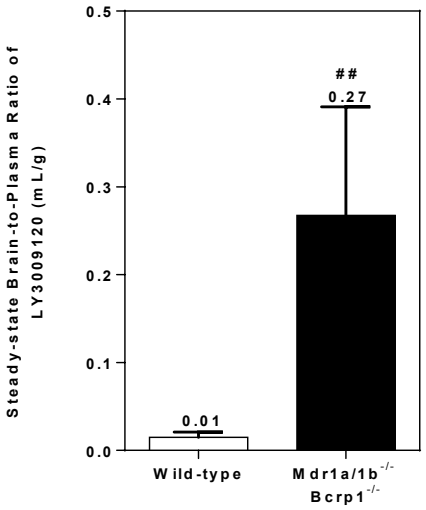
Steady-state Brain-to-Plasma Ratio of LY3009120 (mL/g)
0.5
0.4
0.3
0.2
0.1
0.0
##
0.27
0.01
Wild-type
Mdr1a/1b-/-
Bcrp1-/-

E

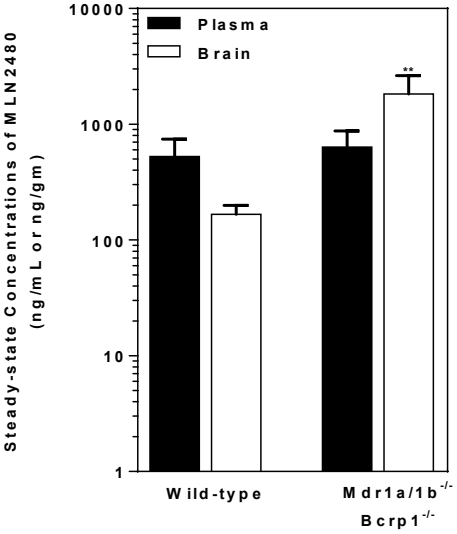
Steady-state Concentrations of MLN2480 (ng/mL or ng/gm)
10000
1000
100
10
1
Plasma
Brain
**
Wild-type
Mdr1a/1b-/-
Bcrp1-/-

F

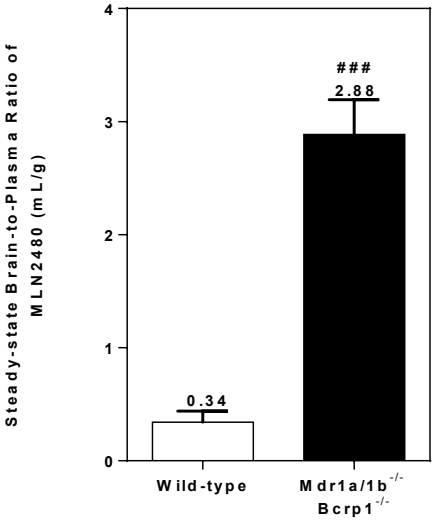
Steady-state Brain-to-Plasma Ratio of MLN2480 (mL/g)
4
3
2
1
0
###
2.88
0.34
Wild-type
Mdr1a/1b-/-
Bcrp1-/-

Figure 5. 10 Plasma and brain unbound concentration-time profiles of (A) CCT196969, (B) LY3009120 and (C) MLN2480 in FVB wild-type mice following 5 mg/kg intravenous drug administration. The unbound concentrations were determined using the in vivo concentrations and the unbound fraction (fu) estimates from in vitro rapid equilibrium dialysis studies. The dashed lines represent the experimentally determined in vitro IC_{50} (free) of the three panRAF inhibitors against BRAF-mutant M12 melanoma cell line. Data represent mean ± S.D., n = 4.

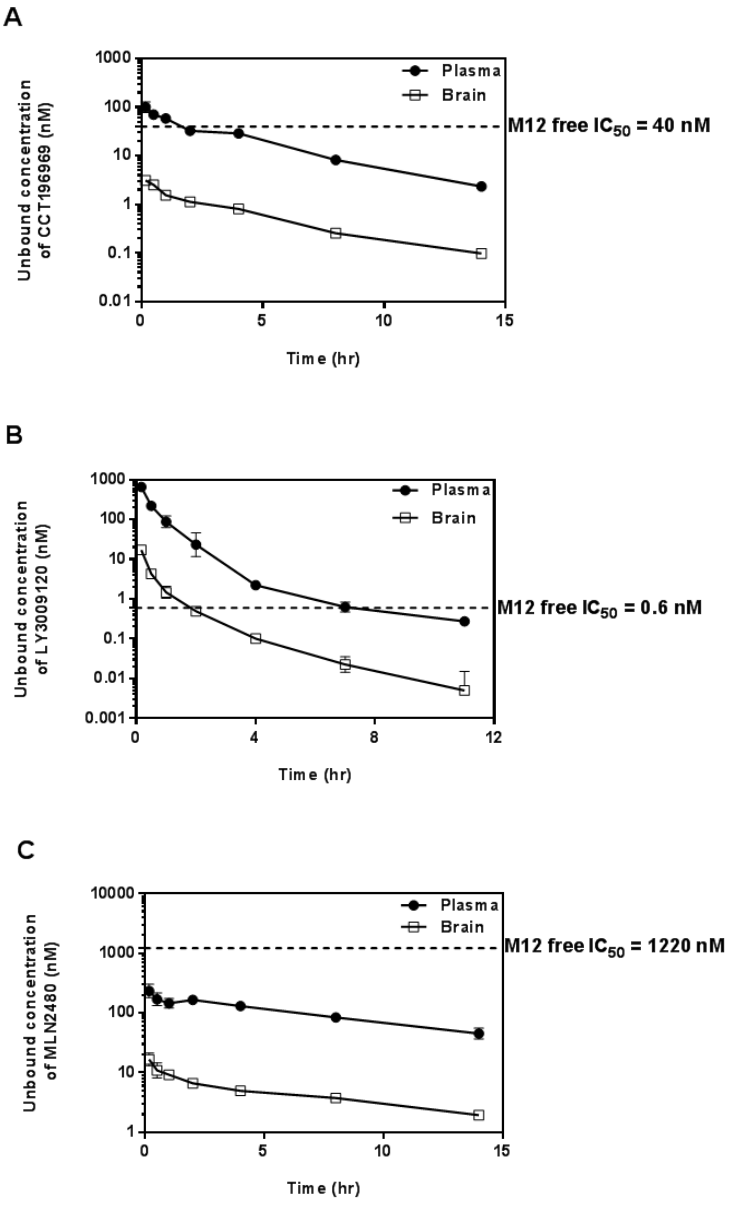

CHAPTER VI. BRAIN DISTRIBUTION OF A NOVEL MEK INHIBITOR E6201: IMPLICATIONS IN THE TREATMENT OF MELANOMA BRAIN METASTASES

Parts of this chapter have been published in:

Gampa G et al. (2018) Brain Distribution of a Novel MEK Inhibitor E6201: Implications in the Treatment of Melanoma Brain Metastases. Drug Metabolism and Disposition 46(5):658-666.

Babiker HM et al. (2018) E6201, an intravenous MEK1 inhibitor, achieves an exceptional response in BRAF V600E-mutated metastatic malignant melanoma with brain metastases. Investigational New Drugs doi: 10.1007/s10637-018-0668-8.

ABSTRACT

Clinically meaningful efficacy in the treatment of brain tumors, including melanoma brain metastases (MBM), requires selection of a potent inhibitor against a suitable target, and adequate drug distribution to target sites in the brain. Deregulated constitutive signaling of mitogen-activated protein kinase (MAPK) pathway has been frequently observed in melanoma, and MEK has been identified to be an important target. E6201 is a potent synthetic small molecule MEK inhibitor. The purpose of this study was to evaluate brain distribution of E6201, and examine the impact of active efflux transport at the BBB on the CNS exposure of E6201. In vitro studies utilizing transfected MDCKII cells indicate that E6201 is not a substrate of P-gp and Bcrp. In vitro efficacy studies in patient-derived cell lines suggest that BRAF-mutant M12 cells are highly sensitive to E6201. In vivo studies also suggest a minimal involvement of P-gp and Bcrp in E6201's brain distribution. The total concentrations in brain were higher than in plasma, resulting in a brain-to-plasma AUC ratio (Kp) of 2.66 in wild-type mice. The brain distribution was modestly enhanced in *Mdr1a/b*$^{-/-}$, *Bcrp1*$^{-/-}$, and *Mdr1a/b*$^{-/-}$*Bcrp1*$^{-/-}$ knockout mice. Drug distribution in an intracranial M12 model was different between tumor and normal brain, with higher drug accumulation in the normal brain compared to the tumor regions. The non-specific binding of E6201 was higher in brain compared to plasma. However, free drug concentrations in brain following 40 mg/kg intravenous dose reach levels that exceed in vitro free IC_{50} values, suggesting that E6201 may be efficacious in inhibiting MEK-driven brain tumors. The brain distribution characteristics of E6201 makes it an

attractive targeted agent for clinical testing in MBM, glioblastoma (GBM) and other CNS tumors that may be effectively targeted with inhibition of MEK signaling.

6.1 INTRODUCTION

Aberrant signaling of the mitogen-activated protein kinase (MAPK) pathway has been observed in about 80% of melanomas and various other types of cancers (Davies et al., 2002). The discovery of activating mutations in the BRAF oncogene, observed in about 50% of melanoma patients, has led to significant advances in therapeutic options for metastatic melanoma (Hocker and Tsao, 2007, Samatar and Poulikakos, 2014). Melanoma patients treated with the newly developed molecularly targeted therapies, e.g., mutant BRAF inhibitors such as vemurafenib and dabrafenib, MEK inhibitors such as trametinib and cobimetinib, have shown improvements in overall survival (OS) (Cohen et al., 2016, Falchook et al., 2012, Long et al., 2012, Margolin et al., 2012, Spagnolo et al., 2016). However, initial responses are often followed by eventual relapse associated with resistance, occurring via mechanisms that cause subsequent hyperactivated downstream MEK signaling (Lito et al., 2013, Samatar and Poulikakos, 2014). In patients with activating BRAF mutations, treatment with BRAF and MEK inhibitor combination showed improved responses compared to single-agent therapy and is an important treatment strategy (Flaherty; Infante; et al., 2012, Larkin et al., 2014, Ribas et al., 2014).

The burden of metastatic melanoma is projected to exceed 87000 new cases and 9700 deaths in the US in 2017 (Siegel et al., 2017). Approximately 70% of patients with metastatic melanoma will develop brain metastases in their lifetime, and after a diagnosis of metastatic spread to the brain, the median overall survival (OS) is less than 6 months (Damsky et al., 2014, Gupta et al., 1997, Raizer et al., 2008, Sloan et al., 2009). Focal therapies with surgical resection and/or radiosurgery can effectively control an individual

metastasis but the risk of developing subsequent brain metastases elsewhere in the brain exceeds 50%, which suggests that integrating these procedures with effective targeted therapies may provide significant clinical benefit (Fife et al., 2004). The successful treatment of brain tumors will need targeted therapies that are: (i) potent against its target, (ii) capable of penetrating an intact blood-brain barrier (BBB) replete with efflux transporters (Osswald et al., 2016), and (iii) capable of reaching the protected tumor cells that are not clinically detectable upon contrast-enhancing MR imaging (Murrell et al., 2015). Many small molecule molecularly-targeted therapies have limited ability to permeate an intact BBB, which in turn can limit their efficacy against brain tumors (Agarwal; Sane; et al., 2011, Gampa; Vaidhyanathan; Resman; et al., 2016, Gampa et al., 2017). While the BBB at the core of larger brain tumors has been observed to be compromised, certain regions of such tumors and micrometastases can have a relatively intact BBB (Essig et al., 2006, Murrell et al., 2015, Osswald et al., 2016). Active drug efflux, mainly by p-glycoprotein (P-gp) and breast cancer resistance protein (Bcrp), is a key mechanism responsible for limiting the entry of various xenobiotics into the brain especially at sites with an intact BBB, including molecularly-targeted therapies approved for melanoma, such as vemurafenib, dabrafenib, trametinib and cobimetinib (Choo et al., 2014, Mittapalli et al., 2013, Mittapalli et al., 2012, Vaidhyanathan et al., 2014). As a consequence, drug delivery to tumor cells residing behind an intact BBB can be severely restricted, causing the establishment of a pharmacological sanctuary. There is a critical need to overcome issues related to brain drug delivery, and develop effective targeted

therapies that can penetrate an intact BBB and reach the target sites on the tumor cells in the brain (Heffron, 2016).

E6201 (Figure 1) is a natural product-inspired synthetic non-allosteric kinase inhibitor that inhibits both MEK1 and FLT3 (Ikemori-Kawada et al., 2012). E6201 is an ATP-competitive MEK inhibitor, in contrast to clinically approved drugs like trametinib and cobimetinib that are allosteric MEK inhibitors (Narita et al., 2014). The binding affinity of E6201 has been shown to be identical for both the active and inactive forms of MEK1 (Goto et al., 2009). The reported in vitro IC_{50} for E6201 against multiple melanoma cell lines (particularly BRAF mutant lines) was less than 100 nmol/L, indicating that E6201 exhibits potent activity against melanoma cells (Byron et al., 2012, Narita et al., 2014).

Given that melanoma has a high propensity to metastasize to the CNS, and inhibition of MEK has been recognized to be an important strategy in treating metastatic melanoma, testing the ability of E6201 to permeate an intact BBB would be essential. The purpose of this study was to determine the brain distribution of E6201 and evaluate the role of major BBB efflux proteins, P-gp and/or Bcrp in limiting the brain delivery of E6201, using mouse models. Such information can be valuable in evaluating the utility of this agent as an effective therapy for patients with melanoma brain metastases (MBM), and can inform future clinical trials. A brain penetrant MEK inhibitor would be particularly useful in patients with MBM, and as such would hold great promise for the treatment of metastatic melanoma.

6.2 MATERIALS AND METHODS

6.2.1 Chemicals

E6201 ((3S,4R,5Z,8S,9S,11E)-14-(ethylamino)-8,9,16-trihydroxy-3,4-dimethyl-3,4,9,10-tetrahydro-1H-2-benzoxacyclotetradecine-1,7(8H)-dione)) and ER807551 were kindly provided by Strategia Therapeutics Inc. (Houston, TX). [^{3}H]-Vinblastine was purchased from Moravek Biochemicals (La Brea, CA). [^{3}H]-Prazosin was purchased from PerkinElmer Life and Analytical Sciences (Waltham, MA). Ko143 [(3S,6S,12aS)-1,2,3,4,6,7,12,12a-octahydro-9-methoxy-6-(2-methylpropyl)-1,4-dioxopyrazino(1',2':1,6) pyrido(3,4-b)indole-3-propanoic acid 1,1-dimethylethyl ester] was purchased from Tocris Bioscience (Ellisville, MO). Zosuquidar [LY335979, (R)-4-([1aR, 6R,10bS]-1,2-difluoro-1,1a,6,10b-tetrahydrodibenzo-[a,e] cyclopropa [c]cycloheptan-6-yl)-([5-quinoloyloxy] methyl)-1-piperazine ethanol, trihydrochloride] was provided by Eli Lilly and Co. (Indianapolis, IN). All other chemicals used were of high-performance-liquid-chromatography or reagent grade and were obtained from Sigma-Aldrich (St. Louis, MO).

6.2.2 In Vitro Accumulation Studies

Polarized Madin-Darby canine kidney II (MDCKII) cells were used for performing in vitro accumulation studies. MDCKII-wild type and Bcrp1-transfected (MDCKII-Bcrp1) cell lines were a kind gift from Dr. Alfred Schinkel (The Netherlands Cancer Institute). MDCKII-wild type and gene encoding the human P-glycoprotein (MDR1)- transfected (MDCKII-MDR1) cell lines were kindly provided by Dr. Piet Borst (The Netherlands Cancer Institute). Cells were cultured in Dulbecco's modified Eagle's medium

supplemented with 10% (v/v) fetal bovine serum and antibiotics (penicillin, 100 U/ml; streptomycin, 100 mg/ml; and amphotericin B, 250 ng/ml). Cells were grown in 25 mL tissue culture-treated flasks before seeding for the intracellular accumulation experiments and were maintained at 37°C in a humidified incubator with 5% carbon dioxide.

The intracellular accumulation of E6201 was performed in 12-well polystyrene plates (Corning Glassworks, Corning, NY). In brief, cells were seeded at a density of 2 x 10^5 cells and grown until ~80% confluent. On the day of experiment, the culture media was aspirated and the cells were washed two times with warm cell assay buffer (122 mM NaCl, 25 mM $NaHCO_3$, 10 mM glucose, 10 mM HEPES, 3 mM KCl, 2.5 mM $MgSO_4$, 1.8 mM $CaCl_2$, and 0.4 mM K_2HPO_4). The cells were then pre-incubated with cell assay buffer for 30 min, after which the buffer was aspirated and the experiment was initiated by adding 1 mL assay buffer containing 5 μM E6201 into each well with further incubation for 60 minutes in an orbital shaker (ShelLab, Cornelius, OR) maintained at 37°C and 60 rpm. At the end of a 60-minute incubation, the experiment was ended by aspirating the E6201 solution followed by washing twice with ice-cold phosphate-buffered saline (PBS). The cell lysis was accomplished by adding 500 μL of 1% Triton-X100 to each well. When the inhibitor was used, it was included in both pre-incubation and accumulation steps. The concentration of E6201 in solubilized cell fractions was analyzed using liquid chromatography–tandem mass spectrometry (LC-MS/ MS) as described later, and was normalized to the protein content (BCA assay).

6.2.3 In vitro binding assay for determination of free (unbound) fractions

The free fraction of E6201 in plasma, brain and serum-containing cell culture media were determined by performing rapid equilibrium dialysis (RED) experiments as per the protocol described by the manufacturer, with some modifications suggested in the literature (Friden et al., 2007, Kalvass and Maurer, 2002). RED base plate (Thermo Fisher Scientific), and single use RED inserts (Thermo Fisher Scientific) with 8 kDa molecular weight cut off (MWCO) were used for these experiments. Briefly, fresh plasma and brain homogenates (prepared in 3 volumes of PBS, w/v) isolated from wild-type FVB mice were used. E6201 stock in DMSO (1 mg/mL) was spiked in plasma and brain homogenate to obtain final concentrations of 10 μM (DMSO <1% of final volume), and in cell culture media to obtain final concentrations of 1 μM. 300 μL of E6201 spiked plasma/brain homogenate/media was placed in the sample chamber (donor), and 500 μL of phosphate buffered saline (1x PBS at pH 7.4; 100 mM sodium phosphate and 150 mM sodium chloride) was placed in buffer chamber (receiver) of the RED inserts in triplicates. The inserts were placed in a base plate, the assembly covered with sealing tape and incubated on an orbital shaker (ShelLab, Cornelius, OR) at 37^{o}C and 300 rpm for 4 hours (preliminary studies show that equilibrium is achieved by 4 hours). After dialysis, 150 μL of both plasma/brain homogenate/media and buffer were collected and the concentrations of E6201 were determined by LC-MS/MS. The Kp for trametinib has been previously reported in literature, but the fu was not available. So, RED experiments were performed to determine the free fractions of trametinib in plasma and brain, as

described for E6201. The experiments were performed with a concentration of 2 μM trametinib in both plasma and brain matrices.

6.2.4 In vitro cytotoxicity in patient-derived cell lines

The in vitro cytotoxicity of E6201 was tested in short-term cultured human primary melanoma cells (BRAF-mutant M12 or BRAF-mutant M27 or NRAS-mutant M15) and glioblastoma (GBM43, loss of NF1 and wild-type PTEN) cells that were maintained by serial passages through subcutaneous implantation in immune-deficient mice (Carlson et al., 2011). The cells were cultured in Dulbecco's modified Eagle's medium (DMEM) supplemented with 10% (v/v) fetal bovine serum (FBS) and antibiotics (penicillin, 100 U/ml and streptomycin, 100 μg/ml), and were maintained in a humidified incubator with 5% carbon dioxide at 37°C.

Briefly, the cells (M12 or M27 or M15 or GBM43) were seeded in 96-well black clear bottom plates (Corning Incorporated, Corning, NY) at a density of 3500 cells per well, and were treated with 9 concentrations of E6201 or trametinib (n = 6 per concentration) 24 hours after plating (about 80% confluency). The plates were incubated for 5 days, and the cell viability was determined using a CyQuant cell proliferation assay (Invitrogen) and fluorescence measurement with a BioTek Synergy HT plate reader. The relative survival of cells was normalized to the untreated controls.

6.2.5 In vivo studies

Animals:

Friend leukemia virus strain B (FVB) wild-type (WT), *Mdr1a/b*$^{-/-}$ (P-gp knockout), *Bcrp1*$^{-/-}$ (Bcrp knockout), and *Mdr1a/b*$^{-/-}$ *Bcrp1*$^{-/-}$ (triple knockout) mice of either sex

(balanced) were used for all the in vivo studies (Taconic Farms, Germantown, NY). All mice used were 8-16 week-old adults, approximately 18 - 35 g, at the time of the experiments. Mice were maintained in a 12-hour light/dark cycle with unlimited access to food and water. All studies carried out were in agreement with the guidelines set by Principles of Laboratory Animal Care (National Institutes of Health, Bethesda, MD), and approved by Institutional Animal Care and Use Committee (IACUC) at University of Minnesota.

Spatial brain distribution studies followed intracranial tumor implantation in female athymic nude mice (Harlan Sprague-Dawley athymic nude-Foxn1nu; Envigo, Indianapolis, IN) that were 6-7 weeks old. These studies were approved by Institutional Animal Care and Use Committee (IACUC) at the Mayo Clinic and were carried out in agreement with the guidelines set by the Principles of Laboratory Animal Care (National Institutes of Health, Bethesda, MD). Animals were housed in a 12-hour light/dark cycle with unrestricted access to water and food.

Plasma and brain pharmacokinetics of E6201 after intravenous, intraperitoneal and oral administration:

All dosing solutions were freshly prepared on the day of the experiment. E6201 dosing formulation was prepared by reconstituting lyophilized powder in single-use vials (received from Strategia Therapeutics Inc.), containing 60 mg E6201 and 3 g Captisol, with 8.5 mL sterile water for injection.

In the first set of studies, an intravenous (i.v.) bolus dose of 40 mg/kg E6201 (a dose previously used in efficacy studies, E6201 investigators brochure) was administered to

FVB wild-type, *Mdr1a/b*$^{-/-}$, *Bcrp1*$^{-/-}$, and *Mdr1a/b*$^{-/-}$ *Bcrp1*$^{-/-}$ knockout mice via tail vein. Blood and brain samples were harvested at 0.083, 0.25, 0.5, 1, 2, 4 and 6 hours post-dose in a serial sacrifice (destructive sampling) design (n = 5 at each time point). At the desired sample collection time point, the animals were euthanized using a carbon dioxide chamber. Blood was collected by cardiac puncture in heparinized tubes. The whole brain was removed from the skull and washed with ice-cold distilled water, and superficial meninges were removed by blotting with tissue paper. Plasma was separated by centrifugation of whole blood at 3500 rpm and 4°C for 15 min. Both plasma and brain samples were stored at -80°C until further analysis for E6201 concentrations by LC-MS/MS. Brain concentrations were corrected for residual drug in brain vasculature assuming a vascular volume of 1.4% in mouse brain (Dai et al., 2003).

In the second set of in vivo studies, 40 mg/kg E6201 was administered to FVB wild-type and *Mdr1a/b*$^{-/-}$ *Bcrp1*$^{-/-}$ knockout mice via intraperitoneal (i.p.) route. Blood and brain samples were harvested at 0.25, 0.5, 1, 2, 4 and 6 hours post-dose in a serial sacrifice design (n = 4 at each time point) as described for i.v. studies.

In the third study, 40 mg/kg E6201 was administered to FVB wild-type mice via oral gavage (p.o.). Blood and brain samples were harvested at 0.25, 0.5, 1, 2, 4 and 6 hours post-dose in a serial sacrifice design (n = 4 at each time point) as described for i.v. studies.

Steady-state brain distribution of E6201 in FVB mice:

The determination of steady-state plasma and brain concentrations of E6201 was accomplished by implanting Alzet osmotic mini pumps (model 1003D; Durect

Corporation, Cupertino, CA) loaded with 6 mg/mL E6201 in the peritoneal cavity of wild-type and *Mdr1a/b*$^{-/-}$ *Bcrp1*$^{-/-}$ mice to deliver the drug at a constant rate of 6 µg/hr. The E6201 formulation was prepared by reconstituting lyophilized powder in single-use vials (received from Strategia Therapeutics Inc.), containing 60 mg E6201 and 3 g Captisol, with 8.5 mL sterile water for injection, which yielded a final concentration of 6 mg/mL E6201. The drug formulation was loaded into minipumps and primed overnight in sterile PBS at 37°C on the day before the experiment. The pumps were implanted into the peritoneal cavity as described previously (Agarwal et al., 2013). Briefly, mice were anaesthetized using isoflurane, and the hair over the skin on the abdominal cavity was removed. A small incision was made in the skin on the lower right abdomen, followed by an incision in the exposed peritoneal membrane under the cutaneous opening, and the primed pump was inserted into the peritoneal cavity. The peritoneal membrane was sutured with absorbable sutures, and the opening in the skin was sealed with surgical clips. The whole procedure was performed on a heating pad until the animals fully recovered. The half-life for E6201 in mice is approximately 45 minutes and so an infusion lasting for 7 hours was considered sufficient to attain steady-state E6201 levels in both plasma and brain. The mice were sacrificed, and blood and brain samples were isolated 7 hours (steady state) following the implantation of osmotic minipumps. Plasma was obtained by centrifugation of blood samples at 3500 rpm for 15 minutes. The plasma and brain samples were stored at -80°C until analysis by LC-MS/MS.

Spatial brain distribution of E6201 in an intracranial tumor model:

The spatial brain distribution of E6201 was examined in an intracranial mouse model. M12 patient-derived melanoma cells, that were transduced with green fluorescent protein and luciferase (M12-GFPLUC), were implanted via stereotaxic intracranial injections as described previously (Carlson et al., 2011). Briefly, mice were anesthetized with ketamine (100 mg/kg) and xylazine (10 mg/kg), and intracranial stereotaxic injections of cell suspension (100,000 cells per mouse, 3 μL volume) were performed at 1 mm anterior and 2 mm lateral from the bregma. After 2-3 weeks, mice with intracranial M12 tumors received a single intraperitoneal dose of 40 mg/kg E6201. The blood and brain (tumor-bearing) samples were collected 30 minutes post dose (n = 9). The harvested whole brains were flash frozen immediately. Plasma was obtained by centrifugation of blood samples at 3500 rpm and 4°C for 15 minutes. The samples were stored at -80°C until further processing.

A fluorescence microscopy based technique was utilized for the dissection of tumor core, tumor rim (brain adjacent to tumor, BAT) and normal (non-tumor) brain tissues from the whole brain specimens. Briefly, thick coronal sections of tumor-bearing brains that were 1-2 mm in thickness were obtained using an acrylic mouse brain matrix (WPI). A fluorescence microscope (Nikon AZ100M) was employed to visualize GFP labelled M12 tumors in the brain slices. The boundaries of tumor core were identified by relative fluorescence, and biospy punches (Harris Uni-Core, Miltex) of varying diameters were used to carefully dissect the tumor core from the rim regions. The tumor core was identified as the region of the tumor with a fluorescence signal that was about 10-fold or higher than the background fluorescence signal observed in the normal brain. The tumor

rim was identified as the region surrounding the tumor core that has a fluorescence signal about 5 to 10-fold higher than the background fluorescence signal. The brain tissue with similar or lower signal than the background signal was isolated as the normal brain (i.e, without tumor) regions. The tissues from the regions of interest were isolated from one or more slices from an individual brain, and pooled together. All the collected samples were stored at -80°C, and the concentrations of E6201 in the tumor core, tumor rim, normal brain and plasma samples were determined using LC-MS/MS.

6.2.6 LC-MS/MS analysis

The concentrations of E6201 in all samples from in vitro and in vivo studies were determined using a specific and sensitive LC-MS/MS assay. E6201 and samples/solutions containing E6201 were protected from light in all experiments to avoid drug degradation. Brain samples were homogenized using a mechanical homogenizer (PowerGen 125; Thermo Fisher Scientific, Waltham, MA) following the addition of three volumes of 5% bovine serum albumin (BSA) to obtain uniform homogenates. For analysis of unknowns, an aliquot of sample (cell lysate, cell assay buffer, PBS, plasma, or brain homogenate) was spiked with 50 ng of ER807551 as an internal standard and liquid-liquid extraction was performed by addition of 5-10 volumes of ethyl acetate, followed by vigorous shaking for 5 minutes and centrifugation at 7500 rpm and 4°C for 5 minutes. The organic layer was separated and transferred to microcentrifuge tubes, and dried under nitrogen gas. The dried powder was reconstituted in 100 μL of mobile phase and transferred into high-performance-liquid-chromatography glass vials with microinserts. Chromatographic analysis was performed using an AQUITY UPLC system

(Waters, Milford, MA). The chromatographic separation was achieved by injection of 7.5 μL sample onto a C18 YMC-ODS-AM (3 μ particle size, 2.0 mm ID x 23 mm length; YMC America, USA) column. A gradient method was employed with mobile phase consisting of 0.1% formic acid in water as the aqueous component (A) and 0.1% formic acid in methanol as the organic component (B). The gradient was as follows: started with 35% B at 0 minutes, increased to 100% B by 0.5 minutes and maintained at 100% B up to 3.2 minutes, decreased to 35% B by 3.5 minutes and maintained at 35% B up to 7 minutes. The mobile phase was delivered at a constant flow rate of 0.3 mL/min.

The column effluent was monitored using a Micromass Quattro Ultima mass spectrometer (Waters, Milford, MA). The instrument was equipped with an electrospray interface, and controlled by the MassLynx (Version 4.1; Waters) data system. The samples were analyzed using an electrospray probe in the positive-ionization mode operating at a spray voltage of 2.5 kV for both E6201 and ER807551. Samples were introduced into the interface through a heated nebulized probe, in which the source temperature and desolvation temperature were set at 100°C and 400°C, respectively. The mass spectrometer was programmed to allow the $[MH]^+$ ions of E6201 and ER807551 at m/z ratios of 390.08 and 450.08, respectively, to pass through the first quadrupole (Q1) and into the collision cell (Q2). The collision energy was set at 20 V and 25 V for E6201 and ER807551, respectively. The daughter ions for E6201 (m/z 232) and ER807551 (m/z 273.96) were monitored through the third quadrupole (Q3). The retention times for E6201 and ER807551 were 1.11 and 1.12 minutes, respectively. The runtime was 7 minutes.

6.2.7 Pharmacokinetic analysis and calculations

Pharmacokinetic parameters from the concentration-time profiles in plasma and brain were obtained by non-compartmental analysis (NCA) performed using Phoenix WinNonlin version 6.4 (Certara USA, Inc., Princeton, NJ). The area under the concentration-time curves (AUC) for plasma (AUC_{plasma}) and brain (AUC_{brain}) were calculated using the linear trapezoidal method. The standard errors around the means of AUC and Cmax were estimated using the sparse sampling module in WinNonlin (Nedelman and Jia, 1998).

Free (unbound) fraction (fu) in plasma and brain homogenate were calculated as the ratio of buffer to matrix concentrations of E6201 (Kalvass and Maurer, 2002).

$$\text{fu, diluted} = \frac{\text{E6201 concentration in buffer (receiver)}}{\text{E6201 concentration in matrix (donor)}} \quad (Equation\ 1)$$

The fraction unbound for brain was determined from the measured fraction unbound in diluted brain homogenate (fu,diluted), using the following equation (Kalvass and Maurer, 2002).

$$\text{fu, brain} = \frac{1/\text{D}}{(1/\text{fu, diluted} - 1) + 1/\text{D}} \quad (Equation\ 2)$$

where D (equal to 4) represents the dilution factor, accounting for the diluted brain homogenate.

The recovery was estimated using the equation,

$$\text{Recovery (\%)} = \frac{(\text{donor mass} + \text{receiver mass})\text{after dialysis}}{\text{donor mass, before dialysis}} \text{ x } 100 \quad (Equation\ 3)$$

The brain-to-plasma ratio (Kp) was calculated as the ratio of AUC_{brain} to AUC_{plasma}.

$$\mathrm{Kp} = \frac{\mathrm{AUCbrain}}{\mathrm{AUCplasma}} \quad (Equation\ 4)$$

A comparison of relative drug exposure in the brain between wild-type and knockout (*Mdr1a/b*$^{-/-}$*, Bcrp1*$^{-/-}$*, and Mdr1a/b*$^{-/-}$ *Bcrp1*$^{-/-}$) mice was made using the distribution advantage (DA).

$$\mathrm{DA} = \frac{\mathrm{Kp}, knockout}{\mathrm{Kp}, wild\ type} \quad (Equation\ 5)$$

The unbound partition coefficient (Kp,uu) was calculated for the four genotypes using the equation,

$$\mathrm{Kp, uu} = \frac{\mathrm{AUCbrain\ x\ fu, brain}}{\mathrm{AUCplasma\ x\ fu, plasma}} \quad (Equation\ 6)$$

6.2.8 Statistical Analysis

GraphPad Prism version 6.04 (GraphPad, L Jolla, CA) software was used for the statistical analysis. The sample sizes used were based on previous work and were determined based on approximately 80% power to detect 50% difference between groups. Data from all experiments are represented as mean ± standard deviation (S.D.) or mean ± standard error of the mean (S.E.M) unless otherwise indicated. Comparisons between two groups were made using an unpaired t-test. Comparisons between multiple groups were made using one-way analysis of variance (ANOVA), followed by Bonferroni's multiple comparison test. A significance level of $P < 0.05$ was used for all statistical analysis.

6.3 RESULTS

6.3.1 In vitro accumulation of E6201 in MDCKII-Bcrp1 and MDCKII-MDR1 cells

The intracellular accumulation of E6201 in MDCKII wild-type, Bcrp1-transfected, and MDR1-transfected cell lines is summarized in Figure 2. [^{3}H]-Prazosin and [^{3}H]-vinblastine were used as positive controls for Bcrp1 and MDR1, respectively. As expected, the cellular accumulation of [^{3}H]-prazosin was significantly lower as compared with wild-type controls (WT: 100±29%; Bcrp1: 25±5%; $P<0.05$). Similarly, the cellular accumulation of [^{3}H]-vinblastine was also significantly lower when compared with wild-type controls (WT: 100±31%; MDR1: 7±1%; $P<0.01$). These results validate the significant elevation of efflux transporter activity in the relevant transfected cell lines. In the same experiment, incubation with 5 μM E6201 showed that the accumulation of E6201 was not significantly different in Bcrp1 cells (Bcrp: 107±29%; WT: 100±29%), and in MDR1 cells (MDR1: 89±16%; WT: 100±9%) when compared with corresponding wild-type controls. The addition of 0.2 μM Ko143, a specific Bcrp1 inhibitor, to the Bcrp1 cells and 1 μM LY335979, a specific MDR1 inhibitor, to MDR1 cells did not lead to significant differences in intracellular accumulation when compared to transfected cells without inhibitor. These data indicate that E6201 is not a substrate for either P-gp or Bcrp1.

6.3.2 Determination of free (unbound) fraction of E6201 and trametinib

In vitro rapid equilibrium dialysis was used for the determination of free fraction (equations 1 and 2) in plasma, brain and cell culture media. The free fraction (fu) for E6201 in plasma was determined to be 2.63 ± 0.18% and the mass balance recovery of

the experiment was 94.04 ± 3.32% (Table 1). The fu for E6201 in brain was found to be 0.14 ± 0.02% and the mass balance recovery was 113.20 ± 9.50% (Table 1). The fu for E6201 in cell culture media was found to be 0.39 ± 0.04% and the recovery was 79.96 ± 1.80% (Table 1). The fu for trametinib in plasma was found to be 0.21 ± 0.03% and the mass balance recovery of the experiment was 99.9% ± 8.42% (Table 1). The fu for trametinib in brain was determined to be 0.21 ± 0.02% and the mass balance recovery was 106.56 ± 2.35% (Table 1). The estimated fu values were used for the determination of unbound partition coefficient, Kp,uu.

6.3.3 In vitro efficacy in patient-derived cell lines

The in vitro efficacy studies were performed in 4 patient-derived cell lines. The total IC_{50} for trametinib (control) and E6201 were estimated using the total drug concentration-response curves determined in BRAF-mutant M12, BRAF-mutant M27, and NRAS-mutant M15 melanoma cell lines, and GBM43 cell line. The free IC_{50} values were estimated using the total IC_{50} estimates and the free fraction of E6201 in cell culture media. The dose-response curves are shown in Figure 3, and the IC_{50} values are listed in Table 2, respectively. The results indicate that M12 is the most sensitive and GBM43 is the least sensitive cell line to treatment with E6201, among the cell lines tested.

6.3.4 Plasma and brain pharmacokinetics following intravenous, intraperitoneal and oral E6201 administration

The pharmacokinetic parameters for E6201 were determined in FVB wild-type and transporter deficient (knockout) mice following various routes of E6201 administration. The brain and plasma concentration time profiles and brain-to-plasma ratio profiles in

FVB wild-type, *Mdr1a/b*$^{-/-}$, *Bcrp1*$^{-/-}$, *and Mdr1a/b*$^{-/-}$ *Bcrp1*$^{-/-}$ mice following a single intravenous bolus dose of 40 mg/kg E6201 are as shown in Figure 4. The total plasma E6201 concentrations (Figure 4A) were similar between the four genotypes at any given time point. The total brain E6201 concentrations (Figure 4B) at the indicated time points were higher than the total plasma concentrations in all the four genotypes. Table 3 summarizes the estimated pharmacokinetic parameters in the four genotypes of mice studied. There were no statistically significant differences between the wild-type plasma AUC and any of the transporter knockout plasma AUCs. The estimated AUCs in the brain for *Mdr1a/b*$^{-/-}$, *Bcrp1*$^{-/-}$, *and Mdr1a/b*$^{-/-}$ *Bcrp1*$^{-/-}$ mice were significantly higher when compared with the AUC in wild-type mice ($P<0.05$). The observed systemic clearance and volume of distribution were similar in the wild-type and knockout mice. The brain-to-plasma AUC ratios (Kp, equation 4) in the wild-type, *Mdr1a/b*$^{-/-}$, *Bcrp1*$^{-/-}$, *and Mdr1a/b*$^{-/-}$ *Bcrp1*$^{-/-}$ mice were 2.66, 4.37, 3.72 and 5.40, respectively. A comparison of relative drug exposure in the brain between wild-type and knockout (*Mdr1a/b*$^{-/-}$, *Bcrp1*$^{-/-}$, *and Mdr1a/b*$^{-/-}$ *Bcrp1*$^{-/-}$) mice was made using the distribution advantage (DA), which is defined as the Kp in knockout mice normalized by the Kp in wild-type mice (equation 5). The DA in *Mdr1a/b*$^{-/-}$, *Bcrp1*$^{-/-}$, *and Mdr1a/b*$^{-/-}$ *Bcrp1*$^{-/-}$ mice were 1.64, 1.39 and 2.03, suggesting minimal involvement of P-gp and Bcrp in limiting the brain distribution of E6201. The extent of distribution of free drug is represented by term "Kpuu" and can be defined as the ratio of the unbound drug exposure in the brain over the unbound drug exposure in plasma (equation 6). The Kp,uu in the wild-type, *Mdr1a/b*$^{-/-}$, *Bcrp1*$^{-/-}$, *and Mdr1a/b*$^{-/-}$ *Bcrp1*$^{-/-}$ mice were 0.14, 0.24, 0.20 and 0.29, respectively.

The concentration time profiles and brain-to-plasma ratio profiles in FVB wild-type *and* *Mdr1a/b*$^{-/-}$ *Bcrp1*$^{-/-}$ mice following a single intraperitoneal dose of 40 mg/kg E6201 are shown in Figure 5. The estimated pharmacokinetic parameters are summarized in Table 4. There was no statistically significant difference between the wild-type plasma AUC and *Mdr1a/b*$^{-/-}$ *Bcrp1*$^{-/-}$ plasma AUC. The AUC in the brain for *Mdr1a/b*$^{-/-}$ *Bcrp1*$^{-/-}$ mice was significantly higher when compared to the AUC in wild-type mice ($P<0.05$). The Kp in wild-type *and Mdr1a/b*$^{-/-}$ *Bcrp1*$^{-/-}$ mice were 2.2 and 3.83, respectively. The Kp,uu values in wild-type *and Mdr1a/b*$^{-/-}$ *Bcrp1*$^{-/-}$ mice were 0.12 and 0.21, respectively. The absolute bioavailability (F) following i.p. administration was found to be 0.95.

The concentration time profiles and brain-to-plasma ratio profile in FVB wild-type mice following single oral dose of 40 mg/kg E6201 are shown in Figure 6. The estimated pharmacokinetic parameters are summarized in Table 5. The Kp and Kp,uu were found to be 2.35 and 0.13, respectively. The absolute bioavailability following p.o. administration was 0.39.

6.3.5 Steady-state brain distribution of E6201 in FVB mice

The steady-state concentrations of E6201 in brain (48.22 ± 20.99 ng/g in wild-type mice; 82.32 ± 21.59 ng/g in *Mdr1a/b*$^{-/-}$*Bcrp1*$^{-/-}$ mice) were higher than that in plasma (26.54 ± 4.60 ng/mL in wild-type mice; 18.57 ± 2.46 ng/mL in *Mdr1a/b*$^{-/-}$*Bcrp1*$^{-/-}$ mice), for both wild-type and *Mdr1a/b*$^{-/-}$*Bcrp1*$^{-/-}$ mice (Figure 7A). The corresponding brain-to-plasma ratios (Kp) in wild-type and *Mdr1a/b*$^{-/-}$*Bcrp1*$^{-/-}$ mice were 1.8 and 4.38, respectively (Figure 7B).

6.3.6 Spatial distribution of E6201 in an intracranial tumor model

The representative microscopy images of a brain slice and dissected regions of interest, as well as the concentrations of E6201 in plasma, tumor core, tumor rim and normal brain at 30 minutes following administration of a single intraperitoneal dose of 40 mg/kg E6201 are shown in Figure 8. Also shown are the brain (tumor tissue)-to-plasma concentration ratios (Kp) in tumor core, tumor rim and normal brain. The results indicate a heterogeneous distribution of E6201 across the BBB (assuming similar binding in the different regions) in the M12 intracranial mouse model, with the relative distribution of E6201 being lowest to the tumor core and highest to the normal brain region. The average Kp in the normal brain was higher than that in the tumor rim, and the Kp in tumor rim was higher than that in the tumor core.

6.4 DISCUSSION

The approved small molecule targeted therapies for melanoma; inhibitors of MAP kinase signaling (BRAF inhibitors, vemurafenib and dabrafenib; MEK inhibitors, trametinib and cobimetinib) and large molecule immune checkpoint inhibitors (CTLA-4 inhibitors such as ipilimumab, and PD-1 inhibitors such as nivolumab) have shown improvements in overall survival (OS) and progression-free survival (PFS) by a few months in patients with MBM (Cohen et al., 2016, Dummer et al., 2014, Falchook et al., 2012, Long et al., 2012, Margolin et al., 2012, Spagnolo et al., 2016). While encouraging (Bates, 2013), it is still difficult to treat advanced metastatic disease that has spread to the brain. The modest efficacy in patients with MBM may be related to both inadequate drug delivery and specific brain microenvironment driven changes in gene expression. Previous studies have shown that vemurafenib, dabrafenib, trametinib and cobimetinib have limited brain distribution due to active efflux by Bcrp and/or P-gp (Choo et al., 2014, Mittapalli et al., 2013, Mittapalli et al., 2012, Vaidhyanathan et al., 2014).

E6201, a novel MEK inhibitor, may be beneficial in treatment of melanoma either in combination with a BRAF inhibitor or as a single agent. In the current study, we investigated brain distribution of E6201 in mice, examined the role of efflux transport on brain distribution, and determined its free fraction in plasma and brain. The results help us understand if E6201 can distribute across the BBB to achieve therapeutically active levels, and also allow us to compare E6201's brain distribution profile with currently available MEK inhibitors. To our knowledge, this is the first report of the brain distribution and active efflux of E6201.

In vitro intracellular accumulation studies in transfected MDCKII cells overexpressing either murine Bcrp or human P-gp, strongly suggest that E6201 is not a substrate of Bcrp or P-gp. The intracellular E6201 concentrations were not different between wild-type and Bcrp1-/MDR1-transfected cells, and also in Bcrp1- and MDR1-transfected cells treated with and without specific inhibitor of transporter (Figure 2). Moreover, directional flux studies showed that E6201 was unlikely to be a substrate of P-gp (E6201 investigators brochure). Subsequent experiments tested the influence of Bcrp and/or P-gp on brain distribution of E6201 in vivo.

The in vitro efficacy experiments were conducted in 3 patient derived melanoma cell lines (BRAF-mutant M12, BRAF-mutant M27, NRAS-mutant M15). MEK inhibition is an important treatment strategy in melanoma tumors that exhibit mutations in RAF or RAS, and so efficacy testing was performed in these cell lines. The results indicate that BRAF-mutant M12 is the most sensitive to E6201 among the 3 patient derived melanoma cell lines tested, with a low nanomolar IC_{50} (Figure 3, Table 2). Moreover, reports suggest that NF1-driven tumors (loss of NF1) are sensitive to MEK inhibition (Ameratunga et al., 2016), and wild-type PTEN status is important for sensitivity to E6201 (Byron et al., 2012). GBM43 exhibits both these features, and so in vitro efficacy testing was also performed in this GBM cell line. However, the results show that the sensitivity of GBM43 to E6201 is much lower compared to the tested melanoma cell lines (Figure 3, Table 2).

In vivo pharmacokinetic experiments following 40 mg/kg single intravenous bolus dose of E6201 indicate that total concentrations in brain were higher than that in plasma at all

measured time points in the four genotypes, while plasma concentrations were similar (Figure 4). Consequently, observed AUCs in brain were higher than AUCs in plasma, as can be recognized from the brain-to-plasma AUC ratios (Kp) of 2.66, 4.37, 3.72 and 5.40 in wild-type, *Mdr1a/b*$^{-/-}$*; Bcrp1*$^{-/-}$*, and Mdr1a/b*$^{-/-}$ *Bcrp1*$^{-/-}$ mice, respectively (Table 3). While plasma AUCs are not significantly different, brain AUCs are significantly higher in knockouts compared to wild-type mice. This indicates that P-gp and Bcrp may play a role in limiting E6201's brain delivery; however, the increase in exposure is minimal (2-fold in *Mdr1a/b*$^{-/-}$ *Bcrp1*$^{-/-}$ mice) when compared to many substrates reported in literature, for instance cobimetinib (30-fold in *Mdr1a/b*$^{-/-}$ *Bcrp1*$^{-/-}$ mice (Choo et al., 2014)) and trametinib (5-fold in *Mdr1a/b*$^{-/-}$ *Bcrp1*$^{-/-}$ mice (Vaidhyanathan et al., 2014)). A possibility for the modest increase in Kp (≤2-fold), given the in vitro results, could be related to changes in transporter expression in knockout mice. Though a change in expression could be possible for some unknown transporter, it is unlikely here, given the results of transporter, receptor, and tight junction proteomic analysis in wild-type compared to *Mdr1a/b*$^{-/-}$ and/or *Bcrp1*$^{-/-}$ mice (Agarwal; Uchida; et al., 2012) indicated no change in expression of BBB proteins. Nevertheless, these results show that E6201, for a molecularly-targeted agent, has brain distribution characteristics that are minimally influenced by Bcrp and P-gp efflux at the BBB.

The brain partitioning following i.p. and p.o. administration of E6201 at the same dose was similar to that observed in i.v. studies. The absolute bioavailability (F) of E6201 was higher following i.p dosing compared to p.o. dosing (F=0.95, i.p., F=0.39, p.o.; Table 4, Table 5). The total E6201 steady-state concentrations in the brain were higher than those

in plasma, in both wild-type and *Mdr1a/b*$^{-/-}$ *Bcrp1*$^{-/-}$ mice. This is reflected in the brain-to-plasma ratio being greater than unity in wild-type mice (Kp = 1.8), again suggesting that E6201 favors distribution to the brain compared to plasma. The increase in Kp by about ~2.5 fold in mice lacking P-gp and Bcrp (Kp = 4.38), indicates that the brain distribution of E6201 is minimally influenced by efflux transport at the blood-brain barrier. Consistent with in vitro results, in vivo studies characterizing the brain exposure of E6201 demonstrate that neither Bcrp nor P-gp show a marked involvement in limiting the brain delivery of E6201.

Furthermore, we have examined the distribution of E6201 across the BBB in an intracranial M12 melanoma model, and the distribution was found to be variable to regions of tumor and normal brain (Figure 8). The average Kp in normal brain (Kp = 2.91 ± 0.39) was similar to the Kp observed at the 30 minute time point in pharmacokinetic studies following intraperitoneal dosing of E6201 in non-tumor bearing FVB mice (Kp = 2.39 ± 0.58). The rank order of the average Kp was normal brain higher than tumor rim and tumor rim higher than tumor core. These results indicate that the accumulation of E6201 in the normal brain and the growing edge of the intracranial M12 tumor (tumor rim) is relatively higher than in the necrotic tumor core. A possible reason for such an observation is perfusion limited drug distribution to the necrotic tumor core. The tumor perfusion can be variable depending on the location within the tumor, and necrotic tumor regions, though leakier, can have a relatively poor perfusion (Jain et al., 2007). For a compound like E6201 that has a high BBB permeability, a perfusion limited distribution to the necrotic tumor core may lead to a relatively lower drug accumulation in the tumor

core compared to the normal brain regions. Another possibility for this finding may be related to differences in drug binding in the tumor regions compared to the normal brain. Previous studies in our lab have shown that the unbound (free) fraction of ponatinib was higher in the core of GBM6 intracranial tumor compared to that in the normal brain (Laramy et al., 2017). A similar behavior for E6201 can result in a lower binding (higher free fraction) in the tumor core compared to normal brain, and that may lead to a lower drug accumulation in the tumor core relative to normal brain. While there exists heterogeneity in regional drug distribution, E6201 has a favorable brain distribution profile and achieves exposures in regions of tumor, including the actively growing edge, as well as in the normal brain that may result in beneficial outcomes.

In vitro rapid equilibrium dialysis experiments indicate that E6201 exhibits higher non-specific binding in brain compared to plasma, possibly related to lipophilic brain environment, with free fractions (fu) of 0.14% and 3.4%, respectively (Table 1). The fu values were used to estimate the unbound partition coefficients (Kp,uu) in wild-type, *Mdr1a/b*$^{-/-}$*, Bcrp1*$^{-/-}$*, and Mdr1a/b*$^{-/-}$ *Bcrp1*$^{-/-}$ mice, 0.14, 0.24, 0.2 and 0.29, respectively, following i.v. dosing (Table 3). The Kp,uu values in all four genotypes of mice were less than one indicating a distribution disequilibrium (Di et al., 2013, Summerfield et al., 2016). It is likely that E6201 has a high passive permeability in the absence of active efflux, since it is a relatively small molecule (389.45 g/mol), highly lipophilic (xlogP3 = 3.3 (Pubchem), logP = 3.63 (E6201 investigators brochure)), and not significantly charged at physiological pH (pKa of basic nitrogen = 8.8 (E6201 investigators brochure)). Also, it can be seen from the brain-to-plasma ratio plot for the four genotypes

(Figure 4C) that an equilibrium between brain and plasma concentrations is achieved rapidly (~0.5 hr) suggesting a high rate into brain. Given these observations, it is possible that Kp,uu less than unity is related to efflux transporter(s) other than Bcrp and P-gp are influencing E6201's brain delivery, especially given that Kp,uu in *Mdr1a/b*$^{-/-}$ *Bcrp1*$^{-/-}$ mice is also less than unity.

The average free drug concentrations in wild-type mice were determined at measured time points to obtain the free concentration-time profile. The free concentrations were then compared to in vitro potency estimates in melanoma cell lines to evaluate the potential of E6201 for treatment of MBM. The free concentrations in brain reached levels higher than the reported IC_{50} value (IC_{50} = 43.7 nmol/L, SK-MEL-28 melanoma cell line; E6201 investigators brochure), suggesting that E6201 may show efficacy in treatment of MEK-driven brain tumors (Figure 9A). Also, since the IC_{50} measurements employed total and not free concentrations in media, the free IC_{50} can be expected to be even lower, giving further credence to the idea that adequate delivery may be achieved in vivo. Also, the unbound concentrations were compared with the free IC_{50} in BRAF-mutant M12 melanoma cell line. The concentrations in the brain were higher than the free IC_{50}, estimated using the total IC_{50} and the free fraction in cell culture media, for about 2 hours in M12 cell line (Figure 9B). Given such insights, it would be valuable to conduct efficacy studies with E6201 in preclinical models of MBM as a next step to better understand in vivo efficacy, and lead to clinical trials. Hence, we are currently evaluating the in vivo efficacy of E6201, in flank (subcutaneous) and intracranial patient-derived xenograft (PDX) mouse models implanted with BRAF-mutant M12 tumors.

The unique macrocyclic structure of E6201 may enhance its brain penetration by avoiding active efflux via Bcrp and P-gp. A macrocyclic structure facilitates a reduction in rotatable bonds, reported to positively correlate with improved brain penetration by lessening active efflux (Heffron, 2016). Also, of at least equal, and probably greater, significance is the opportunity for formation of intramolecular hydrogen bonds that can effectively mask hydrogen-bond donors (HBD), which have a profound correlation with likelihood of transporter mediated efflux (Heffron, 2016). The 3-dimensional x-ray crystal structure of E6201 bound to MEK (see http://www.rcsb.org/pdb/explore.do?structureId=5HZE) shows that each of the alcohol/phenol "OH" groups are capable of intramolecular hydrogen bonding, thereby allowing effective masking of 3 of the 4 available HBDs, essentially leaving only 1 effective HBD. Such observations have been reported for other targeted agents such as lorlatinib (ALK inhibitor) and AZD3759 (EGFR inhibitor) (Johnson et al., 2014, Zeng et al., 2015). Recent literature highlights the fact that an optimal balance of physicochemical properties is necessary to achieve adequate distribution to brain, and drugs having low molecular weight, fewer rotatable bonds, low total polar surface area (TPSA), and fewer HBDs are expected to have better CNS penetration (Heffron, 2016, Rankovic, 2015, Wager et al., 2016). The combination of few rotatable bonds and few effective HBDs readily explains how E6201 achieves significant brain distribution.

In the context of brain tumors, it is important to note that the approved MEK inhibitors, trametinib and cobimetinib, show limited brain distribution due to active efflux. The Kp for trametinib and cobimetinib in wild-type mice were 0.15 and 0.32, respectively (Table

6). As evident from the Kp of 2.66 in wild-type mice, the total concentrations for E6201 are higher in brain compared to plasma, unlike for trametinib and cobimetinib. Given that the three MEK inhibitors are highly protein bound, Kp,uu for E6201 is much higher than that of cobimetinib and similar to that of trametinib (Table 6). The brain distribution profile of E6201 makes it an attractive MEK inhibitor for the treatment of MBM, with potential for achieving improved treatment responses.

The development of targeted agents inhibiting the MAPK pathway and immunotherapies has led to major advances in the treatment of patients with metastatic melanoma. However, it is crucial to realize the challenges that still remain in delivering the molecularly-targeted agents to tumor cells in the brain that may be growing behind an intact BBB. Both the brain microenvironment-driven changes in genetic expression leading to resistance and CNS drug delivery issues need to be addressed to achieve a clinically meaningful response in MBM and other brain tumors. Though single agent treatment may show responses, there is a need to test rational combinations (e.g., a BRAF inhibitor and MEK inhibitor to better inhibit MAPK pathway; a BRAF/MEK inhibitor and a PI3K/mTOR inhibitor to inhibit both MAPK and PI3K pathways) to tackle issues of resistance to therapy. When using combinations, it is important to examine CNS distribution of all agents in the combination regimen since all administered drugs should adequately reach the target site in brain to achieve desired responses and minimize emergence of resistance. Despite the remarkable progress, there remains a need to develop better therapies for MBMs, and drug delivery across the BBB is one crucial factor that requires attention to fulfill this goal.

ACKNOWLEDGEMENTS

The authors thank Jim Fisher, Clinical Pharmacology Analytical Laboratory, University of Minnesota, for his support in the development of the LC-MS/MS assays. The authors would also like to thank Timothy Heffron from Genentech Inc., for his valuable input.

FOOTNOTES

This work was supported by the National Institutes of Health [Grants RO1-NS077921 RO1-NS073610 and U54-CA210180] and Strategia Therapeutics Inc. Gautham Gampa was supported by the Ronald J. Sawchuk Fellowship in Pharmacokinetics and University of Minnesota Doctoral Dissertation Fellowship (DDF).

TABLES

Table 6. 1 Free fraction (fu) for E6201 and trametinib in matrices of interest, determined by in vitro rapid equilibrium dialysis (RED) experiments. Data represent the mean ± S.D. (n = 3).

Inhibitor	Matrix	fu	fu (%)	Recovery (%)	fu_{brain}/fu_{plasma}
E6201	Plasma	0.026 ± 0.002	2.63 ± 0.18	94.04 ± 3.32	0.054
	Brain	0.0014 ± 0.0002	0.14 ± 0.02	113.20 ± 9.49	-
	Media	0.39 ± 0.04	39.16 ± 3.99	79.96 ± 1.80	-
Trametinib	Plasma	0.0021 ± 0.0003	0.21 ± 0.03	99.90 ± 8.42	1
	Brain	0.0021 ± 0.0002	0.21 ± 0.02	106.56 ± 2.35	-

fu, free (unbound) fraction

Table 6. 2 Total and free (unbound) IC_{50} values for trametinib (control) and E6201 in patient derived melanoma (BRAF-mutant M12, BRAF-mutant M27, NRAS-mutant M15) and GBM (GBM43) cell lines. The free IC_{50} for E6201 were determined using the total IC_{50} estimates and the unbound fraction (fu) in cell culture media.

	IC_{50} (nM) (95% confidence intervals)				**Free IC_{50} (nM)**			
	M12	**M27**	**M15**	**GBM43**	**M12**	**M27**	**M15**	**GBM43**
Trametinib	< 1	< 1	< 1	10.04 (6.37-15.84)	-	-	-	-
E6201	15.06 (11.64-19.51)	151.7 (108.7-211.9)	210.9 (165.9-268.2)	1629 (1125-2358)	5.87	59.15	82.26	635.3

Table 6. 3 The pharmacokinetic/metric parameters of E6201 in FVB wild-type, *Mdr1a/b*$^{-/-}$, *Bcrp1*$^{-/-}$, and *Mdr1a/b*$^{-/-}$ *Bcrp1*$^{-/-}$ knockout mice following administration of single intravenous bolus dose of 40 mg/kg. Data are presented as mean or mean ± S.E.M (n=5).

	Plasma				**Brain**			
	Wild-type	*Mdr1a/b*$^{-/-}$	*Bcrp1*$^{-/-}$	*Mdr1a/b*$^{-/-}$ *Bcrp1*$^{-/-}$	Wild-type	*Mdr1a/b*$^{-/-}$	*Bcrp1*$^{-/-}$	*Mdr1a/b*$^{-/-}$ *Bcrp1*$^{-/-}$
Half-life (hr)	0.65	0.78	0.76	0.83	0.62	0.69	0.60	0.66
$AUC_{(0-t)}$ (µg*hr/mL)	10.20 ± 0.29	10.69 ± 0.75	9.89 ± 0.70	9.36 ± 0.45	27.17 ± 0.95	46.68 ± 2.51	36.78 ± 2.04	50.59 ± 3.09
$AUC_{(0-\infty)}$ (µg*hr/mL)	10.21	10.73	9.92	9.40	27.19	46.75	36.81	50.66
CL (mL/min/kg)	65.27	62.17	67.17	70.92	-	-	-	-
Vd (L/kg)	3.7	4.2	4.4	5.1	-	-	-	-
Kp ($AUC_{(0-t)}$ ratio)	-	-	-	-	2.7	4.4	3.7	5.4
Kp,uu ($AUC_{(0-t)}$ ratio)	-	-	-	-	0.14	0.24	0.2	0.29
DA	-	-	-	-	1	1.6	1.4	2

$AUC_{(0-t)}$, area under the curve from zero to the time of last measured concentration
$AUC_{(0-\infty)}$, area under the curve from zero to time infinity
CL, clearance
Vd, volume of distribution
Kp (AUC ratio), the ratio of $AUC_{(0-t,brain)}$ to $AUC_{(0-t,plasma)}$ using total drug concentrations
Kp,uu (AUC ratio), the ratio of $AUC_{(0-t,brain)}$ to $AUC_{(0-t,plasma)}$ using free drug concentrations
DA (Distribution advantage), the ratio of $Kp_{knockout}$ to $Kp_{wild-type}$

Table 6. 4 The pharmacokinetic/metric parameters of E6201 in FVB wild-type and *Mdr1a/b*$^{-/-}$ *Bcrp1*$^{-/-}$ knockout mice following administration of single intraperitoneal dose of 40 mg/kg. Data are presented as mean or mean ± S.E.M (n=4).

	Plasma		**Brain**	
	Wild-type	*Mdr1a/b*$^{-/-}$ *Bcrp1*$^{-/-}$	Wild-type	*Mdr1a/b*$^{-/-}$ *Bcrp1*$^{-/-}$
Half-life (hr)	0.76	0.62	0.58	0.6
Cmax (µg/mL)	11.70 ± 2.25	18.40 ± 5.80	16.72 ± 1.36	30.75 ± 3.93
Tmax (hr)	0.25	0.25	0.5	0.5
$AUC_{(0-t)}$ (µg*hr/mL)	9.69 ± 0.73	11.73 ± 1.57	21.44 ± 1.13	44.93 ± 3.62
$AUC_{(0-\infty)}$ (µg*hr/mL)	9.73	11.75	21.46	44.99
CL/F (mL/min/kg)	68.5	56.75	-	-
Vd/F (L/kg)	4.5	3.1	-	-
Kp ($AUC_{(0-t)}$ ratio)	-	-	2.2	3.83
Kp,uu ($AUC_{(0-t)}$ ratio)	-	-	0.12	0.21
DA	-	-	1	1.75
F	0.95	-	-	-

Cmax, observed maximum concentration
Tmax, time to reach the maximum concentration
$AUC_{(0-t)}$, area under the curve from zero to the time of last measured concentration
$AUC_{(0-\infty)}$, area under the curve from zero to time infinity
CL/F, apparent clearance
Vd/F, apparent volume of distribution
Kp (AUC ratio), the ratio of $AUC_{(0-t,brain)}$ to $AUC_{(0-t,plasma)}$ using total drug concentrations
Kp,uu (AUC ratio), the ratio of $AUC_{(0-t,brain)}$ to $AUC_{(0-t,plasma)}$ using free drug concentrations
DA (Distribution advantage), the ratio of $Kp_{knockout}$ to $Kp_{wild-type}$
F (Absolute bioavailability), ratio of the dose corrected $AUC_{(0-t),ip}$ to dose corrected $AUC_{(0-t),iv}$

Table 6. 5 E6201 pharmacokinetic/metric parameters in FVB wild-type mice following administration of single oral dose of 40 mg/kg. Data are presented as mean or mean ± S.E.M (n=4).

	Plasma	**Brain**
Half-life (hr)	1.37	0.98
Cmax (µg/mL)	2.44 ± 0.41	6.04 ± 1.55
Tmax (hr)	0.5	0.5
$AUC_{(0-t)}$ (µg*hr/mL)	3.94 ± 0.54	9.23 ± 1.95
$AUC_{(0-\infty)}$ (µg*hr/mL)	4.22	9.31
CL/F (mL/min/kg)	158	-
Vd/F (L/kg)	18.7	-
Kp ($AUC_{(0-t)}$ ratio)	-	2.35
Kp,uu ($AUC_{(0-t)}$ ratio)	-	0.13
F	0.39	-

Cmax, observed maximum concentration
Tmax, time to reach the maximum concentration
$AUC_{(0-t)}$, area under the curve from zero to the time of last measured concentration
$AUC_{(0-\infty)}$, area under the curve from zero to time infinity
CL/F, apparent clearance
Vd/F, apparent volume of distribution
Kp (AUC ratio), the ratio of $AUC_{(0-t,brain)}$ to $AUC_{(0-t,plasma)}$ using total drug concentrations
Kp,uu (AUC ratio), the ratio of $AUC_{(0-t,brain)}$ to $AUC_{(0-t,plasma)}$ using free drug concentrations
F (Absolute bioavailability), ratio of the dose corrected $AUC_{(0-t),po}$ to dose corrected $AUC_{(0-t),iv}$

Table 6. 6 Comparison of brain distribution of MEK inhibitors in wild-type mice. Data are presented as means.

MEK inhibitor	Dose mg/kg	Kp	fu_{brain}	fu_{plasma}	Kp,uu
Trametinib	5 (iv)	0.15[a]	0.0021	0.0021	0.15
Cobimetinib[b]	10 (po)	0.32	0.0012	0.014	0.027
E6201	40 (iv)	2.66	0.0014	0.034	0.14

fu, free (unbound) fraction
Kp (AUC ratio), the ratio of $AUC_{(0\text{-}t,brain)}$ to $AUC_{(0\text{-}t,plasma)}$ using total drug concentrations
Kp,uu (AUC ratio), the ratio of $AUC_{(0\text{-}t,brain)}$ to $AUC_{(0\text{-}t,plasma)}$ using free drug concentrations
[a] Kp reported by Vaidhyanathan et al. 2014
[b] Results reported by Choo et al. 2014; Kp and Kp,uu based on plasma and brain concentrations 6 hr post dose

FIGURES

Figure 6. 1 Chemical structure of (A) E6201, (B) cobimetinib, and (C) trametinib.

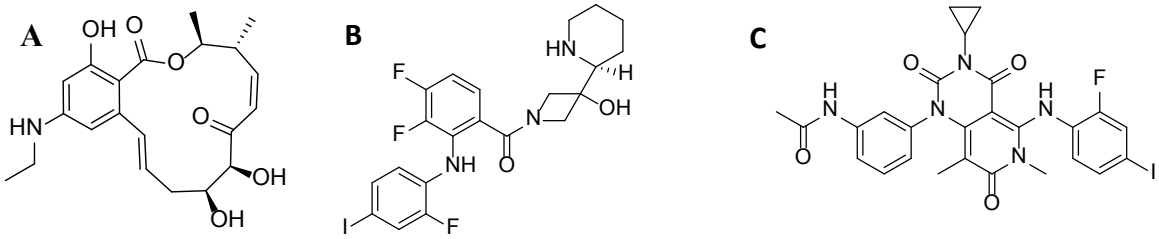

Figure 6. 2 In vitro intracellular accumulation of E6201. (A)The accumulation of prazosin (Bcrp probe substrate; positive control) and E6201 in MDCKII wild-type and Bcrp1-transfected cell lines with and without Bcrp inhibitor Ko143 (0.2 μM). (B) The accumulation of E6201 and vinblastine (probe substrate for P-gp; positive control) in wild-type and MDR1-transfected cells with and without P-gp inhibitor LY335979 (1 μM). Data represent the mean ± S.D.; n = 3 for all data points. **P*< 0.05 compared with respective wild-type controls; #*P*< 0.01 compared with the untreated transfected cell line; ***P*< 0.01 compared with respective wild-type controls; ****P*< 0.001 compared with the untreated transfected cell line.

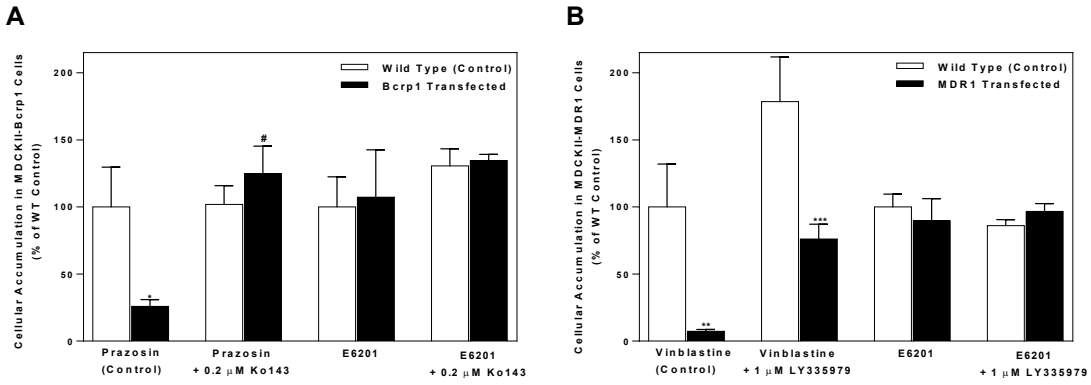

Figure 6. 3 In vitro cytotoxicity of E6201 and trametinib (control) in patient-derived melanoma and GBM cell lines. Dose-response curves showing the effect of various concentrations of E6201 and trametinib on (A) BRAF-mutant M12 melanoma cell line, (B) BRAF-mutant M27 melanoma cell line, (C) NRAS-mutant M15 melanoma cell line, and (D) GBM43 cell line. Data represent the mean ± S.E.M.; n = 6 for all data points.

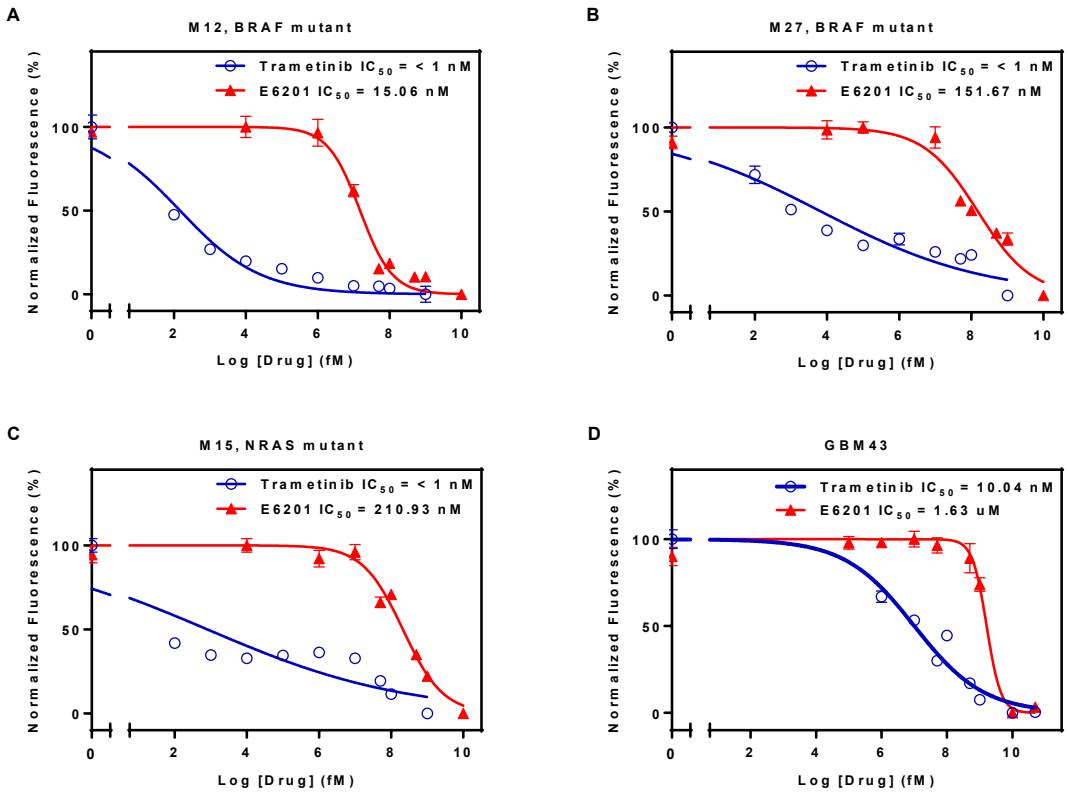

Figure 6. 4 Pharmacokinetic profiles of E6201 in FVB wild-type, *Mdr1a/b*$^{-/-}$, *Bcrp1*$^{-/-}$, *and Mdr1a/b*$^{-/-}$ *Bcrp1*$^{-/-}$ mice following intravenous (i.v.) administration. Plasma concentrations (A), brain concentrations (B), and brain-to-plasma concentration ratios (C) of E6201 in wild-type, *Mdr1a/b*$^{-/-}$, *Bcrp1*$^{-/-}$, *and Mdr1a/b*$^{-/-}$ *Bcrp1*$^{-/-}$ mice following administration of single i.v. bolus dose of 40 mg/kg. The dashed line in (C) represents a brain-to-plasma ratio (Kp) of unity. Data represent mean ± S.D., n = 5.

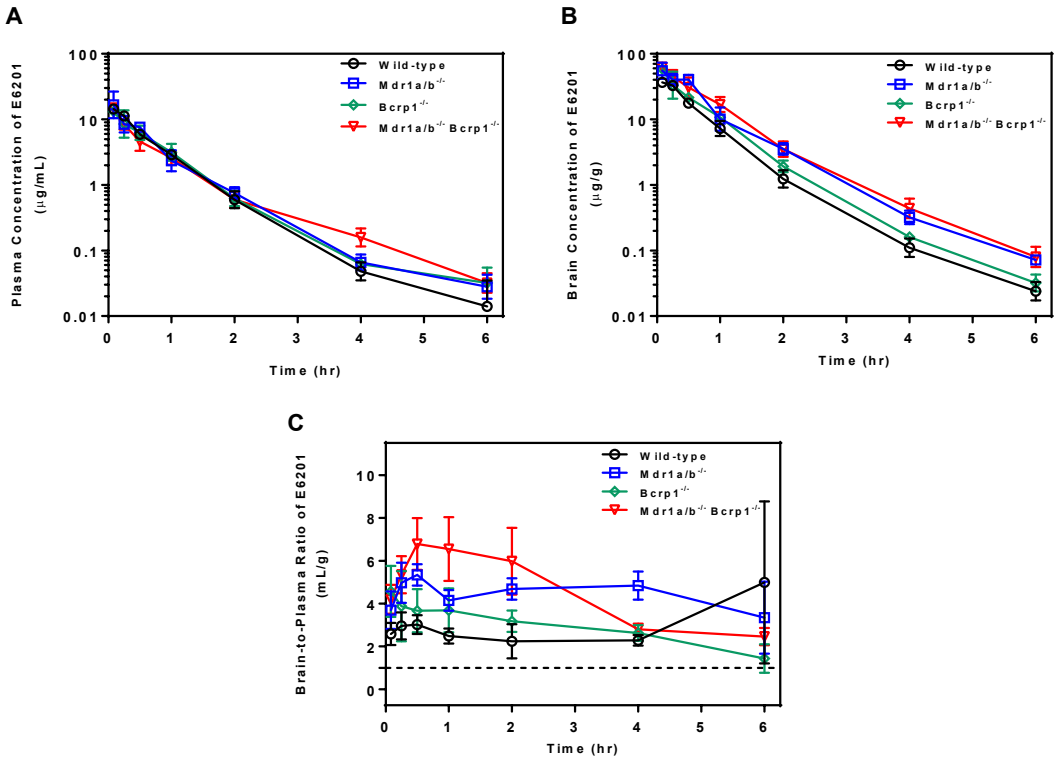

Figure 6. 5 Pharmacokinetic profiles of E6201 in FVB wild-type and *Mdr1a/b*$^{-/-}$ *Bcrp1*$^{-/-}$ mice following intraperitoneal (i.p.) administration. Plasma concentrations (A), brain concentrations (B), and brain-to-plasma concentration ratios (C) of E6201 in wild-type and *Mdr1a/b*$^{-/-}$ *Bcrp1*$^{-/-}$ mice following administration of single i.p. dose of 40 mg/kg. The dashed line in (C) represents a brain-to-plasma ratio (Kp) of unity. Data represent mean ± S.D., n = 4.

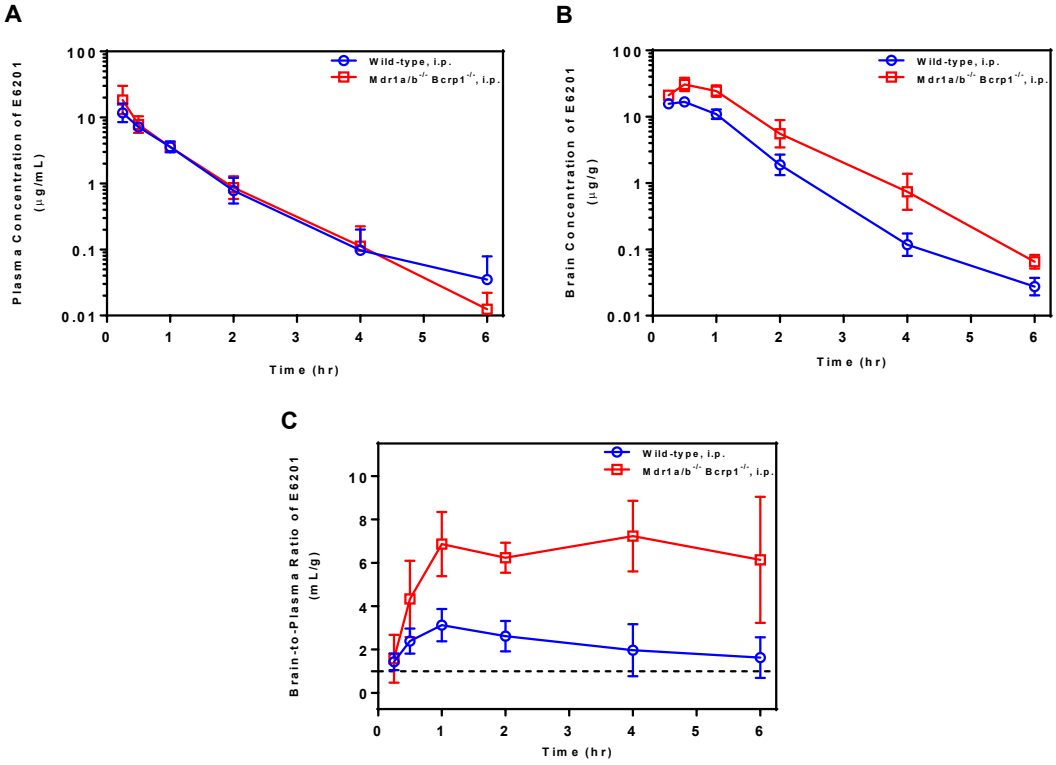

Figure 6. 6 Pharmacokinetic profiles of E6201 in FVB wild-type mice following oral (p.o.) administration. Plasma concentrations and brain concentrations (A), and brain-to-plasma concentration ratios (B) of E6201 in wild-type mice upon single p.o. dose of 40 mg/kg. The dashed line in (B) represents a brain-to-plasma ratio (Kp) of unity. Data represent mean ± S.D., n = 4.

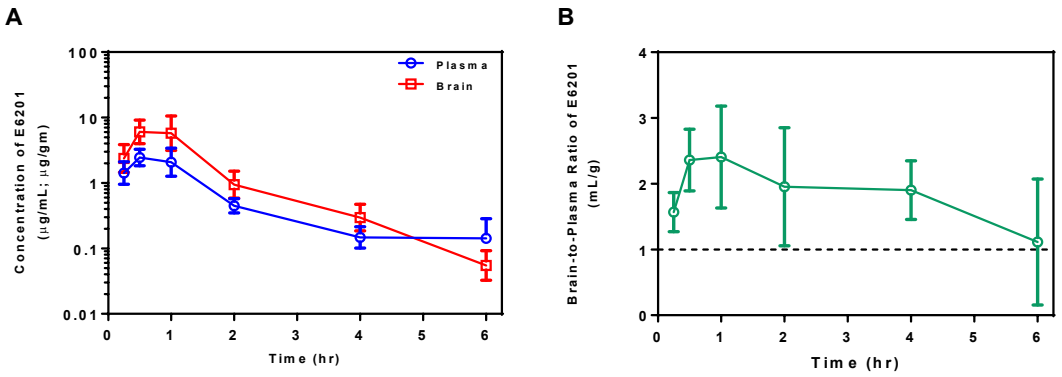

Figure 6. 7 Steady-state distribution of E6201 in FVB wild-type and *Mdr1a/b*$^{-/-}$*Bcrp1*$^{-/-}$ mice. (A) Steady-state plasma and brain concentrations, (B) brain-to-plasma ratios. **P*< 0.05 and ****P*< 0.001, for statistical comparison by unpaired t-test. Data represent mean ± S.D., n = 4.

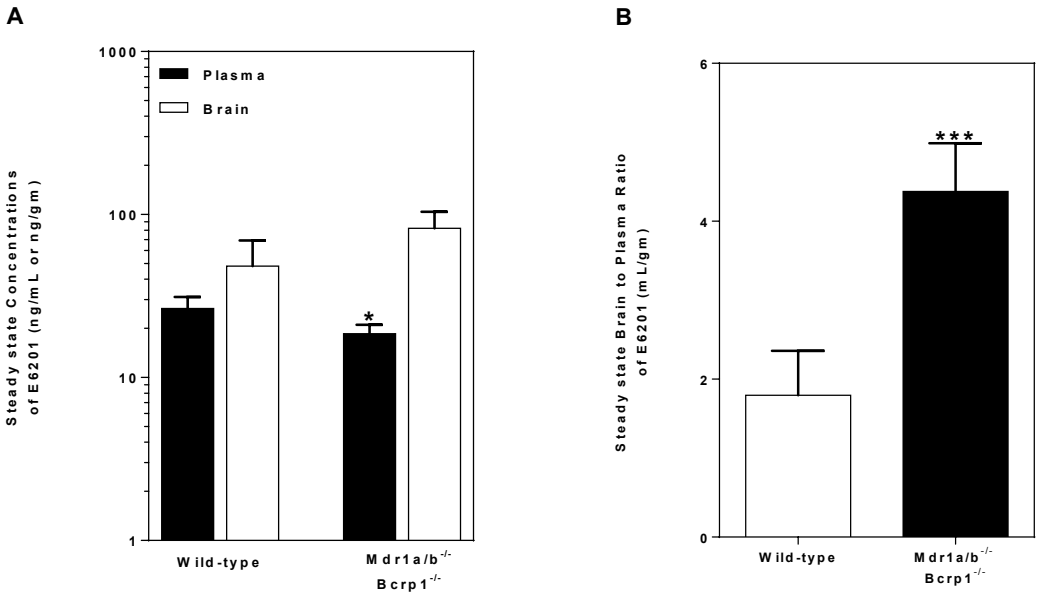

Figure 6. 8 Spatial brain distribution of E6201 in an intracranial melanoma mouse model. (A) Representative fluorescence microscopy image of M12 tumor-bearing thick brain slice marked with tumor core (solid red line) and tumor rim (solid black line) regions, (B) representative image showing dissected tumor core and tumor rim tissues, marked with dashed white lines, (C) E6201 concentrations, and (D) E6201 brain (tumor tissue)-to-plasma ratios. #, concentrations in plasma significantly different from tumor core ($P< 0.05$), tumor rim ($P< 0.01$) and normal brain ($P< 0.0001$). *P< 0.05, ***P< 0.001 and ****P< 0.0001 for statistical comparison by one-way ANOVA. Data represent mean ± S.D., n = 9.

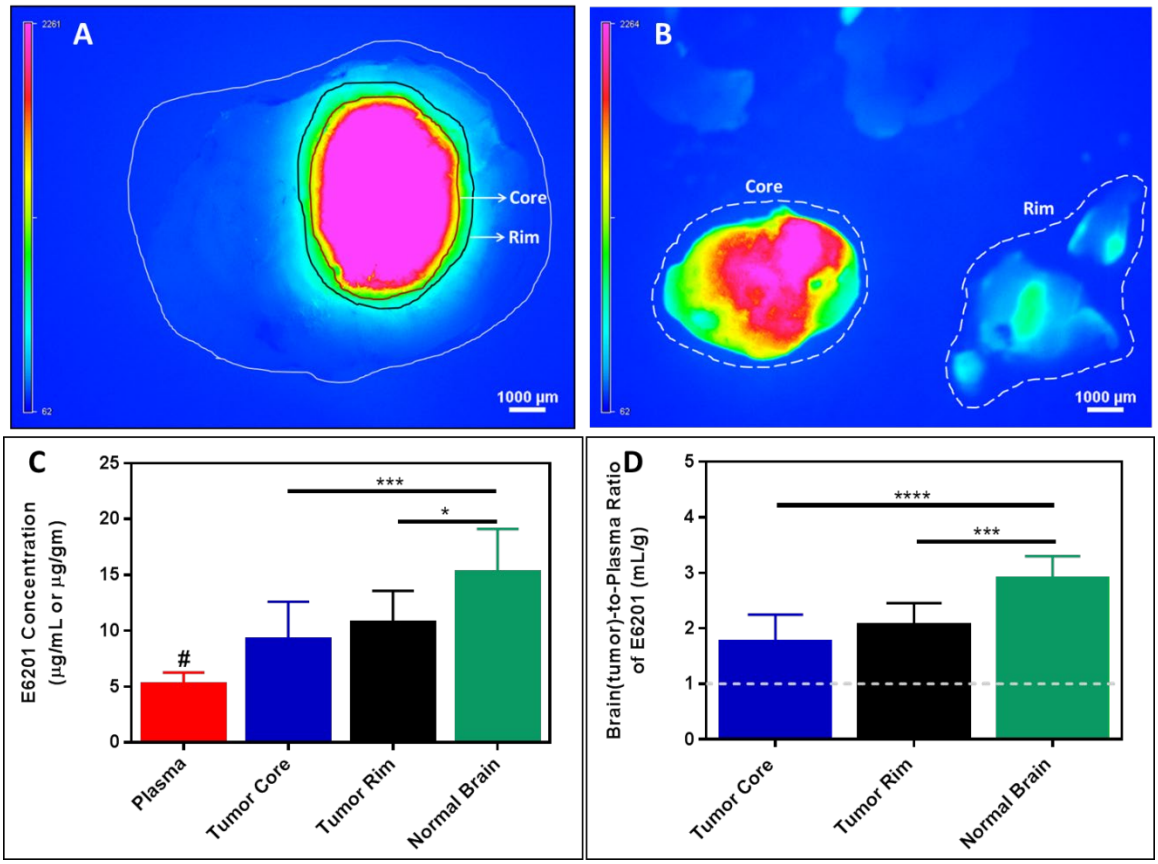

Figure 6. 9 Plasma and brain unbound concentration-time profile of E6201 in FVB wild-type mice, and comparison with in vitro IC_{50}. (A) The dashed green line represents the reported in vitro E6201 IC_{50} against SK-MEL-28 melanoma cell line (IC_{50} = 43.7 nmol/L, E6201 investigator brochure). The dashed orange line represents the free E6201 IC_{50} determined using the plasma free fraction of E6201 (fu_{plasma} = 0.026, free IC_{50} = 1.14nmol/L). Here, the assumption is that the non-specific binding of E6201 in the assay media is similar to the free fraction determined in plasma experimentally. (B) The dashed green line represents the in vitro IC_{50} (free) of E6201 in BRAF-mutant M12 melanoma cell line. The experimentally determined IC_{50} and free fraction in cell culture media from rapid equilibrium dialysis studies was used to determine the free IC_{50} estimate in M12. Data represent mean ± S.D., n = 5.

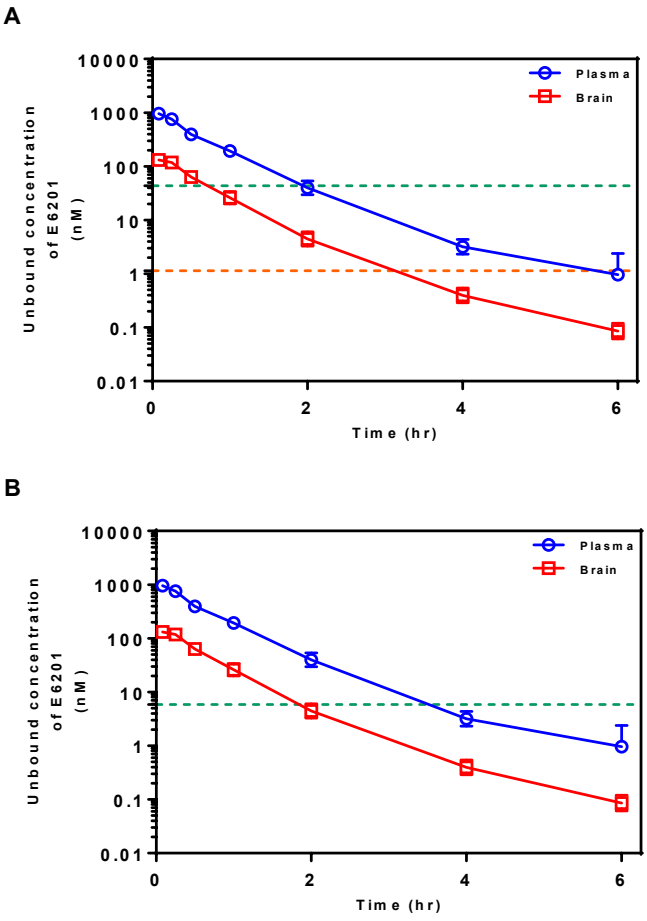

CHAPTER VII. RECAPITULATION

Brain tumors can be devastating and are associated with a poor prognosis. Glioblastoma (GBM) is the most common primary malignant brain tumor in adults. Melanoma, breast and lung cancer are systemic malignancies with a high propensity to metastasize to the brain. The patients diagnosed with tumors in the brain, both primary and metastatic, have a dismal quality of life. The treatment options for brain tumors are limited, and even with aggressive treatment, the patient survival is typically extended only by a few months. There is a critical need to develop more effective treatments to address this severe condition and provide clinically meaningful benefits to the affected patients.

Chapter 1 introduces the problem, presents the structure of this dissertation, and puts forth the research approaches that were undertaken. The challenges in the treatment of brain tumors are manifold and include: (a) accurate and early diagnosis, (b) heterogeneity in genetic drivers and resistance to therapies, and (c) drug delivery to tumor cells protected by a functionally intact blood-brain barrier (BBB). Literature pertaining to CNS pharmacokinetics and challenges in the treatment of tumors in the brain is explored in detail in **Chapters 2 and 3**. Furthermore, some perspectives related to these issues, particularly drug delivery, are discussed. Although a multi-factorial approach is needed to tackle this important problem of brain tumor treatment, the work in this dissertation is mainly centered around the drug delivery challenge.

The blood-brain barrier (BBB) serves as a physical and functional barrier to the entry of xenobiotics into the brain. A key mechanism that limits the brain delivery of several therapeutic agents is active efflux at the BBB, mainly by P-gp and Bcrp, which results in pumping drugs intended for treating CNS diseases back in to the systemic circulation.

Contrast-enhanced magnetic resonance imaging (CE-MRI) identifies regions of the tumor with a disrupted BBB, and this has led to the belief that the BBB is compromised in brain tumors. A major drawback of CE-MRI is that it fails to detect tumor cells in sites with an intact BBB, which includes regions with infiltrative tumor cells and low volume early micro-metastases. The delivery of targeted therapies with a poor BBB penetration can be limited to such protected tumor locations, and result in lack of efficacy. Thus, it is critical to recognize that drug delivery across a functionally intact BBB is crucial to improve responses in brain tumors, and this advocates the need for efforts directed at the development of therapeutic agents capable of penetrating the BBB.

KIF11 is a kinesin involved in both proliferation and invasion, the characteristic hallmarks of GBM. Inhibition of KIF11 using potent targeted agents like ispinesib may translate to beneficial outcomes in GBM. **Chapter 4** examined the brain delivery of ispinesib in normal and tumor-bearing rodent models. Ispinesib was shown to be a substrate of active efflux by P-gp and Bcrp at the BBB using in vivo brain distribution studies in FVB mice. The normalized brain exposure (Kp, AUC ratio) in mice deficient in P-gp and Bcrp (*Mdr1a/b*$^{-/-}$ *Bcrp1*$^{-/-}$) was about 50-fold higher than in wild-type mice. In vitro experiments indicate that ispinesib exhibits high binding in plasma and brain, and the Kp,uu were 0.02 and 1.01 in wild-type and *Mdr1a/b*$^{-/-}$ *Bcrp1*$^{-/-}$ mice, respectively. In vitro efficacy testing reveals low nanomolar sensitivity of ispinesib in MGPP3 GBM cell line. The predicted unbound concentrations in brain were below the in vitro IC_{50} in MGPP3 cells. Moreover, a variable uptake of ispinesib was observed in a rat model of GBM, with lower accumulation in the normal (non-tumor) brain regions and highest

accumulation in the necrotic tumor core. The drug partitioning to the tumor rim, the growing edge of the tumor, was relatively restricted when compared to the tumor core. We also found that elacridar, a dual inhibitor of P-gp and Bcrp, significantly improves the brain delivery of ispinesib, and the unbound concentrations in brain will likely reach the in vitro cytotoxic concentrations. Future studies will test the in vivo efficacy of ispinesib in preclinical models of GBM and also evaluate improvements in efficacy with enhanced drug delivery.

In **chapter 5**, the aim was to compare the brain delivery of three newly developed panRAF inhibitors and understand their potential utility in the treatment of melanoma brain metastases. CCT196969, LY3009120 and MLN2480 are potent panRAF inhibitors that may overcome issues of paradoxical activation and resistance observed with some BRAF inhibitors. LY3009120 and MLN2480 were shown to be substrates of Bcrp using in vitro accumulation studies in MDCKII cells. The three panRAF inhibitors exhibit high binding in both brain and plasma. In vivo studies show that the delivery of the 3 panRAF inhibitors is limited to the brain, and is enhanced in mice deficient in P-gp and Bcrp. BRAF-mutant M12 cell line was most sensitive to the panRAF inhibitors among the cell lines tested. LY3009120 exhibits a superior in vitro efficacy in patient-derived melanoma cell lines. MLN2480 has a superior brain distribution profile. The predicted unbound concentrations in brain achieve levels higher that the in vitro IC50 in M12 for LY3009120 alone. The results demonstrate that an appropriate balance between drug delivery and potency ultimately dictates the efficacy outcomes in the treatment of tumors in the brain.

Targeted inhibition of MEK has been employed as an important strategy in the treatment of melanoma, particularly in combination with BRAF inhibitors. However, the currently approved MEK inhibitors have a restricted brain delivery and this can severely impact the efficacy outcomes in patients with brain metastases. **Chapter 6** aimed to investigate the brain distribution of E6201, a potent inhibitor of MEK with a unique macrocyclic structure that likely reduces its interaction with P-gp and Bcrp. In vitro studies utilizing MDCKII cells and in vivo studies in FVB mice indicate that E6201 is not a substrate of P-gp and Bcrp. In vitro studies in patient-derived cell lines indicate that E6201 has a low nanomolar IC_{50} in BRAF-mutant M12 cell line. The results of the spatial distribution studies reveal a heterogeneity in delivery of E6201 to regions of an intracranial M12 tumor and normal (non-tumor) brain. The drug accumulation was observed to be higher in the normal brain compared to the necrotic tumor core and the invasive edge of the tumor. E6201 has a favorable brain distribution profile that is superior to the approved MEK inhibitors and the predicted unbound concentrations reach levels higher that the in vitro cytotoxic concentrations in patient-derived M12 cell line. Hence, we intend to perform in vivo efficacy testing of E6201 in flank (subcutaneous) and intracranial patient-derived xenograft models of melanoma.

Future work on this project will evaluate the in vivo efficacy of promising selected candidates in preclinical models. The efficacy of ispinesib will be examined in GBM models with and without elacridar co-administration, as well as in mice lacking P-gp and Bcrp. The results of such studies will provide insights on the suitability of KIF11 as a target for GBM, and also if improved delivery of ispinesib will translate to superior

efficacy. Additionally, testing the efficacy of E6201 alone and in combination with RAF inhibitors in patient-derived melanoma models is of interest. Chapter 4 and 6 reveal a regional heterogeneity in drug distribution in intracranial tumor models, and future studies aimed at connecting differences in delivery with possible differences in pharmacodynamics responses will be valuable. The findings of the current research work and outcomes of the outlined future studies will guide the translation of promising experimental therapies to the clinic. The specific ideas related to the brain tumor treatment addressed in this dissertation will provide valuable insights and establish an experimental paradigm for future preclinical testing that will be therapeutically relevant to patients. Also, the current research work raises some critical questions that will generate certain hypotheses and targeted research in the field of brain tumors, the answers to which may lead to important progress in the treatment of this devastating disease.

BIBLIOGRAPHY

CHAPTER I

Agarwal, S., P. Manchanda, M. A. Vogelbaum, J. R. Ohlfest, and W. F. Elmquist (2013) Function of the blood-brain barrier and restriction of drug delivery to invasive glioma cells: findings in an orthotopic rat xenograft model of glioma. *Drug Metab Dispos* 41 (1):33-9. doi: 10.1124/dmd.112.048322.

Agarwal, S., R. Sane, R. Oberoi, J. R. Ohlfest, and W. F. Elmquist (2011) Delivery of molecularly targeted therapy to malignant glioma, a disease of the whole brain. *Expert Rev Mol Med* 13:e17. doi: 10.1017/S1462399411001888.

Babiker, H. M., S. A. Byron, W. P. D. Hendricks, W. F. Elmquist, G. Gampa, J. Vondrak, J. Aldrich, L. Cuyugan, J. Adkins, V. De Luca, R. Tibes, M. J. Borad, K. Marceau, T. J. Myers, L. J. Paradiso, W. S. Liang, R. L. Korn, D. Cridebring, D. D. Von Hoff, J. D. Carpten, D. W. Craig, J. M. Trent, and M. S. Gordon (2018) E6201, an intravenous MEK1 inhibitor, achieves an exceptional response in BRAF V600E-mutated metastatic malignant melanoma with brain metastases. *Invest New Drugs*. doi: 10.1007/s10637-018-0668-8.

Barnholtz-Sloan, J. S., A. E. Sloan, F. G. Davis, F. D. Vigneau, P. Lai, and R. E. Sawaya (2004) Incidence proportions of brain metastases in patients diagnosed (1973 to 2001) in the Metropolitan Detroit Cancer Surveillance System. *J Clin Oncol* 22 (14):2865-72. doi: 10.1200/JCO.2004.12.149.

Blagden, S. P., L. R. Molife, A. Seebaran, M. Payne, A. H. Reid, A. S. Protheroe, L. S. Vasist, D. D. Williams, C. Bowen, S. J. Kathman, J. P. Hodge, M. M. Dar, J. S. de Bono, and M. R. Middleton (2008) A phase I trial of ispinesib, a kinesin spindle protein inhibitor, with docetaxel in patients with advanced solid tumours. *Br J Cancer* 98 (5):894-9. doi: 10.1038/sj.bjc.6604264.

Bray, F., J. Ferlay, I. Soerjomataram, R. L. Siegel, L. A. Torre, and A. Jemal (2018) Global cancer statistics 2018: GLOBOCAN estimates of incidence and mortality worldwide for 36 cancers in 185 countries. *CA Cancer J Clin* 68 (6):394-424. doi: 10.3322/caac.21492.

Burris, H. A., 3rd, S. F. Jones, D. D. Williams, S. J. Kathman, J. P. Hodge, L. Pandite, P. T. Ho, S. A. Boerner, and P. Lorusso (2011) A phase I study of ispinesib, a kinesin spindle protein inhibitor, administered weekly for three consecutive weeks of a 28-day cycle in patients with solid tumors. *Invest New Drugs* 29 (3):467-72. doi: 10.1007/s10637-009-9374-x.

Byron, S. A., D. C. Loch, C. L. Wellens, A. Wortmann, J. Wu, J. Wang, K. Nomoto, and P. M. Pollock (2012) Sensitivity to the MEK inhibitor E6201 in melanoma cells is associated with mutant BRAF and wildtype PTEN status. *Mol Cancer* 11:75. doi: 10.1186/1476-4598-11-75.

Canta, A., A. Chiorazzi, and G. Cavaletti (2009) Tubulin: a target for antineoplastic drugs into the cancer cells but also in the peripheral nervous system. *Curr Med Chem* 16 (11):1315-24.

Chiesa-Vottero, A. G., L. A. Rybicki, and R. A. Prayson (2003) Comparison of proliferation indices in glioblastoma multiforme by whole tissue section vs tissue

microarray. *Am J Clin Pathol* 120 (6):902-8. doi: 10.1309/8UAU-KFK3-NBDM-VTNU.

Choo, E. F., J. Ly, J. Chan, S. K. Shahidi-Latham, K. Messick, E. Plise, C. M. Quiason, and L. Yang (2014) Role of P-glycoprotein on the brain penetration and brain pharmacodynamic activity of the MEK inhibitor cobimetinib. *Mol Pharm* 11 (11):4199-207. doi: 10.1021/mp500435s.

Cross, R. A., and A. McAinsh (2014) Prime movers: the mechanochemistry of mitotic kinesins. *Nat Rev Mol Cell Biol* 15 (4):257-71. doi: 10.1038/nrm3768.

Cuddapah, V. A., S. Robel, S. Watkins, and H. Sontheimer (2014) A neurocentric perspective on glioma invasion. *Nat Rev Neurosci* 15 (7):455-65. doi: 10.1038/nrn3765.

Damsky, W. E., N. Theodosakis, and M. Bosenberg (2014) Melanoma metastasis: new concepts and evolving paradigms. *Oncogene* 33 (19):2413-22. doi: 10.1038/onc.2013.194.

Davies, H., G. R. Bignell, C. Cox, P. Stephens, S. Edkins, S. Clegg, J. Teague, H. Woffendin, M. J. Garnett, W. Bottomley, N. Davis, E. Dicks, R. Ewing, Y. Floyd, K. Gray, S. Hall, R. Hawes, J. Hughes, V. Kosmidou, A. Menzies, C. Mould, A. Parker, C. Stevens, S. Watt, S. Hooper, R. Wilson, H. Jayatilake, B. A. Gusterson, C. Cooper, J. Shipley, D. Hargrave, K. Pritchard-Jones, N. Maitland, G. Chenevix-Trench, G. J. Riggins, D. D. Bigner, G. Palmieri, A. Cossu, A. Flanagan, A. Nicholson, J. W. Ho, S. Y. Leung, S. T. Yuen, B. L. Weber, H. F. Seigler, T. L. Darrow, H. Paterson, R. Marais, C. J. Marshall, R. Wooster, M. R. Stratton, and P. A. Futreal (2002) Mutations of the BRAF gene in human cancer. *Nature* 417 (6892):949-54. doi: 10.1038/nature00766.

de Gooijer, M. C., P. Zhang, N. Thota, I. Mayayo-Peralta, L. C. Buil, J. H. Beijnen, and O. van Tellingen (2015) P-glycoprotein and breast cancer resistance protein restrict the brain penetration of the CDK4/6 inhibitor palbociclib. *Invest New Drugs* 33 (5):1012-9. doi: 10.1007/s10637-015-0266-y.

de Gooijer, M. C., P. Zhang, R. Weijer, L. C. M. Buil, J. H. Beijnen, and O. van Tellingen (2018) The impact of P-glycoprotein and breast cancer resistance protein on the brain pharmacokinetics and pharmacodynamics of a panel of MEK inhibitors. *Int J Cancer* 142 (2):381-391. doi: 10.1002/ijc.31052.

Demuth, T., and M. E. Berens (2004) Molecular mechanisms of glioma cell migration and invasion. *J Neurooncol* 70 (2):217-28. doi: 10.1007/s11060-004-2751-6.

Dummer, R., S. M. Goldinger, C. P. Turtschi, N. B. Eggmann, O. Michielin, L. Mitchell, L. Veronese, P. R. Hilfiker, L. Felderer, and J. D. Rinderknecht (2014) Vemurafenib in patients with BRAF(V600) mutation-positive melanoma with symptomatic brain metastases: final results of an open-label pilot study. *Eur J Cancer* 50 (3):611-21. doi: 10.1016/j.ejca.2013.11.002.

Durmus, S., R. W. Sparidans, E. Wagenaar, J. H. Beijnen, and A. H. Schinkel (2012) Oral availability and brain penetration of the B-RAFV600E inhibitor vemurafenib can be enhanced by the P-GLYCOprotein (ABCB1) and breast cancer resistance protein (ABCG2) inhibitor elacridar. *Mol Pharm* 9 (11):3236-45. doi: 10.1021/mp3003144.

Elenbaas B, Singh L, Boccia A, Cullen P, Peng H, Rohde E, Raimundo B, Kumaravel G, Joseph I. 2010. "BIIB024, a potent pan-Raf kinase inhibitor fro melanoma and solid tumors." EORTC-NCI-AACR Molecular Targets and Cancer Therapeutics, November 16 -19 2010.

Falnikar, A., S. Tole, and P. W. Baas (2011) Kinesin-5, a mitotic microtubule-associated motor protein, modulates neuronal migration. *Mol Biol Cell* 22 (9):1561-74. doi: 10.1091/mbc.E10-11-0905.

Flaherty, K. T., J. R. Infante, A. Daud, R. Gonzalez, R. F. Kefford, J. Sosman, O. Hamid, L. Schuchter, J. Cebon, N. Ibrahim, R. Kudchadkar, H. A. Burris, 3rd, G. Falchook, A. Algazi, K. Lewis, G. V. Long, I. Puzanov, P. Lebowitz, A. Singh, S. Little, P. Sun, A. Allred, D. Ouellet, K. B. Kim, K. Patel, and J. Weber (2012) Combined BRAF and MEK inhibition in melanoma with BRAF V600 mutations. *N Engl J Med* 367 (18):1694-703. doi: 10.1056/NEJMoa1210093.

Flaherty, K. T., C. Robert, P. Hersey, P. Nathan, C. Garbe, M. Milhem, L. V. Demidov, J. C. Hassel, P. Rutkowski, P. Mohr, R. Dummer, U. Trefzer, J. M. Larkin, J. Utikal, B. Dreno, M. Nyakas, M. R. Middleton, J. C. Becker, M. Casey, L. J. Sherman, F. S. Wu, D. Ouellet, A. M. Martin, K. Patel, D. Schadendorf, and Metric Study Group (2012) Improved survival with MEK inhibition in BRAF-mutated melanoma. *N Engl J Med* 367 (2):107-14. doi: 10.1056/NEJMoa1203421.

Freeman, A. K., D. A. Ritt, and D. K. Morrison (2013) Effects of Raf dimerization and its inhibition on normal and disease-associated Raf signaling. *Mol Cell* 49 (4):751-8. doi: 10.1016/j.molcel.2012.12.018.

Gallego Perez-Larraya, J., and J. Hildebrand (2014) Brain metastases. *Handb Clin Neurol* 121:1143-57. doi: 10.1016/B978-0-7020-4088-7.00077-8.

Gampa, G., S. Vaidhyanathan, J. N. Sarkaria, and W. F. Elmquist (2017) Drug delivery to melanoma brain metastases: Can current challenges lead to new opportunities? *Pharmacol Res* 123:10-25. doi: 10.1016/j.phrs.2017.06.008.

Girotti, M. R., F. Lopes, N. Preece, D. Niculescu-Duvaz, A. Zambon, L. Davies, S. Whittaker, G. Saturno, A. Viros, M. Pedersen, B. M. Suijkerbuijk, D. Menard, R. McLeary, L. Johnson, L. Fish, S. Ejiama, B. Sanchez-Laorden, J. Hohloch, N. Carragher, K. Macleod, G. Ashton, A. A. Marusiak, A. Fusi, J. Brognard, M. Frame, P. Lorigan, R. Marais, and C. Springer (2015) Paradox-breaking RAF inhibitors that also target SRC are effective in drug-resistant BRAF mutant melanoma. *Cancer Cell* 27 (1):85-96. doi: 10.1016/j.ccell.2014.11.006.

Gupta, G., A. G. Robertson, and R. M. MacKie (1997) Cerebral metastases of cutaneous melanoma. *Br J Cancer* 76 (2):256-9.

Hatzivassiliou, G., K. Song, I. Yen, B. J. Brandhuber, D. J. Anderson, R. Alvarado, M. J. Ludlam, D. Stokoe, S. L. Gloor, G. Vigers, T. Morales, I. Aliagas, B. Liu, S. Sideris, K. P. Hoeflich, B. S. Jaiswal, S. Seshagiri, H. Koeppen, M. Belvin, L. S. Friedman, and S. Malek (2010) RAF inhibitors prime wild-type RAF to activate the MAPK pathway and enhance growth. *Nature* 464 (7287):431-5. doi: 10.1038/nature08833.

Henry, J. R., M. D. Kaufman, S. B. Peng, Y. M. Ahn, T. M. Caldwell, L. Vogeti, H. Telikepalli, W. P. Lu, M. M. Hood, T. J. Rutkoski, B. D. Smith, S. Vogeti, D.

Miller, S. C. Wise, L. Chun, X. Zhang, Y. Zhang, L. Kays, P. A. Hipskind, A. D. Wrobleski, K. L. Lobb, J. M. Clay, J. D. Cohen, J. L. Walgren, D. McCann, P. Patel, D. K. Clawson, S. Guo, D. Manglicmot, C. Groshong, C. Logan, J. J. Starling, and D. L. Flynn (2015) Discovery of 1-(3,3-dimethylbutyl)-3-(2-fluoro-4-methyl-5-(7-methyl-2-(methylamino)pyrido[2,3- d]pyrimidin-6-yl)phenyl)urea (LY3009120) as a pan-RAF inhibitor with minimal paradoxical activation and activity against BRAF or RAS mutant tumor cells. *J Med Chem* 58 (10):4165-79. doi: 10.1021/acs.jmedchem.5b00067.

Hodis, E., I. R. Watson, G. V. Kryukov, S. T. Arold, M. Imielinski, J. P. Theurillat, E. Nickerson, D. Auclair, L. Li, C. Place, D. Dicara, A. H. Ramos, M. S. Lawrence, K. Cibulskis, A. Sivachenko, D. Voet, G. Saksena, N. Stransky, R. C. Onofrio, W. Winckler, K. Ardlie, N. Wagle, J. Wargo, K. Chong, D. L. Morton, K. Stemke-Hale, G. Chen, M. Noble, M. Meyerson, J. E. Ladbury, M. A. Davies, J. E. Gershenwald, S. N. Wagner, D. S. Hoon, D. Schadendorf, E. S. Lander, S. B. Gabriel, G. Getz, L. A. Garraway, and L. Chin (2012) A landscape of driver mutations in melanoma. *Cell* 150 (2):251-63. doi: 10.1016/j.cell.2012.06.024.

Kromer, C., J. Xu, Q. T. Ostrom, H. Gittleman, C. Kruchko, R. Sawaya, and J. S. Barnholtz-Sloan (2017) Estimating the annual frequency of synchronous brain metastasis in the United States 2010-2013: a population-based study. *J Neurooncol* 134 (1):55-64. doi: 10.1007/s11060-017-2516-7.

Lad, L., L. Luo, J. D. Carson, K. W. Wood, J. J. Hartman, R. A. Copeland, and R. Sakowicz (2008) Mechanism of inhibition of human KSP by ispinesib. *Biochemistry* 47 (11):3576-85. doi: 10.1021/bi702061g.

Long, G. V., U. Trefzer, M. A. Davies, R. F. Kefford, P. A. Ascierto, P. B. Chapman, I. Puzanov, A. Hauschild, C. Robert, A. Algazi, L. Mortier, H. Tawbi, T. Wilhelm, L. Zimmer, J. Switzky, S. Swann, A. M. Martin, M. Guckert, V. Goodman, M. Streit, J. M. Kirkwood, and D. Schadendorf (2012) Dabrafenib in patients with Val600Glu or Val600Lys BRAF-mutant melanoma metastatic to the brain (BREAK-MB): a multicentre, open-label, phase 2 trial. *Lancet Oncol* 13 (11):1087-95. doi: 10.1016/S1470-2045(12)70431-X.

Margolin, K., M. S. Ernstoff, O. Hamid, D. Lawrence, D. McDermott, I. Puzanov, J. D. Wolchok, J. I. Clark, M. Sznol, T. F. Logan, J. Richards, T. Michener, A. Balogh, K. N. Heller, and F. S. Hodi (2012) Ipilimumab in patients with melanoma and brain metastases: an open-label, phase 2 trial. *Lancet Oncol* 13 (5):459-65. doi: 10.1016/S1470-2045(12)70090-6.

Mastronardi, L., A. Guiducci, F. Puzzilli, and A. Ruggeri (1999) Relationship between Ki-67 labeling index and survival in high-grade glioma patients treated after surgery with tamoxifen. *J Neurosurg Sci* 43 (4):263-70.

Mittapalli, R. K., S. Vaidhyanathan, A. Z. Dudek, and W. F. Elmquist (2013) Mechanisms limiting distribution of the threonine-protein kinase B-RaF(V600E) inhibitor dabrafenib to the brain: implications for the treatment of melanoma brain metastases. *J Pharmacol Exp Ther* 344 (3):655-64. doi: 10.1124/jpet.112.201475.

Mittapalli, R. K., S. Vaidhyanathan, R. Sane, and W. F. Elmquist (2012) Impact of P-glycoprotein (ABCB1) and breast cancer resistance protein (ABCG2) on the brain

distribution of a novel BRAF inhibitor: vemurafenib (PLX4032). *J Pharmacol Exp Ther* 342 (1):33-40. doi: 10.1124/jpet.112.192195.

Narita, Y., K. Okamoto, M. I. Kawada, K. Takase, Y. Minoshima, K. Kodama, M. Iwata, N. Miyamoto, and K. Sawada (2014) Novel ATP-competitive MEK inhibitor E6201 is effective against vemurafenib-resistant melanoma harboring the MEK1-C121S mutation in a preclinical model. *Mol Cancer Ther* 13 (4):823-32. doi: 10.1158/1535-7163.MCT-13-0667.

Nayak, L., E. Q. Lee, and P. Y. Wen (2012) Epidemiology of brain metastases. *Curr Oncol Rep* 14 (1):48-54. doi: 10.1007/s11912-011-0203-y.

Ostrom, Q. T., H. Gittleman, P. Liao, T. Vecchione-Koval, Y. Wolinsky, C. Kruchko, and J. S. Barnholtz-Sloan (2017) CBTRUS Statistical Report: Primary brain and other central nervous system tumors diagnosed in the United States in 2010-2014. *Neuro Oncol* 19 (suppl_5):v1-v88. doi: 10.1093/neuonc/nox158.

Parrish, K. E., J. Pokorny, R. K. Mittapalli, K. Bakken, J. N. Sarkaria, and W. F. Elmquist (2015) Efflux transporters at the blood-brain barrier limit delivery and efficacy of cyclin-dependent kinase 4/6 inhibitor palbociclib (PD-0332991) in an orthotopic brain tumor model. *J Pharmacol Exp Ther* 355 (2):264-71. doi: 10.1124/jpet.115.228213.

Peng, S. B., J. R. Henry, M. D. Kaufman, W. P. Lu, B. D. Smith, S. Vogeti, T. J. Rutkoski, S. Wise, L. Chun, Y. Zhang, R. D. Van Horn, T. Yin, X. Zhang, V. Yadav, S. H. Chen, X. Gong, X. Ma, Y. Webster, S. Buchanan, I. Mochalkin, L. Huber, L. Kays, G. P. Donoho, J. Walgren, D. McCann, P. Patel, I. Conti, G. D. Plowman, J. J. Starling, and D. L. Flynn (2015) Inhibition of RAF Isoforms and Active Dimers by LY3009120 Leads to Anti-tumor Activities in RAS or BRAF Mutant Cancers. *Cancer Cell* 28 (3):384-98. doi: 10.1016/j.ccell.2015.08.002.

Polli, J. W., K. L. Olson, J. P. Chism, L. S. John-Williams, R. L. Yeager, S. M. Woodard, V. Otto, S. Castellino, and V. E. Demby (2009) An unexpected synergist role of P-glycoprotein and breast cancer resistance protein on the central nervous system penetration of the tyrosine kinase inhibitor lapatinib (N-{3-chloro-4-[(3-fluorobenzyl)oxy]phenyl}-6-[5-({[2-(methylsulfonyl)ethyl]amino }methyl)-2-furyl]-4-quinazolinamine; GW572016). *Drug Metab Dispos* 37 (2):439-42. doi: 10.1124/dmd.108.024646.

Poulikakos, P. I., C. Zhang, G. Bollag, K. M. Shokat, and N. Rosen (2010) RAF inhibitors transactivate RAF dimers and ERK signalling in cells with wild-type BRAF. *Nature* 464 (7287):427-30. doi: 10.1038/nature08902.

Rasco, D. W.; Olszanski, A. J.; Patnaik, A.; Espino, G.; Neuwirth, R.; Faucette, S.; Bargfrede, M.; Gangolli, E. A.; Walker, R. M.; Kneissl, M.; Bozon, V. 2013. "MLN2480, an Investigational Oral Pan-RAF Kinase Inhibitor, in Patients (Pts) with Relapsed or Refractory Solid Tumors: Phase I Study." ASCO.

Rath, O., and F. Kozielski (2012) Kinesins and cancer. *Nat Rev Cancer* 12 (8):527-39. doi: 10.1038/nrc3310.

Raub, T. J., G. N. Wishart, P. Kulanthaivel, B. A. Staton, R. T. Ajamie, G. A. Sawada, L. M. Gelbert, H. E. Shannon, C. Sanchez-Martinez, and A. De Dios (2015) Brain Exposure of Two Selective Dual CDK4 and CDK6 Inhibitors and the Antitumor

Activity of CDK4 and CDK6 Inhibition in Combination with Temozolomide in an Intracranial Glioblastoma Xenograft. *Drug Metab Dispos* 43 (9):1360-71. doi: 10.1124/dmd.114.062745.

Salphati, L., J. Pang, E. G. Plise, L. B. Lee, A. G. Olivero, W. W. Prior, D. Sampath, S. Wong, and X. Zhang (2012) Preclinical assessment of the absorption and disposition of the phosphatidylinositol 3-kinase/mammalian target of rapamycin inhibitor GDC-0980 and prediction of its pharmacokinetics and efficacy in human. *Drug Metab Dispos* 40 (9):1785-96. doi: 10.1124/dmd.112.046052.

Samatar, A. A., and P. I. Poulikakos (2014) Targeting RAS-ERK signalling in cancer: promises and challenges. *Nat Rev Drug Discov* 13 (12):928-42. doi: 10.1038/nrd4281.

Sarkaria, J. N., L. S. Hu, I. F. Parney, D. H. Pafundi, D. H. Brinkmann, N. N. Laack, C. Giannini, T. C. Burns, S. H. Kizilbash, J. K. Laramy, K. R. Swanson, T. J. Kaufmann, P. D. Brown, N. Y. R. Agar, E. Galanis, J. C. Buckner, and W. F. Elmquist (2018) Is the blood-brain barrier really disrupted in all glioblastomas? A critical assessment of existing clinical data. *Neuro Oncol* 20 (2):184-191. doi: 10.1093/neuonc/nox175.

Siegel, R. L., K. D. Miller, and A. Jemal (2018) Cancer statistics, 2018. *CA Cancer J Clin* 68 (1):7-30. doi: 10.3322/caac.21442.

Spagnolo, F., V. Picasso, M. Lambertini, V. Ottaviano, B. Dozin, and P. Queirolo (2016) Survival of patients with metastatic melanoma and brain metastases in the era of MAP-kinase inhibitors and immunologic checkpoint blockade antibodies: A systematic review. *Cancer Treat Rev* 45:38-45. doi: 10.1016/j.ctrv.2016.03.003.

Stoyanov, G. S., D. L. Dzhenkov, M. Kitanova, I. S. Donev, and P. Ghenev (2017) Correlation Between Ki-67 Index, World Health Organization Grade and Patient Survival in Glial Tumors With Astrocytic Differentiation. *Cureus* 9 (6):e1396. doi: 10.7759/cureus.1396.

Stupp, R., W. P. Mason, M. J. van den Bent, M. Weller, B. Fisher, M. J. Taphoorn, K. Belanger, A. A. Brandes, C. Marosi, U. Bogdahn, J. Curschmann, R. C. Janzer, S. K. Ludwin, T. Gorlia, A. Allgeier, D. Lacombe, J. G. Cairncross, E. Eisenhauer, R. O. Mirimanoff, Research European Organisation for, Tumor Treatment of Cancer Brain, Groups Radiotherapy, and Group National Cancer Institute of Canada Clinical Trials (2005) Radiotherapy plus concomitant and adjuvant temozolomide for glioblastoma. *N Engl J Med* 352 (10):987-96. doi: 10.1056/NEJMoa043330.

Tawbi, H. A., P. A. Forsyth, A. Algazi, O. Hamid, F. S. Hodi, S. J. Moschos, N. I. Khushalani, K. Lewis, C. D. Lao, M. A. Postow, M. B. Atkins, M. S. Ernstoff, D. A. Reardon, I. Puzanov, R. R. Kudchadkar, R. P. Thomas, A. Tarhini, A. C. Pavlick, J. Jiang, A. Avila, S. Demelo, and K. Margolin (2018) Combined Nivolumab and Ipilimumab in Melanoma Metastatic to the Brain. *N Engl J Med* 379 (8):722-730. doi: 10.1056/NEJMoa1805453.

Tibes, R., M. J. Borad, C. E. Dutcus, L. Reyderman, K. Feit, A. Eisen, D. A. Verbel, and D. D. Von Hoff (2018) Safety, pharmacokinetics, and preliminary efficacy of E6201 in patients with advanced solid tumours, including melanoma: results of a

phase 1 study. *Br J Cancer* 118 (12):1580-1585. doi: 10.1038/s41416-018-0099-5.

Vaidhyanathan, S., R. K. Mittapalli, J. N. Sarkaria, and W. F. Elmquist (2014) Factors influencing the CNS distribution of a novel MEK-1/2 inhibitor: implications for combination therapy for melanoma brain metastases. *Drug Metab Dispos* 42 (8):1292-300. doi: 10.1124/dmd.114.058339.

Vaidhyanathan, S., B. Wilken-Resman, D. J. Ma, K. E. Parrish, R. K. Mittapalli, B. L. Carlson, J. N. Sarkaria, and W. F. Elmquist (2016) Factors Influencing the Central Nervous System Distribution of a Novel Phosphoinositide 3-Kinase/Mammalian Target of Rapamycin Inhibitor GSK2126458: Implications for Overcoming Resistance with Combination Therapy for Melanoma Brain Metastases. *J Pharmacol Exp Ther* 356 (2):251-9. doi: 10.1124/jpet.115.229393.

Venere, M., C. Horbinski, J. F. Crish, X. Jin, A. Vasanji, J. Major, A. C. Burrows, C. Chang, J. Prokop, Q. Wu, P. A. Sims, P. Canoll, M. K. Summers, S. S. Rosenfeld, and J. N. Rich (2015) The mitotic kinesin KIF11 is a driver of invasion, proliferation, and self-renewal in glioblastoma. *Sci Transl Med* 7 (304):304ra143. doi: 10.1126/scitranslmed.aac6762.

Wagle, N., E. M. Van Allen, D. J. Treacy, D. T. Frederick, Z. A. Cooper, A. Taylor-Weiner, M. Rosenberg, E. M. Goetz, R. J. Sullivan, D. N. Farlow, D. C. Friedrich, K. Anderka, D. Perrin, C. M. Johannessen, A. McKenna, K. Cibulskis, G. Kryukov, E. Hodis, D. P. Lawrence, S. Fisher, G. Getz, S. B. Gabriel, S. L. Carter, K. T. Flaherty, J. A. Wargo, and L. A. Garraway (2014) MAP kinase pathway alterations in BRAF-mutant melanoma patients with acquired resistance to combined RAF/MEK inhibition. *Cancer Discov* 4 (1):61-8. doi: 10.1158/2159-8290.CD-13-0631.

Wang, J., C. Gan, R. W. Sparidans, E. Wagenaar, S. van Hoppe, J. H. Beijnen, and A. H. Schinkel (2018) P-glycoprotein (MDR1/ABCB1) and Breast Cancer Resistance Protein (BCRP/ABCG2) affect brain accumulation and intestinal disposition of encorafenib in mice. *Pharmacol Res* 129:414-423. doi: 10.1016/j.phrs.2017.11.006.

Wang, J. Y., K. M. Wilcoxen, K. Nomoto, and S. Wu (2007) Recent advances of MEK inhibitors and their clinical progress. *Curr Top Med Chem* 7 (14):1364-78.

Welsh, S. J., H. Rizos, R. A. Scolyer, and G. V. Long (2016) Resistance to combination BRAF and MEK inhibition in metastatic melanoma: Where to next? *Eur J Cancer* 62:76-85. doi: 10.1016/j.ejca.2016.04.005.

Whittaker, S. R., G. S. Cowley, S. Wagner, F. Luo, D. E. Root, and L. A. Garraway (2015) Combined Pan-RAF and MEK Inhibition Overcomes Multiple Resistance Mechanisms to Selective RAF Inhibitors. *Mol Cancer Ther* 14 (12):2700-11. doi: 10.1158/1535-7163.MCT-15-0136-T.

Wojcik, E. J., R. S. Buckley, J. Richard, L. Liu, T. M. Huckaba, and S. Kim (2013) Kinesin-5: cross-bridging mechanism to targeted clinical therapy. *Gene* 531 (2):133-49. doi: 10.1016/j.gene.2013.08.004.

Wood, K. W., W. D. Cornwell, and J. R. Jackson (2001) Past and future of the mitotic spindle as an oncology target. *Curr Opin Pharmacol* 1 (4):370-7.

Wu J, Nomoto K, Wang J, Kuznetsov G, Agoulnik S, Shuck E, Wong N, Towle M, Schnaderbeck M, Wu S, Littlefield B. 2009. "In vivo anticancer activity of E6201, a novel MEK1 inhibitor, against BRAF-mutated human cancer xenografts." Abstract #3687, Denver, CO.

CHAPTER II

Abbott, N. J. (2013). "Blood-brain barrier structure and function and the challenges for CNS drug delivery." J Inherit Metab Dis **36**(3): 437-449.

Agarwal, S., R. Sane, R. Oberoi, J. R. Ohlfest and W. F. Elmquist (2011). "Delivery of molecularly targeted therapy to malignant glioma, a disease of the whole brain." Expert Rev Mol Med **13**: e17.

Barnholtz-Sloan, J. S., A. E. Sloan, F. G. Davis, F. D. Vigneau, P. Lai and R. E. Sawaya (2004). "Incidence proportions of brain metastases in patients diagnosed (1973 to 2001) in the Metropolitan Detroit Cancer Surveillance System." J Clin Oncol **22**(14): 2865-2872.

Bartus, R. T., P. Elliott, N. Hayward, R. Dean, E. L. McEwen and S. K. Fisher (1996). "Permeability of the blood brain barrier by the bradykinin agonist, RMP-7: evidence for a sensitive, auto-regulated, receptor-mediated system." Immunopharmacology **33**(1-3): 270-278.

Basit, S., Z. Ashraf, K. Lee and M. Latif (2017). "First macrocyclic 3(rd)-generation ALK inhibitor for treatment of ALK/ROS1 cancer: Clinical and designing strategy update of lorlatinib." Eur J Med Chem **134**: 348-356.

Baumert, C. and A. Hilgeroth (2009). "Recent advances in the development of P-gp inhibitors." Anticancer Agents Med Chem **9**(4): 415-436.

Begley, D. J. (2004). "ABC transporters and the blood-brain barrier." Curr Pharm Des **10**(12): 1295-1312.

Benjamin, R. K., F. H. Hochberg, E. Fox, P. M. Bungay, W. F. Elmquist, C. F. Stewart, J. M. Gallo, J. M. Collins, R. P. Pelletier, J. F. de Groot, R. C. Hickner, I. Cavus, S. A. Grossman and O. M. Colvin (2004). "Review of microdialysis in brain tumors, from concept to application: first annual Carolyn Frye-Halloran symposium." Neuro Oncol **6**(1): 65-74.

Benson, A. B., 3rd, D. L. Trump, J. M. Koeller, M. I. Egorin, E. A. Olman, R. S. Witte, T. E. Davis and D. C. Tormey (1985). "Phase I study of vinblastine and verapamil given by concurrent iv infusion." Cancer Treat Rep **69**(7-8): 795-799.

Bergenheim, A. T., J. Capala, M. Roslin and R. Henriksson (2005). "Distribution of BPA and metabolic assessment in glioblastoma patients during BNCT treatment: a microdialysis study." J Neurooncol **71**(3): 287-293.

Bickel, U. (2005). "How to measure drug transport across the blood-brain barrier." NeuroRx **2**(1): 15-26.

Blakeley, J. and J. Portnow (2010). "Microdialysis for assessing intratumoral drug disposition in brain cancers: a tool for rational drug development." Expert Opin Drug Metab Toxicol **6**(12): 1477-1491.

Blakeley, J. O., J. Olson, S. A. Grossman, X. He, J. Weingart, J. G. Supko and C. New Approaches to Brain Tumor Therapy (2009). "Effect of blood brain barrier permeability in recurrent high grade gliomas on the intratumoral pharmacokinetics of methotrexate: a microdialysis study." J Neurooncol **91**(1): 51-58.

Blasi, P., S. Giovagnoli, A. Schoubben, M. Ricci and C. Rossi (2007). "Solid lipid nanoparticles for targeted brain drug delivery." Adv Drug Deliv Rev **59**(6): 454-477.

Bleau, A. M., D. Hambardzumyan, T. Ozawa, E. I. Fomchenko, J. T. Huse, C. W. Brennan and E. C. Holland (2009). "PTEN/PI3K/Akt pathway regulates the side population phenotype and ABCG2 activity in glioma tumor stem-like cells." Cell Stem Cell **4**(3): 226-235.
Bohn, J. P., G. Pall, G. Stockhammer and M. Steurer (2016). "Targeted Therapies for the Treatment of Brain Metastases in Solid Tumors." Target Oncol **11**(3): 263-275.
Bonati, M., J. Kanto and G. Tognoni (1982). "Clinical pharmacokinetics of cerebrospinal fluid." Clin Pharmacokinet **7**(4): 312-335.
Bottros, M. M. and P. J. Christo (2014). "Current perspectives on intrathecal drug delivery." J Pain Res **7**: 615-626.
Bregy, A., A. H. Shah, M. V. Diaz, H. E. Pierce, P. L. Ames, D. Diaz and R. J. Komotar (2013). "The role of Gliadel wafers in the treatment of high-grade gliomas." Expert Rev Anticancer Ther **13**(12): 1453-1461.
Bruzzone, M. G., L. D'Incerti, L. L. Farina, V. Cuccarini and G. Finocchiaro (2012). "CT and MRI of brain tumors." Q J Nucl Med Mol Imaging **56**(2): 112-137.
Bynoe, M. S., C. Viret, A. Yan and D. G. Kim (2015). "Adenosine receptor signaling: a key to opening the blood-brain door." Fluids Barriers CNS **12**: 20.
Calatozzolo, C., M. Gelati, E. Ciusani, F. L. Sciacca, B. Pollo, L. Cajola, C. Marras, A. Silvani, L. Vitellaro-Zuccarello, D. Croci, A. Boiardi and A. Salmaggi (2005). "Expression of drug resistance proteins Pgp, MRP1, MRP3, MRP5 and GST-pi in human glioma." J Neurooncol **74**(2): 113-121.
Carman, A. J., J. H. Mills, A. Krenz, D. G. Kim and M. S. Bynoe (2011). "Adenosine receptor signaling modulates permeability of the blood-brain barrier." J Neurosci **31**(37): 13272-13280.
Chen, K. G., J. C. Valencia, J. P. Gillet, V. J. Hearing and M. M. Gottesman (2009). "Involvement of ABC transporters in melanogenesis and the development of multidrug resistance of melanoma." Pigment Cell Melanoma Res **22**(6): 740-749.
Cho, H. S., H. Y. Lee, M. Han, J. R. Choi, S. Ahn, T. Lee, Y. Chang and J. Park (2016). "Localized Down-regulation of P-glycoprotein by Focused Ultrasound and Microbubbles induced Blood-Brain Barrier Disruption in Rat Brain." Scientific Reports **6**: 1-10.
Dantzig, A. H., R. L. Shepard, J. Cao, K. L. Law, W. J. Ehlhardt, T. M. Baughman, T. F. Bumol and J. J. Starling (1996). "Reversal of P-glycoprotein-mediated multidrug resistance by a potent cyclopropyldibenzosuberane modulator, LY335979." Cancer Res **56**(18): 4171-4179.
Davson, H. and M. B. Segal (1995). Physiology of the CSF and Blood Brain Bariers, CRC-Press.
de Lange, E. C. (2013). "Utility of CSF in translational neuroscience." J Pharmacokinet Pharmacodyn **40**(3): 315-326.
de Lange, E. C., M. Danhof, A. G. de Boer and D. D. Breimer (1994). "Critical factors of intracerebral microdialysis as a technique to determine the pharmacokinetics of drugs in rat brain." Brain Res **666**(1): 1-8.
Dean, M., T. Fojo and S. Bates (2005). "Tumour stem cells and drug resistance." Nat Rev Cancer **5**(4): 275-284.

Demeule, M., D. Shedid, E. Beaulieu, R. F. Del Maestro, A. Moghrabi, P. B. Ghosn, R. Moumdjian, F. Berthelet and R. Beliveau (2001). "Expression of multidrug-resistance P-glycoprotein (MDR1) in human brain tumors." Int J Cancer **93**(1): 62-66.
Di, L., H. Rong and B. Feng (2013). "Demystifying brain penetration in central nervous system drug discovery. Miniperspective." J Med Chem **56**(1): 2-12.
Drappatz, J., A. Brenner, E. T. Wong, A. Eichler, D. Schiff, M. D. Groves, T. Mikkelsen, S. Rosenfeld, J. Sarantopoulos, C. A. Meyers, R. M. Fielding, K. Elian, X. Wang, B. Lawrence, M. Shing, S. Kelsey, J. P. Castaigne and P. Y. Wen (2013). "Phase I study of GRN1005 in recurrent malignant glioma." Clin Cancer Res **19**(6): 1567-1576.
Elmquist, W. F. (2005). Targeted bioavailability, a fresh look at pharmacokinetic and pharmacodynamic issues in drug delivery. Drug Delivery: Principles and Applications. B. Wang, Siahaan, T. J., Soltero, R., Wiley Online Library**:** 73-82.
Elmquist, W. F. and R. J. Sawchuk (1997). "Application of microdialysis in pharmacokinetic studies." Pharm Res **14**(3): 267-288.
Emery, I. F., A. Gopalan, S. Wood, K. H. Chow, C. Battelli, J. George, H. Blaszyk, J. Florman and K. Yun (2017). "Expression and function of ABCG2 and XIAP in glioblastomas." J Neurooncol **133**(1): 47-57.
Essig, M., M. A. Weber, H. von Tengg-Kobligk, M. V. Knopp, W. T. Yuh and F. L. Giesel (2006). "Contrast-enhanced magnetic resonance imaging of central nervous system tumors: agents, mechanisms, and applications." Top Magn Reson Imaging **17**(2): 89-106.
Fattori, S., F. Becherini, M. Cianfriglia, G. Parenti, A. Romanini and M. Castagna (2007). "Human brain tumors: multidrug-resistance P-glycoprotein expression in tumor cells and intratumoral capillary endothelial cells." Virchows Arch **451**(1): 81-87.
Fife, K. M., M. H. Colman, G. N. Stevens, I. C. Firth, D. Moon, K. F. Shannon, R. Harman, K. Petersen-Schaefer, A. C. Zacest, M. Besser, G. W. Milton, W. H. McCarthy and J. F. Thompson (2004). "Determinants of outcome in melanoma patients with cerebral metastases." J Clin Oncol **22**(7): 1293-1300.
Fokas, E., J. P. Steinbach and C. Rodel (2013). "Biology of brain metastases and novel targeted therapies: time to translate the research." Biochim Biophys Acta **1835**(1): 61-75.
Fox, E. and S. E. Bates (2007). "Tariquidar (XR9576): a P-glycoprotein drug efflux pump inhibitor." Expert Rev Anticancer Ther **7**(4): 447-459.
Frank, N. Y., A. Margaryan, Y. Huang, T. Schatton, A. M. Waaga-Gasser, M. Gasser, M. H. Sayegh, W. Sadee and M. H. Frank (2005). "ABCB5-mediated doxorubicin transport and chemoresistance in human malignant melanoma." Cancer Res **65**(10): 4320-4333.
Gaillard, P. J., C. C. Appeldoorn, R. Dorland, J. van Kregten, F. Manca, D. J. Vugts, B. Windhorst, G. A. van Dongen, H. E. de Vries, D. Maussang and O. van Tellingen (2014). "Pharmacokinetics, brain delivery, and efficacy in brain tumor-bearing mice of glutathione pegylated liposomal doxorubicin (2B3-101)." PLoS One **9**(1): e82331.
Gallego Perez-Larraya, J. and J. Hildebrand (2014). "Brain metastases." Handb Clin Neurol **121**: 1143-1157.
Gampa, G., M. Kim, N. Cook-Rostie, J. K. Laramy, J. N. Sarkaria, L. Paradiso, L. DePalatis and W. F. Elmquist (2018). "Brain Distribution of a Novel MEK Inhibitor

E6201: Implications in the Treatment of Melanoma Brain Metastases." Drug Metab Dispos **46**(5): 658-666.
Gampa, G., S. Vaidhyanathan, B. W. Resman, K. E. Parrish, S. N. Markovic, J. N. Sarkaria and W. F. Elmquist (2016). "Challenges in the delivery of therapies to melanoma brain metastases." Curr Pharmacol Rep **2**(6): 309-325.
Gampa, G., S. Vaidhyanathan, J. N. Sarkaria and W. F. Elmquist (2017). "Drug delivery to melanoma brain metastases: Can current challenges lead to new opportunities?" Pharmacol Res **123**: 10-25.
Gazzin, S., N. Strazielle, C. Schmitt, M. Fevre-Montange, J. D. Ostrow, C. Tiribelli and J. F. Ghersi-Egea (2008). "Differential expression of the multidrug resistance-related proteins ABCb1 and ABCc1 between blood-brain interfaces." J Comp Neurol **510**(5): 497-507.
Goldwirt, L., K. Beccaria, A. Carpentier, R. Farinotti and C. Fernandez (2014). "Irinotecan and temozolomide brain distribution: a focus on ABCB1." Cancer Chemother Pharmacol **74**(1): 185-193.
Goodman, J. C. (2011). "Clinical microdialysis in neuro-oncology: principles and applications." Chin J Cancer **30**(3): 173-181.
Groothuis, D. R., S. Ward, K. E. Schlageter, A. C. Itskovich, S. C. Schwerin, C. V. Allen, C. Dills and R. M. Levy (1998). "Changes in blood-brain barrier permeability associated with insertion of brain cannulas and microdialysis probes." Brain Res **803**(1-2): 218-230.
Gu, J., X. Fang, J. Hao and X. Sha (2015). "Reversal of P-glycoprotein-mediated multidrug resistance by CD44 antibody-targeted nanocomplexes for short hairpin RNA-encoding plasmid DNA delivery." Biomaterials **45**: 99-114.
Hammarlund-Udenaes, M., M. Friden, S. Syvanen and A. Gupta (2008). "On the rate and extent of drug delivery to the brain." Pharm Res **25**(8): 1737-1750.
Hanley, M. J., P. Cancalon, W. W. Widmer and D. J. Greenblatt (2011). "The effect of grapefruit juice on drug disposition." Expert Opin Drug Metab Toxicol **7**(3): 267-286.
Heffron, T. P. (2016). "Small Molecule Kinase Inhibitors for the Treatment of Brain Cancer." J Med Chem **59**(22): 10030-10066.
Heffron, T. P. (2018). "Challenges of developing small-molecule kinase inhibitors for brain tumors and the need for emphasis on free drug levels." Neuro Oncol **20**(3): 307-312.
Hirschberg, H., F. A. Uzal, D. Chighvinadze, M. J. Zhang, Q. Peng and S. J. Madsen (2008). "Disruption of the blood-brain barrier following ALA-mediated photodynamic therapy." Lasers Surg Med **40**(8): 535-542.
Huang, L., X. Li, J. Roberts, B. Janosky and M. H. Lin (2015). "Differential role of P-glycoprotein and breast cancer resistance protein in drug distribution into brain, CSF and peripheral nerve tissues in rats." Xenobiotica **45**(6): 547-555.
Hyafil, F., C. Vergely, P. Du Vignaud and T. Grand-Perret (1993). "In vitro and in vivo reversal of multidrug resistance by GF120918, an acridonecarboxamide derivative." Cancer Res **53**(19): 4595-4602.
Hynynen, K., N. McDannold, N. Vykhodtseva, S. Raymond, R. Weissleder, F. A. Jolesz and N. Sheikov (2006). "Focal disruption of the blood-brain barrier due to 260-kHz

ultrasound bursts: a method for molecular imaging and targeted drug delivery." J Neurosurg **105**(3): 445-454.
Jacus, M. O., V. M. Daryani, K. E. Harstead, Y. T. Patel, S. L. Throm and C. F. Stewart (2016). "Pharmacokinetic Properties of Anticancer Agents for the Treatment of Central Nervous System Tumors: Update of the Literature." Clin Pharmacokinet **55**(3): 297-311.
Jain, R. K., E. di Tomaso, D. G. Duda, J. S. Loeffler, A. G. Sorensen and T. T. Batchelor (2007). "Angiogenesis in brain tumours." Nat Rev Neurosci **8**(8): 610-622.
Johnson, T. W., P. F. Richardson, S. Bailey, A. Brooun, B. J. Burke, M. R. Collins, J. J. Cui, J. G. Deal, Y. L. Deng, D. Dinh, L. D. Engstrom, M. He, J. Hoffman, R. L. Hoffman, Q. Huang, R. S. Kania, J. C. Kath, H. Lam, J. L. Lam, P. T. Le, L. Lingardo, W. Liu, M. McTigue, C. L. Palmer, N. W. Sach, T. Smeal, G. L. Smith, A. E. Stewart, S. Timofeevski, H. Zhu, J. Zhu, H. Y. Zou and M. P. Edwards (2014). "Discovery of (10R)-7-amino-12-fluoro-2,10,16-trimethyl-15-oxo-10,15,16,17-tetrahydro-2H-8,4-(m etheno)pyrazolo[4,3-h][2,5,11]-benzoxadiazacyclotetradecine-3-carbonitrile (PF-06463922), a macrocyclic inhibitor of anaplastic lymphoma kinase (ALK) and c-ros oncogene 1 (ROS1) with preclinical brain exposure and broad-spectrum potency against ALK-resistant mutations." J Med Chem **57**(11): 4720-4744.
Kalvass, J. C., J. W. Polli, D. L. Bourdet, B. Feng, S. M. Huang, X. Liu, Q. R. Smith, L. K. Zhang, M. J. Zamek-Gliszczynski and C. International Transporter (2013). "Why clinical modulation of efflux transport at the human blood-brain barrier is unlikely: the ITC evidence-based position." Clin Pharmacol Ther **94**(1): 80-94.
Keep, R. F. and D. E. Smith (2011). "Choroid plexus transport: gene deletion studies." Fluids Barriers CNS **8**(1): 26.
Kemper, E. M., W. Boogerd, I. Thuis, J. H. Beijnen and O. van Tellingen (2004). "Modulation of the blood-brain barrier in oncology: Therapeutic opportunities for the treatment of brain tumours?" Cancer Treatment Reviews **30**: 415-423.
Kenneth, D. (1969). "THE USE OF PROBENECID FOR INCREASING PENICILLIN CONCENTRATIONS IN CEREBROSPINAL FLUID." Acta Neurologica Scandinavica **45**(2): 253-256.
Khan, A. R., M. Liu, M. W. Khan and G. Zhai (2017). "Progress in brain targeting drug delivery system by nasal route." J Control Release **268**: 364-389.
Kim, D. G. and M. S. Bynoe (2016). "A2A adenosine receptor modulates drug efflux transporter P-glycoprotein at the blood-brain barrier." J Clin Invest **126**(5): 1717-1733.
Kim, H. G., T. T. Hien, E. H. Han, Y. P. Hwang, J. H. Choi, K. W. Kang, K. I. Kwon, B. H. Kim, S. K. Kim, G. Y. Song, T. C. Jeong and H. G. Jeong (2011). "Metformin inhibits P-glycoprotein expression via the NF-kappaB pathway and CRE transcriptional activity through AMPK activation." Br J Pharmacol **162**(5): 1096-1108.
Kodaira, H., H. Kusuhara, T. Fujita, J. Ushiki, E. Fuse and Y. Sugiyama (2011). "Quantitative evaluation of the impact of active efflux by p-glycoprotein and breast cancer resistance protein at the blood-brain barrier on the predictability of the unbound concentrations of drugs in the brain using cerebrospinal fluid concentration as a surrogate." J Pharmacol Exp Ther **339**(3): 935-944.
Kreuter, J. (2014). "Drug delivery to the central nervous system by polymeric nanoparticles: what do we know?" Adv Drug Deliv Rev **71**: 2-14.

Kroll, R. A., M. A. Pagel, L. L. Muldoon, S. Roman-Goldstein, S. A. Fiamengo and E. A. Neuwelt (1998). "Improving drug delivery to intracerebral tumor and surrounding brain in a rodent model: a comparison of osmotic versus bradykinin modification of the blood-brain and/or blood-tumor barriers." Neurosurgery **43**: 879.
Kromer, C., J. Xu, Q. T. Ostrom, H. Gittleman, C. Kruchko, R. Sawaya and J. S. Barnholtz-Sloan (2017). "Estimating the annual frequency of synchronous brain metastasis in the United States 2010-2013: a population-based study." J Neurooncol **134**(1): 55-64.
Kuppens, I. E., E. O. Witteveen, R. C. Jewell, S. A. Radema, E. M. Paul, S. G. Mangum, J. H. Beijnen, E. E. Voest and J. H. Schellens (2007). "A phase I, randomized, open-label, parallel-cohort, dose-finding study of elacridar (GF120918) and oral topotecan in cancer patients." Clin Cancer Res **13**(11): 3276-3285.
Laramy, J. K., M. Kim, S. K. Gupta, K. E. Parrish, S. Zhang, K. K. Bakken, B. L. Carlson, A. C. Mladek, D. J. Ma, J. N. Sarkaria and W. F. Elmquist (2017). "Heterogeneous Binding and Central Nervous System Distribution of the Multitargeted Kinase Inhibitor Ponatinib Restrict Orthotopic Efficacy in a Patient-Derived Xenograft Model of Glioblastoma." J Pharmacol Exp Ther **363**(2): 136-147.
Lin, F., M. C. de Gooijer, E. M. Roig, L. C. Buil, S. M. Christner, J. H. Beumer, T. Wurdinger, J. H. Beijnen and O. van Tellingen (2014). "ABCB1, ABCG2, and PTEN determine the response of glioblastoma to temozolomide and ABT-888 therapy." Clin Cancer Res **20**(10): 2703-2713.
Lin, J. H. (2008). "CSF as a surrogate for assessing CNS exposure: an industrial perspective." Curr Drug Metab **9**(1): 46-59.
Liu, L., X. Zhang, Y. Lou, Y. Rao and X. Zhang (2014). "Cerebral microdialysis in glioma studies, from theory to application." J Pharm Biomed Anal **96**: 77-89.
Liu, X., C. Chen and B. J. Smith (2008). "Progress in brain penetration evaluation in drug discovery and development." J Pharmacol Exp Ther **325**(2): 349-356.
Lockman, P. R., R. K. Mittapalli, K. S. Taskar, V. Rudraraju, B. Gril, K. A. Bohn, C. E. Adkins, A. Roberts, H. R. Thorsheim, J. A. Gaasch, S. Huang, D. Palmieri, P. S. Steeg and Q. R. Smith (2010). "Heterogeneous blood-tumor barrier permeability determines drug efficacy in experimental brain metastases of breast cancer." Clin Cancer Res **16**(23): 5664-5678.
Lonser, R. R., M. Sarntinoranont, P. F. Morrison and E. H. Oldfield (2015). "Convection-enhanced delivery to the central nervous system." J Neurosurg **122**(3): 697-706.
Loryan, I., V. Sinha, C. Mackie, A. Van Peer, W. Drinkenburg, A. Vermeulen, D. Morrison, M. Monshouwer, D. Heald and M. Hammarlund-Udenaes (2014). "Mechanistic understanding of brain drug disposition to optimize the selection of potential neurotherapeutics in drug discovery." Pharm Res **31**(8): 2203-2219.
Loscher, W. and H. Potschka (2005). "Drug resistance in brain diseases and the role of drug efflux transporters." Nat Rev Neurosci **6**(8): 591-602.
Luo, Y., L. Z. Ellis, K. Dallaglio, M. Takeda, W. A. Robinson, S. E. Robinson, W. Liu, K. D. Lewis, M. D. McCarter, R. Gonzalez, D. A. Norris, D. R. Roop, R. A. Spritz, N. G. Ahn and M. Fujita (2012). "Side population cells from human melanoma tumors reveal diverse mechanisms for chemoresistance." J Invest Dermatol **132**(10): 2440-2450.

Madsen, S. J., H. Hirschberg, J. J. Choi, S. Wang, Y. S. Tung, B. Morrison, E. E. Konofagou, A. Burgess, K. Shah, O. Hough and K. Hynynen (2010). "Site-specific opening of the blood-brain barrier." Journal of Biophotonics **3**: 356-367.
Matsumoto, T., E. Tani, K. Kaba, H. Shindo and K. Miyaji (1991). "Expression of P-glycoprotein in human glioma cell lines and surgical glioma specimens." J Neurosurg **74**(3): 460-466.
Mcmahon, D., R. Bendayan and K. Hynynen (2017). "Acute effects of focused ultrasound-induced increases in blood-brain barrier permeability on rat microvascular transcriptome." Nature Publishing Group: 1-15.
Miller, D. S. (2010). "Regulation of P-glycoprotein and other ABC drug transporters at the blood-brain barrier." Trends Pharmacol Sci **31**(6): 246-254.
Morrison, P. F., D. W. Laske, H. Bobo, E. H. Oldfield and R. L. Dedrick (1994). "High-flow microinfusion: tissue penetration and pharmacodynamics." Am J Physiol **266**(1 Pt 2): R292-305.
Munoz, J. L., V. Rodriguez-Cruz, S. J. Greco, V. Nagula, K. W. Scotto and P. Rameshwar (2014). "Temozolomide induces the production of epidermal growth factor to regulate MDR1 expression in glioblastoma cells." Mol Cancer Ther **13**(10): 2399-2411.
Nayak, L., E. Q. Lee and P. Y. Wen (2012). "Epidemiology of brain metastases." Curr Oncol Rep **14**(1): 48-54.
Neuwelt, E. A., E. P. Frenkel, J. Diehl, L. H. Vu, S. Rapoport and S. Hill (1980). "Reversible osmotic blood-brain barrier disruption in humans: implications for the chemotherapy of malignant brain tumors." Neurosurgery **7**(1): 44-52.
Oberoi, R. K., K. E. Parrish, T. T. Sio, R. K. Mittapalli, W. F. Elmquist and J. N. Sarkaria (2016). Strategies to improve delivery of anticancer drugs across the blood-brain barrier to treat glioblastoma. Neuro-Oncology. **18:** 27-36.
Osswald, M., J. Blaes, Y. Liao, G. Solecki, M. Gommel, A. S. Berghoff, L. Salphati, J. J. Wallin, H. S. Phillips, W. Wick and F. Winkler (2016). "Impact of Blood-Brain Barrier Integrity on Tumor Growth and Therapy Response in Brain Metastases." Clin Cancer Res **22**(24): 6078-6087.
Ostrom, Q. T., H. Gittleman, P. Liao, T. Vecchione-Koval, Y. Wolinsky, C. Kruchko and J. S. Barnholtz-Sloan (2017). "CBTRUS Statistical Report: Primary brain and other central nervous system tumors diagnosed in the United States in 2010-2014." Neuro Oncol **19**(suppl_5): v1-v88.
Pajic, M., J. K. Iyer, A. Kersbergen, E. van der Burg, A. O. Nygren, J. Jonkers, P. Borst and S. Rottenberg (2009). "Moderate increase in Mdr1a/1b expression causes in vivo resistance to doxorubicin in a mouse model for hereditary breast cancer." Cancer Res **69**(16): 6396-6404.
Pardridge, W. M. (2012). "Drug transport across the blood-brain barrier." J Cereb Blood Flow Metab **32**(11): 1959-1972.
Pardridge, W. M. (2016). "CSF, blood-brain barrier, and brain drug delivery." Expert Opin Drug Deliv **13**(7): 963-975.
Parrish, K. E., J. N. Sarkaria and W. F. Elmquist (2015). "Improving drug delivery to primary and metastatic brain tumors: strategies to overcome the blood-brain barrier." Clin Pharmacol Ther **97**(4): 336-346.

Pasko, P., T. Rodacki, R. Domagala-Rodacka, K. Palimonka, M. Marcinkowska and D. Owczarek (2017). "Second generation H1 - antihistamines interaction with food and alcohol-A systematic review." Biomed Pharmacother **93**: 27-39.
Patchell, R. A., P. A. Tibbs, J. W. Walsh, R. J. Dempsey, Y. Maruyama, R. J. Kryscio, W. R. Markesbery, J. S. Macdonald and B. Young (1990). "A randomized trial of surgery in the treatment of single metastases to the brain." N Engl J Med **322**(8): 494-500.
Patel, Y. (2016). "PDTB-12. CNS PENETRATION OF THE CDK4/6 INHIBITOR RIBOCICLIB (LEE011) IN NON-TUMOR BEARING MICE AND MICE BEARING ORTHOTOPIC PEDIATRIC BRAIN TUMORS." Neuro-Oncology **18**(suppl_6): vi152-vi152.
Pitz, M. W., A. Desai, S. A. Grossman and J. O. Blakeley (2011). "Tissue concentration of systemically administered antineoplastic agents in human brain tumors." J Neurooncol **104**(3): 629-638.
Poon, C., D. McMahon and K. Hynynen (2017). Noninvasive and targeted delivery of therapeutics to the brain using focused ultrasound. Neuropharmacology, Elsevier Ltd. **120:** 20-37.
Prados, M. D., S. C. Schold, Jr., H. A. Fine, K. Jaeckle, F. Hochberg, L. Mechtler, M. R. Fetell, S. Phuphanich, L. Feun, T. J. Janus, K. Ford and W. Graney (2003). "A randomized, double-blind, placebo-controlled, phase 2 study of RMP-7 in combination with carboplatin administered intravenously for the treatment of recurrent malignant glioma." Neuro Oncol **5**(2): 96-103.
Rambeck, B., U. H. Jurgens, T. W. May, H. W. Pannek, F. Behne, A. Ebner, A. Gorji, H. Straub, E. J. Speckmann, B. Pohlmann-Eden and W. Loscher (2006). "Comparison of brain extracellular fluid, brain tissue, cerebrospinal fluid, and serum concentrations of antiepileptic drugs measured intraoperatively in patients with intractable epilepsy." Epilepsia **47**(4): 681-694.
Rankovic, Z. (2015). "CNS drug design: balancing physicochemical properties for optimal brain exposure." J Med Chem **58**(6): 2584-2608.
Rao, V. V., J. L. Dahlheimer, M. E. Bardgett, A. Z. Snyder, R. A. Finch, A. C. Sartorelli and D. Piwnica-Worms (1999). "Choroid plexus epithelial expression of MDR1 P glycoprotein and multidrug resistance-associated protein contribute to the blood-cerebrospinal-fluid drug-permeability barrier." Proc Natl Acad Sci U S A **96**(7): 3900-3905.
Raub, T. J., G. N. Wishart, P. Kulanthaivel, B. A. Staton, R. T. Ajamie, G. A. Sawada, L. M. Gelbert, H. E. Shannon, C. Sanchez-Martinez and A. De Dios (2015). "Brain Exposure of Two Selective Dual CDK4 and CDK6 Inhibitors and the Antitumor Activity of CDK4 and CDK6 Inhibition in Combination with Temozolomide in an Intracranial Glioblastoma Xenograft." Drug Metab Dispos **43**(9): 1360-1371.
Regina, A., M. Demeule, A. Laplante, J. Jodoin, C. Dagenais, F. Berthelet, A. Moghrabi and R. Beliveau (2001). "Multidrug resistance in brain tumors: roles of the blood-brain barrier." Cancer Metastasis Rev **20**(1-2): 13-25.
Reichel, A. (2015). Pharmacokinetics of CNS penetration. Blood-Brain Barrier in Drug Discovery: Optimizing Brain Exposure of CNS. L. Di, Kerns, E. H., Wiley**:** 7-41.

Roe, M., A. Folkes, P. Ashworth, J. Brumwell, L. Chima, S. Hunjan, I. Pretswell, W. Dangerfield, H. Ryder and P. Charlton (1999). "Reversal of P-glycoprotein mediated multidrug resistance by novel anthranilamide derivatives." Bioorg Med Chem Lett **9**(4): 595-600.
Ronaldson, P. T., M. Bendayan, D. Gingras, M. Piquette-Miller and R. Bendayan (2004). "Cellular localization and functional expression of P-glycoprotein in rat astrocyte cultures." J Neurochem **89**(3): 788-800.
Rong, H., Feng, B., Di, L. (2012). Integrated Approaches to Blood–Brain Barrier. In Encyclopedia of Drug Metabolism and Interactions. A. V. Lyubimov, Wiley Online Library.
Rubin, E. H., D. P. de Alwis, I. Pouliquen, L. Green, P. Marder, Y. Lin, R. Musanti, S. L. Grospe, S. L. Smith, D. L. Toppmeyer, J. Much, M. Kane, A. Chaudhary, C. Jordan, M. Burgess and C. A. Slapak (2002). "A phase I trial of a potent P-glycoprotein inhibitor, Zosuquidar.3HCl trihydrochloride (LY335979), administered orally in combination with doxorubicin in patients with advanced malignancies." Clin Cancer Res **8**(12): 3710-3717.
Salphati, L., B. Alicke, T. P. Heffron, S. Shahidi-Latham, M. Nishimura, T. Cao, R. A. Carano, J. Cheong, J. Greve, H. Koeppen, S. Lau, L. B. Lee, M. Nannini-Pepe, J. Pang, E. G. Plise, C. Quiason, L. Rangell, X. Zhang, S. E. Gould, H. S. Phillips and A. G. Olivero (2016). "Brain Distribution and Efficacy of the Brain Penetrant PI3K Inhibitor GDC-0084 in Orthotopic Mouse Models of Human Glioblastoma." Drug Metab Dispos **44**(12): 1881-1889.
Salphati, L., T. P. Heffron, B. Alicke, M. Nishimura, K. Barck, R. A. Carano, J. Cheong, K. A. Edgar, J. Greve, S. Kharbanda, H. Koeppen, S. Lau, L. B. Lee, J. Pang, E. G. Plise, J. L. Pokorny, H. B. Reslan, J. N. Sarkaria, J. J. Wallin, X. Zhang, S. E. Gould, A. G. Olivero and H. S. Phillips (2012). "Targeting the PI3K pathway in the brain--efficacy of a PI3K inhibitor optimized to cross the blood-brain barrier." Clin Cancer Res **18**(22): 6239-6248.
Salphati, L., S. Shahidi-Latham, C. Quiason, K. Barck, M. Nishimura, B. Alicke, J. Pang, R. A. Carano, A. G. Olivero and H. S. Phillips (2014). "Distribution of the phosphatidylinositol 3-kinase inhibitors Pictilisib (GDC-0941) and GNE-317 in U87 and GS2 intracranial glioblastoma models-assessment by matrix-assisted laser desorption ionization imaging." Drug Metab Dispos **42**(7): 1110-1116.
Sandler, A., M. Gordon, D. P. De Alwis, I. Pouliquen, L. Green, P. Marder, A. Chaudhary, K. Fife, L. Battiato, C. Sweeney, C. Jordan, M. Burgess and C. A. Slapak (2004). "A Phase I trial of a potent P-glycoprotein inhibitor, zosuquidar trihydrochloride (LY335979), administered intravenously in combination with doxorubicin in patients with advanced malignancy." Clin Cancer Res **10**(10): 3265-3272.
Sanovich, E., R. T. Bartus, P. M. Friden, R. L. Dean, H. Q. Le and M. W. Brightman (1995). "Pathway across blood-brain barrier opened by the bradykinin agonist, RMP-7." Brain Res **705**(1-2): 125-135.
Sarkaria, J. N., L. S. Hu, I. F. Parney, D. H. Pafundi, D. H. Brinkmann, N. N. Laack, C. Giannini, T. C. Burns, S. H. Kizilbash, J. K. Laramy, K. R. Swanson, T. J. Kaufmann, P. D. Brown, N. Y. R. Agar, E. Galanis, J. C. Buckner and W. F. Elmquist (2018). "Is the

blood-brain barrier really disrupted in all glioblastomas? A critical assessment of existing clinical data." Neuro Oncol **20**(2): 184-191.
Semyachkina-Glushkovskaya, O., J. Kurths, E. Borisova, S. Sokolovski, V. Mantareva, I. Angelov, A. Shirokov, N. Navolokin, N. Shushunova, A. Khorovodov, M. Ulanova, M. Sagatova, I. Agranivich, O. Sindeeva, A. Gekalyuk, A. Bodrova and E. Rafailov (2017). "Photodynamic opening of blood-brain barrier." Biomed Opt Express **8**(11): 5040-5048.
Shen, D. D., A. A. Artru and K. K. Adkison (2004). "Principles and applicability of CSF sampling for the assessment of CNS drug delivery and pharmacodynamics." Adv Drug Deliv Rev **56**(12): 1825-1857.
Siegel, R. L., K. D. Miller and A. Jemal (2017). "Cancer Statistics, 2017." CA Cancer J Clin **67**(1): 7-30.
Slater, L. M., P. Sweet, M. Stupecky and S. Gupta (1986). "Cyclosporin A reverses vincristine and daunorubicin resistance in acute lymphatic leukemia in vitro." J Clin Invest **77**(4): 1405-1408.
Stieger, B. and B. Hagenbuch (2014). "Organic anion-transporting polypeptides." Curr Top Membr **73**: 205-232.
Stupp, R., W. P. Mason, M. J. van den Bent, M. Weller, B. Fisher, M. J. Taphoorn, K. Belanger, A. A. Brandes, C. Marosi, U. Bogdahn, J. Curschmann, R. C. Janzer, S. K. Ludwin, T. Gorlia, A. Allgeier, D. Lacombe, J. G. Cairncross, E. Eisenhauer, R. O. Mirimanoff, R. European Organisation for, T. Treatment of Cancer Brain, G. Radiotherapy and G. National Cancer Institute of Canada Clinical Trials (2005). "Radiotherapy plus concomitant and adjuvant temozolomide for glioblastoma." N Engl J Med **352**(10): 987-996.
Summerfield, S. G., Y. Zhang and H. Liu (2016). "Examining the Uptake of Central Nervous System Drugs and Candidates across the Blood-Brain Barrier." J Pharmacol Exp Ther **358**(2): 294-305.
Sun, H., H. Dai, N. Shaik and W. F. Elmquist (2003). "Drug efflux transporters in the CNS." Adv Drug Deliv Rev **55**(1): 83-105.
Sutherlin, D. P., D. Sampath, M. Berry, G. Castanedo, Z. Chang, I. Chuckowree, J. Dotson, A. Folkes, L. Friedman, R. Goldsmith, T. Heffron, L. Lee, J. Lesnick, C. Lewis, S. Mathieu, J. Nonomiya, A. Olivero, J. Pang, W. W. Prior, L. Salphati, S. Sideris, Q. Tian, V. Tsui, N. C. Wan, S. Wang, C. Wiesmann, S. Wong and B. Y. Zhu (2010). "Discovery of (thienopyrimidin-2-yl)aminopyrimidines as potent, selective, and orally available pan-PI3-kinase and dual pan-PI3-kinase/mTOR inhibitors for the treatment of cancer." J Med Chem **53**(3): 1086-1097.
Szakacs, G., J. K. Paterson, J. A. Ludwig, C. Booth-Genthe and M. M. Gottesman (2006). "Targeting multidrug resistance in cancer." Nat Rev Drug Discov **5**(3): 219-234.
Tamai, I. and A. Tsuji (2000). "Transporter-mediated permeation of drugs across the blood-brain barrier." J Pharm Sci **89**(11): 1371-1388.
Taylor, E. M. (2002). "The impact of efflux transporters in the brain on the development of drugs for CNS disorders." Clin Pharmacokinet **41**(2): 81-92.
Tollner, K., C. Brandt, K. Romermann and W. Loscher (2015). "The organic anion transport inhibitor probenecid increases brain concentrations of the NKCC1 inhibitor bumetanide." Eur J Pharmacol **746**: 167-173.

Tsuruo, T., H. Iida, S. Tsukagoshi and Y. Sakurai (1981). "Overcoming of vincristine resistance in P388 leukemia in vivo and in vitro through enhanced cytotoxicity of vincristine and vinblastine by verapamil." Cancer Res **41**(5): 1967-1972.
Twentyman, P. R. and N. M. Bleehen (1991). "Resistance modification by PSC-833, a novel non-immunosuppressive cyclosporin [corrected]." Eur J Cancer **27**(12): 1639-1642.
Uchida, Y., S. Ohtsuki, J. Kamiie and T. Terasaki (2011). "Blood-brain barrier (BBB) pharmacoproteomics: reconstruction of in vivo brain distribution of 11 P-glycoprotein substrates based on the BBB transporter protein concentration, in vitro intrinsic transport activity, and unbound fraction in plasma and brain in mice." J Pharmacol Exp Ther **339**(2): 579-588.
van Tellingen, O., B. Yetkin-Arik, M. C. de Gooijer, P. Wesseling, T. Wurdinger and H. E. de Vries (2015). "Overcoming the blood-brain tumor barrier for effective glioblastoma treatment." Drug Resist Updat **19**: 1-12.
Verweij, J., H. Herweijer, R. Oosterom, M. E. van der Burg, A. S. Planting, C. Seynaeve, G. Stoter and K. Nooter (1991). "A phase II study of epidoxorubicin in colorectal cancer and the use of cyclosporin-A in an attempt to reverse multidrug resistance." Br J Cancer **64**(2): 361-364.
Wager, T. T., X. Hou, P. R. Verhoest and A. Villalobos (2010). "Moving beyond rules: the development of a central nervous system multiparameter optimization (CNS MPO) approach to enable alignment of druglike properties." ACS Chem Neurosci **1**(6): 435-449.
Westerhout, J., M. Danhof and E. C. De Lange (2011). "Preclinical prediction of human brain target site concentrations: considerations in extrapolating to the clinical setting." J Pharm Sci **100**(9): 3577-3593.
Widmer, N., H. Rumpold, G. Untergasser, A. Fayet, T. Buclin and L. A. Decosterd (2007). "Resistance reversal by RNAi silencing of MDR1 in CML cells associated with increase in imatinib intracellular levels." Leukemia **21**(7): 1561-1562; author reply 1562-1564.
Xing, F., R. J. Yong, A. D. Kaye and R. D. Urman (2018). "Intrathecal Drug Delivery and Spinal Cord Stimulation for the Treatment of Cancer Pain." Curr Pain Headache Rep **22**(2): 11.
Zamek-Gliszczynski, M. J., J. C. Kalvass, G. M. Pollack and K. L. Brouwer (2009). "Relationship between drug/metabolite exposure and impairment of excretory transport function." Drug Metab Dispos **37**(2): 386-390.
Zeng, Q., J. Wang, Z. Cheng, K. Chen, P. Johnstrom, K. Varnas, D. Y. Li, Z. F. Yang and X. Zhang (2015). "Discovery and Evaluation of Clinical Candidate AZD3759, a Potent, Oral Active, Central Nervous System-Penetrant, Epidermal Growth Factor Receptor Tyrosine Kinase Inhibitor." J Med Chem **58**(20): 8200-8215.
Zheng, L. H., Y. L. Bao, Y. Wu, C. L. Yu, X. Meng and Y. X. Li (2008). "Cantharidin reverses multidrug resistance of human hepatoma HepG2/ADM cells via down-regulation of P-glycoprotein expression." Cancer Lett **272**(1): 102-109.
Zhou, S., J. D. Schuetz, K. D. Bunting, A. M. Colapietro, J. Sampath, J. J. Morris, I. Lagutina, G. C. Grosveld, M. Osawa, H. Nakauchi and B. P. Sorrentino (2001). "The

ABC transporter Bcrp1/ABCG2 is expressed in a wide variety of stem cells and is a molecular determinant of the side-population phenotype." Nat Med **7**(9): 1028-1034.
Zhu, H., H. Wu, X. Liu, B. R. Evans, D. J. Medina, C. G. Liu and J. M. Yang (2008). "Role of MicroRNA miR-27a and miR-451 in the regulation of MDR1/P-glycoprotein expression in human cancer cells." Biochem Pharmacol **76**(5): 582-588.
Zlokovic, B. V. and M. L. Apuzzo (1998). "Strategies to circumvent vascular barriers of the central nervous system." Neurosurgery **43**(4): 877-878.

CHAPTER III

Abbott NJ. Blood-brain barrier structure and function and the challenges for CNS drug delivery. J Inherit Metab Dis. 2013;36(3):437-49. doi:10.1007/s10545-013-9608-0.

Abbott NJ, Patabendige AA, Dolman DE, Yusof SR, Begley DJ. Structure and function of the blood-brain barrier. Neurobiol Dis. 2010;37(1):13-25. doi:10.1016/j.nbd.2009.07.030.

Adkins CE, Mohammad AS, Terrell-Hall TB, Dolan EL, Shah N, Sechrest E et al. Characterization of passive permeability at the blood-tumor barrier in five preclinical models of brain metastases of breast cancer. Clin Exp Metastasis. 2016;33(4):373-83. doi:10.1007/s10585-016-9784-z.

Agarwal S, Hartz AM, Elmquist WF, Bauer B. Breast cancer resistance protein and P-glycoprotein in brain cancer: two gatekeepers team up. Curr Pharm Des. 2011a;17(26):2793-802.

Agarwal S, Sane R, Oberoi R, Ohlfest JR, Elmquist WF. Delivery of molecularly targeted therapy to malignant glioma, a disease of the whole brain. Expert Rev Mol Med. 2011b;13:e17. doi:10.1017/S1462399411001888.

Aikawa H, Hayashi M, Ryu S, Yamashita M, Ohtsuka N, Nishidate M et al. Visualizing spatial distribution of alectinib in murine brain using quantitative mass spectrometry imaging. Sci Rep. 2016;6:23749. doi:10.1038/srep23749.

Barkan D, Chambers AF. beta1-integrin: a potential therapeutic target in the battle against cancer recurrence. Clin Cancer Res. 2011;17(23):7219-23. doi:10.1158/1078-0432.CCR-11-0642.

Bates SE. A sea change in melanoma. Clin Cancer Res. 2013;19(19):5282. doi:10.1158/1078-0432.CCR-13-2219.

Brastianos PK, Carter SL, Santagata S, Cahill DP, Taylor-Weiner A, Jones RT et al. Genomic Characterization of Brain Metastases Reveals Branched Evolution and Potential Therapeutic Targets. Cancer Discov. 2015;5(11):1164-77. doi:10.1158/2159-8290.CD-15-0369.

Bruzzone MG, D'Incerti L, Farina LL, Cuccarini V, Finocchiaro G. CT and MRI of brain tumors. Q J Nucl Med Mol Imaging. 2012;56(2):112-37.

Bucheit AD, Chen G, Siroy A, Tetzlaff M, Broaddus R, Milton D et al. Complete loss of PTEN protein expression correlates with shorter time to brain metastasis and survival in stage IIIB/C melanoma patients with BRAFV600 mutations. Clin Cancer Res. 2014;20(21):5527-36. doi:10.1158/1078-0432.CCR-14-1027.

Chartrain M, Riond J, Stennevin A, Vandenberghe I, Gomes B, Lamant L et al. Melanoma chemotherapy leads to the selection of ABCB5-expressing cells. PLoS One. 2012;7(5):e36762. doi:10.1371/journal.pone.0036762.

Chen G, Chakravarti N, Aardalen K, Lazar AJ, Tetzlaff MT, Wubbenhorst B et al. Molecular profiling of patient-matched brain and extracranial melanoma metastases implicates the PI3K pathway as a therapeutic target. Clin Cancer Res. 2014;20(21):5537-46. doi:10.1158/1078-0432.CCR-13-3003.

Choo EF, Ly J, Chan J, Shahidi-Latham SK, Messick K, Plise E et al. Role of P-glycoprotein on the brain penetration and brain pharmacodynamic activity of the MEK inhibitor cobimetinib. Mol Pharm. 2014;11(11):4199-207. doi:10.1021/mp500435s.
Cohen JV, Tawbi H, Margolin KA, Amravadi R, Bosenberg M, Brastianos PK et al. Melanoma central nervous system metastases: current approaches, challenges, and opportunities. Pigment Cell Melanoma Res. 2016;29(6):627-42. doi:10.1111/pcmr.12538.
Cruz-Munoz W, Man S, Xu P, Kerbel RS. Development of a preclinical model of spontaneous human melanoma central nervous system metastasis. Cancer Res. 2008;68(12):4500-5. doi:10.1158/0008-5472.CAN-08-0041.
Damsky WE, Theodosakis N, Bosenberg M. Melanoma metastasis: new concepts and evolving paradigms. Oncogene. 2014;33(19):2413-22. doi:10.1038/onc.2013.194.
Davies MA, Liu P, McIntyre S, Kim KB, Papadopoulos N, Hwu WJ et al. Prognostic factors for survival in melanoma patients with brain metastases. Cancer. 2011;117(8):1687-96. doi:10.1002/cncr.25634.
Davies MA, Saiag P, Robert C, Grob JJ, Flaherty KT, Arance A et al. Dabrafenib plus trametinib in patients with BRAFV600-mutant melanoma brain metastases (COMBI-MB): a multicentre, multicohort, open-label, phase 2 trial. Lancet Oncol. 2017. doi:10.1016/S1470-2045(17)30429-1.
de Gooijer MC, Zhang P, Thota N, Mayayo-Peralta I, Buil LC, Beijnen JH et al. P-glycoprotein and breast cancer resistance protein restrict the brain penetration of the CDK4/6 inhibitor palbociclib. Invest New Drugs. 2015;33(5):1012-9. doi:10.1007/s10637-015-0266-y.
Di Giacomo AM, Margolin K. Immune checkpoint blockade in patients with melanoma metastatic to the brain. Semin Oncol. 2015;42(3):459-65. doi:10.1053/j.seminoncol.2015.02.006.
Dolgikh E, Watson IA, Desai PV, Sawada GA, Morton S, Jones TM et al. QSAR Model of Unbound Brain-to-Plasma Partition Coefficient, Kp,uu,brain: Incorporating P-glycoprotein Efflux as a Variable. J Chem Inf Model. 2016;56(11):2225-33. doi:10.1021/acs.jcim.6b00229.
Dummer R, Goldinger SM, Turtschi CP, Eggmann NB, Michielin O, Mitchell L et al. Vemurafenib in patients with BRAF(V600) mutation-positive melanoma with symptomatic brain metastases: final results of an open-label pilot study. Eur J Cancer. 2014;50(3):611-21. doi:10.1016/j.ejca.2013.11.002.
Durmus S, Hendrikx JJ, Schinkel AH. Apical ABC transporters and cancer chemotherapeutic drug disposition. Adv Cancer Res. 2015;125:1-41. doi:10.1016/bs.acr.2014.10.001.
Durmus S, Sparidans RW, Wagenaar E, Beijnen JH, Schinkel AH. Oral availability and brain penetration of the B-RAFV600E inhibitor vemurafenib can be enhanced by the P-GLYCOprotein (ABCB1) and breast cancer resistance protein (ABCG2) inhibitor elacridar. Mol Pharm. 2012;9(11):3236-45. doi:10.1021/mp3003144.
Einarsdottir BO, Bagge RO, Bhadury J, Jespersen H, Mattsson J, Nilsson LM et al. Melanoma patient-derived xenografts accurately model the disease and develop fast enough to guide treatment decisions. Oncotarget. 2014;5(20):9609-18. doi:10.18632/oncotarget.2445.

Eisele SC, Gill CM, Shankar GM, Brastianos PK. PLEKHA5: A Key to Unlock the Blood-Brain Barrier? Clin Cancer Res. 2015;21(9):1978-80. doi:10.1158/1078-0432.CCR-14-2604.
Engelhardt B, Ransohoff RM. Capture, crawl, cross: the T cell code to breach the blood-brain barriers. Trends Immunol. 2012;33(12):579-89. doi:10.1016/j.it.2012.07.004.
Essig M, Weber MA, von Tengg-Kobligk H, Knopp MV, Yuh WT, Giesel FL. Contrast-enhanced magnetic resonance imaging of central nervous system tumors: agents, mechanisms, and applications. Top Magn Reson Imaging. 2006;17(2):89-106. doi:10.1097/01.rmr.0000245464.36148.dc.
Falchook GS, Long GV, Kurzrock R, Kim KB, Arkenau TH, Brown MP et al. Dabrafenib in patients with melanoma, untreated brain metastases, and other solid tumours: a phase 1 dose-escalation trial. Lancet. 2012;379(9829):1893-901. doi:10.1016/S0140-6736(12)60398-5.
Fidler IJ. The role of the organ microenvironment in brain metastasis. Semin Cancer Biol. 2011;21(2):107-12. doi:10.1016/j.semcancer.2010.12.009.
Fife KM, Colman MH, Stevens GN, Firth IC, Moon D, Shannon KF et al. Determinants of outcome in melanoma patients with cerebral metastases. J Clin Oncol. 2004;22(7):1293-300. doi:10.1200/JCO.2004.08.140.
Fortin D. The blood-brain barrier: its influence in the treatment of brain tumors metastases. Curr Cancer Drug Targets. 2012;12(3):247-59.
Francia G, Cruz-Munoz W, Man S, Xu P, Kerbel RS. Mouse models of advanced spontaneous metastasis for experimental therapeutics. Nat Rev Cancer. 2011;11(2):135-41. doi:10.1038/nrc3001.
Gampa G, Vaidhyanathan S, Wilken-Resman B, Parrish KE, Markovic SN, Sarkaria JN et al. Challenges in the Delivery of Therapies to Melanoma Brain Metastases. Current Pharmacology Reports. 2016;2:309-25.
Gerstner ER, Fine RL. Increased permeability of the blood-brain barrier to chemotherapy in metastatic brain tumors: establishing a treatment paradigm. J Clin Oncol. 2007;25(16):2306-12. doi:10.1200/JCO.2006.10.0677.
Gibney GT, Gauthier G, Ayas C, Galebach P, Wu EQ, Abhyankar S et al. Treatment patterns and outcomes in BRAF V600E-mutant melanoma patients with brain metastases receiving vemurafenib in the real-world setting. Cancer Med. 2015;4(8):1205-13. doi:10.1002/cam4.475.
Gorantla V, Kirkwood JM, Tawbi HA. Melanoma brain metastases: an unmet challenge in the era of active therapy. Curr Oncol Rep. 2013;15(5):483-91. doi:10.1007/s11912-013-0335-3.
Gupta G, Robertson AG, MacKie RM. Cerebral metastases of cutaneous melanoma. Br J Cancer. 1997;76(2):256-9.
Harding JJ, Catalanotti F, Munhoz RR, Cheng DT, Yaqubie A, Kelly N et al. A Retrospective Evaluation of Vemurafenib as Treatment for BRAF-Mutant Melanoma Brain Metastases. Oncologist. 2015;20(7):789-97. doi:10.1634/theoncologist.2014-0012.
Heffron TP. Small Molecule Kinase Inhibitors for the Treatment of Brain Cancer. J Med Chem. 2016;59(22):10030-66. doi:10.1021/acs.jmedchem.6b00618.

Hidalgo M, Amant F, Biankin AV, Budinska E, Byrne AT, Caldas C et al. Patient-derived xenograft models: an emerging platform for translational cancer research. Cancer Discov. 2014;4(9):998-1013. doi:10.1158/2159-8290.CD-14-0001.
Izraely S, Sagi-Assif O, Klein A, Meshel T, Ben-Menachem S, Zaritsky A et al. The metastatic microenvironment: Claudin-1 suppresses the malignant phenotype of melanoma brain metastasis. Int J Cancer. 2015;136(6):1296-307. doi:10.1002/ijc.29090.
Jilaveanu LB, Parisi F, Barr ML, Zito CR, Cruz-Munoz W, Kerbel RS et al. PLEKHA5 as a Biomarker and Potential Mediator of Melanoma Brain Metastasis. Clin Cancer Res. 2015;21(9):2138-47. doi:10.1158/1078-0432.CCR-14-0861.
Jung BC, Arevalo-Perez J, Lyo JK, Holodny AI, Karimi S, Young RJ et al. Comparison of Glioblastomas and Brain Metastases using Dynamic Contrast-Enhanced Perfusion MRI. J Neuroimaging. 2016;26(2):240-6. doi:10.1111/jon.12281.
Kalscheuer H, Danzl N, Onoe T, Faust T, Winchester R, Goland R et al. A model for personalized in vivo analysis of human immune responsiveness. Sci Transl Med. 2012;4(125):125ra30. doi:10.1126/scitranslmed.3003481.
Kerbel RS. A Decade of Experience in Developing Preclinical Models of Advanced- or Early-Stage Spontaneous Metastasis to Study Antiangiogenic Drugs, Metronomic Chemotherapy, and the Tumor Microenvironment. Cancer J. 2015;21(4):274-83. doi:10.1097/PPO.0000000000000134.
Krepler C, Xiao M, Sproesser K, Brafford PA, Shannan B, Beqiri M et al. Personalized Preclinical Trials in BRAF Inhibitor-Resistant Patient-Derived Xenograft Models Identify Second-Line Combination Therapies. Clin Cancer Res. 2016;22(7):1592-602. doi:10.1158/1078-0432.CCR-15-1762.
Larkin J, Ascierto PA, Dreno B, Atkinson V, Liszkay G, Maio M et al. Combined vemurafenib and cobimetinib in BRAF-mutated melanoma. N Engl J Med. 2014;371(20):1867-76. doi:10.1056/NEJMoa1408868.
Liu X, Ide JL, Norton I, Marchionni MA, Ebling MC, Wang LY et al. Molecular imaging of drug transit through the blood-brain barrier with MALDI mass spectrometry imaging. Sci Rep. 2013;3:2859. doi:10.1038/srep02859.
Lockman PR, Mittapalli RK, Taskar KS, Rudraraju V, Gril B, Bohn KA et al. Heterogeneous blood-tumor barrier permeability determines drug efficacy in experimental brain metastases of breast cancer. Clin Cancer Res. 2010;16(23):5664-78. doi:10.1158/1078-0432.CCR-10-1564.
Long GV, Trefzer U, Davies MA, Kefford RF, Ascierto PA, Chapman PB et al. Dabrafenib in patients with Val600Glu or Val600Lys BRAF-mutant melanoma metastatic to the brain (BREAK-MB): a multicentre, open-label, phase 2 trial. Lancet Oncol. 2012;13(11):1087-95. doi:10.1016/S1470-2045(12)70431-X.
Luo Y, Ellis LZ, Dallaglio K, Takeda M, Robinson WA, Robinson SE et al. Side population cells from human melanoma tumors reveal diverse mechanisms for chemoresistance. J Invest Dermatol. 2012;132(10):2440-50. doi:10.1038/jid.2012.161.
Margolin K. The Promise of Molecularly Targeted and Immunotherapy for Advanced Melanoma. Curr Treat Options Oncol. 2016;17(9):48. doi:10.1007/s11864-016-0421-5.

Margolin K, Ernstoff MS, Hamid O, Lawrence D, McDermott D, Puzanov I et al. Ipilimumab in patients with melanoma and brain metastases: an open-label, phase 2 trial. Lancet Oncol. 2012;13(5):459-65. doi:10.1016/S1470-2045(12)70090-6.
McArthur GA, Maio M, Arance A, Nathan P, Blank C, Avril MF et al. Vemurafenib in Metastatic Melanoma Patients with Brain Metastases: An Open-Label, Single-Arm, Phase 2, Multicentre Study. Ann Oncol. 2016. doi:10.1093/annonc/mdw641.
McWilliams RR, Brown PD, Buckner JC, Link MJ, Markovic SN. Treatment of brain metastases from melanoma. Mayo Clin Proc. 2003;78(12):1529-36. doi:10.4065/78.12.1529.
Mittapalli RK, Adkins CE, Bohn KA, Mohammad AS, Lockman JA, Lockman PR. Quantitative Fluorescence Microscopy Measures Vascular Pore Size in Primary and Metastatic Brain Tumors. Cancer Res. 2017;77(2):238-46. doi:10.1158/0008-5472.CAN-16-1711.
Mittapalli RK, Vaidhyanathan S, Dudek AZ, Elmquist WF. Mechanisms limiting distribution of the threonine-protein kinase B-RaF(V600E) inhibitor dabrafenib to the brain: implications for the treatment of melanoma brain metastases. J Pharmacol Exp Ther. 2013;344(3):655-64. doi:10.1124/jpet.112.201475.
Mittapalli RK, Vaidhyanathan S, Sane R, Elmquist WF. Impact of P-glycoprotein (ABCB1) and breast cancer resistance protein (ABCG2) on the brain distribution of a novel BRAF inhibitor: vemurafenib (PLX4032). J Pharmacol Exp Ther. 2012;342(1):33-40. doi:10.1124/jpet.112.192195.
Murrell DH, Hamilton AM, Mallett CL, van Gorkum R, Chambers AF, Foster PJ. Understanding Heterogeneity and Permeability of Brain Metastases in Murine Models of HER2-Positive Breast Cancer Through Magnetic Resonance Imaging: Implications for Detection and Therapy. Transl Oncol. 2015;8(3):176-84. doi:10.1016/j.tranon.2015.03.009.
Murrell DH, Zarghami N, Jensen MD, Chambers AF, Wong E, Foster PJ. Evaluating Changes to Blood-Brain Barrier Integrity in Brain Metastasis over Time and after Radiation Treatment. Transl Oncol. 2016;9(3):219-27. doi:10.1016/j.tranon.2016.04.006.
Niessner H, Schmitz J, Tabatabai G, Schmid AM, Calaminus C, Sinnberg T et al. PI3K Pathway Inhibition Achieves Potent Antitumor Activity in Melanoma Brain Metastases In Vitro and In Vivo. Clin Cancer Res. 2016;22(23):5818-28. doi:10.1158/1078-0432.CCR-16-0064.
Osswald M, Blaes J, Liao Y, Solecki G, Gommel M, Berghoff AS et al. Impact of Blood-Brain Barrier Integrity on Tumor Growth and Therapy Response in Brain Metastases. Clin Cancer Res. 2016;22(24):6078-87. doi:10.1158/1078-0432.CCR-16-1327.
Park ES, Kim SJ, Kim SW, Yoon SL, Leem SH, Kim SB et al. Cross-species hybridization of microarrays for studying tumor transcriptome of brain metastasis. Proc Natl Acad Sci U S A. 2011;108(42):17456-61. doi:10.1073/pnas.1114210108.
Parrish KE, Pokorny J, Mittapalli RK, Bakken K, Sarkaria JN, Elmquist WF. Efflux transporters at the blood-brain barrier limit delivery and efficacy of cyclin-dependent kinase 4/6 inhibitor palbociclib (PD-0332991) in an orthotopic brain tumor model. J Pharmacol Exp Ther. 2015a;355(2):264-71. doi:10.1124/jpet.115.228213.

Parrish KE, Sarkaria JN, Elmquist WF. Improving drug delivery to primary and metastatic brain tumors: strategies to overcome the blood-brain barrier. Clin Pharmacol Ther. 2015b;97(4):336-46. doi:10.1002/cpt.71.
Peng W, Chen JQ, Liu C, Malu S, Creasy C, Tetzlaff MT et al. Loss of PTEN Promotes Resistance to T Cell-Mediated Immunotherapy. Cancer Discov. 2016;6(2):202-16. doi:10.1158/2159-8290.CD-15-0283.
Pitz MW, Desai A, Grossman SA, Blakeley JO. Tissue concentration of systemically administered antineoplastic agents in human brain tumors. J Neurooncol. 2011;104(3):629-38. doi:10.1007/s11060-011-0564-y.
Quintana E, Piskounova E, Shackleton M, Weinberg D, Eskiocak U, Fullen DR et al. Human melanoma metastasis in NSG mice correlates with clinical outcome in patients. Sci Transl Med. 2012;4(159):159ra49. doi:10.1126/scitranslmed.3004599.
Quintana E, Shackleton M, Sabel MS, Fullen DR, Johnson TM, Morrison SJ. Efficient tumour formation by single human melanoma cells. Nature. 2008;456(7222):593-8. doi:10.1038/nature07567.
Raizer JJ, Hwu WJ, Panageas KS, Wilton A, Baldwin DE, Bailey E et al. Brain and leptomeningeal metastases from cutaneous melanoma: survival outcomes based on clinical features. Neuro Oncol. 2008;10(2):199-207. doi:10.1215/15228517-2007-058.
Rizzo A, Vasco C, Girgenti V, Fugnanesi V, Calatozzolo C, Canazza A et al. Melanoma cells homing to the brain: an in vitro model. Biomed Res Int. 2015;2015:476069. doi:10.1155/2015/476069.
Rochet NM, Dronca RS, Kottschade LA, Chavan RN, Gorman B, Gilbertson JR et al. Melanoma brain metastases and vemurafenib: need for further investigation. Mayo Clin Proc. 2012;87(10):976-81. doi:10.1016/j.mayocp.2012.07.006.
Ruggeri BA, Camp F, Miknyoczki S. Animal models of disease: pre-clinical animal models of cancer and their applications and utility in drug discovery. Biochem Pharmacol. 2014;87(1):150-61. doi:10.1016/j.bcp.2013.06.020.
Sakji-Dupre L, Le Rhun E, Templier C, Desmedt E, Blanchet B, Mortier L. Cerebrospinal fluid concentrations of vemurafenib in patients treated for brain metastatic BRAF-V600 mutated melanoma. Melanoma Res. 2015;25(4):302-5. doi:10.1097/CMR.0000000000000162.
Salphati L, Alicke B, Heffron TP, Shahidi-Latham S, Nishimura M, Cao T et al. Brain Distribution and Efficacy of the Brain Penetrant PI3K Inhibitor GDC-0084 in Orthotopic Mouse Models of Human Glioblastoma. Drug Metab Dispos. 2016;44(12):1881-9. doi:10.1124/dmd.116.071423.
Salphati L, Heffron TP, Alicke B, Nishimura M, Barck K, Carano RA et al. Targeting the PI3K pathway in the brain--efficacy of a PI3K inhibitor optimized to cross the blood-brain barrier. Clin Cancer Res. 2012;18(22):6239-48. doi:10.1158/1078-0432.CCR-12-0720.
Salphati L, Shahidi-Latham S, Quiason C, Barck K, Nishimura M, Alicke B et al. Distribution of the phosphatidylinositol 3-kinase inhibitors Pictilisib (GDC-0941) and GNE-317 in U87 and GS2 intracranial glioblastoma models-assessment by matrix-assisted laser desorption ionization imaging. Drug Metab Dispos. 2014;42(7):1110-6. doi:10.1124/dmd.114.057513.

Samala R, Thorsheim HR, Goda S, Taskar K, Gril B, Steeg PS et al. Vinorelbine Delivery and Efficacy in the MDA-MB-231BR Preclinical Model of Brain Metastases of Breast Cancer. Pharm Res. 2016;33(12):2904-19. doi:10.1007/s11095-016-2012-3.
Saunus JM, Quinn MC, Patch AM, Pearson JV, Bailey PJ, Nones K et al. Integrated genomic and transcriptomic analysis of human brain metastases identifies alterations of potential clinical significance. J Pathol. 2015;237(3):363-78. doi:10.1002/path.4583.
Siegel RL, Miller KD, Jemal A. Cancer Statistics, 2017. CA Cancer J Clin. 2017;67(1):7-30. doi:10.3322/caac.21387.
Sloan AE, Nock CJ, Einstein DB. Diagnosis and treatment of melanoma brain metastasis: a literature review. Cancer Control. 2009;16(3):248-55.
Spagnolo F, Picasso V, Lambertini M, Ottaviano V, Dozin B, Queirolo P. Survival of patients with metastatic melanoma and brain metastases in the era of MAP-kinase inhibitors and immunologic checkpoint blockade antibodies: A systematic review. Cancer Treat Rev. 2016;45:38-45. doi:10.1016/j.ctrv.2016.03.003.
Steeg PS, Zimmer A, Gril B. Therapeutics for Brain Metastases, v3. Clin Cancer Res. 2016;22(24):5953-5. doi:10.1158/1078-0432.CCR-16-2035.
Stewart DJ. A critique of the role of the blood-brain barrier in the chemotherapy of human brain tumors. J Neurooncol. 1994;20(2):121-39.
Tan CS, Cho BC, Soo RA. Next-generation epidermal growth factor receptor tyrosine kinase inhibitors in epidermal growth factor receptor -mutant non-small cell lung cancer. Lung Cancer. 2016;93:59-68. doi:10.1016/j.lungcan.2016.01.003.
Taylor EM. The impact of efflux transporters in the brain on the development of drugs for CNS disorders. Clin Pharmacokinet. 2002;41(2):81-92. doi:10.2165/00003088-200241020-00001.
Tentler JJ, Tan AC, Weekes CD, Jimeno A, Leong S, Pitts TM et al. Patient-derived tumour xenografts as models for oncology drug development. Nat Rev Clin Oncol. 2012;9(6):338-50. doi:10.1038/nrclinonc.2012.61.
Toyokawa G, Inamasu E, Shimamatsu S, Yoshida T, Nosaki K, Hirai F et al. Identification of a Novel ALK G1123S Mutation in a Patient with ALK-rearranged Non-small-cell Lung Cancer Exhibiting Resistance to Ceritinib. J Thorac Oncol. 2015;10(7):e55-7. doi:10.1097/JTO.0000000000000509.
Vaidhyanathan S, Mittapalli RK, Sarkaria JN, Elmquist WF. Factors influencing the CNS distribution of a novel MEK-1/2 inhibitor: implications for combination therapy for melanoma brain metastases. Drug Metab Dispos. 2014;42(8):1292-300. doi:10.1124/dmd.114.058339.
Vaidhyanathan S, Wilken-Resman B, Ma DJ, Parrish KE, Mittapalli RK, Carlson BL et al. Factors Influencing the Central Nervous System Distribution of a Novel Phosphoinositide 3-Kinase/Mammalian Target of Rapamycin Inhibitor GSK2126458: Implications for Overcoming Resistance with Combination Therapy for Melanoma Brain Metastases. J Pharmacol Exp Ther. 2016;356(2):251-9. doi:10.1124/jpet.115.229393.
Welsh SJ, Rizos H, Scolyer RA, Long GV. Resistance to combination BRAF and MEK inhibition in metastatic melanoma: Where to next? Eur J Cancer. 2016;62:76-85. doi:10.1016/j.ejca.2016.04.005.

Wu CP, S VA. The pharmacological impact of ATP-binding cassette drug transporters on vemurafenib-based therapy. Acta Pharm Sin B. 2014;4(2):105-11. doi:10.1016/j.apsb.2013.12.001.
Yang Z, Guo Q, Wang Y, Chen K, Zhang L, Cheng Z et al. AZD3759, a BBB-penetrating EGFR inhibitor for the treatment of EGFR mutant NSCLC with CNS metastases. Sci Transl Med. 2016;8(368):368ra172. doi:10.1126/scitranslmed.aag0976.
Zeng Q, Wang J, Cheng Z, Chen K, Johnstrom P, Varnas K et al. Discovery and Evaluation of Clinical Candidate AZD3759, a Potent, Oral Active, Central Nervous System-Penetrant, Epidermal Growth Factor Receptor Tyrosine Kinase Inhibitor. J Med Chem. 2015;58(20):8200-15. doi:10.1021/acs.jmedchem.5b01073.

CHAPTER IV

Agarwal, S., R. K. Mittapalli, D. M. Zellmer, J. L. Gallardo, R. Donelson, C. Seiler, S. A. Decker, K. S. Santacruz, J. L. Pokorny, J. N. Sarkaria, W. F. Elmquist, and J. R. Ohlfest (2012) Active efflux of Dasatinib from the brain limits efficacy against murine glioblastoma: broad implications for the clinical use of molecularly targeted agents. *Mol Cancer Ther* 11 (10):2183-92. doi: 10.1158/1535-7163.MCT-12-0552.

Agarwal, S., R. Sane, R. Oberoi, J. R. Ohlfest, and W. F. Elmquist (2011) Delivery of molecularly targeted therapy to malignant glioma, a disease of the whole brain. *Expert Rev Mol Med* 13:e17. doi: 10.1017/S1462399411001888.

Assanah, M. C., J. N. Bruce, S. O. Suzuki, A. Chen, J. E. Goldman, and P. Canoll (2009) PDGF stimulates the massive expansion of glial progenitors in the neonatal forebrain. *Glia* 57 (16):1835-47. doi: 10.1002/glia.20895.

Blagden, S. P., L. R. Molife, A. Seebaran, M. Payne, A. H. Reid, A. S. Protheroe, L. S. Vasist, D. D. Williams, C. Bowen, S. J. Kathman, J. P. Hodge, M. M. Dar, J. S. de Bono, and M. R. Middleton (2008) A phase I trial of ispinesib, a kinesin spindle protein inhibitor, with docetaxel in patients with advanced solid tumours. *Br J Cancer* 98 (5):894-9. doi: 10.1038/sj.bjc.6604264.

Burris, H. A., 3rd, S. F. Jones, D. D. Williams, S. J. Kathman, J. P. Hodge, L. Pandite, P. T. Ho, S. A. Boerner, and P. Lorusso (2011) A phase I study of ispinesib, a kinesin spindle protein inhibitor, administered weekly for three consecutive weeks of a 28-day cycle in patients with solid tumors. *Invest New Drugs* 29 (3):467-72. doi: 10.1007/s10637-009-9374-x.

Canta, A., A. Chiorazzi, and G. Cavaletti (2009) Tubulin: a target for antineoplastic drugs into the cancer cells but also in the peripheral nervous system. *Curr Med Chem* 16 (11):1315-24.

Chiesa-Vottero, A. G., L. A. Rybicki, and R. A. Prayson (2003) Comparison of proliferation indices in glioblastoma multiforme by whole tissue section vs tissue microarray. *Am J Clin Pathol* 120 (6):902-8. doi: 10.1309/8UAU-KFK3-NBDM-VTNU.

Cross, R. A., and A. McAinsh (2014) Prime movers: the mechanochemistry of mitotic kinesins. *Nat Rev Mol Cell Biol* 15 (4):257-71. doi: 10.1038/nrm3768.

Cuddapah, V. A., S. Robel, S. Watkins, and H. Sontheimer (2014) A neurocentric perspective on glioma invasion. *Nat Rev Neurosci* 15 (7):455-65. doi: 10.1038/nrn3765.

Dai, H., P. Marbach, M. Lemaire, M. Hayes, and W. F. Elmquist (2003) Distribution of STI-571 to the brain is limited by P-glycoprotein-mediated efflux. *J Pharmacol Exp Ther* 304 (3):1085-92. doi: 10.1124/jpet.102.045260.

Demuth, T., and M. E. Berens (2004) Molecular mechanisms of glioma cell migration and invasion. *J Neurooncol* 70 (2):217-28. doi: 10.1007/s11060-004-2751-6.

Falnikar, A., S. Tole, and P. W. Baas (2011) Kinesin-5, a mitotic microtubule-associated motor protein, modulates neuronal migration. *Mol Biol Cell* 22 (9):1561-74. doi: 10.1091/mbc.E10-11-0905.

Friden, M., A. Gupta, M. Antonsson, U. Bredberg, and M. Hammarlund-Udenaes (2007) In vitro methods for estimating unbound drug concentrations in the brain interstitial and intracellular fluids. *Drug Metab Dispos* 35 (9):1711-9. doi: 10.1124/dmd.107.015222.

Gampa, G., S. Vaidhyanathan, B. W. Resman, K. E. Parrish, S. N. Markovic, J. N. Sarkaria, and W. F. Elmquist (2016) Challenges in the delivery of therapies to melanoma brain metastases. *Curr Pharmacol Rep* 2 (6):309-325. doi: 10.1007/s40495-016-0072-z.

Gampa, G., S. Vaidhyanathan, J. N. Sarkaria, and W. F. Elmquist (2017) Drug delivery to melanoma brain metastases: Can current challenges lead to new opportunities? *Pharmacol Res* 123:10-25. doi: 10.1016/j.phrs.2017.06.008.

Gomez, H. L., M. Philco, P. Pimentel, M. Kiyan, M. L. Monsalvo, M. G. Conlan, K. G. Saikali, M. M. Chen, J. J. Seroogy, A. A. Wolff, and R. D. Escandon (2012) Phase I dose-escalation and pharmacokinetic study of ispinesib, a kinesin spindle protein inhibitor, administered on days 1 and 15 of a 28-day schedule in patients with no prior treatment for advanced breast cancer. *Anticancer Drugs* 23 (3):335-41. doi: 10.1097/CAD.0b013e32834e74d6.

Hegde PS, Cogswell J, Carrick K, Jackson J, Wood KW, Eng WK, Brawner M, Huang PS, Bergsma D (2003) Differential gene expression analysis of kinesin spindle protein in human solid tumors. *Proc Am Soc Clin Oncol* 22 (535).

Jain, R. K., E. di Tomaso, D. G. Duda, J. S. Loeffler, A. G. Sorensen, and T. T. Batchelor (2007) Angiogenesis in brain tumours. *Nat Rev Neurosci* 8 (8):610-22. doi: 10.1038/nrn2175.

Kalvass, J. C., and T. S. Maurer (2002) Influence of nonspecific brain and plasma binding on CNS exposure: implications for rational drug discovery. *Biopharm Drug Dispos* 23 (8):327-38. doi: 10.1002/bdd.325.

Kim, M., D. J. Ma, D. Calligaris, S. Zhang, R. W. Feathers, R. A. Vaubel, I. Meaux, A. C. Mladek, K. E. Parrish, F. Jin, C. Barriere, L. Debussche, J. Watters, S. Tian, P. A. Decker, J. E. Eckel-Passow, G. J. Kitange, A. J. Johnson, I. F. Parney, P. Z. Anastasiadis, N. Y. R. Agar, W. F. Elmquist, and J. N. Sarkaria (2018) Efficacy of the MDM2 Inhibitor SAR405838 in Glioblastoma Is Limited by Poor Distribution Across the Blood-Brain Barrier. *Mol Cancer Ther* 17 (9):1893-1901. doi: 10.1158/1535-7163.MCT-17-0600.

Lad, L., L. Luo, J. D. Carson, K. W. Wood, J. J. Hartman, R. A. Copeland, and R. Sakowicz (2008) Mechanism of inhibition of human KSP by ispinesib. *Biochemistry* 47 (11):3576-85. doi: 10.1021/bi702061g.

Mastronardi, L., A. Guiducci, F. Puzzilli, and A. Ruggeri (1999) Relationship between Ki-67 labeling index and survival in high-grade glioma patients treated after surgery with tamoxifen. *J Neurosurg Sci* 43 (4):263-70.

Matsukado, Y., C. S. Maccarty, and J. W. Kernohan (1961) The growth of glioblastoma multiforme (astrocytomas, grades 3 and 4) in neurosurgical practice. *J Neurosurg* 18:636-44. doi: 10.3171/jns.1961.18.5.0636.

Nedelman, J. R., and X. Jia (1998) An extension of Satterthwaite's approximation applied to pharmacokinetics. *J Biopharm Stat* 8 (2):317-28. doi: 10.1080/10543409808835241.

Osswald, M., J. Blaes, Y. Liao, G. Solecki, M. Gommel, A. S. Berghoff, L. Salphati, J. J. Wallin, H. S. Phillips, W. Wick, and F. Winkler (2016) Impact of Blood-Brain Barrier Integrity on Tumor Growth and Therapy Response in Brain Metastases. *Clin Cancer Res* 22 (24):6078-6087. doi: 10.1158/1078-0432.CCR-16-1327.

Ostrom, Q. T., H. Gittleman, P. Liao, T. Vecchione-Koval, Y. Wolinsky, C. Kruchko, and J. S. Barnholtz-Sloan (2017) CBTRUS Statistical Report: Primary brain and other central nervous system tumors diagnosed in the United States in 2010-2014. *Neuro Oncol* 19 (suppl_5):v1-v88. doi: 10.1093/neuonc/nox158.

Parrish, K. E., J. Pokorny, R. K. Mittapalli, K. Bakken, J. N. Sarkaria, and W. F. Elmquist (2015) Efflux transporters at the blood-brain barrier limit delivery and efficacy of cyclin-dependent kinase 4/6 inhibitor palbociclib (PD-0332991) in an orthotopic brain tumor model. *J Pharmacol Exp Ther* 355 (2):264-71. doi: 10.1124/jpet.115.228213.

Rath, O., and F. Kozielski (2012) Kinesins and cancer. *Nat Rev Cancer* 12 (8):527-39. doi: 10.1038/nrc3310.

Sarkaria, J. N., L. S. Hu, I. F. Parney, D. H. Pafundi, D. H. Brinkmann, N. N. Laack, C. Giannini, T. C. Burns, S. H. Kizilbash, J. K. Laramy, K. R. Swanson, T. J. Kaufmann, P. D. Brown, N. Y. R. Agar, E. Galanis, J. C. Buckner, and W. F. Elmquist (2018) Is the blood-brain barrier really disrupted in all glioblastomas? A critical assessment of existing clinical data. *Neuro Oncol* 20 (2):184-191. doi: 10.1093/neuonc/nox175.

Sarli, V., and A. Giannis (2008) Targeting the kinesin spindle protein: basic principles and clinical implications. *Clin Cancer Res* 14 (23):7583-7. doi: 10.1158/1078-0432.CCR-08-0120.

Souid, A. K., R. L. Dubowy, A. M. Ingle, M. G. Conlan, J. Sun, S. M. Blaney, and P. C. Adamson (2010) A pediatric phase I trial and pharmacokinetic study of ispinesib: a Children's Oncology Group phase I consortium study. *Pediatr Blood Cancer* 55 (7):1323-8. doi: 10.1002/pbc.22609.

Stoyanov, G. S., D. L. Dzhenkov, M. Kitanova, I. S. Donev, and P. Ghenev (2017) Correlation Between Ki-67 Index, World Health Organization Grade and Patient Survival in Glial Tumors With Astrocytic Differentiation. *Cureus* 9 (6):e1396. doi: 10.7759/cureus.1396.

Venere, M., C. Horbinski, J. F. Crish, X. Jin, A. Vasanji, J. Major, A. C. Burrows, C. Chang, J. Prokop, Q. Wu, P. A. Sims, P. Canoll, M. K. Summers, S. S. Rosenfeld, and J. N. Rich (2015) The mitotic kinesin KIF11 is a driver of invasion, proliferation, and self-renewal in glioblastoma. *Sci Transl Med* 7 (304):304ra143. doi: 10.1126/scitranslmed.aac6762.

Wang, F., and S. L. Lin (2014) Knockdown of kinesin KIF11 abrogates directed migration in response to epidermal growth factor-mediated chemotaxis. *Biochem Biophys Res Commun* 452 (3):642-8. doi: 10.1016/j.bbrc.2014.08.136.

Wojcik, E. J., R. S. Buckley, J. Richard, L. Liu, T. M. Huckaba, and S. Kim (2013) Kinesin-5: cross-bridging mechanism to targeted clinical therapy. *Gene* 531 (2):133-49. doi: 10.1016/j.gene.2013.08.004.

Wood, K. W., W. D. Cornwell, and J. R. Jackson (2001) Past and future of the mitotic spindle as an oncology target. *Curr Opin Pharmacol* 1 (4):370-7.

CHAPTER V

Agarwal, S., P. Manchanda, M. A. Vogelbaum, J. R. Ohlfest, and W. F. Elmquist (2013) Function of the blood-brain barrier and restriction of drug delivery to invasive glioma cells: findings in an orthotopic rat xenograft model of glioma. *Drug Metab Dispos* 41 (1):33-9. doi: 10.1124/dmd.112.048322.

Ahmed, K. A., D. G. Stallworth, Y. Kim, P. A. Johnstone, L. B. Harrison, J. J. Caudell, H. H. Yu, A. B. Etame, J. S. Weber, and G. T. Gibney (2016) Clinical outcomes of melanoma brain metastases treated with stereotactic radiation and anti-PD-1 therapy. *Ann Oncol* 27 (3):434-41. doi: 10.1093/annonc/mdv622.

Ascierto, P. A., D. Schadendorf, C. Berking, S. S. Agarwala, C. M. van Herpen, P. Queirolo, C. U. Blank, A. Hauschild, J. T. Beck, A. St-Pierre, F. Niazi, S. Wandel, M. Peters, A. Zubel, and R. Dummer (2013) MEK162 for patients with advanced melanoma harbouring NRAS or Val600 BRAF mutations: a non-randomised, open-label phase 2 study. *Lancet Oncol* 14 (3):249-56. doi: 10.1016/S1470-2045(13)70024-X.

Atefi, M., B. Titz, E. Avramis, C. Ng, D. J. Wong, A. Lassen, M. Cerniglia, H. Escuin-Ordinas, D. Foulad, B. Comin-Anduix, T. G. Graeber, and A. Ribas (2015) Combination of pan-RAF and MEK inhibitors in NRAS mutant melanoma. *Mol Cancer* 14:27. doi: 10.1186/s12943-015-0293-5.

Barnholtz-Sloan, J. S., A. E. Sloan, F. G. Davis, F. D. Vigneau, P. Lai, and R. E. Sawaya (2004) Incidence proportions of brain metastases in patients diagnosed (1973 to 2001) in the Metropolitan Detroit Cancer Surveillance System. *J Clin Oncol* 22 (14):2865-72. doi: 10.1200/JCO.2004.12.149.

Carlson, B. L., J. L. Pokorny, M. A. Schroeder, and J. N. Sarkaria (2011) Establishment, maintenance and in vitro and in vivo applications of primary human glioblastoma multiforme (GBM) xenograft models for translational biology studies and drug discovery. *Curr Protoc Pharmacol* Chapter 14:Unit 14 16. doi: 10.1002/0471141755.ph1416s52.

Chapman, P. B., A. Hauschild, C. Robert, J. B. Haanen, P. Ascierto, J. Larkin, R. Dummer, C. Garbe, A. Testori, M. Maio, D. Hogg, P. Lorigan, C. Lebbe, T. Jouary, D. Schadendorf, A. Ribas, S. J. O'Day, J. A. Sosman, J. M. Kirkwood, A. M. Eggermont, B. Dreno, K. Nolop, J. Li, B. Nelson, J. Hou, R. J. Lee, K. T. Flaherty, G. A. McArthur, and Brim- Study Group (2011) Improved survival with vemurafenib in melanoma with BRAF V600E mutation. *N Engl J Med* 364 (26):2507-16. doi: 10.1056/NEJMoa1103782.

Chen, S. H., Y. Zhang, R. D. Van Horn, T. Yin, S. Buchanan, V. Yadav, I. Mochalkin, S. S. Wong, Y. G. Yue, L. Huber, I. Conti, J. R. Henry, J. J. Starling, G. D. Plowman, and S. B. Peng (2016) Oncogenic BRAF Deletions That Function as Homodimers and Are Sensitive to Inhibition by RAF Dimer Inhibitor LY3009120. *Cancer Discov* 6 (3):300-15. doi: 10.1158/2159-8290.CD-15-0896.

Choo, E. F., J. Ly, J. Chan, S. K. Shahidi-Latham, K. Messick, E. Plise, C. M. Quiason, and L. Yang (2014) Role of P-glycoprotein on the brain penetration and brain

pharmacodynamic activity of the MEK inhibitor cobimetinib. *Mol Pharm* 11 (11):4199-207. doi: 10.1021/mp500435s.

Dai, H., P. Marbach, M. Lemaire, M. Hayes, and W. F. Elmquist (2003) Distribution of STI-571 to the brain is limited by P-glycoprotein-mediated efflux. *J Pharmacol Exp Ther* 304 (3):1085-92. doi: 10.1124/jpet.102.045260.

Davies, H., G. R. Bignell, C. Cox, P. Stephens, S. Edkins, S. Clegg, J. Teague, H. Woffendin, M. J. Garnett, W. Bottomley, N. Davis, E. Dicks, R. Ewing, Y. Floyd, K. Gray, S. Hall, R. Hawes, J. Hughes, V. Kosmidou, A. Menzies, C. Mould, A. Parker, C. Stevens, S. Watt, S. Hooper, R. Wilson, H. Jayatilake, B. A. Gusterson, C. Cooper, J. Shipley, D. Hargrave, K. Pritchard-Jones, N. Maitland, G. Chenevix-Trench, G. J. Riggins, D. D. Bigner, G. Palmieri, A. Cossu, A. Flanagan, A. Nicholson, J. W. Ho, S. Y. Leung, S. T. Yuen, B. L. Weber, H. F. Seigler, T. L. Darrow, H. Paterson, R. Marais, C. J. Marshall, R. Wooster, M. R. Stratton, and P. A. Futreal (2002) Mutations of the BRAF gene in human cancer. *Nature* 417 (6892):949-54. doi: 10.1038/nature00766.

de Gooijer, M. C., P. Zhang, R. Weijer, L. C. M. Buil, J. H. Beijnen, and O. van Tellingen (2018) The impact of P-glycoprotein and breast cancer resistance protein on the brain pharmacokinetics and pharmacodynamics of a panel of MEK inhibitors. *Int J Cancer* 142 (2):381-391. doi: 10.1002/ijc.31052.

Delord, J. P., C. Robert, M. Nyakas, G. A. McArthur, R. Kudchakar, A. Mahipal, Y. Yamada, R. Sullivan, A. Arance, R. F. Kefford, M. S. Carlino, M. Hidalgo, C. Gomez-Roca, D. Michel, A. Seroutou, V. Aslanis, G. Caponigro, D. D. Stuart, L. Moutouh-de Parseval, T. Demuth, and R. Dummer (2017) Phase I Dose-Escalation and -Expansion Study of the BRAF Inhibitor Encorafenib (LGX818) in Metastatic BRAF-Mutant Melanoma. *Clin Cancer Res* 23 (18):5339-5348. doi: 10.1158/1078-0432.CCR-16-2923.

Dummer, R., P. A. Ascierto, H. J. Gogas, A. Arance, M. Mandala, G. Liszkay, C. Garbe, D. Schadendorf, I. Krajsova, R. Gutzmer, V. Chiarion-Sileni, C. Dutriaux, J. W. B. de Groot, N. Yamazaki, C. Loquai, L. A. Moutouh-de Parseval, M. D. Pickard, V. Sandor, C. Robert, and K. T. Flaherty (2018) Encorafenib plus binimetinib versus vemurafenib or encorafenib in patients with BRAF-mutant melanoma (COLUMBUS): a multicentre, open-label, randomised phase 3 trial. *Lancet Oncol* 19 (5):603-615. doi: 10.1016/S1470-2045(18)30142-6.

Dummer, R., S. M. Goldinger, C. P. Turtschi, N. B. Eggmann, O. Michielin, L. Mitchell, L. Veronese, P. R. Hilfiker, L. Felderer, and J. D. Rinderknecht (2014) Vemurafenib in patients with BRAF(V600) mutation-positive melanoma with symptomatic brain metastases: final results of an open-label pilot study. *Eur J Cancer* 50 (3):611-21. doi: 10.1016/j.ejca.2013.11.002.

Dummer, R., D. Schadendorf, P. A. Ascierto, A. Arance, C. Dutriaux, A. M. Di Giacomo, P. Rutkowski, M. Del Vecchio, R. Gutzmer, M. Mandala, L. Thomas, L. Demidov, C. Garbe, D. Hogg, G. Liszkay, P. Queirolo, E. Wasserman, J. Ford, M. Weill, L. A. Sirulnik, V. Jehl, V. Bozon, G. V. Long, and K. Flaherty (2017) Binimetinib versus dacarbazine in patients with advanced NRAS-mutant

melanoma (NEMO): a multicentre, open-label, randomised, phase 3 trial. *Lancet Oncol* 18 (4):435-445. doi: 10.1016/S1470-2045(17)30180-8.

Elenbaas B, Singh L, Boccia A, Cullen P, Peng H, Rohde E, Raimundo B, Kumaravel G, Joseph I. 2010. "BIIB024, a potent pan-Raf kinase inhibitor fro melanoma and solid tumors." EORTC-NCI-AACR Molecular Targets and Cancer Therapeutics, November 16 -19 2010.

Flaherty, K. T., J. R. Infante, A. Daud, R. Gonzalez, R. F. Kefford, J. Sosman, O. Hamid, L. Schuchter, J. Cebon, N. Ibrahim, R. Kudchadkar, H. A. Burris, 3rd, G. Falchook, A. Algazi, K. Lewis, G. V. Long, I. Puzanov, P. Lebowitz, A. Singh, S. Little, P. Sun, A. Allred, D. Ouellet, K. B. Kim, K. Patel, and J. Weber (2012) Combined BRAF and MEK inhibition in melanoma with BRAF V600 mutations. *N Engl J Med* 367 (18):1694-703. doi: 10.1056/NEJMoa1210093.

Flaherty, K. T., C. Robert, P. Hersey, P. Nathan, C. Garbe, M. Milhem, L. V. Demidov, J. C. Hassel, P. Rutkowski, P. Mohr, R. Dummer, U. Trefzer, J. M. Larkin, J. Utikal, B. Dreno, M. Nyakas, M. R. Middleton, J. C. Becker, M. Casey, L. J. Sherman, F. S. Wu, D. Ouellet, A. M. Martin, K. Patel, D. Schadendorf, and Metric Study Group (2012) Improved survival with MEK inhibition in BRAF-mutated melanoma. *N Engl J Med* 367 (2):107-14. doi: 10.1056/NEJMoa1203421.

Friden, M., A. Gupta, M. Antonsson, U. Bredberg, and M. Hammarlund-Udenaes (2007) In vitro methods for estimating unbound drug concentrations in the brain interstitial and intracellular fluids. *Drug Metab Dispos* 35 (9):1711-9. doi: 10.1124/dmd.107.015222.

Gampa, G., S. Vaidhyanathan, B. W. Resman, K. E. Parrish, S. N. Markovic, J. N. Sarkaria, and W. F. Elmquist (2016) Challenges in the delivery of therapies to melanoma brain metastases. *Curr Pharmacol Rep* 2 (6):309-325. doi: 10.1007/s40495-016-0072-z.

Gampa, G., S. Vaidhyanathan, J. N. Sarkaria, and W. F. Elmquist (2017) Drug delivery to melanoma brain metastases: Can current challenges lead to new opportunities? *Pharmacol Res* 123:10-25. doi: 10.1016/j.phrs.2017.06.008.

Girotti, M. R., F. Lopes, N. Preece, D. Niculescu-Duvaz, A. Zambon, L. Davies, S. Whittaker, G. Saturno, A. Viros, M. Pedersen, B. M. Suijkerbuijk, D. Menard, R. McLeary, L. Johnson, L. Fish, S. Ejiama, B. Sanchez-Laorden, J. Hohloch, N. Carragher, K. Macleod, G. Ashton, A. A. Marusiak, A. Fusi, J. Brognard, M. Frame, P. Lorigan, R. Marais, and C. Springer (2015) Paradox-breaking RAF inhibitors that also target SRC are effective in drug-resistant BRAF mutant melanoma. *Cancer Cell* 27 (1):85-96. doi: 10.1016/j.ccell.2014.11.006.

Goldberg, S. B., S. N. Gettinger, A. Mahajan, A. C. Chiang, R. S. Herbst, M. Sznol, A. J. Tsiouris, J. Cohen, A. Vortmeyer, L. Jilaveanu, J. Yu, U. Hegde, S. Speaker, M. Madura, A. Ralabate, A. Rivera, E. Rowen, H. Gerrish, X. Yao, V. Chiang, and H. M. Kluger (2016) Pembrolizumab for patients with melanoma or non-small-cell lung cancer and untreated brain metastases: early analysis of a non-randomised, open-label, phase 2 trial. *Lancet Oncol* 17 (7):976-983. doi: 10.1016/S1470-2045(16)30053-5.

Gupta, G., A. G. Robertson, and R. M. MacKie (1997) Cerebral metastases of cutaneous melanoma. *Br J Cancer* 76 (2):256-9.

Hatzivassiliou, G., K. Song, I. Yen, B. J. Brandhuber, D. J. Anderson, R. Alvarado, M. J. Ludlam, D. Stokoe, S. L. Gloor, G. Vigers, T. Morales, I. Aliagas, B. Liu, S. Sideris, K. P. Hoeflich, B. S. Jaiswal, S. Seshagiri, H. Koeppen, M. Belvin, L. S. Friedman, and S. Malek (2010) RAF inhibitors prime wild-type RAF to activate the MAPK pathway and enhance growth. *Nature* 464 (7287):431-5. doi: 10.1038/nature08833.

Heidorn, S. J., C. Milagre, S. Whittaker, A. Nourry, I. Niculescu-Duvas, N. Dhomen, J. Hussain, J. S. Reis-Filho, C. J. Springer, C. Pritchard, and R. Marais (2010) Kinase-dead BRAF and oncogenic RAS cooperate to drive tumor progression through CRAF. *Cell* 140 (2):209-21. doi: 10.1016/j.cell.2009.12.040.

Henry, J. R., M. D. Kaufman, S. B. Peng, Y. M. Ahn, T. M. Caldwell, L. Vogeti, H. Telikepalli, W. P. Lu, M. M. Hood, T. J. Rutkoski, B. D. Smith, S. Vogeti, D. Miller, S. C. Wise, L. Chun, X. Zhang, Y. Zhang, L. Kays, P. A. Hipskind, A. D. Wrobleski, K. L. Lobb, J. M. Clay, J. D. Cohen, J. L. Walgren, D. McCann, P. Patel, D. K. Clawson, S. Guo, D. Manglicmot, C. Groshong, C. Logan, J. J. Starling, and D. L. Flynn (2015) Discovery of 1-(3,3-dimethylbutyl)-3-(2-fluoro-4-methyl-5-(7-methyl-2-(methylamino)pyrido[2,3- d]pyrimidin-6-yl)phenyl)urea (LY3009120) as a pan-RAF inhibitor with minimal paradoxical activation and activity against BRAF or RAS mutant tumor cells. *J Med Chem* 58 (10):4165-79. doi: 10.1021/acs.jmedchem.5b00067.

Hocker, T., and H. Tsao (2007) Ultraviolet radiation and melanoma: a systematic review and analysis of reported sequence variants. *Hum Mutat* 28 (6):578-88. doi: 10.1002/humu.20481.

Hodis, E., I. R. Watson, G. V. Kryukov, S. T. Arold, M. Imielinski, J. P. Theurillat, E. Nickerson, D. Auclair, L. Li, C. Place, D. Dicara, A. H. Ramos, M. S. Lawrence, K. Cibulskis, A. Sivachenko, D. Voet, G. Saksena, N. Stransky, R. C. Onofrio, W. Winckler, K. Ardlie, N. Wagle, J. Wargo, K. Chong, D. L. Morton, K. Stemke-Hale, G. Chen, M. Noble, M. Meyerson, J. E. Ladbury, M. A. Davies, J. E. Gershenwald, S. N. Wagner, D. S. Hoon, D. Schadendorf, E. S. Lander, S. B. Gabriel, G. Getz, L. A. Garraway, and L. Chin (2012) A landscape of driver mutations in melanoma. *Cell* 150 (2):251-63. doi: 10.1016/j.cell.2012.06.024.

Johnson, D. B., A. M. Menzies, L. Zimmer, Z. Eroglu, F. Ye, S. Zhao, H. Rizos, A. Sucker, R. A. Scolyer, R. Gutzmer, H. Gogas, R. F. Kefford, J. F. Thompson, J. C. Becker, C. Berking, F. Egberts, C. Loquai, S. M. Goldinger, G. M. Pupo, W. Hugo, X. Kong, L. A. Garraway, J. A. Sosman, A. Ribas, R. S. Lo, G. V. Long, and D. Schadendorf (2015) Acquired BRAF inhibitor resistance: A multicenter meta-analysis of the spectrum and frequencies, clinical behaviour, and phenotypic associations of resistance mechanisms. *Eur J Cancer* 51 (18):2792-9. doi: 10.1016/j.ejca.2015.08.022.

Kalvass, J. C., and T. S. Maurer (2002) Influence of nonspecific brain and plasma binding on CNS exposure: implications for rational drug discovery. *Biopharm Drug Dispos* 23 (8):327-38. doi: 10.1002/bdd.325.

Kim, M., S. H. Kizilbash, J. K. Laramy, G. Gampa, K. E. Parrish, J. N. Sarkaria, and W. F. Elmquist (2018) Barriers to Effective Drug Treatment for Brain Metastases: A Multifactorial Problem in the Delivery of Precision Medicine. *Pharm Res* 35 (9):177. doi: 10.1007/s11095-018-2455-9.

Larkin, J., P. A. Ascierto, B. Dreno, V. Atkinson, G. Liszkay, M. Maio, M. Mandala, L. Demidov, D. Stroyakovskiy, L. Thomas, L. de la Cruz-Merino, C. Dutriaux, C. Garbe, M. A. Sovak, I. Chang, N. Choong, S. P. Hack, G. A. McArthur, and A. Ribas (2014) Combined vemurafenib and cobimetinib in BRAF-mutated melanoma. *N Engl J Med* 371 (20):1867-76. doi: 10.1056/NEJMoa1408868.

Lockman, P. R., R. K. Mittapalli, K. S. Taskar, V. Rudraraju, B. Gril, K. A. Bohn, C. E. Adkins, A. Roberts, H. R. Thorsheim, J. A. Gaasch, S. Huang, D. Palmieri, P. S. Steeg, and Q. R. Smith (2010) Heterogeneous blood-tumor barrier permeability determines drug efficacy in experimental brain metastases of breast cancer. *Clin Cancer Res* 16 (23):5664-78. doi: 10.1158/1078-0432.CCR-10-1564.

Long, G. V., D. Stroyakovskiy, H. Gogas, E. Levchenko, F. de Braud, J. Larkin, C. Garbe, T. Jouary, A. Hauschild, J. J. Grob, V. Chiarion Sileni, C. Lebbe, M. Mandala, M. Millward, A. Arance, I. Bondarenko, J. B. Haanen, J. Hansson, J. Utikal, V. Ferraresi, N. Kovalenko, P. Mohr, V. Probachai, D. Schadendorf, P. Nathan, C. Robert, A. Ribas, D. J. DeMarini, J. G. Irani, M. Casey, D. Ouellet, A. M. Martin, N. Le, K. Patel, and K. Flaherty (2014) Combined BRAF and MEK inhibition versus BRAF inhibition alone in melanoma. *N Engl J Med* 371 (20):1877-88. doi: 10.1056/NEJMoa1406037.

Long, G. V., U. Trefzer, M. A. Davies, R. F. Kefford, P. A. Ascierto, P. B. Chapman, I. Puzanov, A. Hauschild, C. Robert, A. Algazi, L. Mortier, H. Tawbi, T. Wilhelm, L. Zimmer, J. Switzky, S. Swann, A. M. Martin, M. Guckert, V. Goodman, M. Streit, J. M. Kirkwood, and D. Schadendorf (2012) Dabrafenib in patients with Val600Glu or Val600Lys BRAF-mutant melanoma metastatic to the brain (BREAK-MB): a multicentre, open-label, phase 2 trial. *Lancet Oncol* 13 (11):1087-95. doi: 10.1016/S1470-2045(12)70431-X.

Margolin, K., M. S. Ernstoff, O. Hamid, D. Lawrence, D. McDermott, I. Puzanov, J. D. Wolchok, J. I. Clark, M. Sznol, T. F. Logan, J. Richards, T. Michener, A. Balogh, K. N. Heller, and F. S. Hodi (2012) Ipilimumab in patients with melanoma and brain metastases: an open-label, phase 2 trial. *Lancet Oncol* 13 (5):459-65. doi: 10.1016/S1470-2045(12)70090-6.

Mittapalli, R. K., S. Vaidhyanathan, A. Z. Dudek, and W. F. Elmquist (2013) Mechanisms limiting distribution of the threonine-protein kinase B-RaF(V600E) inhibitor dabrafenib to the brain: implications for the treatment of melanoma brain metastases. *J Pharmacol Exp Ther* 344 (3):655-64. doi: 10.1124/jpet.112.201475.

Mittapalli, R. K., S. Vaidhyanathan, R. Sane, and W. F. Elmquist (2012) Impact of P-glycoprotein (ABCB1) and breast cancer resistance protein (ABCG2) on the brain distribution of a novel BRAF inhibitor: vemurafenib (PLX4032). *J Pharmacol Exp Ther* 342 (1):33-40. doi: 10.1124/jpet.112.192195.

Nedelman, J. R., and X. Jia (1998) An extension of Satterthwaite's approximation applied to pharmacokinetics. *J Biopharm Stat* 8 (2):317-28. doi: 10.1080/10543409808835241.

Osswald, M., J. Blaes, Y. Liao, G. Solecki, M. Gommel, A. S. Berghoff, L. Salphati, J. J. Wallin, H. S. Phillips, W. Wick, and F. Winkler (2016) Impact of Blood-Brain Barrier Integrity on Tumor Growth and Therapy Response in Brain Metastases. *Clin Cancer Res* 22 (24):6078-6087. doi: 10.1158/1078-0432.CCR-16-1327.

Peng, S. B., J. R. Henry, M. D. Kaufman, W. P. Lu, B. D. Smith, S. Vogeti, T. J. Rutkoski, S. Wise, L. Chun, Y. Zhang, R. D. Van Horn, T. Yin, X. Zhang, V. Yadav, S. H. Chen, X. Gong, X. Ma, Y. Webster, S. Buchanan, I. Mochalkin, L. Huber, L. Kays, G. P. Donoho, J. Walgren, D. McCann, P. Patel, I. Conti, G. D. Plowman, J. J. Starling, and D. L. Flynn (2015) Inhibition of RAF Isoforms and Active Dimers by LY3009120 Leads to Anti-tumor Activities in RAS or BRAF Mutant Cancers. *Cancer Cell* 28 (3):384-98. doi: 10.1016/j.ccell.2015.08.002.

Poulikakos, P. I., C. Zhang, G. Bollag, K. M. Shokat, and N. Rosen (2010) RAF inhibitors transactivate RAF dimers and ERK signalling in cells with wild-type BRAF. *Nature* 464 (7287):427-30. doi: 10.1038/nature08902.

Rasco, D.W. , A. J. Olszanski, A. Patnaik, G. Espino, R. Neuwirth, S. Faucette, M. Bargfrede, E. A. Gangolli, R. M. Walker, M. Kneissl, and V. Bozon (2013) MLN2480, an investigational oral panRAF kinase inhibitor, in patients (pts) with relapsed or refractory solid tumors: Phase I study. *J Clin Oncol* 31.

Samatar, A. A., and P. I. Poulikakos (2014) Targeting RAS-ERK signalling in cancer: promises and challenges. *Nat Rev Drug Discov* 13 (12):928-42. doi: 10.1038/nrd4281.

Shi, H., W. Hugo, X. Kong, A. Hong, R. C. Koya, G. Moriceau, T. Chodon, R. Guo, D. B. Johnson, K. B. Dahlman, M. C. Kelley, R. F. Kefford, B. Chmielowski, J. A. Glaspy, J. A. Sosman, N. van Baren, G. V. Long, A. Ribas, and R. S. Lo (2014) Acquired resistance and clonal evolution in melanoma during BRAF inhibitor therapy. *Cancer Discov* 4 (1):80-93. doi: 10.1158/2159-8290.CD-13-0642.

Spagnolo, F., V. Picasso, M. Lambertini, V. Ottaviano, B. Dozin, and P. Queirolo (2016) Survival of patients with metastatic melanoma and brain metastases in the era of MAP-kinase inhibitors and immunologic checkpoint blockade antibodies: A systematic review. *Cancer Treat Rev* 45:38-45. doi: 10.1016/j.ctrv.2016.03.003.

Sun, Y., J. A. Alberta, C. Pilarz, D. Calligaris, E. J. Chadwick, S. H. Ramkissoon, L. A. Ramkissoon, V. M. Garcia, E. Mazzola, L. Goumnerova, M. Kane, Z. Yao, M. W. Kieran, K. L. Ligon, W. C. Hahn, L. A. Garraway, N. Rosen, N. S. Gray, N. Y. Agar, S. J. Buhrlage, R. A. Segal, and C. D. Stiles (2017) A brain-penetrant RAF dimer antagonist for the noncanonical BRAF oncoprotein of pediatric low-grade astrocytomas. *Neuro Oncol* 19 (6):774-785. doi: 10.1093/neuonc/now261.

Tawbi, H. A., P. A. Forsyth, A. Algazi, O. Hamid, F. S. Hodi, S. J. Moschos, N. I. Khushalani, K. Lewis, C. D. Lao, M. A. Postow, M. B. Atkins, M. S. Ernstoff, D. A. Reardon, I. Puzanov, R. R. Kudchadkar, R. P. Thomas, A. Tarhini, A. C. Pavlick, J. Jiang, A. Avila, S. Demelo, and K. Margolin (2018) Combined

Nivolumab and Ipilimumab in Melanoma Metastatic to the Brain. *N Engl J Med* 379 (8):722-730. doi: 10.1056/NEJMoa1805453.

Vaidhyanathan, S., R. K. Mittapalli, J. N. Sarkaria, and W. F. Elmquist (2014) Factors influencing the CNS distribution of a novel MEK-1/2 inhibitor: implications for combination therapy for melanoma brain metastases. *Drug Metab Dispos* 42 (8):1292-300. doi: 10.1124/dmd.114.058339.

Wagle, N., E. M. Van Allen, D. J. Treacy, D. T. Frederick, Z. A. Cooper, A. Taylor-Weiner, M. Rosenberg, E. M. Goetz, R. J. Sullivan, D. N. Farlow, D. C. Friedrich, K. Anderka, D. Perrin, C. M. Johannessen, A. McKenna, K. Cibulskis, G. Kryukov, E. Hodis, D. P. Lawrence, S. Fisher, G. Getz, S. B. Gabriel, S. L. Carter, K. T. Flaherty, J. A. Wargo, and L. A. Garraway (2014) MAP kinase pathway alterations in BRAF-mutant melanoma patients with acquired resistance to combined RAF/MEK inhibition. *Cancer Discov* 4 (1):61-8. doi: 10.1158/2159-8290.CD-13-0631.

Wang, J., C. Gan, R. W. Sparidans, E. Wagenaar, S. van Hoppe, J. H. Beijnen, and A. H. Schinkel (2018) P-glycoprotein (MDR1/ABCB1) and Breast Cancer Resistance Protein (BCRP/ABCG2) affect brain accumulation and intestinal disposition of encorafenib in mice. *Pharmacol Res* 129:414-423. doi: 10.1016/j.phrs.2017.11.006.

Welsh, S. J., H. Rizos, R. A. Scolyer, and G. V. Long (2016) Resistance to combination BRAF and MEK inhibition in metastatic melanoma: Where to next? *Eur J Cancer* 62:76-85. doi: 10.1016/j.ejca.2016.04.005.

Whittaker, S. R., G. S. Cowley, S. Wagner, F. Luo, D. E. Root, and L. A. Garraway (2015) Combined Pan-RAF and MEK Inhibition Overcomes Multiple Resistance Mechanisms to Selective RAF Inhibitors. *Mol Cancer Ther* 14 (12):2700-11. doi: 10.1158/1535-7163.MCT-15-0136-T.

CHAPTER VI

Agarwal, S., P. Manchanda, M. A. Vogelbaum, J. R. Ohlfest, and W. F. Elmquist (2013) Function of the blood-brain barrier and restriction of drug delivery to invasive glioma cells: findings in an orthotopic rat xenograft model of glioma. *Drug Metab Dispos* 41 (1):33-9. doi: 10.1124/dmd.112.048322.

Agarwal, S., R. Sane, R. Oberoi, J. R. Ohlfest, and W. F. Elmquist (2011) Delivery of molecularly targeted therapy to malignant glioma, a disease of the whole brain. *Expert Rev Mol Med* 13:e17. doi: 10.1017/S1462399411001888.

Agarwal, S., Y. Uchida, R. K. Mittapalli, R. Sane, T. Terasaki, and W. F. Elmquist (2012) Quantitative proteomics of transporter expression in brain capillary endothelial cells isolated from P-glycoprotein (P-gp), breast cancer resistance protein (Bcrp), and P-gp/Bcrp knockout mice. *Drug Metab Dispos* 40 (6):1164-9. doi: 10.1124/dmd.112.044719.

Ameratunga, M., G. McArthur, H. Gan, and L. Cher (2016) Prolonged disease control with MEK inhibitor in neurofibromatosis type I-associated glioblastoma. *J Clin Pharm Ther* 41 (3):357-359. doi: 10.1111/jcpt.12378.

Bates, S. E. (2013) A sea change in melanoma. *Clin Cancer Res* 19 (19):5282. doi: 10.1158/1078-0432.CCR-13-2219.

Byron, S. A., D. C. Loch, C. L. Wellens, A. Wortmann, J. Wu, J. Wang, K. Nomoto, and P. M. Pollock (2012) Sensitivity to the MEK inhibitor E6201 in melanoma cells is associated with mutant BRAF and wildtype PTEN status. *Mol Cancer* 11:75. doi: 10.1186/1476-4598-11-75.

Carlson, B. L., J. L. Pokorny, M. A. Schroeder, and J. N. Sarkaria (2011) Establishment, maintenance and in vitro and in vivo applications of primary human glioblastoma multiforme (GBM) xenograft models for translational biology studies and drug discovery. *Curr Protoc Pharmacol* Chapter 14:Unit 14 16. doi: 10.1002/0471141755.ph1416s52.

Choo, E. F., J. Ly, J. Chan, S. K. Shahidi-Latham, K. Messick, E. Plise, C. M. Quiason, and L. Yang (2014) Role of P-glycoprotein on the brain penetration and brain pharmacodynamic activity of the MEK inhibitor cobimetinib. *Mol Pharm* 11 (11):4199-207. doi: 10.1021/mp500435s.

Cohen, J. V., H. Tawbi, K. A. Margolin, R. Amravadi, M. Bosenberg, P. K. Brastianos, V. L. Chiang, J. de Groot, I. C. Glitza, M. Herlyn, S. L. Holmen, L. B. Jilaveanu, A. Lassman, S. Moschos, M. A. Postow, R. Thomas, J. A. Tsiouris, P. Wen, R. M. White, T. Turnham, M. A. Davies, and H. M. Kluger (2016) Melanoma central nervous system metastases: current approaches, challenges, and opportunities. *Pigment Cell Melanoma Res* 29 (6):627-642. doi: 10.1111/pcmr.12538.

Dai, H., P. Marbach, M. Lemaire, M. Hayes, and W. F. Elmquist (2003) Distribution of STI-571 to the brain is limited by P-glycoprotein-mediated efflux. *J Pharmacol Exp Ther* 304 (3):1085-92. doi: 10.1124/jpet.102.045260.

Damsky, W. E., N. Theodosakis, and M. Bosenberg (2014) Melanoma metastasis: new concepts and evolving paradigms. *Oncogene* 33 (19):2413-22. doi: 10.1038/onc.2013.194.

Davies, H., G. R. Bignell, C. Cox, P. Stephens, S. Edkins, S. Clegg, J. Teague, H. Woffendin, M. J. Garnett, W. Bottomley, N. Davis, E. Dicks, R. Ewing, Y. Floyd, K. Gray, S. Hall, R. Hawes, J. Hughes, V. Kosmidou, A. Menzies, C. Mould, A. Parker, C. Stevens, S. Watt, S. Hooper, R. Wilson, H. Jayatilake, B. A. Gusterson, C. Cooper, J. Shipley, D. Hargrave, K. Pritchard-Jones, N. Maitland, G. Chenevix-Trench, G. J. Riggins, D. D. Bigner, G. Palmieri, A. Cossu, A. Flanagan, A. Nicholson, J. W. Ho, S. Y. Leung, S. T. Yuen, B. L. Weber, H. F. Seigler, T. L. Darrow, H. Paterson, R. Marais, C. J. Marshall, R. Wooster, M. R. Stratton, and P. A. Futreal (2002) Mutations of the BRAF gene in human cancer. *Nature* 417 (6892):949-54. doi: 10.1038/nature00766.

Di, L., H. Rong, and B. Feng (2013) Demystifying brain penetration in central nervous system drug discovery. Miniperspective. *J Med Chem* 56 (1):2-12. doi: 10.1021/jm301297f.

Dummer, R., S. M. Goldinger, C. P. Turtschi, N. B. Eggmann, O. Michielin, L. Mitchell, L. Veronese, P. R. Hilfiker, L. Felderer, and J. D. Rinderknecht (2014) Vemurafenib in patients with BRAF(V600) mutation-positive melanoma with symptomatic brain metastases: final results of an open-label pilot study. *Eur J Cancer* 50 (3):611-21. doi: 10.1016/j.ejca.2013.11.002.

Essig, M., M. A. Weber, H. von Tengg-Kobligk, M. V. Knopp, W. T. Yuh, and F. L. Giesel (2006) Contrast-enhanced magnetic resonance imaging of central nervous system tumors: agents, mechanisms, and applications. *Top Magn Reson Imaging* 17 (2):89-106. doi: 10.1097/01.rmr.0000245464.36148.dc.

Falchook, G. S., G. V. Long, R. Kurzrock, K. B. Kim, T. H. Arkenau, M. P. Brown, O. Hamid, J. R. Infante, M. Millward, A. C. Pavlick, S. J. O'Day, S. C. Blackman, C. M. Curtis, P. Lebowitz, B. Ma, D. Ouellet, and R. F. Kefford (2012) Dabrafenib in patients with melanoma, untreated brain metastases, and other solid tumours: a phase 1 dose-escalation trial. *Lancet* 379 (9829):1893-901. doi: 10.1016/S0140-6736(12)60398-5.

Fife, K. M., M. H. Colman, G. N. Stevens, I. C. Firth, D. Moon, K. F. Shannon, R. Harman, K. Petersen-Schaefer, A. C. Zacest, M. Besser, G. W. Milton, W. H. McCarthy, and J. F. Thompson (2004) Determinants of outcome in melanoma patients with cerebral metastases. *J Clin Oncol* 22 (7):1293-300. doi: 10.1200/JCO.2004.08.140.

Flaherty, K. T., J. R. Infante, A. Daud, R. Gonzalez, R. F. Kefford, J. Sosman, O. Hamid, L. Schuchter, J. Cebon, N. Ibrahim, R. Kudchadkar, H. A. Burris, 3rd, G. Falchook, A. Algazi, K. Lewis, G. V. Long, I. Puzanov, P. Lebowitz, A. Singh, S. Little, P. Sun, A. Allred, D. Ouellet, K. B. Kim, K. Patel, and J. Weber (2012) Combined BRAF and MEK inhibition in melanoma with BRAF V600 mutations. *N Engl J Med* 367 (18):1694-703. doi: 10.1056/NEJMoa1210093.

Friden, M., A. Gupta, M. Antonsson, U. Bredberg, and M. Hammarlund-Udenaes (2007) In vitro methods for estimating unbound drug concentrations in the brain interstitial and intracellular fluids. *Drug Metab Dispos* 35 (9):1711-9. doi: 10.1124/dmd.107.015222.

Gampa, G., S. Vaidhyanathan, B. W. Resman, K. E. Parrish, S. N. Markovic, J. N. Sarkaria, and W. F. Elmquist (2016) Challenges in the delivery of therapies to melanoma brain metastases. *Curr Pharmacol Rep* 2 (6):309-325. doi: 10.1007/s40495-016-0072-z.

Gampa, G., S. Vaidhyanathan, J. N. Sarkaria, and W. F. Elmquist (2017) Drug delivery to melanoma brain metastases: Can current challenges lead to new opportunities? *Pharmacol Res* 123:10-25. doi: 10.1016/j.phrs.2017.06.008.

Goto, M., J. Chow, K. Muramoto, K. Chiba, S. Yamamoto, M. Fujita, H. Obaishi, K. Tai, Y. Mizui, I. Tanaka, D. Young, H. Yang, Y. J. Wang, H. Shirota, and F. Gusovsky (2009) E6201 [(3S,4R,5Z,8S,9S,11E)-14-(ethylamino)-8, 9,16-trihydroxy-3,4-dimethyl-3,4,9,19-tetrahydro-1H-2-benzoxacyclotetradecine-1,7 (8H)-dione], a novel kinase inhibitor of mitogen-activated protein kinase/extracellular signal-regulated kinase kinase (MEK)-1 and MEK kinase-1: in vitro characterization of its anti-inflammatory and antihyperproliferative activities. *J Pharmacol Exp Ther* 331 (2):485-95. doi: 10.1124/jpet.109.156554.

Gupta, G., A. G. Robertson, and R. M. MacKie (1997) Cerebral metastases of cutaneous melanoma. *Br J Cancer* 76 (2):256-9.

Heffron, T. P. (2016) Small Molecule Kinase Inhibitors for the Treatment of Brain Cancer. *J Med Chem* 59 (22):10030-10066. doi: 10.1021/acs.jmedchem.6b00618.

Hocker, T., and H. Tsao (2007) Ultraviolet radiation and melanoma: a systematic review and analysis of reported sequence variants. *Hum Mutat* 28 (6):578-88. doi: 10.1002/humu.20481.

Ikemori-Kawada, M., A. Inoue, M. Goto, Y. J. Wang, and Y. Kawakami (2012) Docking simulation study and kinase selectivity of f152A1 and its analogs. *J Chem Inf Model* 52 (8):2059-68. doi: 10.1021/ci300135g.

Jain, R. K., E. di Tomaso, D. G. Duda, J. S. Loeffler, A. G. Sorensen, and T. T. Batchelor (2007) Angiogenesis in brain tumours. *Nat Rev Neurosci* 8 (8):610-22. doi: 10.1038/nrn2175.

Johnson, T. W., P. F. Richardson, S. Bailey, A. Brooun, B. J. Burke, M. R. Collins, J. J. Cui, J. G. Deal, Y. L. Deng, D. Dinh, L. D. Engstrom, M. He, J. Hoffman, R. L. Hoffman, Q. Huang, R. S. Kania, J. C. Kath, H. Lam, J. L. Lam, P. T. Le, L. Lingardo, W. Liu, M. McTigue, C. L. Palmer, N. W. Sach, T. Smeal, G. L. Smith, A. E. Stewart, S. Timofeevski, H. Zhu, J. Zhu, H. Y. Zou, and M. P. Edwards (2014) Discovery of (10R)-7-amino-12-fluoro-2,10,16-trimethyl-15-oxo-10,15,16,17-tetrahydro-2H-8,4-(m etheno)pyrazolo[4,3-h][2,5,11]-benzoxadiazacyclotetradecine-3-carbonitrile (PF-06463922), a macrocyclic inhibitor of anaplastic lymphoma kinase (ALK) and c-ros oncogene 1 (ROS1) with preclinical brain exposure and broad-spectrum potency against ALK-resistant mutations. *J Med Chem* 57 (11):4720-44. doi: 10.1021/jm500261q.

Kalvass, J. C., and T. S. Maurer (2002) Influence of nonspecific brain and plasma binding on CNS exposure: implications for rational drug discovery. *Biopharm Drug Dispos* 23 (8):327-38. doi: 10.1002/bdd.325.

Laramy, J. K., M. Kim, S. K. Gupta, K. E. Parrish, S. Zhang, K. K. Bakken, B. L. Carlson, A. C. Mladek, D. J. Ma, J. N. Sarkaria, and W. F. Elmquist (2017)

Heterogeneous Binding and Central Nervous System Distribution of the Multitargeted Kinase Inhibitor Ponatinib Restrict Orthotopic Efficacy in a Patient-Derived Xenograft Model of Glioblastoma. *J Pharmacol Exp Ther* 363 (2):136-147. doi: 10.1124/jpet.117.243477.

Larkin, J., P. A. Ascierto, B. Dreno, V. Atkinson, G. Liszkay, M. Maio, M. Mandala, L. Demidov, D. Stroyakovskiy, L. Thomas, L. de la Cruz-Merino, C. Dutriaux, C. Garbe, M. A. Sovak, I. Chang, N. Choong, S. P. Hack, G. A. McArthur, and A. Ribas (2014) Combined vemurafenib and cobimetinib in BRAF-mutated melanoma. *N Engl J Med* 371 (20):1867-76. doi: 10.1056/NEJMoa1408868.

Lito, P., N. Rosen, and D. B. Solit (2013) Tumor adaptation and resistance to RAF inhibitors. *Nat Med* 19 (11):1401-9. doi: 10.1038/nm.3392.

Long, G. V., U. Trefzer, M. A. Davies, R. F. Kefford, P. A. Ascierto, P. B. Chapman, I. Puzanov, A. Hauschild, C. Robert, A. Algazi, L. Mortier, H. Tawbi, T. Wilhelm, L. Zimmer, J. Switzky, S. Swann, A. M. Martin, M. Guckert, V. Goodman, M. Streit, J. M. Kirkwood, and D. Schadendorf (2012) Dabrafenib in patients with Val600Glu or Val600Lys BRAF-mutant melanoma metastatic to the brain (BREAK-MB): a multicentre, open-label, phase 2 trial. *Lancet Oncol* 13 (11):1087-95. doi: 10.1016/S1470-2045(12)70431-X.

Margolin, K., M. S. Ernstoff, O. Hamid, D. Lawrence, D. McDermott, I. Puzanov, J. D. Wolchok, J. I. Clark, M. Sznol, T. F. Logan, J. Richards, T. Michener, A. Balogh, K. N. Heller, and F. S. Hodi (2012) Ipilimumab in patients with melanoma and brain metastases: an open-label, phase 2 trial. *Lancet Oncol* 13 (5):459-65. doi: 10.1016/S1470-2045(12)70090-6.

Mittapalli, R. K., S. Vaidhyanathan, A. Z. Dudek, and W. F. Elmquist (2013) Mechanisms limiting distribution of the threonine-protein kinase B-RaF(V600E) inhibitor dabrafenib to the brain: implications for the treatment of melanoma brain metastases. *J Pharmacol Exp Ther* 344 (3):655-64. doi: 10.1124/jpet.112.201475.

Mittapalli, R. K., S. Vaidhyanathan, R. Sane, and W. F. Elmquist (2012) Impact of P-glycoprotein (ABCB1) and breast cancer resistance protein (ABCG2) on the brain distribution of a novel BRAF inhibitor: vemurafenib (PLX4032). *J Pharmacol Exp Ther* 342 (1):33-40. doi: 10.1124/jpet.112.192195.

Murrell, D. H., A. M. Hamilton, C. L. Mallett, R. van Gorkum, A. F. Chambers, and P. J. Foster (2015) Understanding Heterogeneity and Permeability of Brain Metastases in Murine Models of HER2-Positive Breast Cancer Through Magnetic Resonance Imaging: Implications for Detection and Therapy. *Transl Oncol* 8 (3):176-84. doi: 10.1016/j.tranon.2015.03.009.

Narita, Y., K. Okamoto, M. I. Kawada, K. Takase, Y. Minoshima, K. Kodama, M. Iwata, N. Miyamoto, and K. Sawada (2014) Novel ATP-competitive MEK inhibitor E6201 is effective against vemurafenib-resistant melanoma harboring the MEK1-C121S mutation in a preclinical model. *Mol Cancer Ther* 13 (4):823-32. doi: 10.1158/1535-7163.MCT-13-0667.

Nedelman, J. R., and X. Jia (1998) An extension of Satterthwaite's approximation applied to pharmacokinetics. *J Biopharm Stat* 8 (2):317-28. doi: 10.1080/10543409808835241.

Osswald, M., J. Blaes, Y. Liao, G. Solecki, M. Gommel, A. S. Berghoff, L. Salphati, J. J. Wallin, H. S. Phillips, W. Wick, and F. Winkler (2016) Impact of Blood-Brain Barrier Integrity on Tumor Growth and Therapy Response in Brain Metastases. *Clin Cancer Res* 22 (24):6078-6087. doi: 10.1158/1078-0432.CCR-16-1327.

Raizer, J. J., W. J. Hwu, K. S. Panageas, A. Wilton, D. E. Baldwin, E. Bailey, C. von Althann, L. A. Lamb, G. Alvarado, M. H. Bilsky, and P. H. Gutin (2008) Brain and leptomeningeal metastases from cutaneous melanoma: survival outcomes based on clinical features. *Neuro Oncol* 10 (2):199-207. doi: 10.1215/15228517-2007-058.

Rankovic, Z. (2015) CNS drug design: balancing physicochemical properties for optimal brain exposure. *J Med Chem* 58 (6):2584-608. doi: 10.1021/jm501535r.

Ribas, A., R. Gonzalez, A. Pavlick, O. Hamid, T. F. Gajewski, A. Daud, L. Flaherty, T. Logan, B. Chmielowski, K. Lewis, D. Kee, P. Boasberg, M. Yin, I. Chan, L. Musib, N. Choong, I. Puzanov, and G. A. McArthur (2014) Combination of vemurafenib and cobimetinib in patients with advanced BRAF(V600)-mutated melanoma: a phase 1b study. *Lancet Oncol* 15 (9):954-65. doi: 10.1016/S1470-2045(14)70301-8.

Samatar, A. A., and P. I. Poulikakos (2014) Targeting RAS-ERK signalling in cancer: promises and challenges. *Nat Rev Drug Discov* 13 (12):928-42. doi: 10.1038/nrd4281.

Siegel, R. L., K. D. Miller, and A. Jemal (2017) Cancer Statistics, 2017. *CA Cancer J Clin* 67 (1):7-30. doi: 10.3322/caac.21387.

Sloan, A. E., C. J. Nock, and D. B. Einstein (2009) Diagnosis and treatment of melanoma brain metastasis: a literature review. *Cancer Control* 16 (3):248-55. doi: 10.1177/107327480901600307.

Spagnolo, F., V. Picasso, M. Lambertini, V. Ottaviano, B. Dozin, and P. Queirolo (2016) Survival of patients with metastatic melanoma and brain metastases in the era of MAP-kinase inhibitors and immunologic checkpoint blockade antibodies: A systematic review. *Cancer Treat Rev* 45:38-45. doi: 10.1016/j.ctrv.2016.03.003.

Summerfield, S. G., Y. Zhang, and H. Liu (2016) Examining the Uptake of Central Nervous System Drugs and Candidates across the Blood-Brain Barrier. *J Pharmacol Exp Ther* 358 (2):294-305. doi: 10.1124/jpet.116.232447.

Vaidhyanathan, S., R. K. Mittapalli, J. N. Sarkaria, and W. F. Elmquist (2014) Factors influencing the CNS distribution of a novel MEK-1/2 inhibitor: implications for combination therapy for melanoma brain metastases. *Drug Metab Dispos* 42 (8):1292-300. doi: 10.1124/dmd.114.058339.

Wager, T. T., X. Hou, P. R. Verhoest, and A. Villalobos (2016) Central Nervous System Multiparameter Optimization Desirability: Application in Drug Discovery. *ACS Chem Neurosci* 7 (6):767-75. doi: 10.1021/acschemneuro.6b00029.

Zeng, Q., J. Wang, Z. Cheng, K. Chen, P. Johnstrom, K. Varnas, D. Y. Li, Z. F. Yang, and X. Zhang (2015) Discovery and Evaluation of Clinical Candidate AZD3759, a Potent, Oral Active, Central Nervous System-Penetrant, Epidermal Growth Factor Receptor Tyrosine Kinase Inhibitor. *J Med Chem* 58 (20):8200-15. doi: 10.1021/acs.jmedchem.5b01073.